Center for Radiological Research – 630 W. 168th St., New York, NY 10032 – http://crr-cu.org

ANNUAL REPORT 2006

Eric J. Hall
Director

Howard B. Lieberman
Editor

Moshe Y. Friedman
Jinshuang Lu
Assistant Editors

COLUMBIA UNIVERSITY

College of Physicians and Surgeons

Table of Contents

Collaborating Institutions

Individuals from the following institutions collaborated with the Center's faculty and staff in the research reports included in this year's publication (for individual attributions see specific reports):

Collaborating Columbia University Departments:

- Columbia Center for New Media Teaching and Lecturing
- Department of Mechanical Engineering
- Department of Neurology
- Department of Pathology
- Department of Radiation Oncology

Collaborating Institutions:

- City University of New York, Department of Natural Sciences, HCC, New York
- Gray Cancer Institute, Mount Vernon Hospital, Northwood, Middlesex, UK
- Imperial College, London, UK
- Institute for Advanced Research, Tarapaca, University Arica, Chile
- Princess Margaret Hospital, Toronto, Ontario, Canada
- Tufts School of Medicine, Boston, MA
- University of California, Department of Mathematics, Berkeley
- U.S. Department of Health and Human Services
  - National Institutes of Health, Bethesda, MD
    - National Cancer Institute, Laboratory of Molecular Pharmacology, Center for Cancer Research ■

Acknowledgment of Support

In 2006 the Center for Radiological Research was supported by competitively awarded grants from the following agencies:

State:

- New York State Department of Health, Health Research Science Board

Federal:

- Department of Defense
  - Defense Threat Reduction Agency
- Department of Energy
  - Office of International Health Programs
  - Office of Science, Office of Biological and Environmental Research [Low Dose Radiation Research Program]
- Department of Health and Human Services
  - National Institutes of Health:
    - National Cancer Institute [Program Project (PO1) & Individual Research Grants (RO1s)]
    - National Center for Research Resources (S10)
    - National Institute of Biomedical Imaging and Bioengineering (P41)
    - National Institute of Allergy and Infectious Disease (U19)
    - National Institute of Environmental Health and Safety (RO1s)
    - National Institute of General Medical Sciences (RO1)
- National Aeronautics and Space Administration ■

Web Sites

- **Center for Radiological Research** ..... **http://crr-cu.org**
- **Radiological Research Accelerator Facility**..... **http://www.raraf.org**
- **Center for High-Throughput Minimally-Invasive Radiation Biodosimetry** ..... **http://www.cmcr.columbia.edu**
- **Web-Rad-Train**..... **http://www.web-rad-train.org**
- **Department of Radiation Oncology** .....**http://cpmcnet.columbia.edu/dept/radoncology**
- **Radiation Safety Office** .....**http://cpmcnet.columbia.edu/dept/radsafety**

- **CRR Annual Reports *(1998–present)*** .....**http://crr-cu.org/reports.htm**

Introduction

This introduction is primarily designed to provide a brief overview of the life and times of the Center in the past year, especially to give a flavor of the principal research initiatives and academic activities.

2006 was a year of significant change. It was the first full year of funding for the "Center for Minimally Invasive Biodosimetry" with Dr. Brenner as P.I., which has significantly broadened the base of our research and brought a measure of pragmatism to our activities, since the new Center is focused on developing a product. The increased funding prompted the Trustees to allocate funds to renovate some of the laboratory space to make it more efficient. For the first time since 1944, when Dr. Failla moved his research activities to the newly built 11th floor of the Vanderbilt Clinic Building, the Center was invaded by builders, plumbers, electricians and painters, all intent on renovation. At the same time, research space at our Nevis laboratory was more than doubled by building an additional floor.

Research activities of the Center for Radiological Research address diverse goals:

- To probe the mechanisms of the biological effects of radiation at the molecular level.
- Radiation Protection and the effects of low doses of radiation of concern to the U.S. Department of Energy.
- The biological effects of high energy heavy ions, unique to the space environment, that are of concern to NASA.
- Research of relevance to Radiation Oncology, especially altered fractionation patterns and the impact of radiation-induced second cancers.
- To examine the basic mechanism of diverse environmental carcinogen effects at both cellular and molecular levels.

For the first time, Dr. David Brenner's group has produced realistic mechanistically-based models which can predict radiation-induced second cancer risks (leukemia and solid tumors) after contemporary radiotherapeutic regimens. This is important both from the perspective of a patient's understanding of the risks associated with treatment, as well as for future efforts to reduce second cancer risks.

International collaboration and training remain an integral part of the Center activities, in line with the increasing emphasis on global activities of Columbia University as a whole. Investigators from Japan and China have conducted experiments at our RARAF facilities and Dr. Tom K. Hei has coordinated many training opportunities for medical and doctoral students from these countries.

Studies conducted in Dr. Hei's laboratory in the past year have firmly established the important role of mitochondrial function/mitochondrial DNA mutations in modulating radiation-induced bystander effects, as well as the response of cells to many environmental toxicants in which their activities are linked to reactive oxygen species.

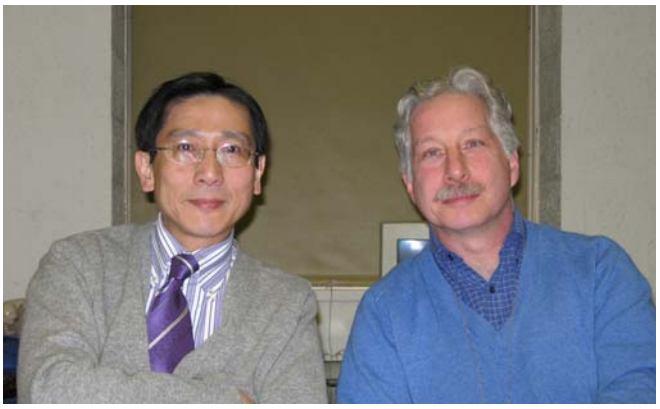

Dr. Tom K. Hei and Dr. Howard B. Lieberman.

Continuing studies with the DNA damage resistance gene Rad9 in Dr. Howard Lieberman's laboratory have revealed an important link between the encoded protein and human prostate cancer. These studies are being pursued to understand the basic mechanism of prostate carcinogenesis, as well as for the potential to develop novel therapeutic strategies to combat the disease.

Dr. Charles Geard's group, with Dr. Brian Ponnaiya and Gloria Jenkins based at RARAF and Drs. Peter Grabham and Burong Hu in the Center, have successfully utilized 3D tissue systems to show widely disseminated phosphorylation profiles in bystander cells (at RARAF) and space-related radiation effects on endothelial cell vessel formation (at Brookhaven National Laboratory).

Studies conducted in the past year have optimized gene expression profiling in human blood to enable identification and testing of radiation biomarkers. Early analysis of ongoing microarray experiments is extremely encouraging, indicating that gene expression can be used to predict exposure dose to samples irradiated both *ex vivo* and *in vivo*.

The productivity of the Center continues at a high level, as evidenced by a steady stream of scientific papers in peer-reviewed journals, including several in high profile journals. Given our success during the previous year for obtaining funding for research, we anticipate that the upcoming year will bring many important advances in understanding the biological effects of radiation exposure.

Members of the staff are frequently invited to participate in national and international meetings, and are frequently called upon to serve as consultants, reviewers or site visitors by government and private agencies.

The Center's teaching activities include presenting radiation biology and radiation physics to undergraduates, medical students and graduate students in the School of Public Health, and to residents in Radiology and Radiation Oncology, and a City-wide course for residents in Radiology. ■

Staff News

Dr. Eric Hall was named a fellow of the American Society of Therapeutic Radiology and Oncology (ASTRO) at a ceremony held on November 5 2006 during the ASTRO's 48th annual meeting in Philadelphia (see picture). Members of ASTRO are eligible to become a Fellow if they have served in a leadership role for the organization and made a significant contribution to the field of Radiation Oncology.

At the end of 2006 Dr. Eric Hall announced his plans to retire as Chair of the Joint Radiation Safety Committee (JRSC) and the Radioactive Drug Research Committee (RDRC) having served in these capacities for 22 years. In the beginning of 2007 Dr. David Brenner was appointed to succeed him in these roles.

Dr. Howard Lieberman was elected a Fellow of the American Association for the Advancement of Science.

Dr. Tom K. Hei continues to serve as an *ad hoc* member of the NCI cancer etiology study section and as chairman of several special emphasis panels.

Dr. Tom K. Hei has been elected Vice-Chairman of Subcommittee F on space radiation environment, biology and health of the Committee on Space Research for a period of four years.

Miss Ilana Yurkiewicz, a high school senior from the Lawrence High School in Cederhurst, New York under the mentorship of Professor Tom K. Hei was named one of the top twenty high school graduates in the United States in 2006 by the USA Today.

Mr. Daniel Lim, a science teacher from the Dunman Secondary School in Singapore spent three months in Dr. Hei's laboratory studying mutagenesis and apoptotic pathways in human melanoma cells.

Mr. Takuro Fushimi, a third year medical student from the Okayama Medical University spent three months in Dr. Hei's laboratory studying mitochondrial DNA function and mutagenesis in arsenic exposed human cohort as part of a physician scientist training program.

We will miss a number of staff members who have left the Center in the past year, either for retirement or new adventures in other research institutions:

Ms. Mary Coady, who has been on the staff as an Administrative Coordinator in the Center assisting Dr. Eric Hall for 25 years, retired in December.

A few Post-Doctoral Research Scientists, Drs. Genze Shao, Giuseppe Schettino and Naved Alam, have left the Center for new positions elsewhere.

Two staff associates, Gregory Ross and Shenbing Gu, and Instrument Maker Robert Archigian, have moved on for new positions.

Administrative Assistant Moshe Friedman left the center for a new position in the CUMC Radiation Safety Office.

Also leaving in 2006 were Senior Technician Ronald Baker and Administrative Assistant Diana Morrison.

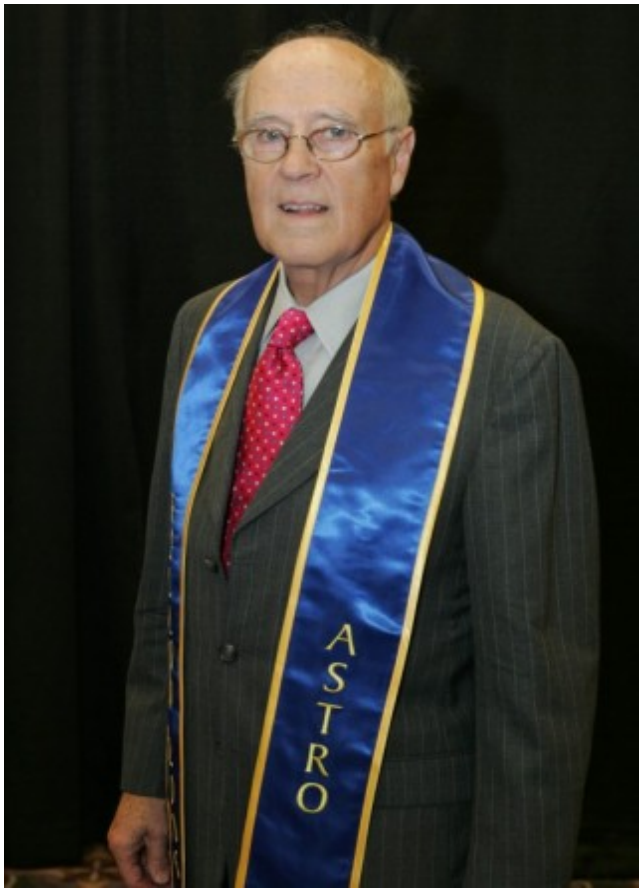

Dr. Eric Hall was named a fellow of the American Society of Therapeutic Radiology and Oncology at ASTRO's 48th annual meeting in Philadelphia on November 5, 2006.

The Center is pleased to have a number of new staff members who have been recruited to pursue research:

Dr. Alexandre Mesentsen and Sunirmal Paul have joined the Center as Associate Research Scientists in Dr. Sally Amundson's lab.

A number of new Post-Doctoral Research Scientists, including Dr. Cindy Liu in Dr. Yin's lab, Jarah A. Meador and Yanrong Su in Dr. Balajee's lab, Shanaz Ghandhi in Dr. Amundson's lab, and Yu-Chen Lien in Dr. Hei's lab, have also joined the Center. Dr. Ye Zhang came to Dr. Hei's lab as a Visiting Associate Research Scientist.

Dr. Igor Shuryak and Ms. Sasha Oleksandra Lyulko have joined the Center in pursuing their PhD degrees under the supervision of Dr. Brenner.

Mr. Dimitar Zlatev has also joined our team as a Research Worker in Dr. Smilenov's lab.

Jinshuang Lu, a junior programmer, joined the Center at the beginning of 2007, and has filled in nicely as assistant editor to produce this report. ■

Faculty and Staff

Faculty:

ERIC J. HALL, D.Phil., D.Sc., FACR, FRCR, FASTRO, FSRP
— ***Director***
Higgins Professor of Radiation Biophysics
Professor of Radiology and Radiation Oncology

CHARLES R. GEARD, Ph.D.
— ***Associate Director***
Professor of Clinical Radiation Oncology

DAVID J. BRENNER, Ph.D., D.Sc.
— ***RARAF Director***
Professor of Radiation Oncology and Public Health (Environmental Health Science)
Chairman, Joint Radiation Safety Committee
Chairman, Radioactive Drug Research Committee

TOM K. HEI, Ph.D.
Professor of Radiation Oncology
Professor of Environmental Health Sciences

HOWARD B. LIEBERMAN, Ph.D.
Professor of Radiation Oncology

SALLY A. AMUNDSON, Sc.D.
Associate Professor of Radiation Oncology

LUBOMIR SMILENOV, Ph.D.
Assistant Professor of Radiation Oncology

YUXIN YIN, M.D., Ph.D.
Assistant Professor of Radiation Oncology

YONG-LIANG ZHAO, Ph.D.
Assistant Professor of Radiation Oncology

Research Staff:

ADAYABALAM BALAJEE, Ph.D.
Research Scientist

GERHARD RANDERS-PEHRSON, Ph.D.
Research Scientist

ALAN BIGELOW, Ph.D.
Associate Research Scientist

GLORIA CALAF, Ph.D.
Adj. Associate Research Scientist

PETER GRABHAM, Ph.D.
Associate Research Scientist

VLADIMIR IVANOV, Ph.D.
Associate Research Scientist

ALEXANDRE MEZENTSEV, Ph.D.
Associate Research Scientist

SUNIRMAL PAUL, Ph.D.
Associate Research Scientist

BRIAN PONNAIYA, Ph.D.
Associate Research Scientist

HONGNING ZHOU, M.D.
Associate Research Scientist

KEVIN M. HOPKINS, M.S.
Senior Staff Associate

STEPHEN A. MARINO, M.S.
Senior Staff Associate

JAEYONG AHN, M.S.
Staff Associate

CARL ELLISTON, M.S.
Staff Associate

GUY GARTY, Ph.D.
Staff Associate

JING NIE, B.S.
Staff Associate

GREGORY ROSS, M.S.
Programmer Analyst

JINGJING WU, M.S.
Staff Associate

AIPING ZHU, M.D.
Staff Associate

Post-Doctoral Research Scientists:

APARAJITA DUTTA, Ph.D.
ANDREW HARKEN, Ph.D.
BURONG HU, Ph.D.
CORINNE LELOUP, Ph.D.
YU-CHIN LIEN, Ph.D.
CYNTHIA LIU, Ph.D.
JARAH MEADOR, Ph.D.
MICHAEL PARTRIDGE, Ph.D.
GIUSEPPE SCHETTINO, Ph.D. (until Dec. 2006)
GENZE SHAO, Ph.D. (until Sep. 2006)
WENHONG SHEN, Ph.D.
YANRONG SU, Ph.D.
GENGYUN WEN, Ph.D.
AN XU, Ph.D.
YANPING XU, Ph.D.
GUANGMING ZHOU, Ph.D.

Visiting Research Scientists:

YE ZHANG, Ph.D.
Visiting Associate Research Scientist

YIGAL HOROWITZ, Ph.D.
Visiting Senior Research Scientist

ATARA HOROWITZ, Ph.D.
Visiting Senior Research Scientist

TOMOO FUNAYAMA, Ph.D.
Visiting Research Scientist

Design & Instrument Shop:

GARY W. JOHNSON, A.A.S., Senior Staff Associate
— ***Design & Instrument Shop Director***

DAVID CUNIBERTI, B.A., Instrument Maker

ROBERT C. MORTON, Instrument Maker

Technical Staff:

GLORIA JENKINS-BAKER, B.S., Research Worker
XIAOJIAN WANG, M.S., Research Worker
CUI-XIA KUAN, Technical Assistant
DIMITAR ZLATEV, M.S., Technician B

Administrative & Secretarial Staff:

MONIQUE REY, B.A., Center Administrator
ANNE SUTTHOFF, M.A., Administrator
MARY COADY, Administrative Coordinator
YVETTE ACEVEDO, Administrative Assistant
DIANA MORRISON, Administrative Assistant
HEIDY HERNANDEZ, Jr. Accountant
ANGELA LUGO, Clerk Typist

Faculty and Staff

Front row (*l-r*): Dr. Gerhard Randers-Pehrson, Dr. Sally Amundson, Dr. Tom Hei, Dr. Charles Geard, Dr. Eric Hall, Dr. David Brenner, Dr. Howard Lieberman, Ms. Monique Rey.

2nd row: Mrs. Cui-Xia Kuan, Dr. Natalia Sotnik, Dr. Wenhong Shen, Dr. Shanaz Ghandhi, Dr. Aparajita Dutta, Bingyan Li, Ms. Sarah Huang, Dr. Aiping Zhu, Ms. Xiaojian Wang, Dr. Corinne Leloup, Ms. Gloria Jenkins-Baker, Dr. Yu-Chen Lien, Ms. Anne Sutthoff, Ms. Sasha Lyulko, Ms. Jing Nie, Dr. An Xu, Dr. Jarah Meador, Ms. Yvette Acevedo, Dr. Yanrong Su, Ms. Angela Lugo, Dr. Vladimir Ivanov, Ms. Heidy Hernandez, Mr. Gary Johnson.

3rd row: Dr. Ye Zhang, Mr. David Cuniberti, Dr. Yuxin Yin, Dr. Lubomir Smilenov, Dr. Yong-Liang Zhao, Dr. Adayabalam Balajee, Dr. Hongning Zhou, Dr. Guy Garty, Dr. Guangming Zhou, Dr. Alan Bigelow, Dr. Yanping Xu.

Back row: Mr. Yunfei Chai, Mr. Carl Elliston, Dr. Gengyun Wen, Mr. Robert Morton, Mr. Dimitar Zlatev, Dr. Andrew Harken, Dr. Brian Ponnaiya, Mr. Stephen Marino, Dr. Burong Hu, Mr. Kevin Hopkins.

Not pictured: Dr. Gloria Calaf, Dr. Michael Partidge, Dr. Igor Shuryak, Dr. Tomoo Funayama, Mr. Jaeyong Ahn, Dr. Peter Grabham.

Columbia Colloquium and Laboratory Seminars

At about monthly intervals during the year the Center for Radiological Research is pleased to welcome accomplished specialists from around the world to present formal seminars and/or spend time discussing ongoing research.

The seminars are attended by Center and RARAF professional staff, senior technical staff and graduate students, as well as doctors and scientists from other departments of the College of Physicians & Surgeons interested in collaborative research. Attention has focused on recent findings and future plans, with special emphasis on the interdisciplinary nature of our research effort.

The 2006 sessions included the following guest speakers (listed alphabetically):

- Dr. Rachel Airley, Instructor, Chanin Cancer Institute, Albert Einstein School of Medicine, Bronx, NY: "The Role of Glucose Transport and Metabolism in Tumour Microenvironment."
- Dr. Mohammad Athar, Department of Dermatology, Columbia University, College of Physicians & Surgeons: "CP-31398 activates mitochondrial apoptosis signaling pathway and blocks skin cancer development."
- Dr. Paul Fisher, Departments of Pathology, Neurosurgery and Urology, Columbia University, College of Physicians & Surgeons: "Cancer terminator viruses: A potential approach for treating primary and metastatic cancers."
- Dr. Jean Gautier, Institute of Cancer Genetics, Irving Cancer Research Center: "The ATM-MRN pathway."
- Dr. Tian Liu, Department of Radiation Oncology, Columbia University, College of Physicians & Surgeons: "Ultrasonic tissue-typing imaging for guiding dose escalation of prostate cancer radiotherapy."
- Dr. Man-ton Mei, South China Agricultural University, Guangzhou, China: "Biological Effects of Space Radiation Environment."
- Dr. Charles Powell, Department of Medicine, Columbia University, College of Physicians & Surgeons: "TGF-beta mediated invasion of lung adenocarcinoma."
- Dr. Qamar Rahman, Head, Fiber Toxicology Division, Industrial Toxicology Research Center, Lucknow, India: "Nanotoxicology: A Threat From Ultrafine Particles."
- Dr. Gloria Su, Otolaryngology/Head and Neck Cancer: "Modeling human pancreatic cancer."
- Dr. Keiji Suzuki, Associate Professor of Radiation Biology, Department of Radiology & Radiation Biology, Nagasaki University, Nagasaki, Japan: "Radiation-Induced Chromatin Disorganization and ATM-Dependent DNA Damage Signals."
- Dr. Eric Tang, Professor of Environmental Health Sciences, Nelson Institute of Environmental Medicine, New York University School of Medicine, Tuxedo, NY: "Searching for the True Villains of Lung and Liver Cancer: Fingerprinting DNA Damage and Repair in the p53 Gene."

The three generations of scientists after a seminar visit to Columbia University: Dr. Keiji Suzuki (left) was a former postdoctoral fellow of Professor Hei (middle) and Dr. Motohiro Yamauchi (right) is a current fellow in Dr. Suzuki's laboratory in Nagasaki University, Japan.

- Dr. Motohiro Yamauchi, Department of Radiology & Radiation Biology, Nagasaki University, Nagasaki, Japan: "Modulation of G1 checkpoint by ATM Protein Kinase."

Seminars were also conducted by professionals from our own Center staff:

- Dr. Alan Bigelow: "Multiphoton microscopy design for a microbeam endstation."
- Dr. Eric J. Hall: "In Memory of Basil Worgul." Dr. Worgul was a Professor of Radiation Biology in Ophthalmology and Radiology and Director Eye Radiation and Environmental Research Laboratory, who had collaborated on reports that appeared in this publication over the years.
- Dr. Tom Hei: "Recent advances in fiber toxicology."
- Dr. Corinne Leloup: "Deletion of *Mrad9B* sensitizes mouse embryonic stem cells to killing by DNA damaging agents."
- Dr. Howard Lieberman: "Role of human Rad9 in prostate cancer."
- Dr. Michael Partridge, "Arsenic induces mitochondrial DNA deletions, depletion of copy number and altered mitochondrial oxidative function."
- Dr. Genze Shao: "Betaig-h3 gene functions as tumor suppressor."
- Dr. Wenhong Shen: "PTEN regulates Rad51-mediated DNA double-strand break repair."
- Dr. An Xu: "New insight into intrachromosomal deletions induced by chrysotile in gpt delta transgenic mutation assay system." ■

Multiphoton Microscope: Incident Optics Characterization

Alan W. Bigelow, Gerhard Randers-Pehrson and David J. Brenner

Introduction

We are currently building a multiphoton microscope at the endstation of our single-cell, single-particle microbeam irradiator for a) detecting and observing the short-term molecular kinetics of radiation response in living cells, and b) allowing direct imaging of targets in thick biological materials, such as 3D tissue. A multiphoton microscope is an infrared laser-based, 3D, minimally-damaging imaging tool that, when compared to conventional confocal microscopy, has greater penetration depth and reduced phototoxicity and photobleaching in the sample bulk. The guiding principle of the multiphoton microscope is: when two photons are spatially and temporally coincident within the excitation cross-section of a fluorophore molecule, they can act as one photon with twice the energy to induce an electronic transition. Hence, multiphoton excitation occurs primarily at the laser focal point. Given their tunable infrared wavelength ranges and high power, ultrafast Titanium:Sapphire (Ti:S) lasers are favored for multiphoton excitation. The multiphoton microscope being constructed (see Fig. 1) incorporates a modified Nikon Eclipse E600-FN research fluorescence microscope and a high-precision stage. The base was physically removed from the microscope for use over a vertical ion beam. Upgrading to a true kinetic mount for the microscope, it is now mounted to a pivot arm with a spring-loaded ball-and-socket connection at the pivot point.

Laser

The excitation light source is a Chameleon (Coherent Inc.) tunable Titanium:Sapphire (Ti:S) laser that provides 140fs pulses at a 90 MHz repetition rate with a wavelength tuning range of 705-950nm. Specifications for this laser mention the $1/e^2$ beam diameter (1.2 ± 0.2mm) at the exit port and at the peak of the tuning curve, but omit mentioning beam divergence. It is important to have a full set of laser beam characterization data when designing an optics system, so in order to have a better grasp of our divergence, $1/e^2$ beam diameter measurements were made at about 25nm increments of wavelength along the 705-950nm tuning curve, at 12.5cm from the laser and at 3m from the laser. The further measurement was done by bending the beam 90 degrees and directing it across the room. In both cases the $1/e^2$ beam diameter was measured using a power meter, a digital camera and an adjustable iris. Images of the iris positions provided an aperture size through analysis by pixel ratios. The divergence curve looks similar to the power-tuning curve, as shown in Figure 2, implying that the divergence variation may be related to laser power.

The probable cause for the laser divergence variation is from Kerr lensing in the Ti:S crystal. The Kerr effect is part of the operating principle for the laser, where a higher-intensity, modelocked beam has a different lensing quality through the crystal. This allows for passive modelocking, which drives the laser from CW to pulsed operation. The Kerr effect is non-linear and it creates a gradient lens, which is dependent on the beam's intensity. With a power curve that varies across the laser's wavelength tuning range, the power variation combined with the Kerr effect can explain the variation in divergence that is similar to the laser power curve.

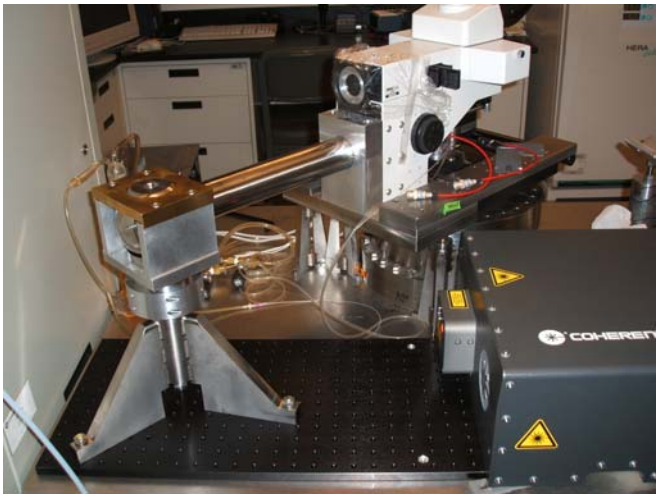

Fig. 1. Picture of the multiphoton microscopy system being assembled at RARAF. The components shown here are the tunable Chameleon Ti:S laser, the microscope mount, and the modified Nikon Eclipse E600-FN microscope, which is positioned above the vertical ion beam exit window.

Beam expander

The geometry of the infinity optics in the microscope provides guidance to establishing the diameter of the incident laser beam. Following specifications for a recommended objective (Nikon CFI LU Epi Plan Fluor 50X, 0.80N.A, 1.0mm WD ESD), the diameter of the back aperture, D, of the lens is found to be 6.4mm through the relationships: 1) $D = 2N.A. \times f_o$, where N.A. is the objective numerical aperture and f_o is the objective focal length, and 2) $M_o = f_t/f_o$, where M_o is the magnification of the objective and f_t is the tube lens focal length, 200mm. Additionally, a diffraction-limited spot is achievable for a microscope objective that has its back aperture filled with a planar wave; and with Gaussian beams, to approximate this condition it is common to overfill the back aperture by a factor of two of the $1/e^2$ beam diameter.[1] With this scenario, the $1/e^2$ laser beam diameter at the objective back aperture should be at

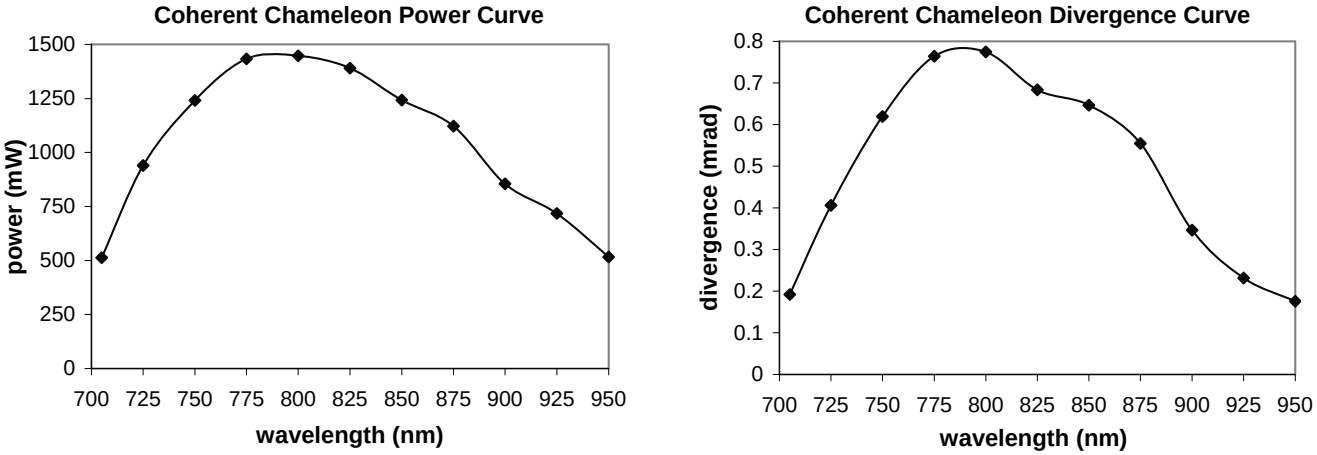

Fig. 2. Power (left panel) and divergence (right panel) measurements for the Chameleon (Coherent, Inc.) Ti:S laser. The divergence measurements were made by comparing $1/e^2$ beam diameters at 12.5cm and at 3m from the laser exit window. At 12.5cm from the exit port, $1/e^2$ beam diameters measured from 1.1mm to 1.4mm and increased linearly as a function of wavelength. At 3m from the exit port, the $1/e^2$ beam diameter was as large as 5.6mm at the peak of the power-tuning curve.

least 12.8mm.

Considering the variation in initial laser beam spot size and divergence, there is a corresponding distribution in the laser beam spot size at the objective back aperture. Optics transport shows that the minimum beam spot size at the objective back aperture is at a wavelength of 705nm, and the expansion requirement for that $1/e^2$ beam diameter is from 1.5mm to 12.8mm, or 8.4X. A beam expander designed for the smallest beam spot size will function for the rest of the laser output spectrum.

Power distribution

For all wavelengths, the truncated portion of the Gaussian laser beam that transmits through the objective back aperture has somewhat of a "top hat" profile. For wavelengths at the peak of the power-tuning curve, where there is greater divergence, a larger percentage of the beam profile is truncated. The power transmitted through a limiting aperture can be found by integrating the intensity distribution from 0 to r, and can be expressed by the following Gaussian beam optics formula, $P(r)=P_T[1-\exp(-2r^2/\omega_0^2)]$, where P_T is the total beam power, r is the radius of the aperture, and ω_0 is the Gaussian beam radius, where the intensity has decreased to $1/e^2$ of its peak value.[2] A plot of P(r) as a function of wavelength is shown in Figure 3. Compared to the large variation in total power across the tuning curve, the limiting aperture at the back of the objective effectively compresses the overall power-tuning curve.

Scanning mirrors

Pairs of mirrors are commonly used with scanning laser systems. The scanning head design for this multiphoton microscope involves a Model 6215H series galvanometer scanner from Cambridge Technology. The scanning head and its associated control electronics were delivered and have passed an initial test run. An assortment of static mirror optics are also on hand, and the multiphoton microscope construction is well underway.

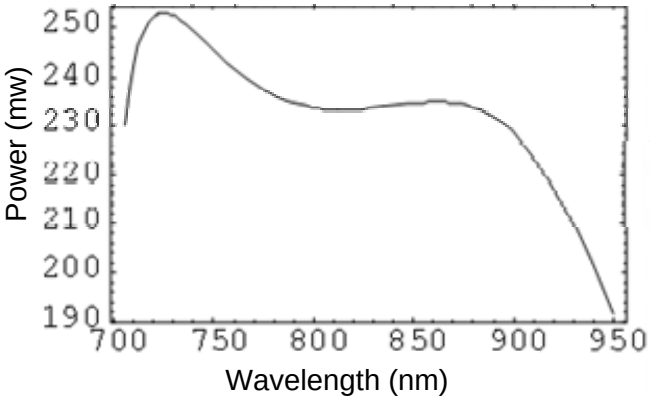

Fig. 3. Power curve for transmitted light through the microscope objective back aperture, as a function of wavelength.

References

1. Stelzer EKH. The intermediate optical system of laser-scanning confocal microscopes, Handbook of Biological Confocal Microscopy. ed Pawley JB (New York: Plenum) pp 141-7, 1995.
2. The Newport Catalog, Optics Technical Reference, p. 580, 2003. ■

Under-Dish Detector for the Microbeam at Columbia University

Guy Garty, Gregory J. Ross, Edmin Sung, Gerhard Randers-Pehrson and David J. Brenner

Introduction

Currently the RARAF microbeam irradiator delivers a precise number of particles by irradiating the sample and counting the particles traversing it, using a gas-based ionization chamber placed immediately above the cells. This method was found to be inadequate for the thicker samples (either tissue or medium-covered cells) now required by RARAF users, where the projectile particles are fully absorbed and do not reach the gas counter. To alleviate this problem we need to be able to detect the irradiating particles *before* they enter the sample.

The "Lumped Delay Line Detector" (LD^2) is a non-scattering device based on a capacitive pickup detector, typically used for detection of ion clusters or highly charged ions within ion traps. The LD^2 will enable single particle irradiation of thick samples by sub-micron beams. It will improve the attainable spot size, since it contains no material within the beam path and therefore does not induce scattering. It will also obviate the current need for removing the medium from cells pre-irradiation.

LD^2 structure

The LD^2 detector, shown in Figure 1, consists of a 1m long string of 300 cylindrical pickup electrodes. Each projectile particle passing through a pickup electrode induces a mirror charge, identical in magnitude and opposite in polarity to its own, on the inside of the pickup electrode. The pickup electrodes are connected by surface mount inductors and capacitively coupled to ground, forming a lumped delay line with a time constant that can be matched to the velocity of the projectile. Thus, the signals from all pickup electrodes add in phase, generating a detectable signal.

Tuning the LD^2 time constant is done, as shown in Figure 1, by pivoting a grounded electrode around the pickup electrodes, thus changing their capacitance to ground and hence the delay line time constant.

Results

Two short LD^2 prototypes, containing 47 and 49 electrodes have been built, using Rexolite and Macor respectively as a dielectric and using 100nH inductors. Figure 2 demonstrates the pulse propagation velocity obtained by measuring the time delay between a pulse injected on the first electrode and measured on subsequent electrodes in the open and closed configurations.

We have seen that both prototypes have roughly the same ratio of pulse propagation velocity in the open and closed configurations (1.4 for the Rexolite and 1.45 for the

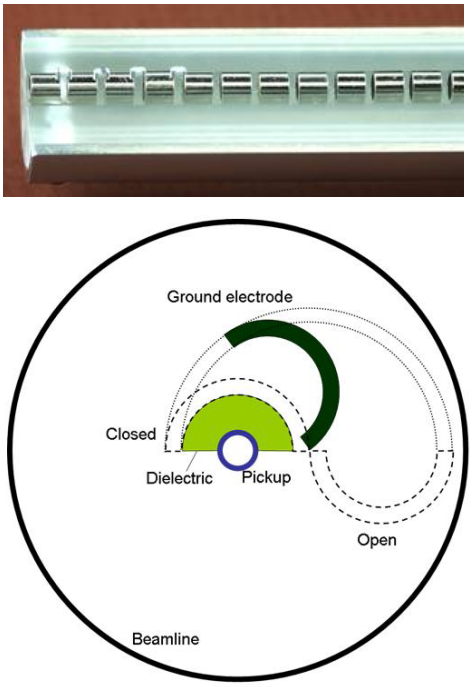

Fig. 1. Top. A close-up photo of the LD^2 prototype. **Bottom**. A sketch of the tuning mechanism. A grounded electrode is pivoted between the closed position (high capacitance) and the open position (low capacitance).

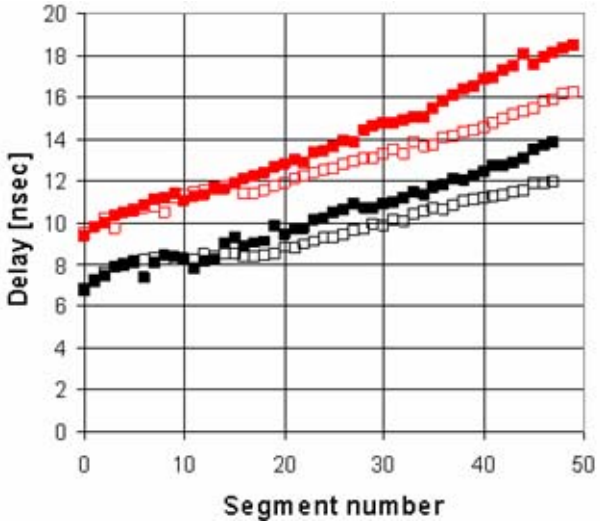

Fig. 2. The measured pulse propagation times. The black symbols are the Rexolite prototype. The red symbols are the Macor prototype. The open and closed symbols correspond to the open and closed configurations respectively.

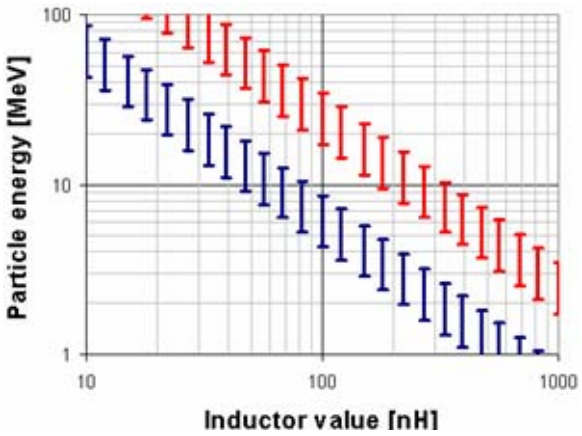

Fig. 3. The range of particle energies the LD^2 can be matched to using commercially available inductors and a rexolite dielectric. The blue ranges are for protons and the red ones are for Helium ions.

Macor) and so we decided to make the full length LD^2 out of Rexolite, to simplify production efforts.

Based on the obtained pulse propagation velocity, we have selected 330nH inductors for the full length LD^2 (currently under construction) providing velocity matching to protons of 1.3 to 2.6 MeV and Helium ions of 5.2 to 10.4 MeV. We expect the LD^2 to be primarily used for 6 MeV He ions. Figure 3 shows the particle energy ranges accessible using different inductor values. ■

7th International Workshop: Microbeam Probes of Cellular Radiation Response, held on March 15-17, 2006 at Columbia University in New York City.

Columbia University, Medical Center, Low Dose Radiation Workshop Meeting, held on April 2-4, 2006. This meeting was organized by Professor Tom K. Hei and Professor Ohtsura Niwa from Kyoto University, Japan.

A Microbeam Study of DNA Double Strand Breaks In Bystander Primary Human Fibroblasts

Lubomir B. Smilenov, Eric J. Hall, William M. Bonner[a] and Olga A. Sedelnikova[a]

Introduction

Bystander cells exhibit a variety of characteristics of IR-induced genomic instability. Recently DNA double-strand breaks (DSBs) have been shown to be involved in the bystander response.[1-3] Using the γ-H2AX focus formation assay as an indicator of DNA DSBs, the authors have shown an increase in γ-H2AX focal incidence in bystander cell populations cultured in media conditioned on gamma irradiated cells or cocultured with microbeam or gamma-irradiated cells. In alpha particle IR experiments we showed[1] that γ-H2AX focus formation in directly irradiated cells exhibited the expected early and linear dose-dependent γ-H2AX focus formation and most of the foci have been repaired by 18h post-IR. In contrast, an increase in γ-H2AX focal incidence has been detected in bystander cells at that time point. The DSB nature of γ-H2AX foci has been confirmed by their colocalization with DNA DSB-repair proteins. In this report we show that DNA DSB incidence in bystander cells lacks a linear dose response. This may indicate that in a specific range, neither the dose nor the proportion of irradiated cells in a population defines the magnitude of the bystander effect.

[a] *Laboratory of Molecular Pharmacology, Center for Cancer Research, National Cancer Institute, NIH, Bethesda, MD.*

Results and discussion

The existence of bystander effects after low dose IR is well documented, but the factors and mechanisms involved

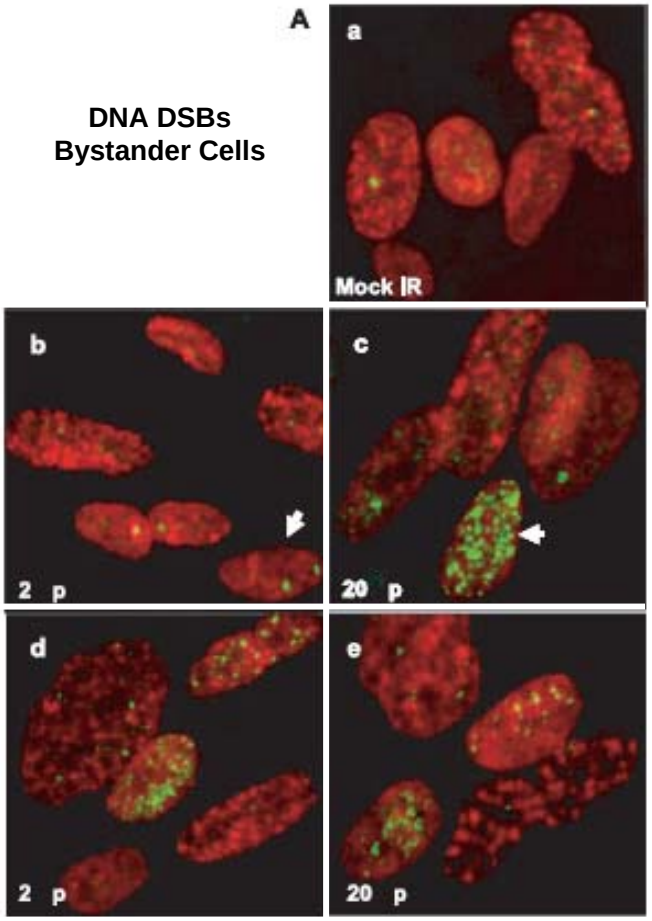

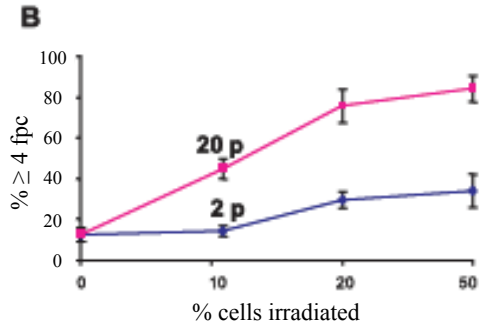

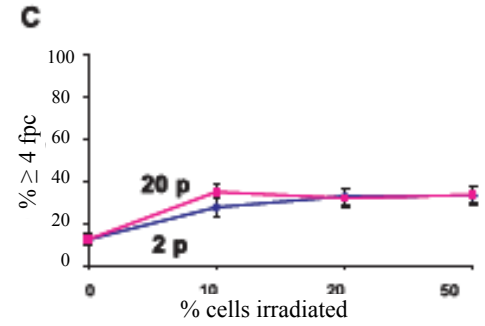

Fig. 1. Presence of γ-H2AX foci at different times post-IR. 10%, 20% or 50% of WI38 cells were selected randomly and irradiated with 2 or 20 alpha particles per cell. The bystander effect was evident at 18h post-IR. **A.** Images of representational fields (experiment with 10% cells irradiated). Nuclei were counterstained with propidium iodide. (a) Non irradiated control cells. (b) Two or (c) twenty alpha particle-irradiated cell populations 30 min post-IR. Arrows mark cells which were irradiated and visually distinct from the majority of the cell populations. (d) Two or (e) twenty alpha particle-irradiated cell populations 18h post-IR. **B.** Focal incidences 30 min post-IR in cell populations irradiated with 2 or 20 alpha particles. **C.** Focal incidences 18h post-IR in cells irradiated with 2 or 20 alpha particles. The numbers of foci at 18h post-IR was similar regardless of the dose of IR or proportion of irradiated cells and persisted for several days.

are still obscure. Most of the evidence supporting the bystander effect phenomena is based on directly measured endpoints or partial molecular analysis of radiation response pathways in the bystander cells. These evidences show that several aspects of the induced response in the bystander cells are similar to the ones in directly hit cells. An important question is whether the pathways activated in the bystander cells recapitulate the pathways activated in directly hit cells, or different mechanism are involved. Another important question is how to quantify the intensity or the time-dependence of bystander effects. Since the γ-H2AX focus formation assay is highly quantitative, we attempted to use it as a tool for bystander effect characterization. Our results show that DNA DSBs are induced in the bystander cells, indicating that this aspect of the overall response is similar to that in directly hit cells. However, the kinetics of the DSB induction in directly hit and bystander cells show different patterns. In the directly hit cells, DSBs appear almost immediately, reaching their maximum at 10–30 min post-IR and mostly disappear by 18h, while in contrast, in the bystander cells DSBs are detected substantially later and persist substantially longer than in the hit cells. The number of DNA DSBs in bystander cells didn't correspond to the dose, indicating that bystander effect factors most probably do not act directly on DNA as radiation does, but rather their effect is induced and filtered through intermediate steps.

The induction of DSBs in bystander cells is a surprising result especially knowing how tightly cells maintain DNA integrity. Mutation frequency of human cells is very low and is in the range of 1–2 mutant genes per cell per individual life time.[4] On the other hand, the induced mutation frequencies by different factors can be considerably higher. A normal cell encounters almost 200,000 DNA mutations daily induced by reactive oxygen species and DNA depurination.[5] Usually these mutations are promptly repaired by DNA repair mechanisms. Assuming that the directly hit cells secrete factors inducing stress in the neighbouring cells, one conclusion might be that the stress response makes DNA repair pathways less efficient in the bystander cells leading to higher rates of mutation accumulation and to the formation of DSBs.

Conclusion

The appearance of DNA DSBs in bystander cells confirms that the effects of ionizing radiation are intense, complex and difficult to measure, and that the effects of radiation at low doses cannot be extrapolated from high-dose effects.

References

1. Sokolov MV, Smilenov LB, Hall EJ, Panyutin IG, Bonner WM and Sedelnikova OA. Ionizing radiation induces DNA double-strand breaks in bystander primary human fibroblasts. *Oncogene* **24**:7257–65, 2005.
2. Hu B, Wu L, Han W, Zhang L, Chen S, Xu A, Hei T and Yu Z. The time and spatial effects of bystander response in mammalian cells induced by low dose radiation. *Carcinogenesis* **27**:245–51, 2006.
3. Hu B, Han W, Wu L, Feng H, Liu X, Zhang L, Chen S, Xu A, Hei T and Yu Z. In situ visualization of DSBs to assess the extranuclear/ extracellular effects induced by low-dose alpha-particle irradiation. *Radiat. Res* **164**: 286–91, 2005.
4. Nakamura J and Swenberg JA. Endogenous apurinic/apyrimidinic sites in genomic DNA of mammalian tissues. *Cancer Res* **59**:2522-6, 1999.
5. Cervantes RB, Stringer JR, Shao C, Tischfield JA and Stambrook PJ. Embryonic stem cells and somatic cells differ in mutation frequency and type. *Proc. Natl Acad. Sci. USA* **99**:3586–90, 2002. ■

Further Studies of a Low LET Radiation-Induced Bystander Effect in a 3D Cell Cluster Model

Rudranath Persaud, Honging Zhou, Sarah E. Baker, Tom K. Hei and Eric J. Hall

This study involved a three-dimensional cell culture model composed of a mixture of human-hamster hybrid (A_L) and Chinese hamster ovary (CHO) cells. The CHO cells were labeled with tritiated thymidine and mixed with A_L cells before being centrifuged briefly to produce a "cluster" of 4×10^6 cells, as illustrated in Figure 1.

Clusters were incubated overnight, resuspended into single cell suspensions, and passed twice through MACS separation columns to produce two independent cell populations. The A_L fraction was plated for a 7-day expression period and subsequently subjected to the CD59 Antibody-Complement Cell Lysis Mutation Assay. These cells never incorporated the radioactive material, but were in close contact with cells that did. They constitute, therefore, a bystander population.

In last year's report we showed a significant incidence of mutations in the Bystander A_L cells, when the CHO cells had been incubated with 100μCi of tritiated thymidine. In the past year we have repeated the experiments with doses of tritiated thymidine two orders of magnitude lower, namely 0.5μCi. These data are shown in Figure 2.

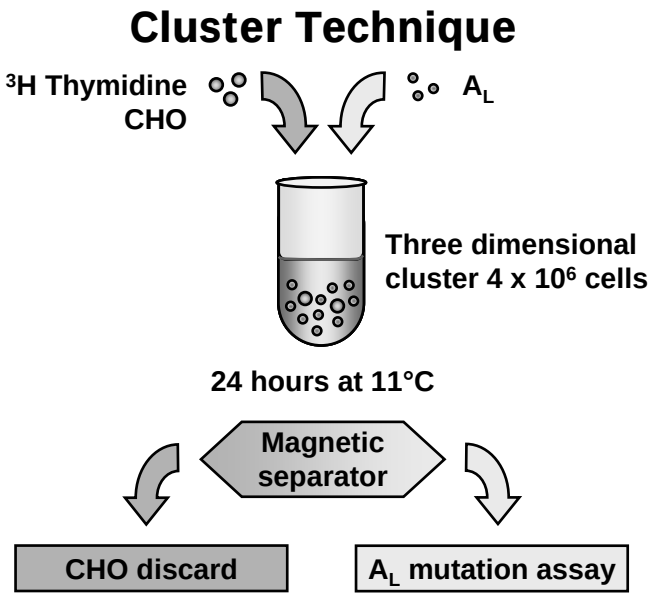

Fig. 1. CHO cells incorporating tritiated thymidine are mixed with A_L cells and centrifuged to form a three-dimensional cluster. Following overnight incubation, the two cell types are separated. The fraction of AL cells showing a mutation is assessed using a standard assay.

There is no easy way to estimate the actual absorbed doses involved since it is difficult to determine the amount of tritiated thymidine involved, and the uptake is likely to be non-uniform. Judging by the fraction of cells surviving the three levels of tritiated thymidine (Fig. 2), and previously published survival data for x-rays, the effective x-ray doses for 0.5, 1.0, and 5.0μCi of tridiated thymide are 0.2, 0.75 and 1.0Gy respectively.

In addition, multiplex PCR was used to determine the types of mutations produced in the bystander cells. Individual clones were isolated and analyzed for five markers on human chromosome 11. Over 100 mutants were analyzed including 22 of spontaneous origin. As shown in Figure 3, mutations in bystander cells involved large deletions more frequently than in mutations of spontaneous origin. ■

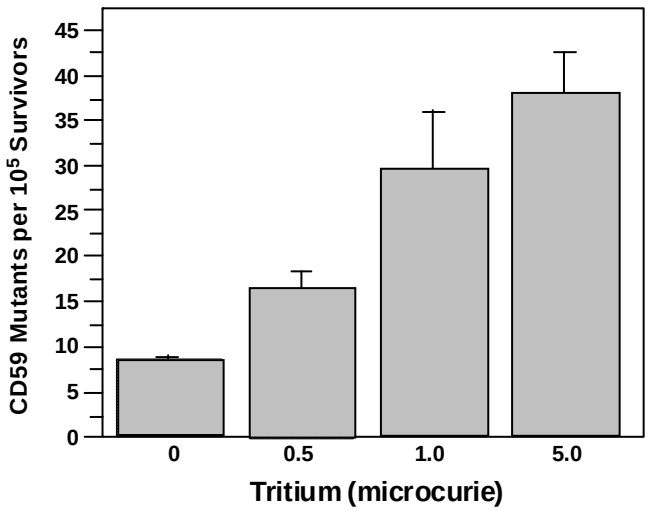

Fig. 2. Incidence of bystander CD59$^-$ mutants among A_L cells clustered with CHO cells that were either labeled with 0, 0.5, 1.0 or 5.0μCi ^{3}HdTTP. Data represent mean ± S.D. of four experiments.

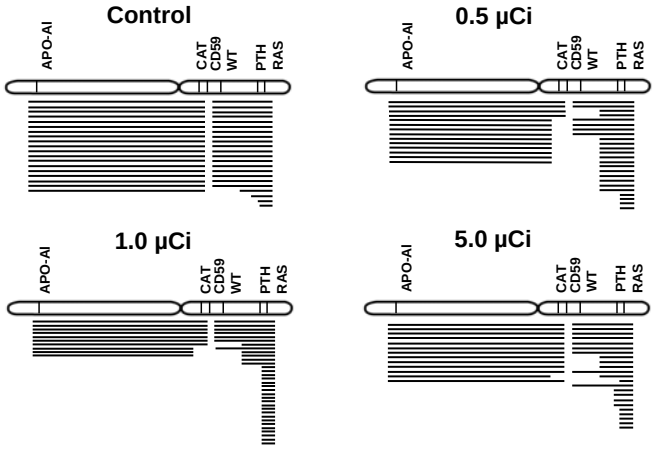

Fig. 3. Mutant spectrum of bystander CD59$^-$ mutants among A_L cells clustered with CHO cells that were labeled with 0, 0.5, 1.0 or 5.0μCi ^{3}HdTTP. Note that the radiation-induced mutants consist principally of large deletions compared with spontaneous mutations which are mostly small deletions.

The Function of DNA-PKcs in the Radiation-Induced Bystander Effect

Hongning Zhou, Muria Sutton, Joseph A. Gillispie, Guillermo Taccioli and Tom K. Hei

Considerable evidence is now emerging that targeted nuclei may not always be required in mediating the genotoxic effects of radiation. Non-irradiated bystander cells have been shown to present similar cytotoxic and genotoxic responses to those detected in directly irradiated cells. This is known as the bystander effect. There is evidence that gap junction mediated cell-cell communication plays a critical role in the bystander response, and that secretion of cytokines or other growth promoting factors by irradiated cells has been suggested to modulate the bystander response.

However, the precise mechanism of the bystander effect is not clear. It is likely that multiple signaling pathways are required to mediate the bystander response in either confluent or sparsely populated cultures.[1-5]

One of the most damaging lesions that can occur in a cell is a DNA double-strand break (DSB). The major pathway in mammalian cells dedicated to the repair of DSBs is by the non-homologous end-joining machinery (NHEJ). Among the six components that play a role in NHEJ, the DNA-PK catalytic subunit (DNA-PKcs) complex, constituted by Ku heterodimer and DNA-PKcs, is fundamental in the first steps of the process. Mutant cells deficient in one of the DNA-PK complex components are defective in DSB repair and in V (D) J recombination and are hypersensitive to DSB inducing agents such as radiation and many carcinogenic chemicals.[6,7]

In the present study, a DNA-PKcs deficient hamster cell line (V3) and its parental cell line (AA8) were used to study the function of DNA-PKcs in radiation-induced the bystander effect. To approach this goal, newly designed strip dishes were used in the experiments. Briefly, the bottom of the well-fit outer and inner stainless rings was covered with 6μm and 38μm thick mylar sheets, respectively. The mylar of the inner rings was cut as strips. Exponentially growing AA8 and V3 cells were plated in specially designed mylar dishes and cultured for several days to ensure confluency upon subsequent irradiation with alpha particles. Cells were incubated in the mylar dishes overnight before experiments for survival and mutagenesis were conducted. To further explore the radiation induced bystander effect in different cell lines, the charged particle microbeam was employed to lethally irradiate one type of cells in the confluent population, and the other remaining cell line was incubated for further experiments.

The AA8 and V3 cells showed similar growth kinetics as demonstrated by growth curve analysis. However, V3 cells were more sensitive to the cell killing effect of gamma-ray irradiation. 2Gy gamma ray irradiation could reduce the surviving fraction of V3 cells to only 15%, compared with 80% in AA8 cells. There is a dose response in $HGPRT^-$ mutation with increasing gamma ray doses. However, with further increase in the dose of gamma rays, the $HGPRT^-$ mutation frequency decreased, likely due to the significant cell killing effect.

Using specially designed strip dishes, we found that 0.5Gy alpha particle irradiation could induce 3.3 times mutant yield in AA8 bystander cells, compared with the spontaneous background mutation frequency. However, the same radiation can only cause a 2.0 times increase in bystander mutagenesis. To further identify the role of DNA-PKcs in the radiation-induced bystander effect, we transfected V3 cells with a YAC containing human DNA-PKcs (V3 147f), and repeated the experiments using the same conditions. We found in the non-irradiated bystander V3 147f cells, the mutation frequency is 3.8 times higher than the spontaneous background (Fig. 1). These results indicated DNA-PKcs plays some role in radiation induced bystander effects.

To understand the possible mechanisms of the role of DNA-PKcs in radiation-induced bystander effects, we tried

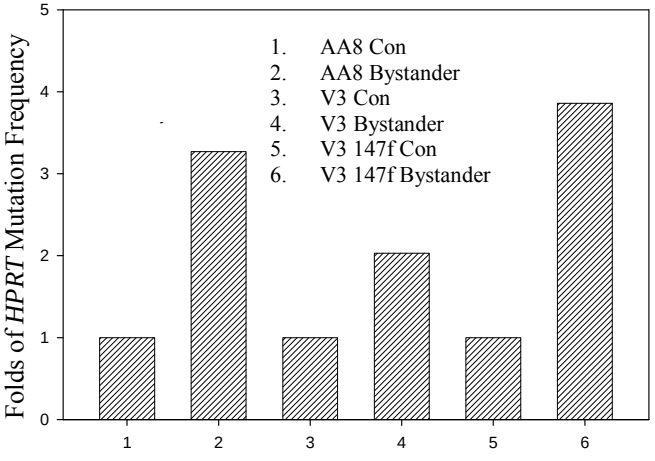

Fig. 1. Alpha particle irradiation induced HGPRT-mutation in non-irradiated bystander DNA-PKcs deficient V3 cells, and the parental AA8 cells.

to identify if there is any problem in delivering or receiving bystander signals in DNA-PKcs deficient V3 cells. Using microbeam irradiation, we found that when 10% of AA8 cells of the population get lethally irradiated, the $HGPRT^-$ mutation frequency was about 4 times higher than the spontaneous yield. However, when 10% of V3 cells in the mixed population (90% AA8 and 10% V3) were irradiated, there was only a limited bystander mutagenesis response in AA8 cells when compared with irradiated AA8 cells (Fig. 2). A similar result was found when 10% of AA8 cells in the mixed population (10% AA8 and 90% V3) were irradiated; there was only a limited bystander mutagenesis response in V3 cells when AA8 cells were lethally irradiated. These data give some clue about the function of DNA-PKcs in the radiation induced bystander effect, and indicate that DNA-PKcs deficiency may cause some problems in either delivering or receiving the bystander signals. Further experiments are needed to determine the possible signaling transduction pathways involved with DNA-PKcs in the radiation induced bystander response.

References

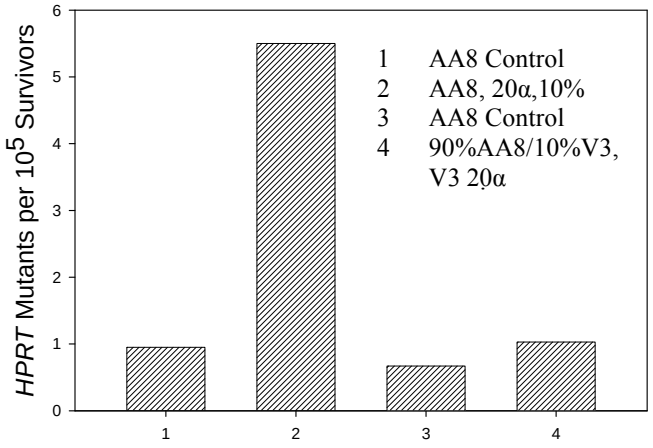

Fig. 2. Response of AA8 cells when 10% of AA8 or V3 cells were traversed by 20 alpha particles through their nuclei.

1. Nagasawa H and Little JB. Induction of sister chromatid exchanges by extremely low doses of alpha-particles. *Cancer Res* **52**:6394-6, 1992.
2. Morgan WF. Non-targeted and delayed effects of exposure to ionizing radiation: I. Radiation-induced genomic instability and bystander effects in vitro. *Radiat Res* **159**:567-80, 2003.
3. Little JB. Genomic instability and bystander effects: a historical perspective. *Oncogene* **22**:6978-87, 2003.
4. Hei TK, Persaud R, Zhou H and Suzuki M. Genotoxicity in the eyes of bystander cells. *Mutat Res* **568**:111-20, 2004.
5. Mothersill C and Seymour CB. Radiation-induced bystander effects--implications for cancer. *Nat Rev Cancer* **4**:158-64, 2004.
6. Rothkamm K, Kruger I, Thompson LH and Lobrich M. Pathways of DNA double-strand break repair during the mammalian cell cycle. *Mol Cell Biol* **23**:5706-15, 2003.
7. Lucero H, Gae D and Taccioli GE. Novel localization of the DNA-PK complex in lipid rafts: a putative role in the signal transduction pathway of the ionizing radiation response. *J Biol Chem* **278**:22136-43, 2003. ■

The Mechanism of Radiation Induced Bystander Effects: Implication from Mitochondrial Function Studies

Hongning Zhou, Vladimir Ivanov, Yu-Chin Lien, Mercy Davidson and Tom K. Hei

The radiation-induced bystander effect is defined as the induction of biological effects in cells that are not directly traversed by a charged particle, but are in close proximity to cells that are, or have received signals from these irradiated cells. There is evidence that very low doses of α-particles induced clastogenic responses (principally sister chromatid exchanges) in both Chinese hamster ovary (CHO) and human fibroblast cultures at levels significantly higher than expected based on the number of cellular nuclei that had been traversed by a particle. In CHO cells irradiated with low doses of alpha particles where less than 1% of the nuclei were estimated to have been traversed by a particle, an increase in sister chromatid exchanges was observed in over 30% of the cells.[1] In other words, either cytoplasmic damages or signals received from an extracellular component may have modulated the observed genotoxic response. While circumstantial evidence in support of a bystander effect appears to be consistent, direct proof of such extranuclear and extracellular effects are most convincingly demonstrated using charged particle microbeams.

Although the bystander effects have been well described over the past decade, the mechanisms of the process remain unclear. In sub-confluent cultures, there is evidence that reactive oxygen species (ROS), nitric oxide, and cytokines such as TGFβ are involved in mediating the process. On the other hand, gap junction-mediated cell-cell communications have been shown to be critical in mediating bystander effects in confluent cultures of either human or rodent cells. It is likely that a combination of pathways involving both primary and secondary signaling processes is involved in producing a bystander process. However, the precise mechanism of the bystander effect is still unclear.[2-5]

To better understand the mechanisms of the radiation-induced bystander effect, the signal transduction pathways related to mitochondrial function were investigated using the Columbia University charged particle microbeam.

Exponentially growing mitochondrial deficient human skin fibroblast (rho^0) and the parental cell line (rho^+) were plated in specially designed strip mylar dishes and irradiated with alpha particles upon confluency. After irradiation, cells were incubated in the mylar dishes overnight before being processed for survival, mutagenesis, and signal pathway studies. To further explore the role of mitochondria in the radiation-induced bystander effect, a microbeam was used to lethally irradiate either rho^0 or rho^+ cells in a mixed, confluent culture and the bystander response was determined in the non-irradiated fraction.

Using specially designed strip dishes, it was found that in rho^+ bystander cells, 0.5Gy alpha particle irradiation could increase the HPRT-mutant yield 2.1 times higher than the spontaneous background level. However, under similar irradiation conditions, rho^0 cells had a bystander mutant fraction that was 4-fold higher than non-irradiated rho^0 cells. Furthermore, a nitric oxide scavenger can significantly decrease the bystander mutagenesis in both cell lines. The observation that rho^0 HSF showed a higher bystander mutagenic response in confluent monolayers was similarly demonstrated using a microbeam when a fraction of the same population was irradiated with lethal doses (Fig. 1). In contrast, using mixed cultures of rho^0 and rho^+ cells and targeting only one population of cells with a lethal dose of alpha particles, decreased bystander mutagenesis was uniformly found in non-irradiated bystander cells, in contrast to data obtained using similar cell types (Fig. 1). These results indicated that mitochondrial deficient cells have deficiencies either in delivering or receiving the bystander signals and that the bystander signals are dependent on mitochondrial function in the human fibroblast model.

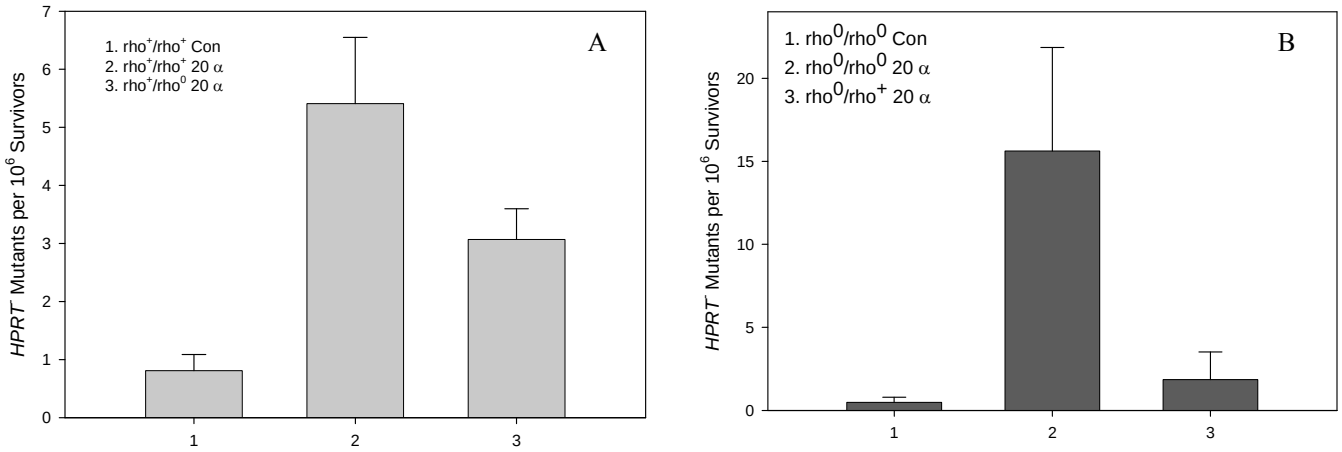

Fig. 1. *HGPRT* mutation of bystander cells in the mixing cultures using Columbia microbeam irradiation. **A.** rho$^+$ cells used as the bystander cells when rho$^+$ or rho^0 cells were irradiated with 20 alpha particles. **B.** rho^0 cells used as the bystander cells when rho^0 or rho$^+$ cells were irradiated with 20 alpha particles.

References

1. Nagasawa H and Little JB. Induction of sister chromatid exchanges by extremely low doses of alpha-particles. *Cancer Res* **52**:6394-6, 1992.
2. Morgan WF. Non-targeted and delayed effects of exposure to ionizing radiation: I. Radiation-induced genomic instability and bystander effects in vitro. *Radiat Res* **159**:567-80, 2003.
3. Little JB. Genomic instability and bystander effects: a historical perspective. *Oncogene* **22**:6978-87, 2003.
4. Hei TK, Persaud R, Zhou H and Suzuki M. Genotoxicity in the eyes of bystander cells. *Mutat Res* **568**:111-20, 2004.
5. Mothersill C and Seymour CB. Radiation-induced bystander effects--implications for cancer. *Nat Rev Cancer* **4**:158-64, 2004. ■

Human Endothelial Cells in 2D and 3D Systems: Effects of Space Related Radiations

Peter Grabham, Burong Hu, Gloria Jenkins and Charles R. Geard

The ionizing radiations to which humans are likely to be exposed in a space environment are rarely encountered in an earth environment. These consist of low LET (linear energy transfer) protons and high LET iron (Fe) ions. Little is known about the effects of space radiation on endothelial cells. This study is aimed at understanding the effects of space radiation on endothelial cells using 2D and 3D culture systems of human umbilical vein endothelial cells (HUVEC). Monolayers are being used to investigate the effects of these radiations on chromosome damage and would thus be of importance to mitotic endothelial stem cells. Since atomic bomb survivors show non-cancer disease mortality including vascular diseases,[1] a 3D tissue model is being used to determine the effects of space radiation on blood vessel formation and maintenance.

Chromosome damage and aberrations

To date both high LET Fe ions and low LET protons, in addition to gamma radiation, have been observed to cause chromosome damage in HUVECs. The G2 phase premature chromosome condensation assay (G2-PCC) 2 hours after Fe irradiation at the NASA Space Research laboratory (Brookhaven) revealed chromosome breaks in and gaps at doses from 0.1Gy to 1Gy. mFISH analysis is being used to identify chromosome aberrations. In response to 0.8Gy Fe ions, endothelial cells showed a large number of chromosome aberrations (94% of cells) involving chromosomes 1, 2, 4, 5, 7, 9 and X. These include stable aberrations such as reciprocal translocations (Fig. 1).

The use of a 3D model of vessel cultures

To date, studies on the effects of irradiation on endothelial cells *in vitro* have been in 2D monolayers. HUVEC cells in such cultures, however, are very different from those cultured in a 3D tissue culture model. When the cells are exposed to growth factors such as VEGF and FGF and embedded in collagen gels they fully differentiate and assemble into capillary tubes. The cytoskeleton changes

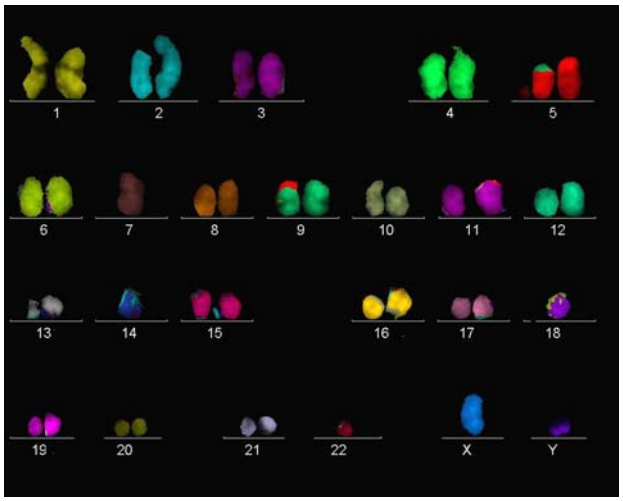

Fig. 1. mFISH karyotype of a cell exposed to 80cGy Fe ions (1GeV). Cells were exposed to Fe ion radiation and then allowed to recover for 36h before the use of G2-PCC and mFISH. This cell shows a reciprocal translocation between chromosomes 5 and 9.

dramatically, and most importantly, the cells express a different profile of genes.[2] Using gene array analysis, differential display and cDNA library screening, hundreds of differentially expressed genes were identified. Thus, these differentiated cultures represent a model far more relevant to cells *in vivo* than 2D cultures. Human umbilical vein endothelial cells (HUVEC) have been successfully cultured in 3D matrices using an adaptation of the protocol described by Davis and Camarillo.[3] Cells are cultured in additional matrix proteins contained in matrigel. This gives a more robust vessel formation and a theoretically more physiologically relevant matrix.

Human umbilical vein endothelial cells (HUVEC) were fluorescently labeled with a long-lived cytotracker, then suspended in collagen gels and stimulated to differentiate and form vessels. Live 3D imaging of cells showed distinct stages of development, starting with the formation of vacuoles, followed by cell elongation and cellular coalescence leading to the formation of capillary tube-like structures resembling vessels (Fig. 2).

Effects of space radiation on vessel formation

HUVECs are irradiated in 2D cultures before suspension in gel (inhibition before differentiation), 1-2 days after suspension in gel (inhibition of vessel formation), and after full development of vessels (maintenance of vessels). The effects of gamma irradiation have been studied widely in radiotherapy patients. Gamma irradiation stimulates vessel

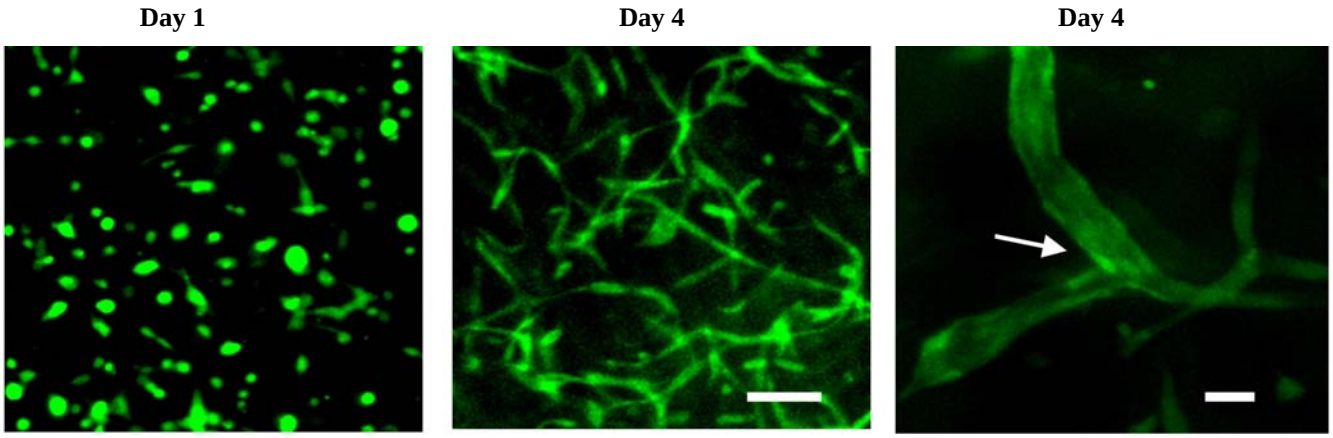

Fig. 2. Left two panels. Confocal images of 20 planes through a 200-micron section of matrix, which have been projected onto a single plane. One day after suspension in collagen/matrigel matrices, cells begin to elongate and continue to elongate through day 4 by which time the cells have formed long structures. Bar = 200μm. **Right panel.** Higher magnification microscopy of 5-micron slices projected onto a single plane reveals that tubular structures contain lumens and often branch (arrow). Bar = 30μm.

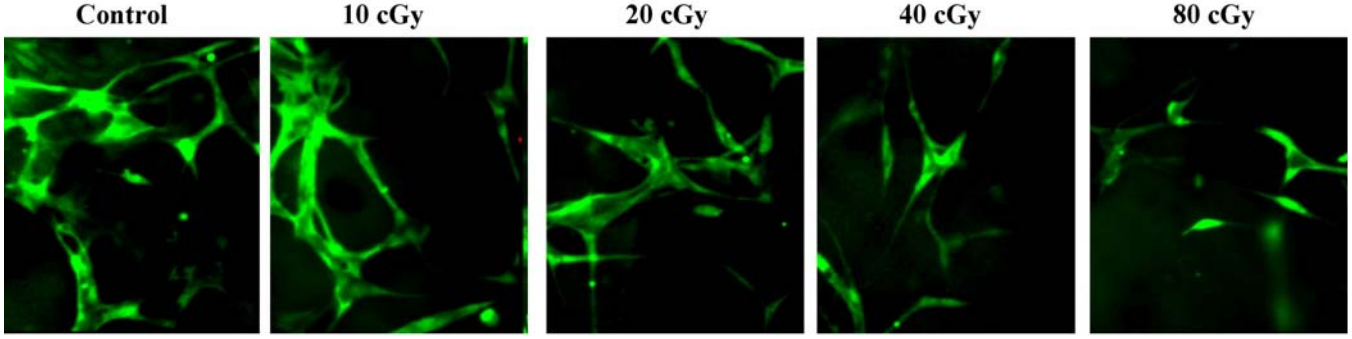

Fig. 3. Effect of Fe ion irradiation on vessel formation. HUVECs were irradiated with various doses of Fe ions, allowed to recover for 72 hours then plated into collagen matrix gels. Live vessels were observed 4 days later. Each panel represents 10 frames (10 microns thick) projected onto a single frame. Up to 20 cGy, vessels formed with characteristic lumens. At doses of 20 cGy or higher the cells elongate but fail to join together and form lumens.

formation via its ability to stimulate secretion of VEGF. High LET Fe ions, however, caused a significant decrease in vessel formation at a dose of 0.2Gy (Fig. 3). In our assay gamma rays did not induce vessel formation up to 0.8Gy. Interestingly, this was also true for protons (1GeV). Continuing studies are investigating this apparent difference in response according to LET.

Apoptosis in vessels

We have developed a technique whereby mature vessels in gels can be fixed and labeled by immunocytochemistry much the same as monolyers (Fig. 4). This will be used to investigate certain apoptosis markers, e.g., Cytochrome C to determine the effect of space radiation on apoptosis in mature vessels.

References

1. Preston DL, Shimizu Y, Pierce DA, Suyama A and Mabuchi K. Studies of mortality of atomic bomb survivors. Report 13: Solid cancer and noncancer disease mortality: 1950-1997. *Radiat Res* **160**:381-407, 2003.
2. Bell SE, Mavila A, Salazar R, Bayless KJ, Kanagala S, Maxwell SA and Davis G. Differential gene expression during capillary morphogenesis in 3D collagen matrices: regulated expression of genes genes involved in basement membrane matrix assembly, cell cycle progression, cellular differentiation and G-protein signaling. *J. Cell Sci.* **114**: 2755-73, 2001.
3. Davis GE and Camarillo CW. An a2b1 integrin-dependent pinocytic mechanism involving intracellular vacuole formation and coalescence regulates capillary lumen and tube formationin three dimensional collagen matrix. *J. Cell Sci.* **114**: 917-30, 1996. ■

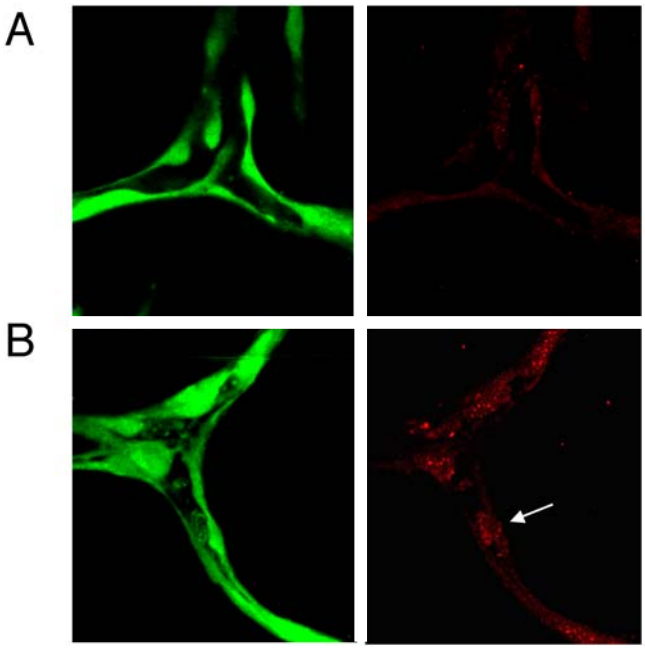

Fig. 4. H2AX phosphorylation in HUVEC vessels. Cells were stained with cell tracker (green, left panels) and immunostained for phosphorylated H2AX (red, right panels). **A.** Nuclei in unirradiated control showed few foci. **B.** Irradiated cells contained a number of foci comparable to those in monolayers (arrow).

Delayed Genomic Instability in Bystander Cells

Burong Hu, Peter Grabham, Adayabalam Balajee, Brian Ponnaiya, Stephen Marino, Gloria Jenkins-Baker and Charles R. Geard

Radiation-induced bystander effects pose a challenge to the assessment of radiation risk and the understanding of basic mechanisms of radiation action.[1-3] There is considerable evidence that exposure to ionizing radiation may induce a heritable, genomic instability that leads to a persisting increased frequency of genetic and functional changes in the progeny of irradiated cells. These may be considered to be a driving force behind carcinogenic change.[4-6] Over the past decade studies on non-irradiated bystander cells have shown effects on chromosome damage, for example, mutation, micronuclei and clonal survival.[7,8] Although there is indication that genomic instability may occur in the progeny of bystander cells,[3-6] more evidence is needed to establish this phenomenon.

In this study, we examine heritable genomic instability in the progeny of bystander cells. Two novel protocols were used to ensure pure populations of bystander cells and their progeny. 1) Normal human fibroblast cells cultured in double sided mylar dishes were irradiated on one side with random short penetrability 3Gy alpha-particles (track segment). Cells on the opposite side are bystander cells which could only be influenced by signal transfer through the medium. 2) 20% of cell nuclei of near-confluent fibroblasts were irradiated with 30 alpha-particles each using the Columbia University microbeam facility. This high dose ensures that only contacting but non-hit bystander cells can survive over many cell generations. In both scenarios cells were harvested at specific time points post-irradiation. The G_2 phase premature chromosome condensation assay (G_2-PCC) shows, that in both irradiation protocols, there was a higher level of chromosomal damage in the bystander cell population compared with the corresponding control. Moreover, there are significant differences in induced chromatid breaks a few days after track segment (by 5 days)

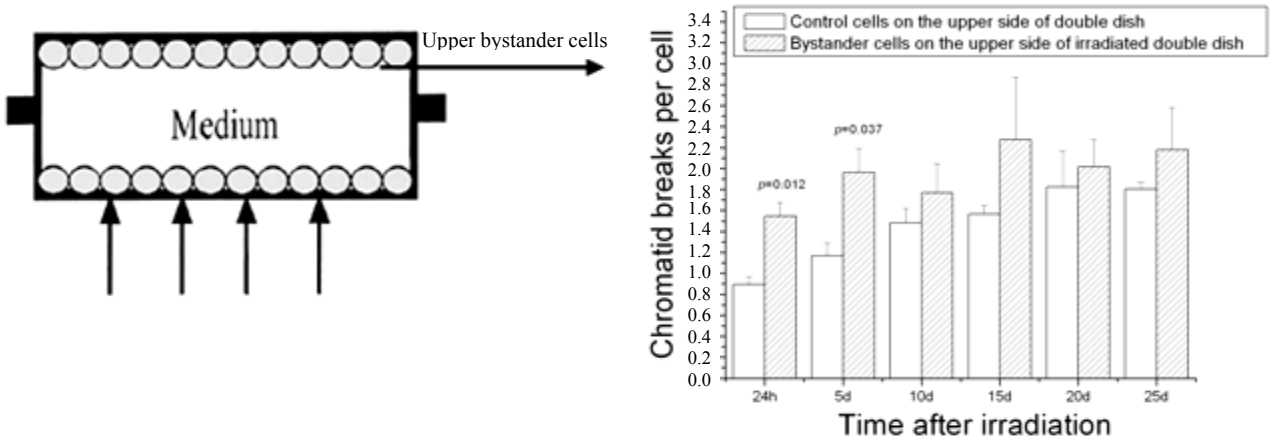

Fig. 1. Induced chromatid breaks per cell as a function of time after the bottom cells of the double dish were exposed to 3Gy alpha particles (track segment irradiation) and their parallel controls. Data are pooled from 3 independent experiments. Error bars represent ±SE.

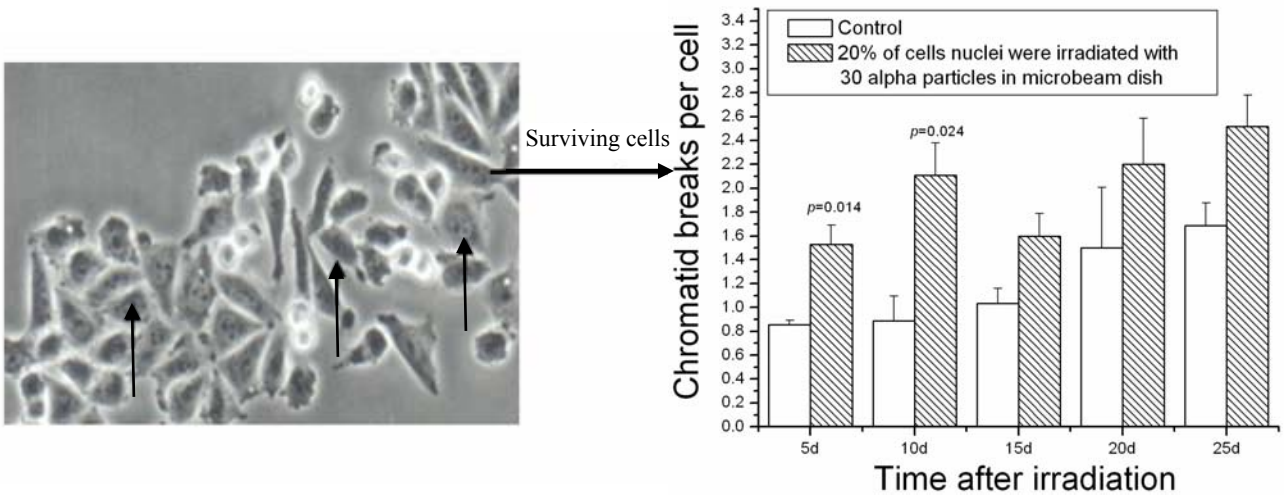

Fig. 2. Induced chromatid breaks per cell as a function of time after 20% of cell nuclei were irradiated with 30 alpha particles (microbeam irradiation) each and their parallel controls. Data are pooled from 3 independent experiments. Error bars represent ±SE.

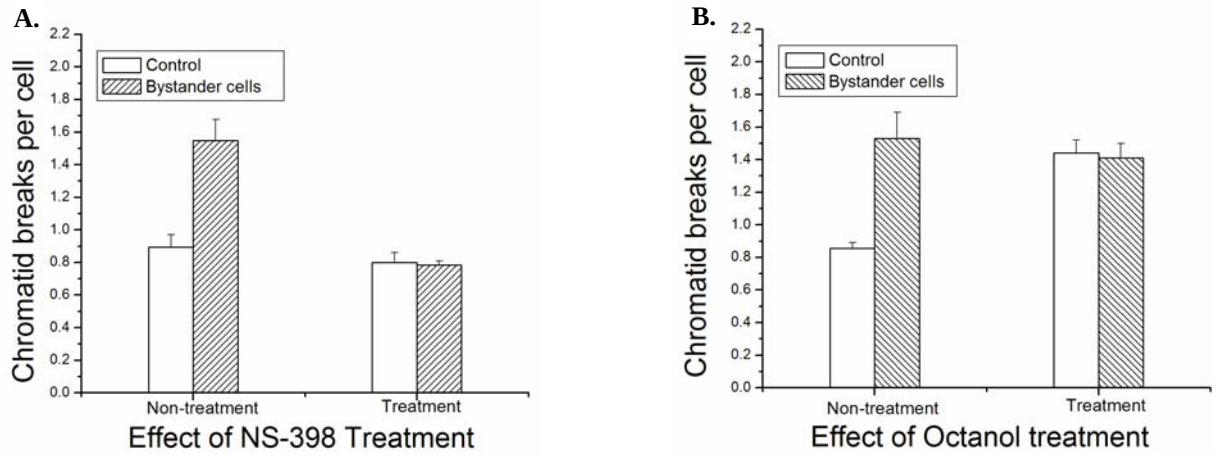

Fig. 3. Induced chromosome aberration in bystander cells was suppressed after treatment with NS-398 or Octanol. **A.** Effect of 50μM NS-398 (24h before irradiation, and maintained 24h after track segment irradiation) treatment on chromosome aberrations in bystander cells cultured for 24h after irradiation. **B.** Effect of 1 mM Octanol (2h before irradiation, and maintained 24h after microbeam irradiation) treatment on chromosome aberrations in bystander cells cultured for 5 days after irradiation. Data are pooled from two independent experiments. Error bars represent ±SE.

and microbeam (10 days) irradiations (Figs. 1 and 2). Elevated chromosomal damage can be suppressed by NS-398 (inhibitor of cyclooxygenase-2 activity) in track segment irradiation (Fig. 3a) and by Octanol (inhititor of gap junctional intercellular communication) in microbeam irradiation (Fig. 3b). These results suggest that the bystander signal(s) was transferred from irradiated cells and genomic instability can be induced in bystander cell populations in both protocols. Ongoing mFISH experiments will further indicate whether the large scale damages in chromosomes of the bystander cells' progeny are induced.

References

1. Nagasawa H and Little JB. Induction of sister chromatid exchanges by extremely low doses of alpha-particles. *Cancer Res.* **52**:6394–6, 1992.
2. Zhou H, Randers-Pehrson G, Waldren CA, Vannais D, Hall EJ and Hei TK. Induction of a bystander mutagenic effect of alpha particles in mammalian cells. *Proc Natl Acad Sci U S A* **97**:2099-2104, 2000.
3. Hall EJ and Hei TK. Genomic instability and bystander effects induced by high-LET radiation. *Oncogene* **22**:7034-42, 2003. Review.
4. Morgan WF. Non-targeted and delayed effects of exposure to ionizing radiation: II. Radiation-induced genomic instability and bystander effects in vivo, clastogenic factors and transgenerational effects. *Radiat Res* **159**:581-96, 2003. Review.
5. Morgan WF. Non-targeted and delayed effects of exposure to ionizing radiation: I. Radiation-induced genomic instability and bystander effects in vitro. *Radiat Res* **159**:567-80, 2003. Review.
6. Lorimore SA, Coates PJ and Wright EG. Radiation-induced genomic instability and bystander effects: inter-related nontargeted effects of exposure to ionizing radiation. *Oncogene* **22**: 7058-69, 2003. Review.
7. Shao C, Furusawa Y, Kobayashi Y, Funayama T and Wada S. Bystander effect induced by counted high-LET particles in confluent human fibroblasts: a mechanistic study. *FASEB J.* **17**:1422-7, 2003.
8. Hu B, Wu L, Han W, Zhang L, Chen S, Xu A, Hei TK and Yu Z. The time and spatial effects of bystander response in mammalian cells induced by low dose radiation. *Carcinogenesis* **27**:245-51, 2006. ■

External advisory committee members of Center for Radiological Research program project grant on mechanism of Radiation-induced bystander effect. (L-r): Dr. Charles Waldren, Dr. Eleanor Blakely, Dr. Gayle Woloschak, Dr. Richard B. Setlow and Dr. Albert Fornace Jr.

A visiting seminar speaker, Professor Qamar Rahman, Head, Fiber Toxicology Division, Industrial Toxicology Research Center, Lucknow, India, with Dr. Mohammmad Athar, Department of dermatology, Columbia University and Dr. Tom K. Hei.

HRAD9 Expression in Human Prostate Normal And Cancer Tissue

Aiping Zhu, Xia Zhang, Xiangyuan Wang, Harshwardhan M. Thaker,[a] Mahesh M. Mansukhani[a] and Howard B. Lieberman

HRAD9 was identified as homologous to yeast *S. pombe* rad9, serving many functions that could involve carcinogenesis, such as acting as a DNA damage sensor, inducing cell cycle checkpoints and apoptosis, and maintenance of genomic stability.[1] Recently, several reports showed that HRAD9 was also associated with tumorgenesis. For example, HRAD9 has aberrantly high expression in lung and breast cancer.[2,3] Similarly, we found high HRAD9 expression in prostate cancer cell lines (DU145, PC-3, CWR22 and LNCaP) when compared to the level in normal prostate epithelia cells (by western-blot).[4] In this report, we focus on our new findings of high HRAD9 expression in human prostate cancer tissues and almost no expression in normal prostate tissue.

Human prostate normal and cancer tissue slides were purchased from US Biomax and Imgenex. Fifty two different normal prostate tissue cases and 339 different prostate cancer tissue cases were examined by immunostaining. We followed the company's deparaffinization, hydration and immunohistochemistry protocols. Slides were deparaffinized in safeclear reagent (Fisher Corp) and stepwise rehydrated with 100% ethanol, to 95%, to 75%, and finally to 50% ethanol. Citrate buffer (0.01M, PH 6.0) was used for antigen retrieval. VECTASTAIN elite ABC kit was used for immunostaining (Vector Laboratories, Inc.). HRAD9 monoclonal antibody was used as the primary antibody (BD Biosciences). Counterstaining was performed with Meyer's hematoxylin. The dehydration was carried out in 75%, 80%, 95% and 100% ethanol. Clear slides in safeclear reagent and cover slips were mounted with Permount.

The results showed that brown dots, representing HRAD9 staining, appeared in the tumor cell nuclei. Prostate tumor samples (153) with brown dots in the nuclei were detected out of a total of 339 prostate cancer samples, although HRAD9 expression levels and staining intensities varied case to case. Only two normal prostate cases showed very weak brown dot staining out of a total of 52 normal prostate samples. The percentage of positive HRAD9 immunostaining is 45.1 percent in tumor sections and 3.8 percent in normal tissue sections. We also found that the intensity of HRAD9 immunostaining depended on the tumor grade–the

[a] *Department of Pathology, College of Physicians & Surgeons, Columbia University, NY*

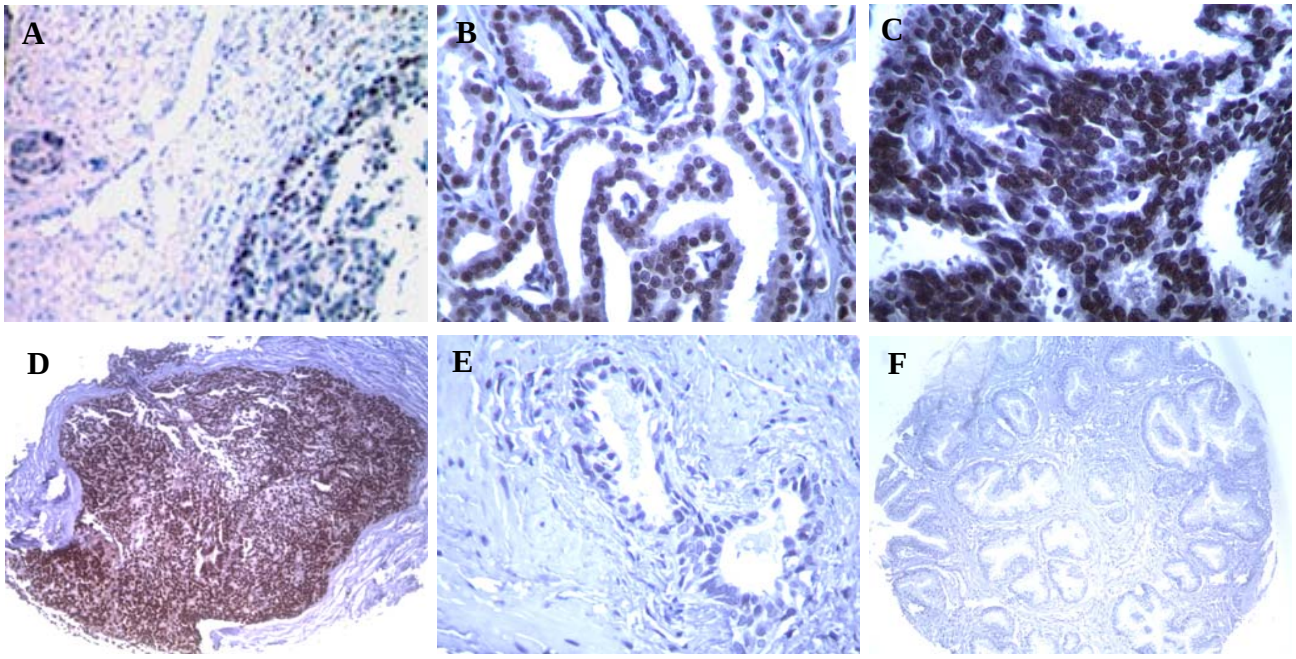

Fig. 1. Immunostaining analysis of tissue slides showed different HRAD9 abundance in prostate cancer tissue and normal tissues. **A.** part of HRAD9 immunostaining in prostate tumor cell nuclei, the intensity was considered +; **B.** and **C.** HRAD9 accumulated in most of the prostate tumor cell nuclei, the intensity was considered ++; **D.** HRAD9 accumulated extensively in the prostate tumor cell nuclei, the intensity was considered +++; **E.** and **F.** showed normal prostate tissue sections. There was no HRAD9 immunostaining in these cell nuclei.

Table 1.
Positive staining intensity and percentage in different grade in the prostate tissues

Grade	Total cases	0	+	++	+++	Total positive percentage (%)
Normal	52	50	2			3.8
I	43	33	10			23.3
II	65	38	23	4		41.5
III	155	79	52	24		49
IV	72	36	25	8	3	50
M	4	0	2		2	100
Prostate cancer cases	339					
Positive Cases	153					45.1

higher grades showed higher intensity of HRAD9 staining. See Figure 1 and Table 1 for articles.

From the pictures and table summary, HRAD9 protein is clearly aberrantly high in human prostate cancer tissues. This is the first demonstration that HRAD9 overexpression is associated with human prostate cancer. This is a very important finding because prostate cancer is the most frequent type of cancer in American men. Over 200,000 new cases of prostate cancer are diagnosed annually in the U.S. Prostate cancer is the third most common cause of death from cancer in men of all ages and is the most common cause of death from cancer in men over 75 years old. The disease's mechanism is unclear so far. The high expression of HRAD9 in prostate cancer found provides us with a new clue to understanding mechanism. In the future, perhaps we can use this information in the prevention and treatment of this disease.

References

1. Lieberman HB. Rad9, an evolutionarily conserved gene with multiple functions for preserving genomic integrity. *J Cell Biochem* **97**:690-7, 2006.
2. Maniwa Y, Yoshimura M, Bermudez VP, Yuki T, Okada K, Kanomata N, Ohbayashi C, Hayashi Y, Hurwitz J and Okita Y. Accumulation of hRad9 protein in the nuclei of nonsmall cell lung carcinoma cells. *Cancer* **103**:126-32, 2005.
3. Cheng CK, Chow LW, Loo WT, Chan TK and Chan V. The cell cycle checkpoint gene Rad9 is a novel oncogene activated by 11q13 amplification and DNA methylation in breast cancer. *Cancer Res* **65**:8646-54, 2005.
4. Lieberman HB and Zhu A. Rad9 Expression is aberrantly high in human prostate cancer cells. *Center for Radiology Research. Annual Report*, p32, 2005. ■

Mrad9B Is Essential for Early Development

Kevin M. Hopkins, Xiangyuan Wang, Corinne Leloup, Aiping Zhu, Debra J. Wolgemuth and Howard B. Lieberman

Introduction

Human *HRAD9B* and mouse *Mrad9B* were identified as paralogs of the cell cycle checkpoint control genes *HRAD9* and *Mrad9*, respectively.[1] In the adult mouse and human, RAD9B is predominantly localized in the testis. HRAD9B is localized in the nucleus and can coimmunoprecipitate with the checkpoint control proteins HRAD1, HRAD9, HHUS1 and HHUS1B.[1]

In order to determine the function(s) of Mrad9B, *Mrad9B*$^{-/-}$ mouse embryonic stem cells have been generated by deleting the first two exons of the gene and replacing them with a neomycin resistance gene. Mutant cells are more sensitive than wild type controls to DNA damage induced by 254nm UV-light, γ-rays and mitomycin C but not by cisplatin, hydroxyurea or ethyl methane-sulfonate (unpublished data).

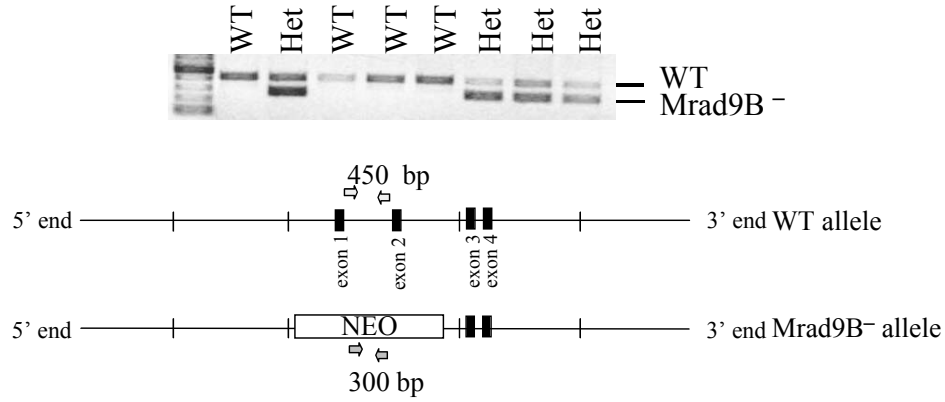

Fig. 1. PCR analysis of heterozygous mice. Genomic DNA was extracted from mouse tails and genotyped by PCR.

	Number of Embryos with Indicated Genotype		
Stage(Day)	Mrad9B$^{+/+}$	Mrad9B$^{+/-}$	Mrad9B$^{-/-}$
9.5	7	13(4)	6(6)
10.5	5	13(4)	5(4)
12.5	1	2	1(1)

Fig. 2. Genotypes of embryos from timed *Mrad9B*$^{+/-}$ × *Mrad9B*$^{+/-}$ crosses. Numbers represent the sum of three liters for each stage, except for E12.5 which represents only one liter. The numbers in parentheses represent the number of embryos with an open brain phenotype in the *Mrad9B*$^{+/-}$ column and the number of resorbed embryos in the *Mrad9B*$^{+/-}$ column.

Generation of MRAD9B$^{+/-}$ mice

MRAD9B$^{+/-}$ ES cells have been injected into blastocytes to generate mutant mice. Male chimeric offspring were mated with wild type females. The offspring mice were genotyped by PCR (Fig. 1). Five heterozygous *Mrad9B*$^{+/-}$ mice out of 35 born were obtained.

Mrad9B$^{-/-}$ genotype causes embryonic lethality

Mrad9B$^{+/-}$ mice were mated to each other. The genotypes obtained are presented in Figure 2. Eleven out of twelve *Mrad9B*$^{-/-}$ mice were resorbed. This indicates that *Mrad9B* is essential for early embryonic development, before day E9.

MRAD9B$^{+/-}$ embryos display brain abnormality

A large percentage (30%) of the *Mrad9B*$^{+/-}$ mice displayed an open brain phenotype (Fig. 3). Therefore Mrad9B might be more specifically involved in brain development.

References

1. Hopkins KM, Wang X, Berlin A, Hang H, Thaker HM and Lieberman HB. Expression of Mammalian Paralogues of HRAD9 and Mrad9 Checkpoint Control Genes in Normal and Cancerous Testicular Tissue. *Cancer Res.* **63:**5291-8, 2003. ■

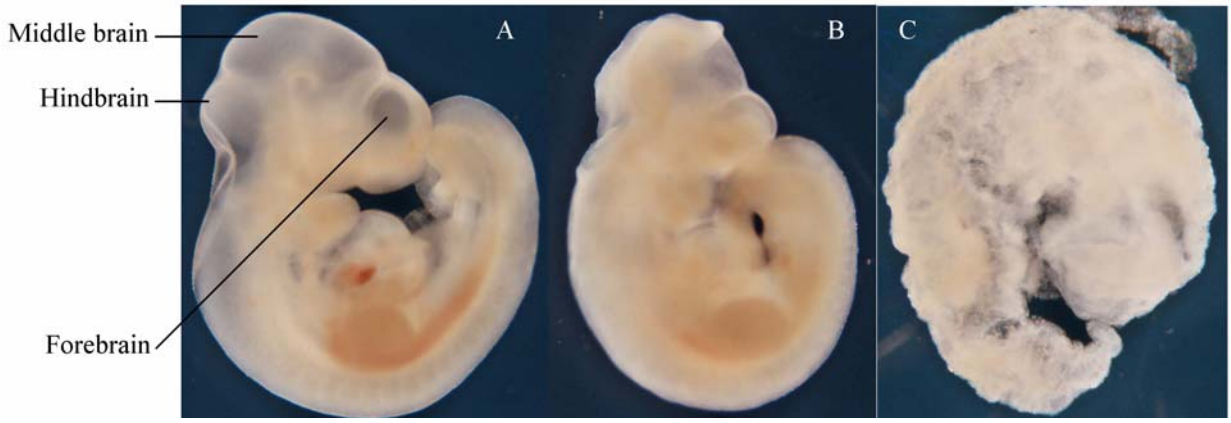

Fig. 3. Mrad9B$^{+/-}$ mice at day E10.5 displaying **A.** normal and **B.** open brain phenotypes. **C.** Resorbed Mrad9B$^{+/-}$ mouse at day E10.5.

Regulation of Gene Expression In Response to 1GeV ^{56}Fe Ions

Sally A. Amundson and Jaeyong Ahn

As the U.S. contemplates a renewed human presence in space, with plans for a moon base and possible manned missions to Mars, an understanding of the biological effects of the space radiation environment becomes more important. Exposure to the heavy ions that make up galactic cosmic rays poses a serious radiological health concern for such extended space missions. ^{56}Fe ions are an important component of Galactic Cosmic Rays. At 1GeV/amu. ^{56}Fe ions have a LET of approximately 148 keV/µm, which is near the maximum reported RBE for cell killing.

We previously reported on the cellular responses of p53 wild-type (TK6) and null (NH32) human lymphoblasts exposed to various doses of 1GeV ^{56}Fe ions at the NASA Space Radiation Laboratory during NSRL-5 and NSRL-6. We now report on analysis of gene expression by microarray analysis, with confirmation and follow-up of several genes by quantitative real-time PCR.

Microarray analysis

RNA from cultures exposed to 0.5 or 1.67Gy 1GeV ^{56}Fe particles were compared to controls by microarray analysis at representative early (3 hours) and late (24 hours) times

after irradiation. Labeling was performed by amino-allyl incorporation followed by coupling with mono-reactive Cy3 or Cy5 dyes. Hybridizations were carried out under standard conditions using active sample mixing on the MAUI® hybridization station (BioMicro Systems). We used arrays printed with the 19200 long oligonucleotides of the Compugen library.

For analysis of the microarray data, we used the BRB Array tools (http://linus.nci.nih.gov/BRB-ArrayTools.html). With the class comparison tools, 34 genes were found with p53 dependent regulation following ^{56}Fe-particle irradiation. Similar analysis revealed 114 genes that were differentially regulated at early and late times. When only the higher dose treatments were considered, 45 genes showed time-specific regulation by ^{56}Fe-particle irradiation.

A further comparison was made between roughly equitoxic doses of ^{56}Fe (1.67Gy) and gamma-rays (2.5Gy) at early and late times in the p53 wild-type cell line TK6. Analyzing the combined results from the two LETs yielded a set of 249 genes differing between early and late times. Interestingly, a four-way comparison was able to reveal a set of 183 genes that could discriminate between the treatments both in terms of time since exposure and radiation quality. Hierarchical clustering of this gene set recapitulated the four categories, with a greater effect of time rather than LET being evident. Part of the resulting heat-map is illustrated in Figure 1.

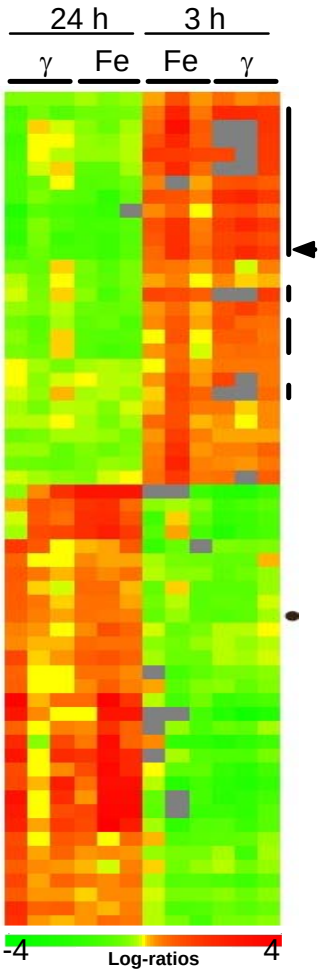

Fig. 1. Heat-map of log ratios of time and LET specific genes. Line to right marks histone genes. Grey squares: filtered data. Arrowhead: HISTH1B. Dot: MAML3.

Histone gene expression

One of the most immediately striking patterns in this data set was the robust down-regulation of a large cluster of histone genes (marked by black bar in Figure 1) at the 24-hour time-point by both high and low LET irradiation. Although Figure 1 illustrates only data from the p53 wild-type cell line (TK6), a similar pattern of coordinate histone gene down-regulation was also observed in p53-null NH32 cells. Although previously published studies have found coordinate down-regulation of histone genes to be induced by stresses including ionizing radiation, this has previously been reported to be dependent on expression of both wild-type p53 and CDKN1A.[1]

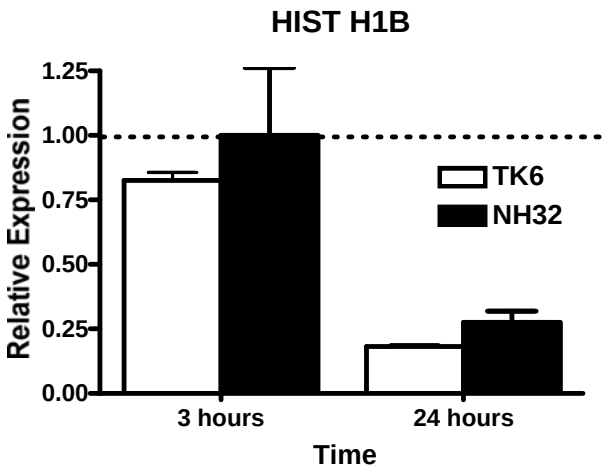

Fig. 2. Expression of HISTH1B by qRT-PCR. Dashed line: level of expression in untreated controls.

We therefore used quantitative real-time PCR (qRT-PCR) to confirm the observ-ed expression of HISTH1B as a representative of this gene cluster (Fig. 2). We found that while levels in treated cells remained simi-lar to control levels at three hours, by 24 hours after treatment, both TK6 and NH32 had significantly reduced expression of HISTH1B, in agreement with the microarray results. Thus, in this cell line, histone gene expression appears to be coordinately down-regulated by both gamma and ^{56}Fe irradiation independently of p53 status.

Genes up-regulated at late times

Despite the very striking histone cluster among the down-regulated genes, many responsive genes were also up-regulated. This is consistent with our earlier studies of global gene expression response to ionizing radiation.[2,3] In contrast to our prior studies, which have focused largely on the first peak of gene expression, we here focused our analysis on genes regulated at late times. As an example of a gene with p53-independent regulation at 24 hours after irradiation, we examined the gene for the transcriptional cofactor mastermind-like 3 (MAML3). The results of qRT-PCR analysis of MAML3 are illustrated in Figure 3. Although this gene

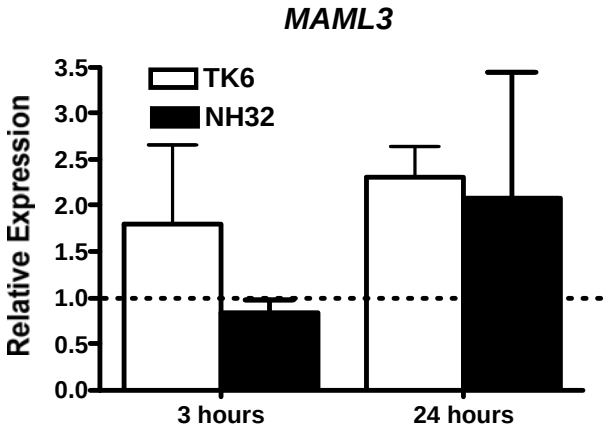

Fig. 3. Expression of HISTH1B by qRT-PCR. Dashed line: level of expression in untreated controls.

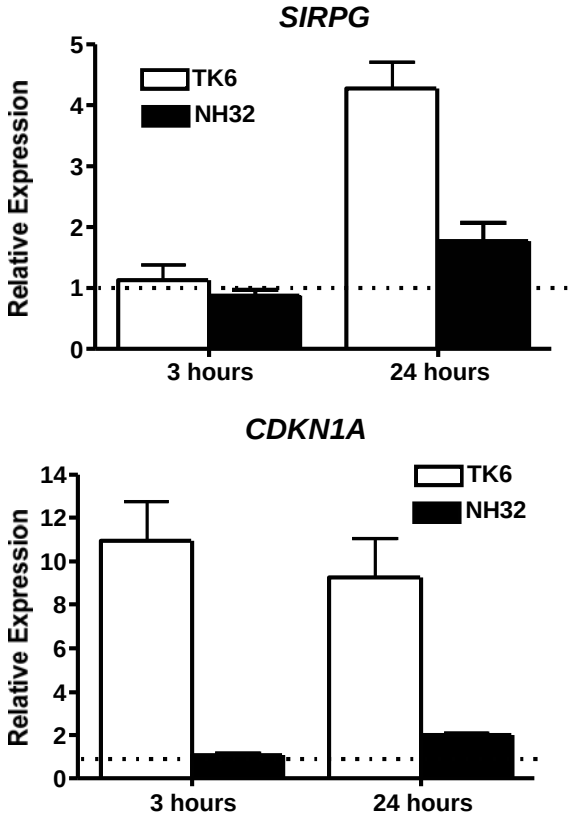

Fig. 4. *Expression of SIRPG by qRT-PCR and CDKN1A by quantitative dot blot.*[4] Dashed line:Expression in untreated controls.

showed more biological variability between experiments than others in this study, its expression was significantly increased at 24 but not three hours after irradiation. At 24 hours, expression ratios were significantly and consistently elevated in both the p53 wild-type and knock-out lines, although more variability was observed in the knock-out line.

Late responding genes with p53 regulation

In contrast to our results with MAML3 and the histone genes, we did also find genes responding at the late time point that showed a p53-dependent response. As an example, we verified the expression response of the gene for signal regulatory protein protein γ (SIRPG) using qRT-PCR (Fig. 4). SIRPG codes for a cell surface marker that participates in signal transduction through interaction with CD47, and may play a role in apoptosis. While this gene was expressed at control levels three hours after irradiation, it was robustly and reproducibly up-regulated at 24 hours after irradiation in the p53 wild-type cell line. A consistent up-regulation of much lower magnitude, a little less than two-fold, was seen in the p53 null cell line. This level of up-regulation at 24 hours is virtually identical to that seen for the prototypical p53-regulated gene CDKN1A (Fig. 4), and suggests a major role for p53 in regulation of this late responding gene.

Conclusion

This preliminary analysis of microarray data from p53 wild-type and knock-out human cells exposed to ^{56}Fe ions and γ-rays has revealed some intriguing patterns. The responses seen on the microarrays have been well confirmed by qRT-PCR. Further investigation of the regulation of genes responding at late times after irradiation will likely clarify both p53-dependent and -independent levels of control distinct from those characterized at earlier times.

References

1. Su C, Gao G, Schneider S, Helt C, Weiss C, O'Reilly MA, Bohmann D and Zhao J. DNA damage induces downregulation of histone gene expression through the G1 checkpoint pathway. *EMBO J,* **23**:1133-43, 2004.
2. Amundson SA, Bittner M, Chen Y, Trent J, Meltzer P and Fornace AJ Jr. Fluorescent cDNA microarray hybridization reveals complexity and heterogeneity of cellular genotoxic stress responses. *Oncogene* **18**:3666-72, 1999.
3. Amundson SA, Do KT, Vinikoor L, Koch-Paiz CA, Bittner ML, Trent JM, Meltzer P and Fornace AJ, Jr. Stress-specific signatures: expression profiling of p53 wild-type and -null human cells. *Oncogene* **24**:4572-9, 2005.
4. Koch-Paiz CA, Momenan R, Amundson SA, Lamoreaux E and Fornace AJ Jr. Estimation of relative mRNA content by filter hybridization to a polyuridylic probe. *Biotechniques* **29**:706-14, 2000. ■

The Complete Nucleotide Sequence of Chinese Hamster (*Cricetulus griseus*) Mitochondrial DNA

Michael A. Partridge, Mercy M. Davidson and Tom K. Hei

Sequence data from this article has been deposited with GenBank Data Libraries under the accession number **DQ390542**.

Introduction

Mitochondria, the energy-generating organelles in the cell, contain their own extra-nuclear DNA. In most

mammals, mitochondrial DNA is an approximately 16.5kb circular, autonomously replicating genome. It encodes 13 of the proteins involved in the electron transport chain, two ribosomal RNA genes (rRNA) and 22 tRNA genes. In humans, damage to mitochondrial DNA has been associated with aging and is a critical factor in the progression of a number of diseases. Recently, there has also been considerable interest in the involvement of mitochondria in cancer, as the mitochondria are a major source of reactive oxygen species and free radicals which are known to cause DNA mutations.[1]

In our *in vitro* studies of the mutagenic effects of alpha particles and mineral fibers,[2,3] we have specifically used the AL hybrid cell line, which is derived from *C.griseus* (Chinese hamster). The A_L cell line contains a complete set of Chinese hamster ovary-K1 (CHO) chromosomes and a single copy of human chromosome 11. Using the A_L cell culture model we have shown that the mutagenic effects of arsenic are mediated by the mitochondria.[4,5] The complete mitochondrial genome has been sequenced for a variety of mammals including human, cow and pig, and two rodent species, rat and mouse.[6-10] Surprisingly, complete sequences of only three of the thirteen protein-coding genes in hamster were known. This incomplete sequence information fundamentally hampered our mutation analyses. We therefore sequenced the entire mitochondria genome of CHO cells, the progenitor of the A_L cell line.

Results and discussion

We report here the entire 16,284 bp mtDNA sequence of *C. griseus*. The sequence was obtained by generating six overlapping PCR products encompassing the entire 16,284 bp. These fragments were sequenced using primers designed, initially, from published sequences and subsequently from additional data obtained from the sequencing analysis.

Hamster mtDNA is organized in an analogous manner to other mammals.[6-10] The 13 protein coding sequences of hamster mitochondrial genome, the rRNA genes and the 22 tRNAs, are all encoded in the same order and on the same strand as has been reported in other species (Table 1). The genome is, by nuclear DNA standards, remarkably compact, with no introns and very few non-coding regions.

The hamster is the third from the *Sciurognathi* suborder of rodents, after mouse and rat, to have its mitochondrial genome sequenced in its entirety.[8,9] A comparison between these genomes reveals some interesting differences and similarities. Among the protein coding genes of the three rodent species, the seven NADH genes are less conserved than the three cytochrome *c* oxidase (COX) subunit genes. However, the most highly conserved genes are the rRNA genes, in particular the 12S sequence, for which there is a greater than 85% similarity between the rodent species. The least conserved gene, ATPase 8, is also the smallest and its amino acid similarity to other rodent equivalents is even lower (~50%) than its nucleotide similarity (~67%). The most conserved protein coding gene is the COX1 gene, which has a protein sequence with a greater than 96% similarity to the gene in other rodents. Interestingly, in a comparison between human and hamster, the human COX1 gene had the highest similarity to any hamster gene, greater even than the 12S rRNA sequence.

Overall, the hamster mtDNA sequence has only a ~76% similarity to that of mice and rats. However, certain elements of the hamster sequence highlight its close relationship to the mitochondrial genome of other rodent species. First, the length of the hamster genome (16,284 bp) is within 15 bp of the mouse (16,295) and rat (16,298) mtDNA sequences.[8,9] Second, all three rodent NADH1 coding sequences begin with a GTG (Val) codon, whereas in human, cow, pig and frog, the initiator is a methionine (ATG or ATA) codon.[9-11]

Table 1.

Element	nt Position	Size	Strand	Start	Stop
tRNA-Phe	1-70	72			
12S rRNA	71-1023	953			
tRNA-Val	1024-1095	72			
16S rRNA	1096-2656	1561			
tRNA-Leu (UUR)	2658-2732	75			
NADH1	2733-3687	956		GTG	T--
tRNA-Ile	3688-3756	69			
tRNA-Gln	3754-3824	71	L		
tRNA-Met	3829-3897	69			
NADH2	3898-4930	1033		ATT	T--
tRNA-Trp	4931-4997	67			
tRNA-Ala	5000-5069	69	L		
tRNA-Asn	5072-5142	71	L		
Or. L-strand repl.	5144-5174	31			
tRNA-Cys	5174-5241	68	L		
tRNA-Tyr	5241-5308	68	L		
COX-I	5310-6854	1546		ATG	TAA
tRNA-Ser (UCN)	6851-6923	72	L		
tRNA-Asp	6924-6993	69			
COX-II	6994-7677	684		ATG	TAA
tRNA-Lys	7681-7744	64			
ATPase8	7746-7949	204		ATG	TAA
ATPase6	7907-8587	681		ATG	TAA
COX-III	8587-9370	783		ATG	T--
tRNA-Gly	9371-9438	68			
NADH3	9439-9786	348		ATA	TAA
tRNA-Arg	9788-9855	68			
NADH4L	9857-10153	297		ATG	TAA
NADH4	10147-11524	1378		ATG	T--
tRNA-His	11525-11592	68			
tRNA-Ser (AGY)	11593-11652	60			
tRNA-Leu (CUN)	11652-11720	70			
NADH5	11721-13541	1821		ATT	TAA
NADH6	13525-14049	525	L	ATG	TAA
tRNA-Glu	14049-14118	69	L		
Cytochrome b	14123-15265	1143		ATG	TAA
tRNA-Thr	15267-15333	66			
tRNA-Pro	15337-15403	67	L		

Note: The order and location of each element of the Chinese hamster mitochondrial genome has been defined. Numbering begins at the first 5′ nucleotide of the tRNA-Phe. Genomic DNA was isolated from CHO-K1 cells (a gift from G. Taccioli, Boston University) and overlapping PCR products encompassing the entire 16,284 bp were generated and sequenced. Protein encoding regions and rRNA genes are in bold. L indicates that the element is encoded on the light strand; all other elements are encoded on the heavy strand.

Finally, aside from the NADH1 start codon, there are at least two other minor anomalies that are specific to rodent mtDNA; there are spacer bases between tRNA-Arg and the NADH4L gene, and there is a TAA termination codon at the end of the NADH3 gene. These features are absent in other vertebrates.

The Chinese hamster mtDNA sequence presented here is almost identical to most other known *C. griseus* mtDNA sequences. There are six cases where the sequence of the complete mitochondrial genome differs from published sequences, in each case at a single nucleotide. For the 16S rRNA gene, there are two cases where an individual residue differs between the four published sequences, and in each instance the complete hamster mitochondrial genome was identical to three of the four, suggesting that this was the wild type sequence. For the ATPase 6 gene, there are two individual nucleotides that differ between the two published sequences, both conferring a proline to leucine amino acid change in the resulting protein.[12] Importantly, both proline and leucine have relatively small, uncharged and non-polar side chains and consequently these differences are unlikely to dramatically alter the structure or function of the hamster ATPase 6 protein. It is possible that this sequence variation is a common polymorphism occurring in the Chinese hamster species.

The final partial *C. griseus* mtDNA sequence which differs from the complete hamster mtDNA sequence is the 406bp fragment of the NADH4 gene.[13] The nucleotide change in this partial sequence would result in the mutation of a leucine at residue 315 to glutamine. However, as the leucine residue is conserved in human, cow, pig, rat, mouse and frog[6-11] it seems likely that the full mtDNA sequence reported here, and not the previously published partial sequence,[13] encodes the wild type hamster NADH4 gene.

There were three other previously published complete gene sequences, as well as the D-loop regulatory region, attributed to Chinese hamster. The first incorporates the entire 12S rRNA gene, as well as the flanking tRNA-Val, and the second is the complete ATPase 8 gene.[12,14] Both are identical to the sequence reported here. There are also complete 12S rRNA genes published for other hamster species, and phylogenetic comparisons between the species are detailed elsewhere.[15,16] In addition, an analysis of the regulatory region of the mitochondrial genome in several mammalian species has been previously published.[17]

Finally, there are two complete (or nearly complete) coding sequences attributed to Chinese hamster from the cytochrome-b (Cyt-b) gene,[15,18] a component of the cytochrome bc1 complex. One of these sequences differs only at a single nucleotide and does not alter the amino acid of the encoded protein.[15] However, the second sequence, derived from a phylogenetic study of Asian rodents, differs from the complete Chinese hamster mtDNA sequence at 97 nucleotides within the ~1140 bp coding region.[18] This represents only a 91% similarity between the two genes, a much more substantial change than observed with other *C. griseus* sequences. It seems likely that the sequence from the Japanese group[18] represents a different species within the *Cricetulus* genus, given the almost perfect homology between all other published Chinese hamster mtDNA sequences (including the Cyt-b gene)[15] and the complete mitochondria genome presented in this study. Obtaining the exact and complete sequence of the hamster mitochondrial genome enables detailed phylogenetic studies to be performed in addition to providing a valuable tool for analyzing mtDNA damage in *C. griseus* derived cells.

References

1. Dimauro S and Davidzon G. Mitochondrial DNA and disease. *Ann Med* **37**:222-32, 2005.
2. Hei TK, Piao CQ, He ZY, Vannais D and Waldren CA. Chrysotile fiber is a strong mutagen in mammalian cells. *Cancer Res* **52**:6305-9, 1992.
3. Hei TK, Wu LJ, Liu SX, Vannais D, Waldren CA and Randers-Pehrson G. Mutagenic effects of a single and an exact number of alpha particles in mammalian cells. *Proc Natl Acad Sci U S A*, **94**:3765-70, 1997.
4. Hei TK, Liu SX and Waldren C. Mutagenicity of arsenic in mammalian cells: role of reactive oxygen species. *Proc Natl Acad Sci U S A* **95**:8103-7, 1998.
5. Liu SX, Davidson MM, Tang X, Walker WF, Athar M, Ivanov V and Hei TK. Mitochondrial damage mediates genotoxicity of arsenic in mammalian cells. *Cancer Res* **65**:3236-42, 2005.
6. Anderson S, Bankier AT, Barrell BG, de Bruijn MH, Coulson AR, Drouin J, Eperon IC, Nierlich DP, Roe BA, Sanger F, Schreier PH, Smith AJ, Staden R and Young IG. Sequence and organization of the human mitochondrial genome. *Nature* **290**:457-65, 1981.
7. Anderson S, de Bruijn MH, Coulson AR, Eperon IC, Sanger F and Young IG. Complete sequence of bovine mitochondrial DNA. Conserved features of the mammalian mitochondrial genome. *J Mol Biol*, **156**:683-717, 1982.
8. Bibb MJ, Van Etten RA, Wright CT, Walberg MW and Clayton DA. Sequence and gene organization of mouse mitochondrial DNA. *Cell*, **26**:167-80, 1981.
9. Gadaleta G, Pepe G, De Candia G, Quagliariello C, Sbisa E and Saccone C. The complete nucleotide sequence of the Rattus norvegicus mitochondrial genome: cryptic signals revealed by comparative analysis between vertebrates. *J Mol Evol*, **28**:497-516, 1989.
10. Ursing BM and Arnason U. The complete mitochondrial DNA sequence of the pig (Sus scrofa). *J Mol Evol*, **47**:302-6, 1998.
11. Roe BA, Ma DP, Wilson RK and Wong JF. The complete nucleotide sequence of the Xenopus laevis mitochondrial genome. *J Biol Chem*, **260**:9759-74, 1985.
12. Breen GA, Miller DL, Holmans P and Welch G. Mitochondrial DNA of two independent oligomycin-resistant Chinese hamster ovary cell lines contains a single nucleotide change in the ATPase 6 gene. *J Biol Chem*, **261**:11680-5, 1986.
13. Chaudhuri K, Banerjee R, Pandi, B, Mukherjee A, Das S, Sengupta S, Roychoudury S and Bhattacharyya NP. Identification of two differentially expressed mitochondrial genes in a methotrexate-resistant Chinese hamster

cell strain derived from v79 cells using RNA fingerprinting by arbitrary primed polymerase chain reaction. *Radiat Res*, **160**:77-85, 2003.
14. Murphy WJ, Eizirik E, Johnson WE, Zhang YP, Ryder OA and O'Brien SJ. Molecular phylogenetics and the origins of placental mammals. *Nature*, **409**:614-8, 2001.
15. Neumann K, Michaux J, Lebedev V, Yigit N, Colak E, Ivanova N, Poltoraus A, Surov A, Markov G, Maak S, Neumann S and Gattermann R. Molecular phylogeny of the Cricetinae subfamily based on the mitochondrial cytochrome b and 12S rRNA genes and the nuclear vWF gene. *Mol Phylogenet Evol*, **39**:135-48, 2006.
16. Norris RW, Zhou K, Zhou C, Yang G, William Kilpatrick C and Honeycutt RL. The phylogenetic position of the zokors (Myospalacinae) and comments on the families of muroids (Rodentia). *Mol Phylogenet Evol*, **31**:972-8, 2004.
17. Nakamichi N, Rhoads DD, Hayashi JI, Kagawa Y and Matsumura T. Detection, localization, and sequence analyses of mitochondrial regulatory region RNAs in several mammalian species. *J Biochem (Tokyo)*, **123**: 392-8, 1998.
18. Suzuki H, Tsuchiya K and Takezaki N. A molecular phylogenetic framework for the Ryukyu endemic rodents Tokudaia osimensis and Diplothrix legata. *Mol Phylogenet Evol*, **15**:15-24, 2000. ■

Low LET Radiation Induced DNA Double Strand Break Signaling and Repair in Human 3D Skin Model System: Role of PI-3 Kinase-Like Kinases

Yanrong Su, Jarah A. Meador and Adayabalam S. Balajee

Introduction

Exposure of cells to DNA damaging agents such as ionizing radiation (IR) and radiomimetic agents triggers a multitude of signal transduction pathways. Among them, the most notable one is mediated by PI-3 kinase related kinases (PIKK) involving ATM, ATR and DNA-PK. One of the foremost goals of our laboratory is to understand the role of PIKK in the cellular response to low dose radiation and to elucidate the mechanistic differences, if any, in the action of PIKK between low and high dose radiation exposures. Therefore, several low and high dose experiments using γ-rays irradiation have been performed for the detection of PIKK mediated signaling pathways of DSB repair in human 2- and 3- dimensional cell systems by monitoring the kinetic assembly and intra-nuclear organization of various proteins that serve as sensors, effectors and signal transducers for DSB. Some of these proteins include 53BP1, MDC1, SMC1, phosphorylated forms of ATM, histone H2AX, p53, DNA-PK, Chk1 and Chk2.

An important aspect, which is of special concern to the DOE, is the determination of radiation-induced responses in intact tissues or tissue-like constructs. Studies focused on elucidating the tissue specific radiation responses are critically important for improving the accuracy of health risk estimation in intact human tissues. We have initiated studies looking into radiation-induced responses in human EpiDerm tissue constructs (MatTek Incorporation, USA) following low and high doses of low LET radiation. As 53BP1 is a sensitive indicator of DSB, studies were carried out to determine the induction and repair of DSB in tissues by monitoring the kinetics of 53BP1 focus formation as a function of radiation dose and recovery time. Tissues were exposed to different doses of γ-rays (0.1-5Gy) and post incubated for different recovery times (0.5, 2, 4, 8 and 24hr). Unirradiated and irradiated tissues were fixed in buffered formalin and the tissue sections were processed for 53BP1 immunostaining. In unirradiated tissues, 53BP1 was found to be more homogenous similar to that observed in human 2-dimensional cell systems. Upon irradiation, distinct focal sites of 53BP1 were observed in tissues as a function of radiation dose (Fig.1). Upon irradiation with 0.1Gy of γ-rays, 2.3foci/cell were observed 30min after irradiation and the foci number steadily increased with increasing radiation doses. The foci number induced by 0.1Gy of γ-rays (2.32/cell) was lower in 3D tissue constructs as compared to MRC 5 cells (6/cell).

It is interesting to note that the cells in the basal layer showed efficient DSB induction where as the cells beneath the stratum corneum did not show 53BP1 foci after 0.1Gy of γ-rays exposure illustrating the heterogeneous cellular response to IR in a tissue microenvironment. The feasibility of detecting DSB induction and repair in intact tissue-constructs opens up exciting new possibilities for evaluating the radiation responses in tissues.

The kinetics of DSB repair in tissue constructs was next evaluated by 53BP1 foci analysis at different post-irradiation times (2hr, 4hr, 8hr and 24hr). The DSB repair was highly efficient in EpiDerm tissues after 0.1Gy of γ-rays. The efficiency of DSB repair declined with increasing radiation doses and the percentage of cells with persistent DSB increased in number with doses higher than 1Gy of γ-rays exposure. The observation of 53BP1 foci only in the basal layer of cells after 0.1Gy clearly points out the heterogeneity in the induction of DSB in a tissue microenvironment. To further explore this heterogeneity, a full thickness skin

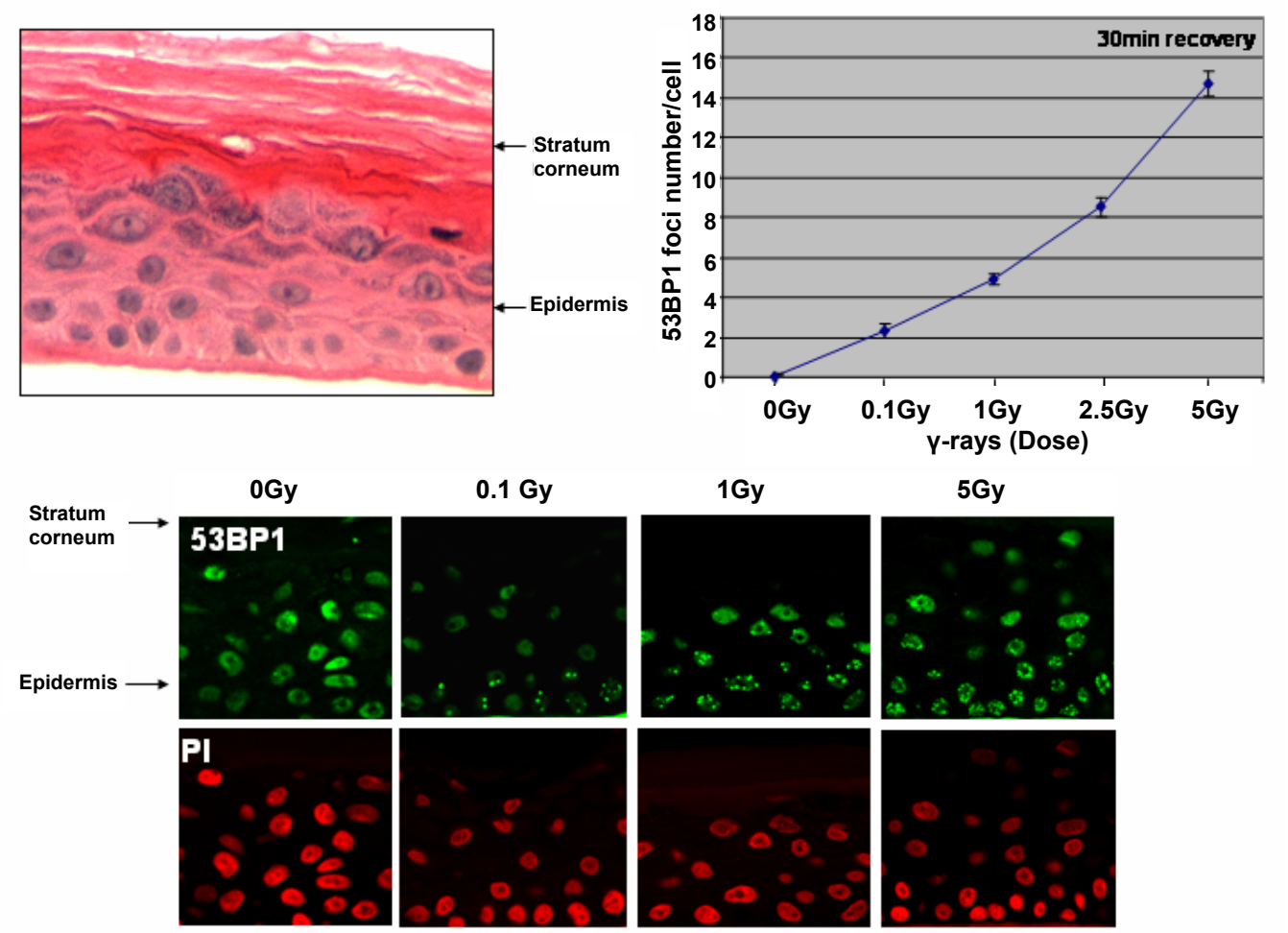

Fig. 1. Dose dependent induction of DSB in human 3-dimensional EpiDerm tissue constructs detected by 53BP1 antibody 30 min after IR treatment. 53BP1 foci number observed per cell basis as a function of radiation dose (γ-rays) is given in the top right panel. Bars indicate the standard error of the mean.

model system is being used presently to determine whether there is differential DSB induction in dermis and epidermis. It would be interesting to determine whether the radiation effects would be different in dermis and epidermis.

In addition to 53BP1, intra-nuclear localization of various DNA repair and cell cycle regulatory factors such as MDC1, DNA-PK^{T2609}, ATM^{ser1981}, γ-H2AX, TRF2, phosphorylated histone H3, poly (ADP) ribose polymerase, Chk1, Chk2, and p53^{ser15} has been performed successfully in EpiDerm tissue constructs. Immunolabeling has also been performed to detect the phosphorylation of target proteins that are phosphorylated at serine/threonine residues by ATM and ATR kinases using a phosphorylation specific pan antibody. It is worth to mention that phosphorylated DNA-PK^{T2609} was detectable only at doses higher than 0.1Gy of γ-rays in EpiDerm tissue constructs and distinct focal sites of phosphorylated DNA-PK were observed upon irradiation with 5Gy of γ-rays. This interesting initial observation will be extended further to determine if there are any mechanistic differences as a function of radiation dose in the activation of ATM, ATR and DNA-PK in the tissue microenvironment.

PI-3 kinase inhibitor abolishes 53BP1 foci formation and causes apoptotic death in EpiDerm tissue constructs

We have demonstrated an efficient induction of various repair and cell cycle checkpoint regulators as a function of radiation dose in 3D human tissue constructs. These observations demonstrate the existence of efficient DSB mediated signaling pathways in tissues. In order to verify whether PI-3 kinase signaling is important for DSB recognition and repair in a tissue microenvironment, EpiDerm tissues were treated with a PI-3 kinase inhibitor LY294002 at a concentration of 100μM prior to radiation exposure. Treatment with PI-3 kinase inhibitor completely abolished 53BP1 foci formation and resulted in apoptotic death of the cells. This clearly illustrates the importance of PIKK mediated signaling pathways in response to DSB in tissues. We intend to use commercially available specific inhibitors for ATM, ATR and DNA-PK to evaluate the effects of low doses of low LET radiation in tissue constructs. ■

Gene Expression in Human Breast Epithelial Cells Altered By a Pesticide and Estrogen

Gloria M. Calaf ,[a] Debasish Roy [b] and Tom K. Hei

Cancer of the breast is the most common form of malignant disease occurring among women of the western world and environmental substances seem to be involved in the etiology of this disease. Many studies have found an association between human cancer and exposure to agricultural pesticides, that among them malathion and parathion, the organophosphorous pesticides have been used in agriculture to control mosquito plagues.[1,2] The association between breast cancer and prolonged exposure to estrogens suggests that this hormone may also have a role in such a process. [3] However, the causative factors for breast carcinogenesis remain an enigma. The current hypothesis of tumorigenesis in humans suggests that cancer cells acquire malignancy through the accumulation of activation and inactivation of genes.[4]

The objective of this study was to determine the effects of 17β estradiol (E), malathion, parathion, a combination of malathion plus E and a combination of parathion plus E on cell transformation *in vitro* of human breast epithelial cells MCF-10F, an immortalized human breast epithelial cell line[5] was treated with malathion and parathion either alone or in combination with estrogen.

Previously, studies have shown that parathion and a combination of parathion and E-induced malignant transformation of MCF-10F as indicated by increased cell proliferation, invasive capabilities and increased PCNA, mutant p53, beta catenin and Rho-A protein expression in comparison to the control MCF-10F cell line.[6] The results of this study showed that malathion and parathion alone and also in combination with E-induced malignant transformation of an immortalized human breast epithelial cell line, MCF-10F, and the malignant feature was confirmed by anchorage independency and invasive capabilities. Table 1 shows the anchorage independence capability of treated cells as well as the invasive characteristics of control and treated MCF-10F cells scored 20h after plating onto matrigel basement membranes using Boyden's chambers (Fig. 1). RNA samples from MCF-10F cells treated with E, malathion, parathion and also in combination with E were compared to control MCF-10F, and the array was able to simultaneously quantify and analyze the expression profile of 408 genes involved in human cancer.

Analysis of gene expression using commercially available OLIGO GEArray® Human Cancer Microarray (from Super Array, Bioscience Corporation, MD) revealed transcriptional alterations in 17 out of a total of 408 genes (Fig. 2). The 17 genes are involved in the regulation of human cancer were altered. The genes represented by this array

Table 1
Origin and phenotypic characteristics of cell lines

Cell lines	Origin	AI	I
MCF-10F	MCF-10F parental cells	-	-
Estrogen	MCF-10F treated with estrogen	-	-
Malathion	MCF-10F treated with malathion	+	+
Parathion	MCF-10F treated with parathion	+	+
Malathion + E	MCF-10F treated with combination	+	+
Parathion + E	MCF-10F treated with combination	+	+

Estrogen: MCF-10F treated with 17β estradiol 10^{-8} M (E) during 20 passages.
Malathion: MCF-10F treated with 0.5μg/ml malathion during 20 passages.
Parathion: MCF-10F treated with 100ng/ml parathion during 20 passages.
Malathion+E: MCF-10F treated with a combination of parathion and E for 20 passages.
Parathion+E: MCF-10F treated with a combination of parathion and E for 20 passages.
AI: Anchorage Independence colony-forming efficiency in soft agar.
I: Invasion assay: Invasive characteristics of control and MCF-10F treated cells scored 20h after plating onto matrigel basement membranes using Boyden's chambers.
Positive signs (+): represent the results in relation to anchorage independent growth and number of cells that crossed the filters.
Negative signs (-): lack of anchorage independent growth and invasiveness.

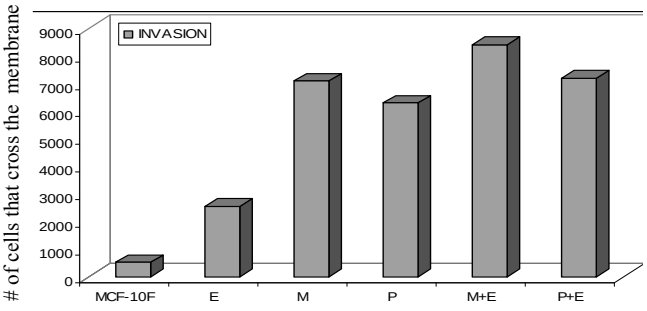

Fig. 1. Invasive capabilities of parental MCF-10F, estrogen (E), malathion (M), parathion (P), malathion + estrogen (M+E), parathion + estrogen (P+E)-treated cells.

[a] *Institute for Advanced Research, Tarapaca, Univ. of Arica, Chile.*
[b] *Dept. of Natural Sciences, HCC, City Univ. of New York, NY.*

include functional gene groupings related to apoptosis, cell cycle, cell growth and differentiation, signal transduction and other cancer related processes. Table 2 shows the genes that were modified in pesticide- and E-treated cells suggesting that these substances had the potency to cause malignant transformation of breast epithelial cells through modulation of expression of such genes.

These studies suggest that organophosphorous pesticides and estradiol induced changes in gene expression in the human breast epithelium influnce the carcinogenesis process.

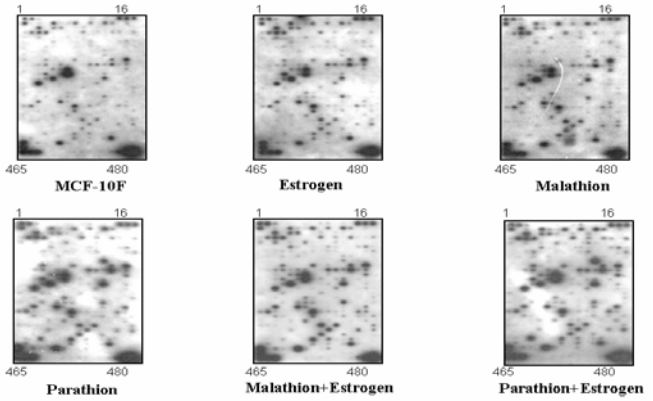

Fig. 2. Expression profile generated using the Oligo GEArray for Human Cancer (Cat. No. OHS-802). Image was recorded by a CCD camera-based imager. Expression of human oligo cancer microarray in the parental MCF-10F, estrogen, malathion, parathion, malathion + estrogen and parathion + estrogen-treated cells.

References

1. Falck A Jr, Ricci A Jr, Wolff MS, Godbold J and Deckers P. Pesticides and polychlorinated biphenyl residues in human breast lipids and their relation to breast cancer. *Arch Environ Health* **47**:143-6, 1992.
2. National Cancer Institute. Bioassay of Malathion for Possible Carcinogenicity. Technical Report Series No. 24. DHEW Publication No. (NIH) 78-824, 1978.
3. Kelsey JL and Bernstein L. Epidemiology and prevention of breast cancer. *Annu Rev Public Health* **17**:47-67, 1996.
4. Loeb LA. Mutator phenotype may be required for multistage carcinogenesis. *Cancer Res* **51**:3075-9, 1991.
5. Soule HD, Maloney TM, Wolman SR, Peterson WD Jr., Brenz R, McGrath CM, Russo J, Pauley RJ, Jones RF and Brooks SC. Isolation and characterization of a spontaneously immortalized human breast epithelial cell line, MCF-10. *Cancer Res* **50**:6075-86, 1990.
6. Calaf G, Roy D and Hei TK. Immunochemical analysis of protein in breast epithelial cells transformed by estrogens and high linear energy transfer (LET) radiation. *Histochem Cell Biol* **124**:261-74, 2005. ■

Table 2 – Human Cancer Microarray

Position	UniGene	Symbol	Description	FGG	MCF+10F	E	M	P	M+E	P+E
28	Hs.179735	ARHC	Ras homolog gene family, member C	Signal transduction pathway	(-)	(-)	↑	(-)	↑	↑
57	Hs.371468	CCND1	Cyclin D1 (PRAD1)	Cell cycle, cell growth and differentiation	(-)	↑	↑	↑	↑	↑
67	Hs.153752	CDC25B	Cell division cycle 25B	Cell cycle, cell growth and differentiation	(-)	↑	(-)	(-)	↑	(-)
71	Hs.95577	CDK4	Cyclin-dependent kinase 4	Cell cycle, cell growth and differentiation	(-)	↑	↑	↑	↑	↑
75	Hs.370771	CDKN1A	Cyclin-dependent kinase inhibitor 1 (p21, Cip1)	Cell cycle, cell growth and differentiation	(-)	(-)	↑	(-)	↑	↑
95	Hs.70312	COX7A2	Cytochrome c oxidase subunit VIIa polypeptide 2(I)	Other cancer-related genes	(-)	(-)	↑	(-)	↑	↑
116	Hs.74375	DVL1	Dishevelled, dsh homolog 1 (Drosophila) Dvs	Signal transduction pathway	(-)	(-)	↑	(-)	(-)	↑
183	Hs.76067	HSPB1	Heat shock 27kDa protein 1	Other cancer-related genes	(-)	(-)	↑	(-)	↑	↑
196	Hs.450230	IGFBP3	Insulin-like growth factor binding protein 3	Cell growth and differentiation	(-)	↑	↑	↑	↑	↑
199	Hs.512226	IGFBP5	Insulin-like growth factor binding protein 5	Cell growth and differentiation	(-)	↑	↑	↑	↑	↑
220	Hs.406013	KRT18	Keratin 18	Other cancer-related genes	(-)	(-)	↑	↑	↑	↑
244	Hs.57101	MCM2	MCM2 minichromosome maintenance deficient 2, mitot	Cell cycle	(-)	(-)	(-)	(-)	↑	↑
265	Hs.437922	MYCL1	V-myc myelocytomatosis viral oncogene homolog 1, I	Other cancer-related genes	(-)	(-)	(-)	↑	↑	↑
343	Hs.444499	REA	Repressor of estrogen receptor activity	Other cancer-related genes	(-)	↑	↑	↑	↑	↓
363	Hs.74335	HSPCB	Heat shock 90kDa protein 1, beta	Other cancer-related genes	(-)	↑	↑	↑	↑	↑
424	Hs.408312	TP53	Tumor protein p53 inducible protein 3	Cell cycle and apoptosis	(-)	↑	↑	(-)	(-)	(-)
426	Hs.50649	TP5313	Tumor protein, translationallycontrolled 1	Other cancer-related genes	(-)	(-)	(-)	(-)	↑	↑

FGG: Functional gene grouping. ↑ Arrow indicates the up-regulated expression of that gene with respect to control MCF-10F. ↓ Arrow indicates the down-regulated expression of that gene with respect to control MCF-10F. **(-)** Indicates no change in expression of that gene with respect to control MCF-10F.

Note: Both up regulated and down regulated by gene expression above or below 2-5 folds are taken into consideration.

Center for Radiological Research 2006 Departmental Picnic. (L-r): Dr. Tom K. Hei, Dr. Brain Ponnaiya**,** Dr. Eric J. Hall and Dr. Charles R. Geard.

Center for Radiological Research 2006 Departmental Picnic. (L-r): Dr. Burong Hu, Dr. Guangming Zhou and Dr. Yongliang Zhao.

Center for Radiological Research 2006 Departmental Picnic. (L-r): Dr. Yu-Chin Lien, Jayoung Yoon (Jaeyong's wife), Jaeyong Ahn, Aiping Zhu, Dr. Hongning Zhou and Dr. Corinne Leloup.

Dr. Vladmir Ivanov, associate research scientist, and Ms. Sarah Huang, a Ph.D student, celebrate their birthday.

Center for Radiological Research 2006 Christmas Party. (L-r): Gary Johnson, Mrs. Bernice Hall and Dr. Tom Hei.

Center for Radiological Research 2006 Christmas Party. (L-r): Cui-Xia Kuan, Jingjing Wu and Yu-Chin Lien.

Arsenic Induced Mitochondrial DNA Damage and Altered Mitochondrial Oxidative Function: Implication for Genotoxic Mechanism in Mammalian Cells

Michael A. Partridge, Sarah X.L. Huang, Evelyn Hernandez-Rosa,[a] Mercy P. Davidson[a] and Tom K. Hei

Introduction

Arsenic is an important environmental carcinogen that affects millions of people worldwide. In West Bengal, India, and Bangladesh alone, more than 35 million people are believed to be exposed to an arsenic concentration in drinking water exceeding 50µg/L, the maximum allowable limit in Bangladesh. Individuals chronically exposed to arsenic have a higher risk of developing skin, lung, liver, kidney and bladder cancers.[1] Although epidemiology studies have identified arsenic as a human carcinogen, the mechanism by which arsenic causes cancer is still poorly understood.[2] Given that millions of people are at risk worldwide, there is an urgent need to understand how arsenic mediates tumorigenesis.

Previous work from our laboratory had established that arsenic is a chromosomal mutagen,[3] and that normal mitochondrial function is required for the genotoxic response to arsenic.[4] Mitochondria are the energy generating organelles of the cell, and structural and functional abnormalities in mitochondria have been demonstrated in cancer cells.[5] Furthermore, mitochondria are a rich source of reactive oxygen species (ROS) and arsenic induced genotoxic effects are also dependent on ROS.[3,6] Mitochondria contain their own extranuclear DNA (mtDNA) which is a potentially susceptible target of various environmental mutagens/carcinogens, including arsenic. This circular genome lacks protective histones, has only a subset of the DNA repair systems available to nuclear DNA and exists inside the organelle in an environment of high oxidative stress.[7] Consequently, the basal mutation rate of mtDNA is high, and a rise in the ROS burden induced by arsenic exposure could further increase the rate of mutation. Therefore, we investigated the consequences of arsenic treatment on mitochondrial function and the role of mtDNA changes in mediating these effects.

[a] *Department of Neurology, College of Physcians & Surgeons, Columbia University, NY.*

Results

Arsenic induced nuclear DNA mutagenesis

In order to more accurately replicate normal environmental exposure conditions, we treated cells with arsenic doses of 1, 0.5 and 0.25µg/mL for up to 60 days and monitored genotoxicity ($CD59^-$ mutations) in the human-hamster A_L cells (CHO cells stably expressing human chromosome 11). Consistent with our previous data, arsenic treatment of A_L cells resulted in a dose dependent increase in mutation frequency (Fig. 1A), measured by the loss of the CD59 cell surface antigen which is encoded by human chromosome 11.[3] Arsenic treatment also caused an almost three-fold increase in the number of micronuclei observed in A_L cells (untreated: 11.6 +/- 2.2%; treated: 32.6 +/- 1.9%) treated for 60 days (Fig. 1B), providing further evidence that arsenic exposure resulted in genomic instability.

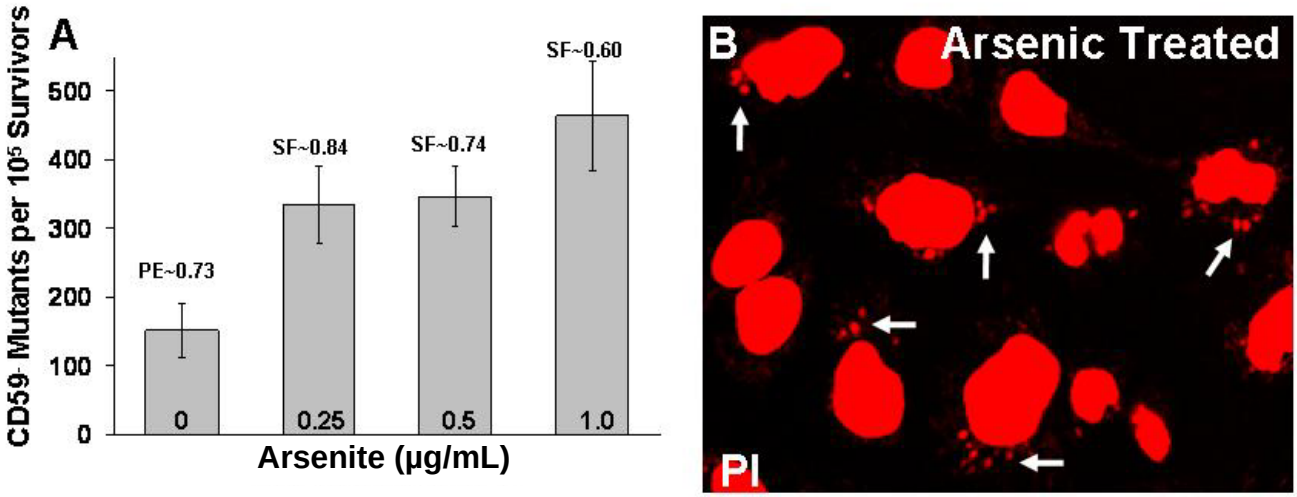

Fig. 1. Cells exposed to arsenic have an increase in both $CD59^-$ mutations and the incidence of micronuclei. **A.** A_L cells exposed to graded doses of sodium arsenite for the indicated times were assessed for mutations at the $CD59^-$ locus. Data are pooled from 3 experiments. PE, plating efficiency. SF, surviving fraction when compared to untreated A_L cells. Bars, +/- SD. **B.** Arsenic treated A_L cells were stained with propidium iodide to visualize the nucleus. Arrows indicate micronuclei formation in arsenic treated cells.

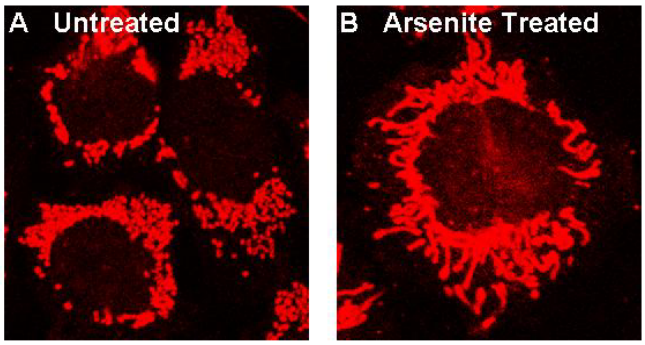

Fig. 2. Sodium arsenite treatment alters the morphology of mitochondria in A_L cells. **A.** Pyruvate dehydrogenase (PDH) staining of untreated cells. **B.** Cells treated with sodium arsenite (1μg/mL) for 60 days.

Mitochondrial oxidative function

Given our previous findings that normal mitochondrial function was required to mediate the genotoxicity of arsenic,[4] we analyzed changes in the morphology of the mitochondria in A_L cells after arsenic treatment by staining cells with an antibody to the mitochondrial enzyme pyruvate dehyrdogenase and examined the cells by fluorescence microscopy. The mitochondria of untreated cells maintained a compact, punctate structure in the perinuclear region with an approximately uniform number of mitochondria from cell to cell (Fig. 2A). In contrast, cultures exposed to arsenic had a distribution of mitochondria that varied considerably between cells and exhibited a dramatically elongated or filamentous morphology (Fig. 2B).

Having identified a change in mitochondrial phenotype, we examined the effect of arsenic on mitochondrial metabolic activity. Cytochrome *c* oxidase (COX) is a 13 subunit enzyme located in the inner mitochondrial membrane. Also known as complex IV in the respiratory chain, COX activity is routinely used as a measure of mitochondrial metabolic function. Interestingly, biochemical analysis of lysates from clonal isolates of arsenic treated and untreated A_L cells revealed that COX activity was reduced by almost 45% after sodium arsenite treatment for 60 days (Fig. 3) indicating that mitochondrial respiration was reduced after arsenic treatment.

Mitochondrial DNA alterations

Cytochrome c oxidase is a complex with 3 of its 13 subunits encoded by mitochondrial DNA.[8] It was possible that the decrease in COX activity after arsenic treatment resulted from mtDNA damage. There are at least two ways in which mtDNA could be altered after arsenic treatment; by depleting the copy number or by deleting sections of the genome.

To test for reduction in mtDNA copy number we performed real-time quantitative PCR. Segments from both mtDNA and nuclear DNA (nDNA) were amplified and the relative mtDNA to nDNA ratio assessed in arsenic treated cells compared to untreated controls. Interestingly, after 60 days of arsenic treatment, mtDNA copy number was reduced to less than 65% of untreated levels. This effect was dose dependent, and was observed in cells exposed to arsenic concentration of 0.5μg/mL. Mitochondrial DNA copy number was also reduced in cells treated with arsenic at 0.25μg/mL, although the effect at this dose was not statistically significant (Fig. 4A).

In an initial screen to identify mtDNA deletions using long extension PCR, we were unable to detect deletions that represented a substantial fraction of the genome. We then used a more sensitive method to detect rare heteroplasmic mtDNA deletions. In humans, a PCR-based technique had been developed to detect heteroplasmic deletions that exploited the physical characteristics of a circular mtDNA molecule containing a large deleted fragment.[9] Primer annealing sites in wild type mtDNA that were thousands of base pairs apart would be substantially closer together after deletion of the intervening sequence and re-circularization of the genome. Using short extension times (30 seconds), sequences flanking the deleted fragment would be selectively amplified, even when present as a fraction of the total mtDNA copy number. In humans, the vast majority of mtDNA deletions that have been identified thus far occur between tandem repeats, including the "common" deletion.[10] Using a pair of nested primers sets, the PCR procedure for detecting the "common" deletion in humans was adapted to hamster mtDNA in an attempt to identify large deletions.

Duplicate cultures were exposed to 0.25, 0.5 and 1μg/mL arsenic for 30 days and analyzed for deletions using two different sets of nested primers. Surprisingly, after arsenic exposure large heteroplasmic deletions were detected by PCR amplification of fragments in A_L cell mtDNA that were not found in untreated cells (Fig. 4B). Deletions were observed even after short (24 hours) treatment times with relatively low concentrations (0.25μg/mL) of arsenic (not shown). Unexpectedly, when we repeatedly assayed a single DNA sample extracted from an exposed culture, we identified many different deletion products, indicating that multiple, possibly single copy, deletions were induced by arsenic treatment. Consistent with this finding, the DNA from the same continuously cultured cells when analyzed after 60 days of arsenic exposure displayed deletions that were not detected after 30 days of treatment (not shown). Deletions

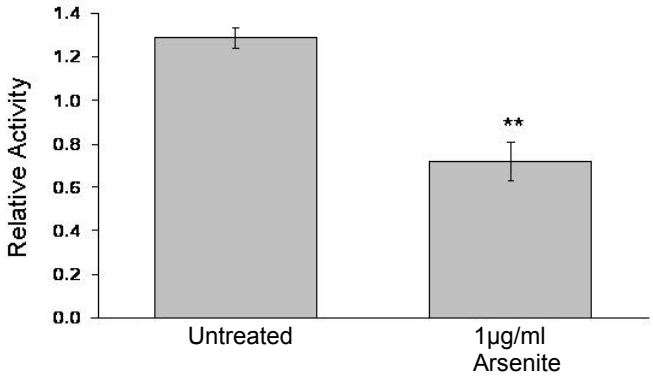

Fig. 3. Treatment of A_L cells with sodium arsenite decreases cytochrome c oxidase (COX) function. Lysates from cells treated with arsenic (1μg/mL) for 60 days were tested for COX function by measuring the quantity of cytochrome *c* (nmol) oxidized/min/mg protein. Data are averaged from duplicate determinations from at least 5 clones. ** = $P < 0.005$, Student's *t*-test.

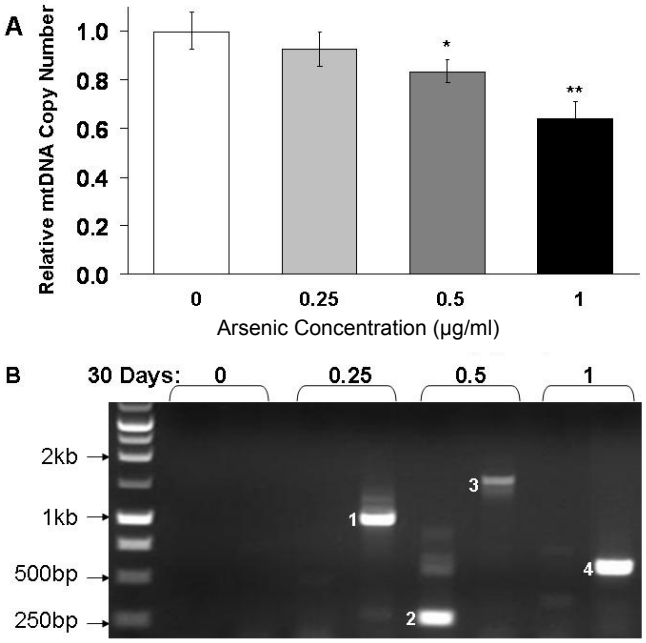

Fig. 4. Mitochondria DNA is depleted and large heteroplasmic deletions occur after sodium arsenite treatment. **A.** mtDNA copy number was determined by comparing the ratio of mtDNA to nuclear DNA amplified using real time quantitative PCR on extracts from cells exposed to arsenite for 60 days as well as controls. Data are averages (+/- SD) of 2 experiments performed on extracts from each of 2 independent cell cultures. * = $P < 0.05$, ** = $P < 0.005$, Student's *t*-test compared to untreated controls. **B.** 0.9% agarose gel of PCR products from second round of amplification of a nested PCR using DNA from A_L cells treated with arsenic for 60 days at the indicated doses as a template for the first round of PCR. Duplicate cultures were screened for each treatment condition. First round of nested PCR performed with primers 6123 sense + 14617 antisense using DNA isolated from cultures as a template. No products were visible (data not shown). The second round of PCR was performed with primers 6716 sense + 14154 antisense and 1µL of first reaction used as a template.

were also not detected in arsenic treated ρ0 A_L cells, indicating that they were not due to pseudogenes present in nuclear DNA (not shown).

Discussion

In this study we observed a reduction in mtDNA copy number, an increased incidence of large heteroplasmic deletions, a reduction of COX activity and an increase in citrate synthase activity, indications that mitochondrial replication and function were abnormal after arsenic treatment. This suggests that exposed cells have moved from an oxidative toward a glycolytic metabolic state. Interestingly, the Warburg theory, advanced many decades ago,[5] implies that cancer cells also have impaired mitochondrial function and increased glycolysis. In addition, the "mitochondrial dysfunction hypothesis" contends that the three deleterious features (increased oxidative stress, energy deprivation and mtDNA damage) contribute to a degenerative cycle and thus compound the effect of each of the other factors individually.[11] At least two of these factors, increased ROS and mtDNA depletion, have been previously implicated in DNA damage and genotoxicity after arsenic exposure.[3,12] In addition to our previous work, we have now demonstrated here that all three factors (including mitochondrial dysfunction, mtDNA depletion and induction of mtDNA deletions) are observed after arsenic treatment of cells and it is possible that a related degenerative cycle of mitochondrial dysfunction may contribute to the carcinogenicity of arsenic in humans. These data support the theory that the mitochondria, and particularly mtDNA, are important mediators of the mutagenic effects of arsenic in mammalian cells.

Our initial experiments confirmed that arsenic was a genotoxic mutagen[4] and also induced genomic instability, measured by an increase in micronuclei. In addition to examining nuclear genotoxicity, we wanted to understand the effects of arsenic on mitochondrial respiratory chain function and, in particular, whether arsenic induced damage in mtDNA. Biochemical analysis on arsenic treated cells revealed that COX activity decreased by nearly 45% after treatment. This was consistent with our previous observation that arsenic induced the formation of peroxynitrites,[4] as these molecules inhibit COX (complex IV), as well as complexes I, II, and V.[13]

We and others have shown that direct mutations to specific nuclear genes (CD59), as well as genomic instability (micronucleus formation), was clearly induced by arsenic exposure and these effects could be ameliorated by reducing the levels of ROS in the cell.[3,14] These findings, combined with the decrease in COX activity in arsenic treated cells, prompted us to examine the integrity of the mitochondrial genome.

There are many hundreds of copies of the mitochondrial genome in any given cell and a reduction in copy number may affect the expression level of the three COX subunits encoded by mtDNA. In our experiments, we observed a clear decrease in the ratio of mtDNA to nuclear DNA after arsenic treatment in a dose-dependent manner. This is probably due to changes in function or expression of DNA polymerase-γ, the polymerase responsible for the replication and repair of mtDNA, as this polymerase is susceptible to oxidative damage *in vitro*[15] and mRNA expression is known to decrease in arsenic exposed cells.[16]

Perhaps the most interesting finding was the evidence that large heteroplasmic deletions in the mitochondrial genome were induced by arsenic exposure. The genome was apparently subjected to repeated damage, as a number of unique deletions were detected in mtDNA from each sample, as well as mtDNA extracted at different times from the same continuously cultured cell line. The detection of deletions in arsenic treated cells likely reveals an increase in the incidence of these mutations after exposure, not their complete absence in unexposed cells. The ability to detect deletions in treated cells may be explained by a number of factors; increased ROS resulting in more double strand breaks, decreased DNA repair capacity or a lower mitotic index. Our data indicate that the mitochondrial genome was subjected to repeated and continuous damage when exposed to arsenic.

Arsenic is an important environmental contaminant that affects millions of people worldwide. Our present findings

illustrate that mitochondria are a primary target in arsenic toxicity and provide a basis for better interventional approaches in both treatment and prevention of arsenic-induced human diseases.

References

1. Smith AH, Lingas EO and Rahman M. Contamination of drinking-water by arsenic in Bangladesh: a public health emergency. *Bull World Health Organ* **78**:1093-103, 2000.
2. Ahsan H, Chen Y, Parvez F, Argos M, Hussain AI, Momotaj H, Levy D, van Geen A, Howe G and Graziano J. Health Effects of Arsenic Longitudinal Study (HEALS): description of a multidisciplinary epidemiologic investigation. *J Expo Sci Environ Epidemiol* **16**:191-205, 2006.
3. Hei TK, Liu SX and Waldren C. Mutagenicity of arsenic in mammalian cells: role of reactive oxygen species. *Proc Natl Acad Sci U S A* **95**:8103-7, 1998.
4. Liu SX, Davidson MM, Tang X, Walker WF, Athar M, Ivanov V and Hei TK. Mitochondrial damage mediates genotoxicity of arsenic in mammalian cells. *Cancer Res* **65**:3236-42, 2005.
5. Warburg O. On respiratory impairment in cancer cells. *Science* **124**:269-70, 1956.
6. Liu SX, Athar M, Lippai I, Waldren C and Hei TK. Induction of oxyradicals by arsenic: implication for mechanism of genotoxicity. *Proc Natl Acad Sci U S A* **98**:1643-8, 2001.
7. Croteau DL, Stierum RH and Bohr VA. Mitochondrial DNA repair pathways. *Mutat Res* **434**:137-48, 1999.
8. Dimauro S and Davidzon G. Mitochondrial DNA and disease. *Ann Med* **37**:222-32, 2005.
9. Soong NW and Arnheim N. Detection and quantification of mitochondrial DNA deletions. *Methods Enzymol* **264**:421-31, 1996.
10. MITOMAP A Human Mitochondrial Genome Database. http://www.mitomap.org. 2006.
11. Lewis W, Copeland WC and Day BJ. Mitochondrial dna depletion, oxidative stress, and mutation: mechanisms of dysfunction from nucleoside reverse transcriptase inhibitors. *Lab Invest* **81**:777-90, 2001.
12. Delsite RL, Rasmussen LJ, Rasmussen AK, Kalen A, Goswami PC and Singh KK. Mitochondrial impairment is accompanied by impaired oxidative DNA repair in the nucleus. *Mutagenesis* **18**:497-503, 2003.
13. Brown GC. Nitric oxide as a competitive inhibitor of oxygen consumption in the mitochondrial respiratory chain. *Acta Physiol Scand* **168**:667-74, 2000.
14. Wang TS and Huang H. Active oxygen species are involved in the induction of micronuclei by arsenite in XRS-5 cells. *Mutagenesis* **9**:253-7, 1994.
15. Graziewicz MA, Day BJ and Copeland WC. The mitochondrial DNA polymerase as a target of oxidative damage. *Nucleic Acids Res* **30**:2817-24, 2002.
16. Andrew AS, Warren AJ, Barchowsky A, Temple KA, Klei L, Soucy NV, O'Hara KA and Hamilton JW. Genomic and proteomic profiling of responses to toxic metals in human lung cells. *Environ Health Perspect* **111**:825-35, 2003. ■

Immortalization of Primary Human Prostate Epithelial Cells by Telomerase

Yongliang Zhao, Genze Shao, Gloria J. Baker, Adayabalam S. Balajee and Tom K. Hei

Cellular senescence or replicative senescence is an irreversible arrest of cellular growth that occurs in normal human somatic cells and has been suggested to be a major barrier against cancerous transformation. The ability to overcome senescence and to obtain an unlimited replicative potential (termed "immortalization) is one of the prerequisites for cancer formation.[1-3] The telomere model postulates that progressive shortening of telomeres with each cell division limits replicative life span in most human somatic cells. Consequently, cellular senescence can be circumvented if telomere shortening is prevented.[2,3]

Telomerase is a RNA-dependent DNA polymerase containing a RNA template for telomere synthesis and a catalytic protein subunit with reverse transcriptase activity (hTERT). The hTERT is tightly suppressed in most types of normal human somatic cells and is upregulated in over 90% of cancerous cells and *in vitro* immortalized cells.[4,5] Ectopic expression of hTERT in telomerase-negative normal cells is sufficient to induce telomerase activity and immortalize a number of normal human cell types.[4,6,7] Furthermore, inhibition of telomerase activity leads to senescence or apoptosis in tumor cells, suggesting that telomerase expression in immortal cancer cells apparently is responsible for their maintenance of a stable telomere length through an indefinite number of cell division.[6,7] However, telomerase activation may not apply to all cell types. A mechanism called alternate lengthening of telomeres (ALT) exists to maintain telomere length in some immortalized and cancer cells.[8]

Prostate cancer is one of the leading causes of cancer death in the male population around the world with approximately 232,090 new cases of prostate cancer being diagnosized in the USA in 2005 alone.[9] Unlike the relatively common somatic genetic alterations observed in colon cancer, such as *p53* and *K-ras* mutations, the molecular patho-

genesis of prostate cancer displays a great deal of heterogeneity both between individuals as well as within an affected organ.[10] Thus *in vitro* prostate epithelial cell culture systems will provide very useful models in delineating the genetic alterations, especially early events, responsible for prostate tumor progression. However, all of the currently available immortalized prostate epithelial cell lines are derived using either oncogene or oncogenic viruses which render them genomically unstable and unsuitable for the study of early events responsible for prostate cancer progression.[11,12] Thus, use of hTERT to immortalize normal prostate epithelial cells provides a much better alternative. However, it has previously been reported that forced expression of hTERT failed to immortalize normal prostate epithelial cells.[12] In this study, we demonstrated that normal human prostate epithelial cells (PrEC) can be immortalized by introduction of hTERT. In addition, decreased expression of $p16^{INK4a}$ is involved in the immortalization process.

Immortalization of human normal PrEC cells by hTERT

To establish an immortalized cell line with human prostate epithelium-origin, normal prostate epithelial cells at PD2 were transfected with retrovirus vector containing hTERT (pLNCX2-neo-hTERT) or a control vector expressing only the drug selection marker gene (pLNCX2-neo). Transfected cells were selected and grown continuously in medium containing 100μg/ml G418. Since hTERT alone had previously been shown to immortalize human normal fibroblasts,[4] human prostate stromal cells were similarly transfected with retrovirus vectors to test the efficiency of transfection of our hTERT vector. Two immortal mass cultures, PrEC-hTERT and PrSC-hTERT, were established after hTERT retrovirus transfection. The population doubling (PD) times of hTERT-transfected PrEC cells compared with vector-transfected PrEC cells are presented in Figure 1a. As expected, vector-transfected PrEC cells underwent replicative senescence by PD12, as evidenced by a lack of increase in cell number accompanied by enlargement and flat morphology of cells in the culture. The replicative senesscence was further confirmed by staining for proliferative marker Ki67 (Fig. 1c). Untransduced parental PrEC cells senesced after approximately the same number of cumulative PD. In contrast to vector-transduced cells, proliferation of hTERT-expressing PrEC cells at PD12 was severely inhibited but not completely arrested, and entered a slow growth phase (SGP).[6] The SGP lasted around 36 days after which uniformly small-sized cells emerged and gradually overtook the entire culture (Fig. 1c). These small and hTERT-expressing cells had a higher proliferation potential as demonstrated by Ki67 staining (Fig. 1c), retained the characteristic epithelial cell morphology and displayed contact-inhibited growth typical of early-passaged, parental PrEC cells (Fig. 1c). However, their population growth rate was much higher than that of the parental cells (Fig. 1b). Thus far, the hTERT-transduced PrEC cells have continuously been grown for more than PD130 and the replicative lifespan has been extended for at least ten times compared with vector-transfected cells. Therefore, these cells were truly immortal. Control PrSC cells transduced with empty vector ceased proliferation (senescence) at around PD24, whereas hTERT-expressing PrSC cells (PrSC-hTERT) continued to divide rapidly without any sign of senescence well over PD110 which is largely beyond the normal limit of their parental cells, and are immortal as well (data not shown).

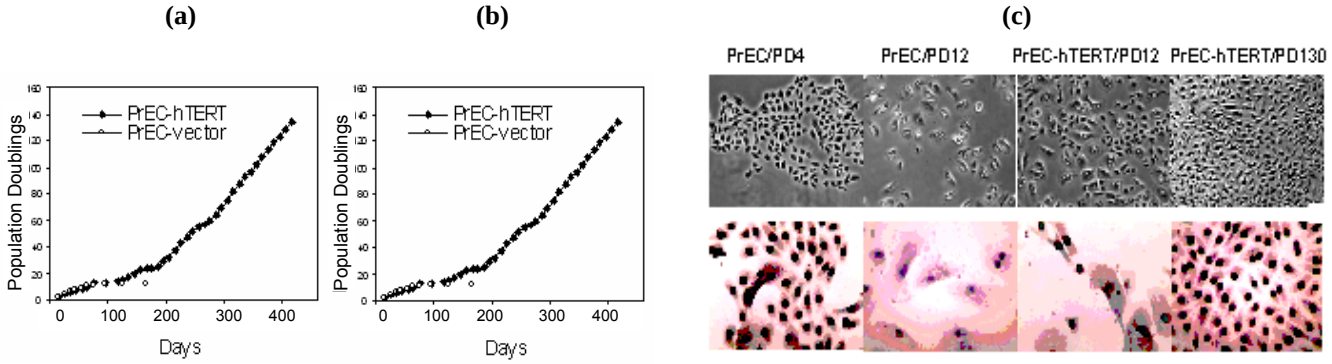

Fig. 1. Growth characteristics of vector and hTERT-transduced human PrEC cells. Normal human prostate epithelial cells (PrEC), normal prostate stromal fibroblast cells (PrSC) were purchased from Clonetics BioWhittaker (Walkersville, MD). **(a)** Cumulative population doubling versus time. pLNCX2-neo-hTERT retroviral vector was generated by digesting whole length cDNA of hTERT from pZeoSV2-hTERT construct using HindIII and NotI restriction sites[13] and cloning into pLNCX2-neo retroviral vector (BD Biosciences Clontech). To create polytropic retroviruses, PT67 packaging cells were transfected with pLNCX2-neo-hTERT and pLNCX2-neo by Lipofectamine Plus reagent (Gibco, Grand Island, NY) and selected with 300μg/ml G418 (Gibco). Stable virus-producing cell lines were then established from large and healthy G418-resistant colonies and used for generating retroviral supernatants. Exponentially-growing PrEC cells at PD2 were transfected with retroviral supernatants in the presence of polybrene (4μg/ml, Sigma). The virus was then removed after 24h, and selection with 300μg/ml of G418 (Gibco) was started 48h after transfection and continued for 2-3 weeks. Retroviral vectors carrying only drug resistance genes were used as control. PD0 is defined as the time of retroviral infection. PrEC cells lacking hTERT (open circle) senesced and ceased to proliferate at PD12. PrEC-hTERT cells entered a slow growth phase (SGP) at around PD12 and restart to grow rapidly at later PDs. (**b**) Growth curves of PrEC-hTERT cells at PD130 and parental PrEC cells at PD4. (**c**) Morphology changes and proliferative potential of parental and hTERT-transduced PrEC cells at different PDs. The cells grown on chamber slides were immunostained with Ki67 (1:100, Lab Vision, CA) by Vestastain Elite ABC kit and counterstained with Meyer's hematoxylin.

Telomerase activity and telomere length measurements

To ascertain whether the hTERT-transfected cells exhibit telomerase activity and telomere stability, telomerase activity and telomere length were measured in PrEC-hTERT and PrSC-hTERT cells using a telomeric repeat amplification protocol (TRAP) assay and the terminal restriction fragment length (TRL) assay, respectively. Primary cultures of PrEC and PrSC cells did not show any telomerase activity. However, transfection of hTERT conferred telomerase activity on the immortal PrEC-hTERT and PrSC-hTERT cells (Fig. 2a, b). In addition, hTERT-immortalized PrEC and PrSC cells acquired and maintained relatively long telomeres with lengths of ~12kb and ~10kb, respectively, compared with the relatively shorter telomeres (~5kb and ~6 kb, respectively) found in the later-PD of control cells (Fig. 2a, b).

In order to determine chromosomal stability in hTERT-immortalized cells, M-FISH analysis was performed on metaphase spreads prepared from PD20 and PD130 cells. Karyotypic chromosomes painted by M-FISH were analyzed in 10-13 well spread metaphases. Both PD20 and PD130 cells displayed a near diploid complement of chromosomes with occasional loss or gain involving chromosomes 5, 9, 10, 17 and 20. In addition, translocation involving chromosomes 9 and 17 was observed in 85% of the metaphases while 15% of the metaphases showed translocation involving chromosomes 6 and 16 in PD20 and PD130 cells. A representative chromosome karyotype is shown in Figure 3.

Telomerase activation is strongly associated with human malignancies including prostate cancer and has facilitated experimental studies in the immortalization of a variety of primary human cells.[4,6,7,14] Use of hTERT to immortalize normal human prostate epithelial cells has advantages for the following reasons. First, it is of particular relevance to clinical findings that over 90% of prostate cancer patients have high levels of telomerase activity, whereas the majority of clinically confirmed benign prostatic hyperplasia does not express any telomerase activity.[15] Second, unlike virally immortalized cells, hTERT-immortalized normal human somatic cells maintain near normal karyotypes and continue to respond in the same manner as pre-senescent, non-immortalized cells to DNA damage insults such as due to γ-irradiation.[16] In the present study, primary human prostate epithelial cells are shown to achieve immortalization by the introduction of telomerase activity. These immortal cells are genotypically stable and express human cytokeratins. In addition, they are anchorage dependent and do not form tumors in immunosuppressed host animals. As primary cells have a finite life-span, the hTERT-immortalized prostate epithelial cells is expected to provide a valuable tool for prolonged molecular and biomedical studies related to progression of prostate cancer.

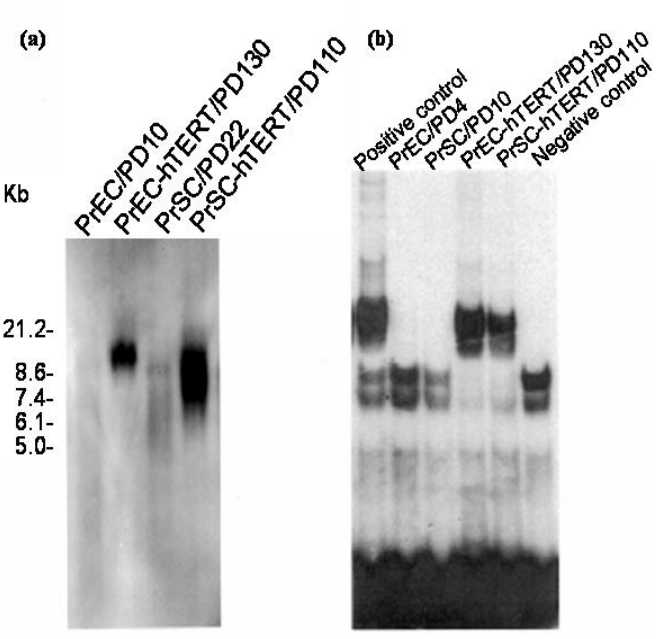

Fig. 2. Telomere length and telomerase activity in the parental and hTERT-immortalized cells determined by telomeric repeat amplification protocol (TRAP) assay and terminal restriction fragment length (TRL) assay. Both hTERT-immortalized PrEC and PrSC cells maintained a longer telomere length (a) and higher telomerase activity (b) relative to their parental cells.

References

1. Hanahan D and Weinberg RA. The hallmarks of cancer. *Cell* **100**:57-70, 2000.
2. Shay JW and Wright WE. Aging. When do telomeres matter? *Science* **291**:839-40, 2001.
3. Stewart SA and Weinberg RA. Telomerase and human tumorigenesis. *Semin Cancer Biol* **10**:399-406, 2000.
4. Bodnar AG, Ouellette M, Frolkis M, Holt SE, Chiu CP, Morin GB, Harley CB, Shay JW, Lichtsteiner S and Wright WE. Extension of life-span by introduction of telomerase into normal human cells. *Science* **279**:349-52, 1998.
5. Kim NW, Piatyszek MA, Prowse KR, Harley CB, West MD, Ho PL, Coviello GM, Wright WE, Weinrich SL and Shay JW. Specific association of human telomerase activity with immortal cells and cancer. *Science* **266**:2011-5, 1994.
6. Dickson MA, Hahn WC, Ino Y, Ronfard V, Wu JY, Weinberg RA, Louis DN, Li FP and Rheinwald JG. Human keratinocytes that express hTERT and also bypass a p16(INK4a)-enforced mechanism that limits life span become immortal yet retain normal growth and differentiation characteristics. *Mol Cell Biol* **20**:1436-47, 2000.
7. Hahn WC. Immortalization and transformation of human cells. *Mol Cells* **13**:351-61, 2002.
8. Bryan TM, Englezou A, Gupta J, Bacchetti S and Reddel RR. Telomere elongation in immortal human cells without detectable telomerase activity. *Embo J* **14**:4240-8, 1995.
9. Jemal A, Murray T, Ward E, Samuels A, Tiwari RC, Ghafoor A, Feuer EJ and Thun MJ. Cancer statistics, 2005. *CA Cancer J Clin* **55**:10-30, 2005.
10. Palapattu GS, Sutcliffe S, Bastian PJ, Platz EA, De Marzo AM, Isaacs WB and Nelson WG. Prostate carcinogenesis and inflammation: emerging insights. *Carcinogenesis* **26**:1170-81, 2005.

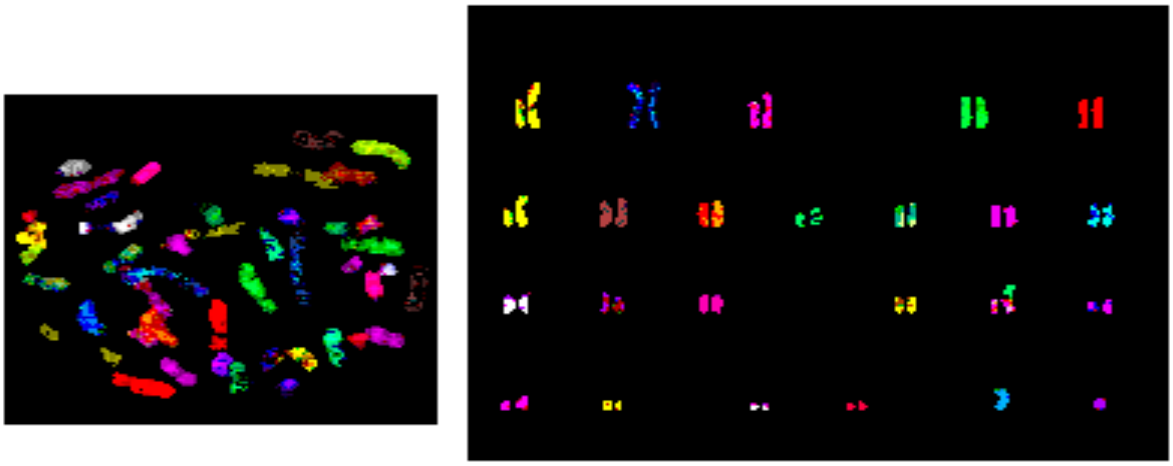

Fig. 3. Representative karyotype from M-FISH analysis in hTERT-immortalized PrEC cells. A cocktail of DNA probes specific for all the human chromosomes (24XCyte, Metasystems) was purchased from MetaSystems (Belmont, MA). M-FISH and post-hybridization washings were performed following the manufacturer's specifications. Images were captured using a Nikon Axioplan fluorescence microscope and the metaphases were analyzed using Metasystems software. A near-diploid number of chromosomes and a stable translocation involving 9p and 17p were demonstrated in majority of metaphases analyzed in PD20 and PD130 cells.

11. Choo CK, Ling MT, Chan KW, Tsao SW, Zheng Z, Zhang D, Chan LC and Wong YC. Immortalization of human prostate epithelial cells by HPV 16 E6/E7 open reading frames. *Prostate* **40**:150-8, 1999.
12. Gil J, Kerai P, Lleonart M, Bernard D, Cigudosa JC, Peters G, Carnero A and Beach D. Immortalization of primary human prostate epithelial cells by c-Myc. *Cancer Res* **65**:2179-85, 2005.
13. Piao CQ, Liu L, Zhao YL, Balajee AS, Suzuki M and Hei TK. Immortalization of human small airway epithelial cells by ectopic expression of telomerase. *Carcinogenesis* **26**:725-31, 2005.
14. Ramirez RD, Sheridan S, Girard L, Sato M, Kim Y, Pollack J, Peyton M, Zou Y, Kurie JM, Dimaio JM, *et al.* Immortalization of human bronchial epithelial cells in the absence of viral oncoproteins. *Cancer Res* **64**:9027-34, 2004.
15. Caldarera E, Crooks NH, Muir GH, Pavone-Macaluso M and Carmichael PL. An appraisal of telomerase activity in benign prostatic hyperplasia. *Prostate* **45**:267-70, 2000.
16. Morales CP, Holt SE, Ouellette M, Kaur KJ, Yan Y, Wilson KS, White MA, Wright WE and Shay JW. Absence of cancer-associated changes in human fibroblasts immortalized with telomerase. *Nat Genet* **21**:115-8, 1999. ■

Immortalized Human Small Airway Epithelial Cells Transformed By Arsenic *in Vitro*

Gengyun Wen, Gloria M. Calaf,[a] Michael A. Partridge, Yongliang Zhao, Xuelian S.Huang, Yunfei Chai and Tom K. Hei

Although inorganic arsenic has been recognized as a human carcinogen for over 100 years, scientists have been unable to elucidate the mechanisms of carcinogenesis in humans. Therefore, developing models of inorganic arsenic carcinogenesis is crucial to characterizing how arsenic affected human cells become transformed, in order to develop effective treatments.

Previous human epithelial cell lines used for arsenic transformation and carcinogenesis study were established by incorporation of a virus and other genes to immortalize the cells.[1,2] It can be argued that these factors may interfere with the genomic stability and intracellular signalling which may facilitate increased transformation. The h-TERT immortalized human small airway epithelial cells, which were established in our lab, has the characteristics as well as advantages that were discussed earlier.[3] In the present study we have developed a model system to study the ability of inorganic arsenic to induce transformation in culture as an *in vitro* model of carcinogenesis. After 8 months arsenic continuously treatment at 0.5µg/ml, we have characterized the following changes:

[a] *Institute for Advanced Research and Research Center for the Man in the Desert, Tarapaca University, Arica, Chile.*

Growth kinetics and plating efficiency

The h-TERT immortalized SAEC cells grew as a contact-inhibited monolayer with a population doubling time of ~24h. At confluency, these cells had a saturation density of ~2.5×10^6 cells/60mm dish, as shown in Figure 1A. The cells were treated with sodium arsenite at 0.5µg/ml for approximately 28 weeks and changes in growth kinetics were observed. The population doubling time of the SAEC-A0.5 cells were similar to the control cell SAEC yet its saturation density considerably increased up to 3.3×10^6/dish, suggesting that arsenic exposed cells were able to partially overcome contact inhibition, a characteristic of transformed cells. Furthermore, SAEC-A0.5 cells had a much higher plating efficiency than SAEC cells as seen in Figure 1B.

Anchorage-independent growth

Anchorage-independence growth usually correlates strongly with invasiveness in many cell types. Our data demonstrated that only SAEC-A0.5 cells formed agar-positive clones, with a rate more than 5% as shown in Figure 1C.

Genomic instability

These results demonstrate that SAEC-A0.5 cells exhibited a much higher frequency in forming PALA resistant clones in comparison to SAEC control cells, indicating that

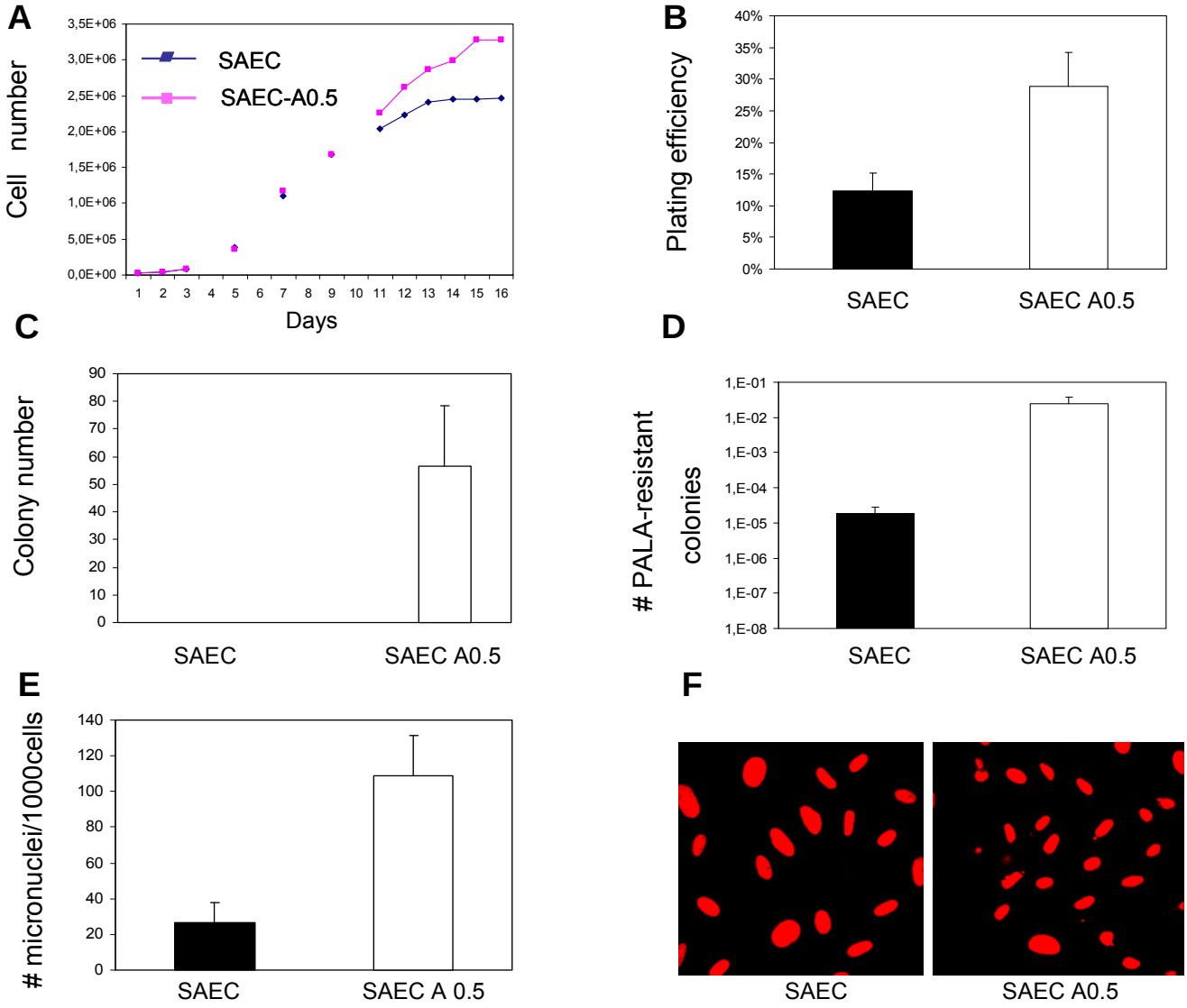

Fig. 1. A. Growth kinetics and **B.** plating efficiency of SAEC cells and SAEC-A0.5 cells in SAGM medium. Data shown are the mean of triplicates. Bars represent ± SD. See details in Methods and Materials. **C.** Colony number: 1 x 10^3 cells in 1 ml of 0.35% agarose were overlaid on a 0.7% agar base in a 24-well culture plate. Cultures were fed every 3 days and colonies with >50 cells were scored after 4 weeks in cultures under a dissecting microscope. The experiment was carried out in triplicate. Bars represent ± SD. **D.** PALA-resistant colonies: Frequency determined at a concentration of 180 µM PALA that corresponds to nine times the LD_{50} of SAEC-A0.5 (data not shown): Data are pooled from three independent experiments. Bars represent ± SD. **E.** Micronuclei formation: cells were incubated with cytochalasin-B (3µg/ml) for 24h. After a hypotonic shock in 0.075 M KCl, cells were stained with acridine orange and examined with a fluorescence microscope under UV light. BN cells with MN were counted with three independent experiments involving 1000 cells. Bars represent ± SD. **F.** Representative images of SAEC cells and SAEC-A0.5 where micronuclei can be observed.

arsenic indeed induced genomic instability in the SAEC cells (Fig. 1D). Transformation/carcinogenesis is a multi-stage process. The importance of maintaining genomic stability is evidenced by the fact that transformed cells often contain a variety of chromosomal abnormalities such as euploidy, translocations, and inversions. Genomic instability induced by chemicals or drugs may contribute to transformation with accumulating genetic changes and ultimately lead to malignant conversion. The micronuclei assay was used as a measure of genotoxicity of arsenic in this study. When cells were analyzed for cell micronuclei formation there was a 4.8 fold increase in micronuclei structures in SAEC-A0.5 cells in comparison to control cells as seen in Figure 1E. Such rate was substantially increased to more than 10%,

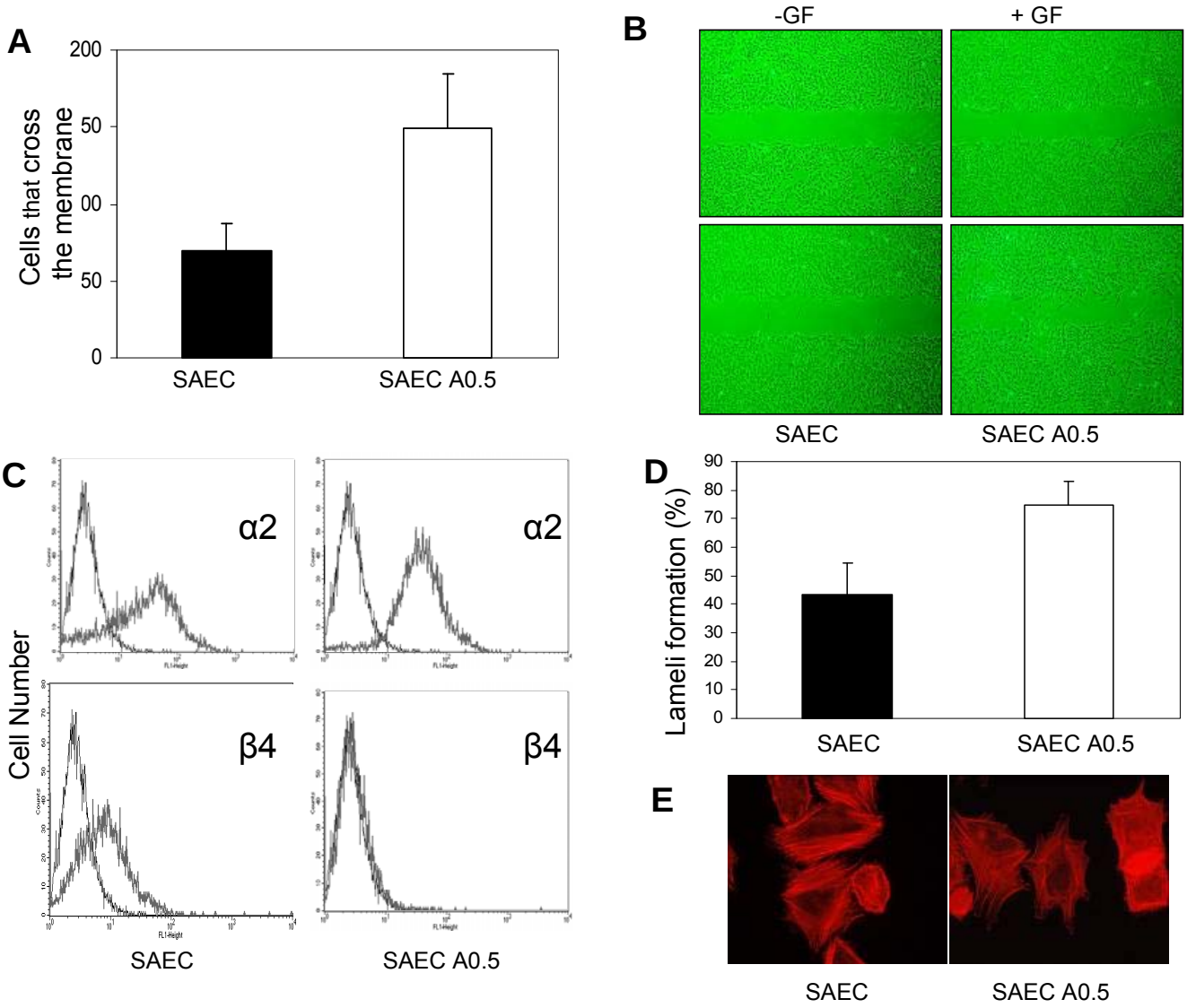

Fig. 2. A. Invasion assay: $1x10^5$ cells were added to the upper compartment of the chamber. Growth factors added in the medium (complete medium) were used as chemo-attractant and placed in the lower chamber. After incubation for 23 h at 37°C in a 5% CO_2 incubator, the cells on the upper surface of the filter were completely removed by wiping with a cotton swab and the cells that had crossed the matrigel and attached to the lower surface of the filter were studied. The filters were fixed, stained with Diff Quick (Sigma Chemical Co.), cut out and mounted on glass slides. The three fields of cell number that crossed the membrane were counted under a light microscope and calculated the average value. Experiments were performed three times with 4 chambers/cell line. Bars represent ± SE. **B.** *in vitro* wound-healing assay: "wound" was created by loading tips as described in Methods and Materials. Images were captured 18 hours after adding the growth factors in both SAEC and SAEC-A0.5 cells. The "wound" closing trend was compared between the two type of cells upon the growth factors' addition. **C.** Surface expression of integrin receptors on arsenic treated SAE cells and controls. Fluorescence flow-cytometry analysis of surface expression of two endogenous integrins, the laminin receptor anti-α2 and the collagen receptor anti-β4, in arsenic treated and untreated SAE cells determined by staining with the correspondent antibodies (BD), respectively. **D.** Rate of lamellipodia formation was compared between SAEC and SAEC-A0.5 cells by scoring the number of cells which actively form lamellipodia. 500 cells in three different coverslips were scored and recorded under a Fluorescence microscope, percentage of cells with lamellipodia was calculated. Bars represent ± SD. **E.** Fluorescence microscopy of phalloidin stained SAEC and SAEC-A0.5 cells. Cells were grown on glass coverslips for 24 hours, fixed and labeled with Rhodamine-phalloidin to visualize actin filaments. Arrows point to lamellipodia areas. Magnification 600x.

contrasting to the 3% micronuclei rate of SAEC control cells, suggesting that chronic arsenic treatment caused the human small airway epithelial cell genome to become unstable. Figure 1F represents normal SAEC (a) and SAEC A0.5 (b) cells in which micronuclei can be observed.

Invasive capability

Figure 2A shows the invasive characteristics of control and treated cells scored 23hr after plating onto matrigel basement membranes using Boyden's chambers. The number of cells which migrated through the membrane was more than double in SAEC-A0.5 cells when compared with SAEC cells, a clear induction that arsenic increased the cells invasive capabilities. To show signs of transformation in arsenic-treated cells other experiments were performed such as an *in vitro* wound-healing assay which showed that arsenic-treated SAEC cells exhibited higher cell motility in response to growth factors than control cells as seen in Figure 2B.

Alterations in protein expression

To determine whether arsenic induced cell transformation another study was done on alterations in surface protein expression as analyzed by the amount of integrin receptors that were present on arsenic-treated cells are compared to the non-treated SAEC cells. Results indicated that integrin α2 did not show any difference in control and treated cells as seen in Figure 2C. However, integrin β4 protein expression was expressed in control and lost in arsenic-treated cells, indicating a change in the Extracellular Matrix (ECM) receptor induced by the chemical used. Figure 2D and 2E shows lamellipodia formation found in control and experimental cells. The arsenic-treated SAEC group presented a higher percentage of lamellipodia formation than control cells indicating an alteration at epithelial morphology and attachment to the fibronectin substrate upon plating, contributing to the process of transformation as seen in representative cells, which could be explained by the lost expression of the β4 integrin.

Malignant transformation is frequently associated with the expression change of specific oncogenes and tumor suppressors. Immunofluorescent studies indicated that there was significantly increase in c-myc, mutant p53, c-Ha-ras and c-fos protein expression in cells in comparison to control cells as in Figure 3A. It was next analyzed whether the alterations of protein expression correlated with cell transformation induced by arsenic. Results indicated that SAEC-A0.5-treated cells had significantly ($P<0.05$) increased the expression of these 3 proteins compared to control cells. Treatment with arsenic elevated the expression of c-myc, c-fos and c-Ha-ras by x-fold in comparison to control cells respectively. Representative images of c-myc, c-Ha-ras and c-fos cells are shown in Figure 3B.

On the other hand, c-Ha-ras, c-myc and c-fos as well as c-jun protein expression were confirmed by Western blot analysis in control and SAEC-A0.5 cells (Fig. 4A and B). Phosphorilation of ERK1 and Rb was examined by Western-blot analysis between SAEC and SAEC-A0.5 cells, as shown in Figure 4C and D. Under these culture conditions, the Rb protein was hyperphosphorylated in SAEC-A0.5 cells, while the control cells maintained a basal level. Thus, it was demonstrated that cell proliferation and transformation markers as c-myc, c-fos and c-Ha-ras protein expression were altered by the treatment.

p53 exhibited a significant decrease in SAEC-A0.5 cells compared with SAEC as seen in Figure 4E. However, the sequence of p53 gene in SAEC-A0.5 cells revealed no

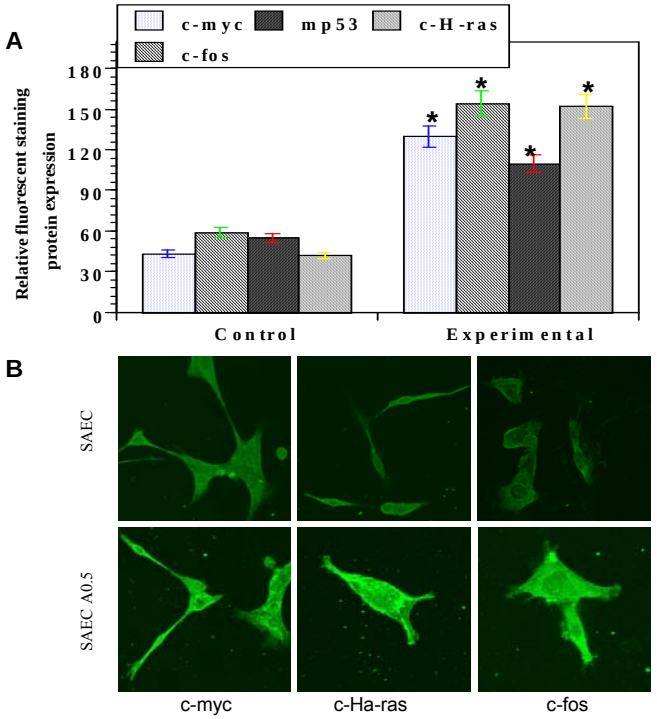

Fig. 3. A. Bars represent the average and standard error of c-myc, mutant p53, c-Ha-ras and c-fos protein expression of SAEC and SAEC-A0.5. **B.** Representative immunofluorescence stained in confocal microscopical images of c-myc**,** c-Ha-ras and c-fos protein expression of SAEC and SAEC A0.5 cells. The primary antibodies used were mouse monoclonal antibody (Biotechnology Inc., Santa Cruz, CA).

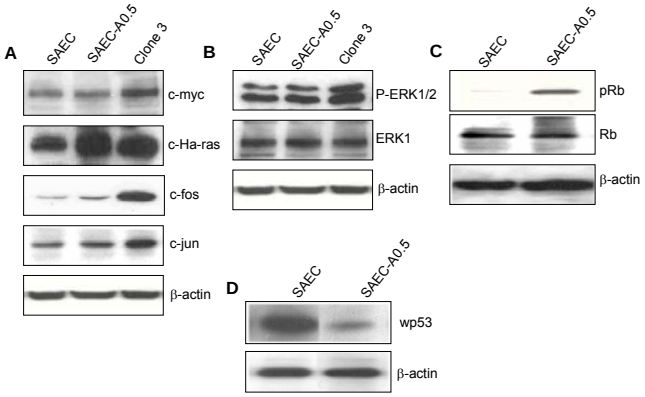

E Query 1019 GCGTGAGCGCTTCGAGATGTTCCGAGAGCTGAATGAGGCCTTGGAA 1065
Sbjct 1256 **TG**-------- GCGCTTCGAGATGTTCCGAGAGCTGAATGAGGCCTTGGAA 1298

Fig. 4. Western blot analysis: **A.-D.** Equal amount of whole cell lysates from SAEC and SAEC-A0.5 prepared in RIPA buffer, resolved on 12% SDS-PAGE and transferred to PVDF membrane, probed with correspondent antibodies shown in each panel. **E.** Sequence of wild p53.

change in the treated and control cells (Fig. 4E). The down-regulation of p53 may partially contribute to the transformation features.

The objective of the study was to establish an *in vitro* arsenic transformation model based on the h-TERT immortalized human small airway epithelial cells. Based on the alterations we detected as shown above, SAEC had been successfully transformed. Therefore as the next step, it will be important to determine whether these cells can progress to induce tumor formation *in vivo*.

References

1. Bryan TM and Reddel RR. SV40-induced immortalization of human cells. *Crit Rev Oncog* **5**:331-57, 1994.
2. Willey JC, Broussoud A, Sleemi A, Bennett WP, Cerutti P and Harris CC. Immortalization of normal human bronchial epithelial cells by human papillomaviruses 16 or 18. *Cancer Res* **51**:5370-7, 1991.
3. Piao CQ, Liu L, Zhao YL, Balajee AS, Suzuki M and Hei TK. Immortalization of human small airway epithelial cells by ectopic expression of telomerase. *Carcinogenesis* **26**:725-31, 2005.
4. Otto E, McCord S and Tlsty TD. Increased incidence of CAD gene amplification in tumorigenic rat lines as an indicator of genomic instability of neoplastic cells. *J Biol Chem* **264**:3390-6, 1989.
5. Wahl GM. overproduction of the first three enzymes of UMP synthesis in N-(phosphonacetyl)-L-aspartate resistant hamster cells. *J Biol Chem* **254**:8679-89, 1979.
6. Lemoine FJ and Marriott SJ. Genomic instability driven by the human T-cell leukemia virus type I (HTLV-I) oncoprotein, Tax. *Oncogene* **21**:7230-4, 2002.
7. Chernova OB, Chernov MV, Ishizaka Y, Agarwal ML and Stark GR. MYC abrogates p53-mediated cell cycle arrest in N-(phosphonacetyl)-L-aspartate-treated cells, permitting CAD gene amplification. *Mol Cell Biol* **18**:536-45, 1998.
8. Mondello C, Riboni R, Rady M, Giulotto E and Nuzzo F. Gene amplification in Chinese hamster DNA repair deficient mutants. *Mutat Res* **346**:61-7, 1995. ■

Intrachromosomal Deletions Induced by Chrysotile In the gpt delta Transgenic Mutation Assay

An Xu, Lubomir B. Smilenov and Tom K. Hei

Introduction

The mechanisms by which asbestos produces malignancy are unclear at present. Although a close link between chromosomal abnormalities has frequently been demonstrated in fiber exposed human and rodent cell lines and carcinogenicity *in vivo*, there is less direct evidence to illustrate chromosomal mutations by asbestos fibers in various organs and tissues in intact organisms.

The use of transgenic mouse systems carrying bacterial reporter genes, such as *lacZ*, *lacI*, and *cII*, has opened a promising opportunity for short-term mutagenicity analysis.[1] To efficiently recover large deletions *in vivo*, *gpt* delta transgenic mice have been established by integrating multiple copies of λ EG10 DNA with the *redBA* and *gam* genes into each chromosome 17 of C57BL/6J mice.[2] Since wild-type λ phage DNA replicate poorly in the presence of P2 lysogens in the host cells (called *Sensitive to P2 interference* or Spi); only mutant λ phages that are deficient in the functions of both the *redBA* and *gam* genes are able to escape from P2 interference (called Spi$^-$) and form visible clear plaques on a bacterial lawn. Simultaneous inactivation of both the *redBA* and *gam* genes, an indication of deletions in the gene loci region, provide an available method to quantify deletion mutations induced by various physical and chemical mutagens, such as x-rays and alkylating agents.[3,4]

Chrysotile asbestos, a fibrous serpentine, is the most commercially used form of asbestos in the world trade and accounts for over 95% of asbestos found in USA buildings.

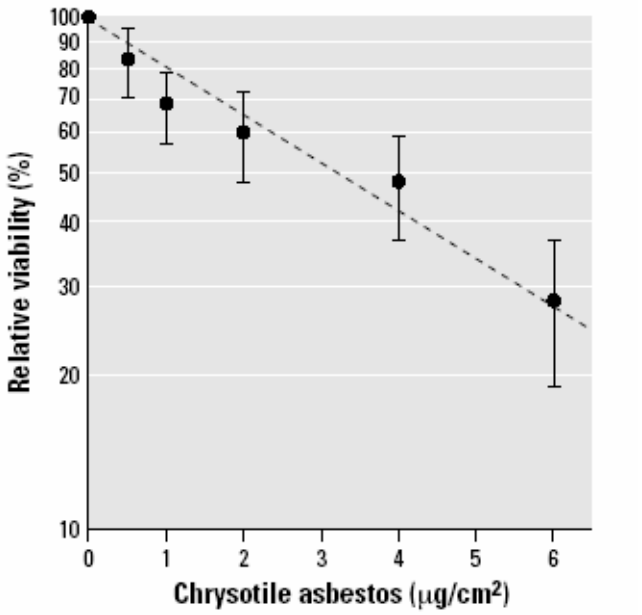

Fig. 1. Cells viability of transgenic MEF cells treated with graded doses of chrysotile for 24hr. Data were the average of three independent experiments. Error bars indicate ± SD.

In the present study, we adapted the *gpt* delta transgenic mouse mutation system to evaluate the genotoxicity of chrysotile in *gpt* delta MEF cells.

Chrysotile induced dose-dependent toxicity in transgenic MEF cells

The viability of MEF cells exposed to graded doses of chrysotile was analyzed by using the MTT assay. As shown in Figure 1, exposure of MEF cells to doses of chrysotiles ranging from 0.5 to 6μg/cm^2 for 24h produced a dose-dependent decrease in cell viability. The viability of MEF cells was reduced by 14%, 29%, and 59%, when the concentrations of chrysotile were 0.5, 1, and 2μg/cm^2, respectively. The LD_{50} dose of chrysotile, which resulted in 50% cell killing, was about 3.2μg/cm^2.

Mutation frequencies at *red/gam* gene loci were elevated in response to chrysotile exposure

We have previously shown that asbestos is mutagenic and induces multilocus deletions in mammalian cells.[5] To investigate the mutagenicity of asbestos in the *gpt* delta assay, a Spi$^-$ mutation assay was used to determine the mutation frequencies induced by chrysotile exposure in transgenic MEF cells. The average number of spontaneous *red/gam* gene mutants per 10^6 recovered plaques in MEF cells used for these experiments was 4.69 ± 1.80. Treatment of MEF cells with chrysotile fibers resulted in a dose-dependent induction of mutation yield at the *red/gam* gene locus (Fig. 2). A significant increase in mutation yield over the background level was observed at fiber concentrations > 1μg/cm^2 ($p<0.005$). The mutant fraction in cells treated with a dose of 1μg/cm^2 of fibers was 2.4-fold higher than background. These results indicated that chrysotile asbestos was able to produce deletion mutations in the *gpt* delta transgenic mutation assay system.

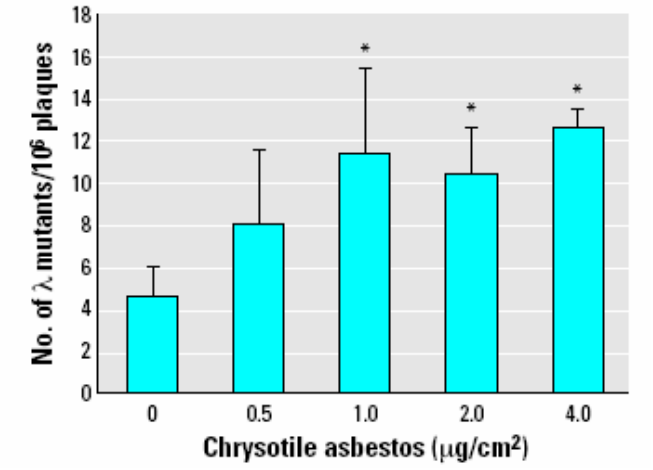

*Significantly different at $p<0.05$.

Fig. 2. Mutagenic potential of chrysotile asbestos at *redBA* and gam loci in transgenic MEF cells. MEF cells, 5×10^5, were treated with graded doses of chrysotile as described in the text. Results were expressed as the total number of rescued phages. The average number of preexisting mutants per 10^6 plaques used for these experiments was 4.69 ± 1.42. Data were pooled from six independent experiments. Error bars indicate ± SD.

Characterization of mutant spectra induced by chrysotile

To determine the spectrum of mutations induced by chrysotile fibers, 93 and 74 λ mutants from control cells and cells treated with chrysotile at 1μg/cm^2, respectively, were subjected to either PCR analysis or DNA sequence analysis. The PCR product of *redBA/gam* in the wild-type lambda EG10 was about 2 kb. If a PCR product did not show any discrete alteration on the gel, the mutant was classified as one containing a point mutation with either a base substitution or a frameshift causing no alteration in the size of the gene product. In contrast, an absence of visible PCR product

Table 1. Type of λ-phage mutants at *redBA/gam* loci either of spontaneous origin or induced by chrysotile treatments (1μg/cm^2) determined by multiplex PCR analyses and DNA sequencing.

Groups	Total no. of mutants	No. of mutants with base substitution	No. of mutants with 1-bp deletion	No. of mutants with > 2-bp and < 1-kb deletions	No. of mutants with > 2-kb deletion
Control	93	7 (8%)	68 (73%)	8 (8%)	10 (11%)
Chrysotile	74	5 (7%)	41 (56%)	10 (14%)	17 (23%)

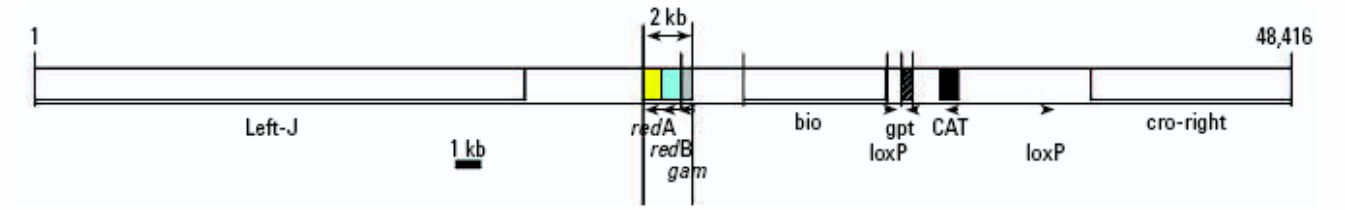

Fig. 3. Schematic map of λ EG10 transgene. Abbreviations: bio, genetic marker used I bacteriophage lambda vectors; *CAT*, chloramphenicol acetyltransferase (GenBank accession no. AJ401050; http://www.ncbi.nlm.nih.gov/GenBank); cro, transcription inhibitor; *gpt,* xanthine phosphoribosyltransferase (GenBank accession no. NP_414773); J, codes for phage tail gene; loxP, locus of X over P1, a site on the bacteriophage P1 consisting of 34 bp; redA, redB, and gam, single copy bacteriophage genes.

Table 2. Mutant fractions of deletions involving the *redBA/gam* region and other smaller deletions including single base changes in either nontreated control cells or cells treated with chrysotile fibers (1μg/cm^2 for 24hr).

	Control	Asbestos
Total mutant fraction at *redBA/gam* loci	4.69×10^{-6}	11.4×10^{-6}
Large deletions (> 2 kb)		
Mutant fraction	0.5×10^{-6}	2.6×10^{-6}
Increase above the control	1.0	5.2
Small deletions plus single base changes		
Mutant fraction	4.2×10^{-6}	8.8×10^{-6}
Increase above the control	1.0	2.1

was taken as evidence of a mutant with a deletion larger than 2kb as a result of losing both *redBA* and *gam* genes. The types of mutations identified from analysis of these mutants are listed in Table 1 and Figure 3. To minimize the possibility that these isolated mutants were spontaneously derived, mutant phages were selected from only the dose of chrysotile that resulted in the highest inductions over background levels. Deletions of various sizes throughout the genes comprised a majority (86/93 or 92%) of the spontaneous mutations. Of these deletion mutants, one base deletion made up 68/93 or 73%, whereas deletions ranging from 2bps to 1kbps comprise 8/93 or 8.6%. 10/93 or 11% of the spontaneous mutations with deletions encompass regions of both the *gam* and *redBA* genes. In contrast, 41/74 or 56% and 10/74 or 14% of mutants recovered from chrysotile treated cells were single-bp deletion and deletions ranging from 2bps to 1kb, respectively. The proportion of mutants induced by chrysotile suffering loss of both the *gam* and *redBA* genes was increased from 10/93 or 11% among spontaneous mutants to 17/74 or 23% in fiber-treated MEF cells (Table 1).

Deletion larger than 2kb contributes to chrysotile-induced mutagenicity

To provide further evidence of the contribution of deletions larger than 2kb to the mutagenicity of chrysotile, we compared the frequencies of deletions larger than 2kb induced by chrysotile at a dose of 1μg/cm^2 with those derived spontaneously from control cultures (Table 2). Although the total Spi$^-$ mutant yield in chrysotile-treated cells was 2.4-fold higher than that of controls, the frequency of deletions larger than 2kb induced by 1μg/cm^2 of fibers was 5.2-fold higher than those derived from non-treated control (2.6 vs. 0.5×10^{-6}, $p<0.005$). The frequency of base substitution and small deletions including single base deletions and deletions less than 1kb formed in fiber-treated MEF cells was only 2-fold higher than those from non-treated cases. These results indicated that the major type of mutations induced by chrysotile was deletions large than 2kb in size.

Our results provide novel information on the frequencies and types of mutations induced by asbestos fibers in the *gpt* delta transgenic mouse mutagenic assay, which shows great promise for evaluating fiber/particle mutagenicity *in vivo*.

Reference

1. Dean SW, Brooks TM, Burlinson B, Mirsalis J, Myhr B, Recio L and Thybaud V. Transgenic mouse mutation assay systems can play an important role in regulatory mutagenicity testing in vivo for the detection of site-of-contact mutagens. *Mutagenesis* **14**:141-51, 1999.
2. Nohmi T and Masumura KI. Gpt delta transgenic mouse: A novel approach for molecular dissection of deletion mutations in vivo. *Adv Biophys* **38**:97-121, 2004.
3. Horiguchi M, Masumura KI, Ikehata H, Ono T, Kanke Y and Nohmi T. Molecular nature of ultraviolet B light-induced deletions in the murine epidermis. *Cancer Res* **61**:3913-8, 2001.
4. Shibata A, Kamada N, Masumura K, Nohmi T, Kobayashi S, Teraoka H, Nakagama H, Sugimura T, Suzuki H and Masutani M. Parp-1 deficiency causes an increase of deletion mutations and insertions/rearrangements in vivo after treatment with an alkylating agent. *Oncogene* **24**:1328-37, 2005.
5. Hei TK, Piao CQ, He ZY, Vannais D and Waldren CA. Chrysotile fiber is a strong mutagen in mammalian cells. *Cancer Res* **52**:6305-9, 1992. ■

Genotoxicity of Nanoparticles

An Xu and Tom K. Hei

Nanotechnology is a rapidly evolving and expanding area and has aroused growing media and public interest for the past decade. Although many nanotechnologies are still in the pre-competitive stage, nano-sized materials, by virtue of extraordinary electronic, light-emitting, and catalytic properties, are increasingly being used in many industries including optoelectronic, electronic, medical imaging, drug delivery, cosmetic, catalytic and materials applications.[1,2] Although

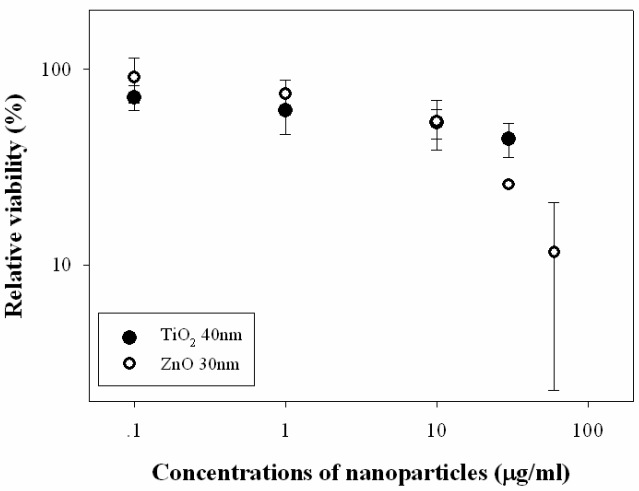

Fig. 1. Viability of transgenic MEF cells treated with graded doses of either TiO_2 40nm or ZnO 30nm for 24 hrs.

benefits of nanotechnology are well recognized, discussion of the potential effects of their widespread use in the consumer and industrial products are just beginning to cause concerns.[3,4]

In recent years, there is a significant body of published information indicating that nanoparticles show signs of toxicity.[5,6] Early in 1997, Dunford et al. reported that titanium dioxide/zinc oxide nanoparticles from sunscreen were found to induce free radicals and catalysed DNA damage both in cell free system and *in vitro*.[7] Results from three independent studies using intratracheal dosing of carbon nanotubes in rodents indicated significant acute inflammatory pulmonary effects that either subsided in rats or were more persistent in mice. Chemically functionalized, water-soluble carbon nanoparticles were shown to enter fibroblasts, promyelocytic leukemia (HL60) cells and T cells.[8-10] Multiwalled carbon nanotubes resulted in proinflammatory effects and were internalized in keratinocytes. Profound cytotoxicity such as mitochondrial dysfunction, cellular morphological modifications, and phagocytic dysfunction were seen for carbon nanotubes, even at a low concentration[11] The recent study by Oberdorster demonstrated that nanomaterials (Fullerences C_{60}) induced oxidative stress in juvenile fish and caused brain damage along with changes in gene function.[12] Hussain et al. showed that Ag nanoparticles induced a depletion of reduced glutathione and oxidized glutathione levels significantly, reduced mitochondrial membrane potential and increased in ROS level in BRL 3A rat liver cells, suggesting nanoparticle cytotoxicity is likely to be mediated through oxidative stress.[13] Sayes et al. reported that lipid peroxidation may play an important role in the cytotoxicity of nano-C (60).[14] Since DNA is a critical target in living cells, it's of great interest to investigate the genotoxic events triggered by nanoparticles.

The viability of MEF cells exposed to graded doses of either TiO_2 or ZnO was analyzed by using the MTT assay. Exposure of MEF cells to either TiO_2 or ZnO induced a dose-dependent decrease in cell viability (Fig. 1). MEF cells were more sensitive to ZnO than TiO_2 at doses higher than $30\mu g/cm^2$. Both TiO_2 and ZnO resulted in a time-dependent induction of mutation yield at the *red/gam* gene locus (Fig. 2).

References

1. Bogunia-Kubik K and Sugisaka M. From molecular biology to nanotechnology and nanomedicine. *Biosystems* **65**:123-38, 2002.
2. Cui Y, Wei Q, Park H and Lieber CM. Nanowire nanosensors for highly sensitive and selective detection of biological and chemical species. *Science* **293**:1289-92, 2001.
3. Biswas P and Wu CY. Nanoparticles and the environment. *J Air Waste Manag Assoc* **55**:708-46, 2005.
4. Hoet PH, Bruske-Hohlfeld I and Salata OV. Nanoparticles - known and unknown health risks. *J Nanobiotechnology* **2**:12, 2004.
5. Colvin VL. The potential environmental impact of engineered nanomaterials. *Nat Biotechnol* **21**:1166-70, 2003.
6. Oberdorster G, Oberdorster E and Oberdorster J. Nanotoxicology: an emerging discipline evolving from studies of ultrafine particles. *Environ Health Perspect* **113**:823-39, 2005.
7. Dunford R, Salinaro A, Cai L, Serpone N, Horikoshi S,

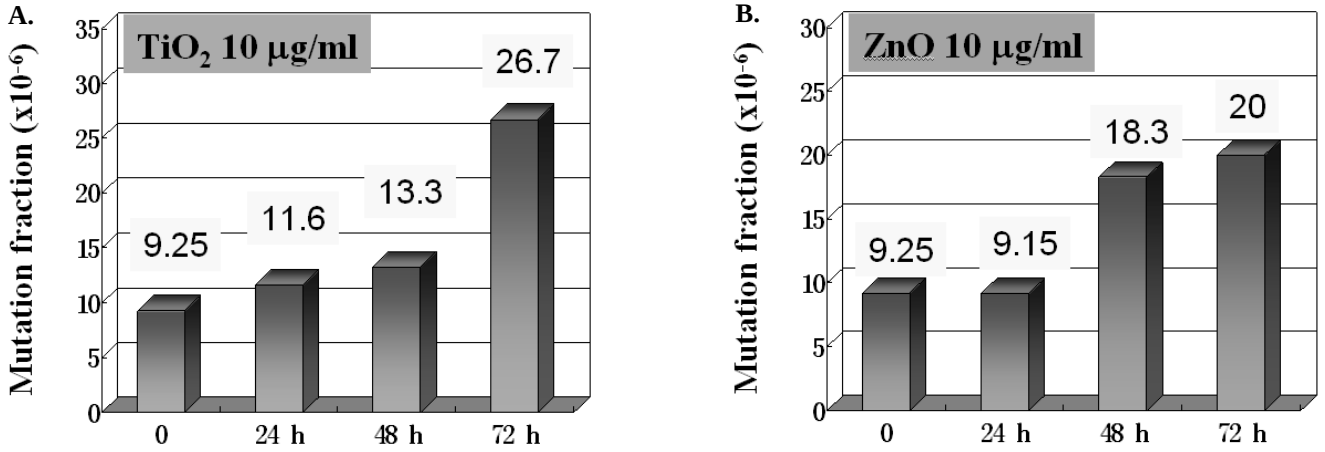

Fig. 2. Representative Mutagenic potential of either **A.** TiO_2 or **B.** ZnO in transgenic MEF cells.

Hidaka H and Knowland J. Chemical oxidation and DNA damage catalysed by inorganic sunscreen ingredients. *FEBS Lett* **418**:87-90, 1997.
8. Lam CW, James JT, McCluskey R and Hunter RL. Pulmonary toxicity of single-wall carbon nanotubes in mice 7 and 90 days after intratracheal instillation. *Toxicol Sci* **77**:126-34, 2004.
9. Shvedova AA, Kisin ER, Mercer R, Murray AR, Johnson VJ, Potapovich AI, Tyurina YY, Gorelik O, Arepalli S, Schwegler-Berry D*, et al.* Unusual inflammatory and fibrogenic pulmonary responses to single-walled carbon nanotubes in mice. *Am J Physiol Lung Cell Mol Physiol* **289**:L698-708, 2005.
10. Warheit DB, Laurence BR, Reed KL, Roach DH, Reynolds GA and Webb TR. Comparative pulmonary toxicity assessment of single-wall carbon nanotubes in rats. *Toxicol Sci* **77**:117-25, 2004.
11. Monteiro-Riviere NA, Nemanich RJ, Inman AO, Wang YY and Riviere JE. Multi-walled carbon nanotube interactions with human epidermal keratinocytes. *Toxicol Lett* **155**:377-84, 2005.
12. Oberdorster E. Manufactured nanomaterials (fullerenes, C60) induce oxidative stress in the brain of juvenile largemouth bass. *Environ Health Perspect* **112**:1058-62, 2004.
13. Hussain SM, Hess KL, Gearhart JM, Geiss KT and Schlager JJ. In vitro toxicity of nanoparticles in BRL 3A rat liver cells. *Toxicol In Vitro* **19**:975-83, 2005.
14. Sayes CM, Gobin AM, Ausman KD, Mendez J, West JL and Colvin VL. Nano-C60 cytotoxicity is due to lipid peroxidation. *Biomaterials* **26**:7587-95, 2005. ■

Luciferase Assay to Detect Base Excision Repair *in Vivo* In Mouse ES Cells Differing in Mrad9 Status

Kevin M. Hopkins and Howard B. Lieberman

Introduction

Our lab generated mouse embryonic stem cells deleted for *Mrad9* to determine the role of the gene in the response of cells to DNA damaging agents. We found that these cells are very sensitive to a number of DNA damaging agents including gamma rays,[1] ultraviolet light,[1] hydroxyurea,[1] methylmethane sulphonate, ethylmethane sulphonate, N-methyl-N'-nitro-N-nitrosoguanidine (MNNG), fluorodeoxyuridine, bromodeoxyuridine, 5-fluorouracil, cisplatin, and mitomycin C (unpublished data).

It has been reported that the Rad9-Rad1-Hus1 complex interacts with and/or stimulates components of the base excision repair (BER) pathway including the *S. pombe* MutY homolog (MYH),[2] human polymerase beta (Polbeta),[3] flap endonuclease 1 (FEN1)[4] and DNA ligase I.[5]

To understand the function of *Mrad9* in promoting cell survival after exposure to DNA damaging agents, we initiated a study to examine the role of the protein in base excision repair.

***In vivo* BER luciferase assay**

With the use of an *in vivo* plasmid based BER assay[6] we tested if Mrad9 deficient cells show a reduction in BER activity. The assay we employed is based on changing the cytosine residues in the luciferase bearing plasmid pGL4.13 to uracil. Treatment of the plasmid with sodium bisulfite in the presence of hydroquinone deaminates cytosine into uracil residues. The uracil containing plasmid along with pRL-TK was then transfected into wild-type and mutant Mrad9 ES cells. Plasmid pRL-TK is used as an internal control to adjust for differences in transfection efficiency. If the cells are capable of repairing the modified plasmid there should be an increase in luciferase activity over time. Four hours after transfection cells were harvested, lysed and the luciferase activity was determined. This time point was considered time zero. Cells were then collected at 24 and 48 hour time points and the luciferase activity was also determined.

Results

Twenty four and 48 hours after transfection of Mrad9$^{+/+}$ and Mrad9$^{-/-}$ mouse ES cells with uracil containing plasmid

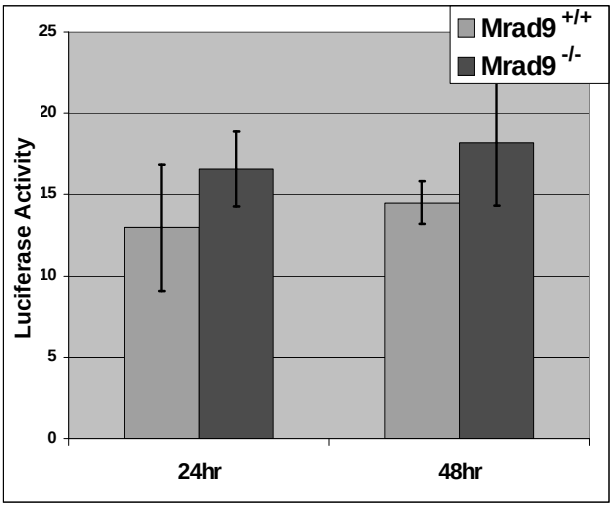

Fig. 1. *In vivo* BER assay. The luciferase gene reporter assay was performed after transfection of uracil containing plasmid pGL4.13 and pRL-TK in Mrad9$^{+/+}$ and Mrad9$^{-/-}$ mouse embryonic stem cells.

pGL4.13 and pRL-TK there is an equivalent increase in luciferase activity in both cell lines. In Mrad9$^{+/+}$ cells luciferase activity increased 13 fold within 24 hours and 14 fold after 48 hours. Mrad9$^{-/-}$ cells increased 16 fold within 24 hours and 18 fold after 48 hours.

Conclusions

Based on the *in vivo* BER assay results it appears that lack of *Mrad9* does not inhibit repair of uracil in DNA via the BER pathway.

Additional studies are underway to understand the role of *Mrad9* in BER, and how these results relate to cellular resistance to DNA damage.

References

1. Hopkins KM, Auerbach W, Wang XY, Hande MP, Hang H, Wolgemuth DJ, Joyner AL and Lieberman HB. Deletion of mouse rad9 causes abnormal cellular responses to DNA damage, genomic instability, and embryonic lethality. *Mol Cell Biol*. **24**:7235-48, 2004.
2. Shi G, Chang DY, Cheng CC, Guan X, Venclovas C and Lu AL. Physical and functional interactions between MutY glycosylase homologue (MYH) and checkpoint proteins Rad9-Rad1-Hus1. *Biochem J*. **400**:53-62, 2006.
3. Toueille M, El-Andaloussi N, Frouin I, Freire R, Funk D, Shevelev I, Friedrich-Heineken E, Villani G, Hottiger MO and Hubscher U. The human Rad9/Rad1/Hus1 damage sensor clamp interacts with DNA polymerase beta and increases its DNA substrate utilisation efficiency: implications for DNA repair. *Nucleic Acids Res* **32**:3316-24, 2004.
4. Wang W, Brandt P, Rossi ML, Lindsey-Boltz L, Podust V, Fanning E, Sancar A and Bambara RA. The human Rad9-Rad1-Hus1 checkpoint complex stimulates flap endonuclease 1. *Proc Natl Acad Sci USA* **101**:16762-7, 2004.
5. Smirnova E, Toueille M, Markkanen E and Hubscher U. The human checkpoint sensor and alternative DNA clamp Rad9-Rad1-Hus1 modulates the activity of DNA ligase I, a component of the long-patch base excision repair machinery. *Biochem J*. **389**:13-7, 2005.
6. Kundu CN, Balusu R, Jaiswal AS, Gairola CG and Narayan S. Cigarette smoke condensate-induced level of adenomatous polyposis coli blocks long-patch base excision repair in breast epithelial cells. *Oncogene* **26**:1428-38, 2007. ■

Mary's retirement party. (L-r): Monique Rey, Mary Coady, Heidy Hernandez and Angela Lugo.

Mary's retirement party. (L-r): Dr. Aiping Zhu, Dr. Corinne Leloup, Dr. Adayabalam Balajee and Gloria Baker.

Protons and the Risk of Second Cancers

Eric J. Hall and David J. Brenner

One of the most significant recent developments in radiotherapy, and certainly the most expensive, is the proliferation of hospital-based proton facilities. A contribution to our 2005 annual report described one of the problems associated with current facilities, namely that when the pencil beam of protons that emerges from a cyclotron or synchrotron is expanded and shaped by passive scattering, neutrons are produced which deliver an undesirable total body dose to the patient. Neutrons are produced whenever protons lose a large amount of energy, so that the principle sources of neutrons are in the scattering foils and collimators. This problem is largely avoided if pencil scanning is used instead of passive scattering, but this involves difficult and complicated technology.

Figure 1, reproduced from the 2005 report, compares the off-axis neutron equivalent doses for a proton beam using passive scattering, with that for the pencil scanning beam in Switzerland – both compared with standard x-ray beams. These data were published in a paper in the September 2006 issue of the International Journal of Radiation Oncology. Biology Physics, and the conclusion drawn that for the full potential of protons to be achieved, it is necessary to have pencil scanning.[1] This conclusion was contested strongly in the correspondence columns of the JJRO by Dr. Gottschalk,[2] a leader in the design of collimators for proton facilities, and by Harold Paganetti,[3] who had supplied us in the first place with much of the neutron data in Figure 1.

The basis of their criticism was that the data for passive modulation in Figure 1 was measured on the Harvard cyclotron (now obsolete) while fewer neutrons are produced in the new hospital based proton facilities. Gottschalk suggested that we were "…incorrect by a factor of ≥ 9 to the detriment of scattered vs. scanned protons." We accept this criticism and in Figure 2 the neutron doses are reduced by this factor. On this basis the off axis (and therefore total body) neutron doses are no worse than IMRT, which is not much of a recommendation since it has been estimated that IMRT may double the risk of radiation-induced second cancers compared with conventional techniques. However, the Paganetti data for neutron equivalent doses were based on a neutron RBE of 10, which is surely too small. Recently published data for neutron RBE as a function of neutron energy would suggest a value of at least 30 for the neutrons of the energy produced in clinical proton facilities. Figure 3 factors in this higher neutron RBE.

Based on these considerations, it still appears reasonable to conclude that proton facilities using passive modulation result in a total body exposure to neutrons where the equivalent dose is greater than that characteristic of IMRT with x-rays and about two orders of magnitude greater than with a pencil scanned proton beam. It is true that the neutron dose is very dependent on the design of the scattering system and

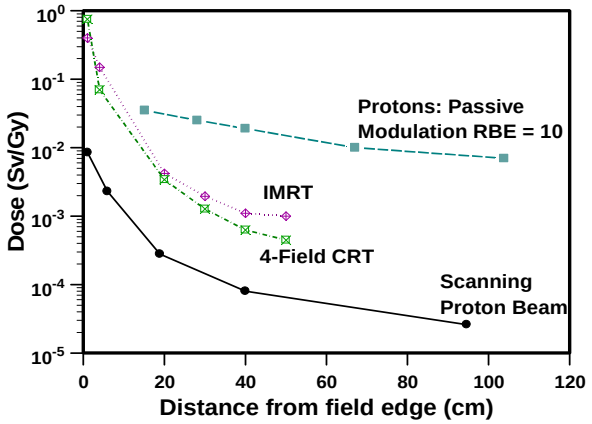

Fig. 1. The equivalent dose outside the edge of the treatment field as a fraction of the dose at the isocenter for protons with passive modulation, for a scanning proton beam and for 6 MV x-rays, either 4 field CRT or IMRT. (Proton data due to Harald Paganetti, Massachusetts General Hospital, Boston.)

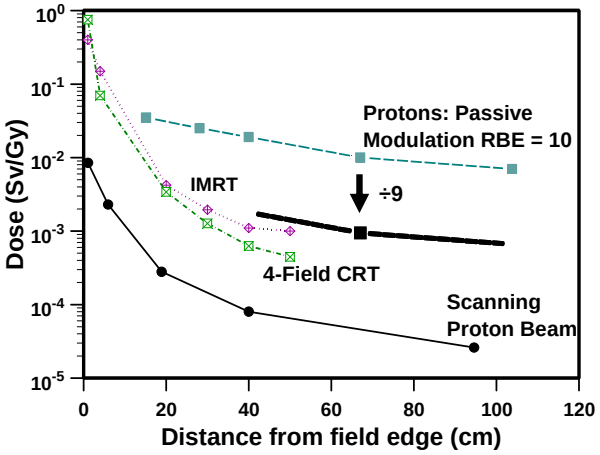

Fig. 2. Same as Fig.1, but with the neutron dose outside the field reduced by a factor of 9.

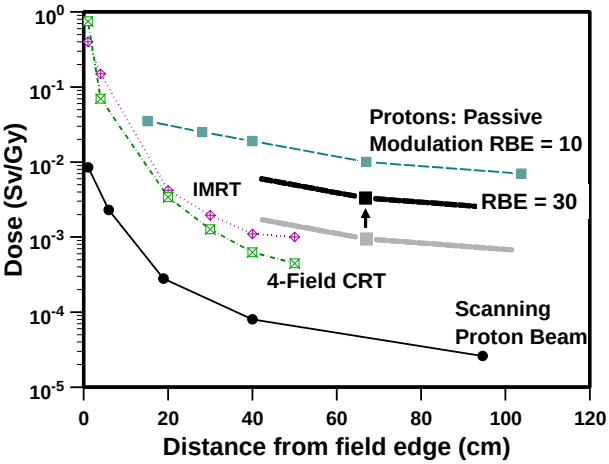

Fig. 3. Same as Fig. 2, but with a neutron RBE of 30 instead of 10.

collimator, and may therefore vary significantly between different facilities. Given this, does it really make sense to spend a million dollars on a proton facility, and then to spray the patient with a non-negligible total-body neutron dose, the risks from which we really don't know, when the technology to virtually eliminate this unwanted dose is available, and indeed is in clinical use elsewhere?

References

1. Hall EJ. Intensity-modulated radiation therapy, protons, and the risk of second cancers. *Int J Radiat Oncol Biol Phys* **65**:1-7, 2006.
2. Gottschalk B. Neutron dose in scattered and scanned proton beams: in regard to Eric J. Hall (Int J Radiat Oncol Biol Phys 2006;65:1-7). *Int J Radiat Oncol Biol Phys* **66**:1594; author reply 5, 2006.
3. Paganetti H, Bortfeld T and Delaney TF. Neutron dose in proton radiation therapy: in regard to Eric J. Hall (Int J Radiat Oncol Biol Phys 2006;65:1-7). *Int J Radiat Oncol Biol Phys* **66**:1594-5; author reply 5, 2006. ■

Potential Risks of Radiation-Induced Breast Cancer With Different Accelerated Partial Breast Irradiation Techniques

Sandra A. Russo,[a] Cheng-Shie Wuu,[a] Andy Xu,[a] Carl D. Elliston and David J. Brenner

There is increasing current interest in treating early stage breast cancer with accelerated partial breast irradiation (APBI). One of the major rationales of APBI is to minimize the long-term risk of a radiation-induced second cancer. The purpose of this study was to determine if different external beam APBI techniques produce significantly different predicted risks of radiation-induced breast and lung cancers, both ipsilateral and contralateral.

An anthropomorphic whole-body phantom (Fig. 1) was used, with realistic breasts based on CT scans of a female in a supine position. Point dose measurements using MOSFET detectors within the ipsilateral left breast, the contralateral right breast, the right and left lung were used to validate calculated organ dose distributions for six different external-beam APBI techniques. APBI techniques compared were 1) a tangential technique *(T)* using a 30º enhanced dynamic wedged pair; 2) a two field multi-segment static (field in field) forward planning IMRT technique *(FF)*; 3) a two field dynamic multi-leaf collimator forward planning intensity modulated radiation therapy (IMRT) technique *(2FDMLC)*; 4) a four-field dynamic multi-leaf collimator forward planning intensity modulated radiation therapy technique *(4FDMLC)*; 5) a three-dimensional conformal radiation therapy technique *(3D-CRT)* using four non-coplanar fields, as outlined in the RTOG-0413 protocol; 6) a dynamic multi-leaf collimator inverse planning IMRT technique *(IDMLC)* using the same four non-coplanar fields as the 3D conformal technique.

[a] *Department of Radiation Oncology, College of Physcians & Surgeons, Columbia University, NY*

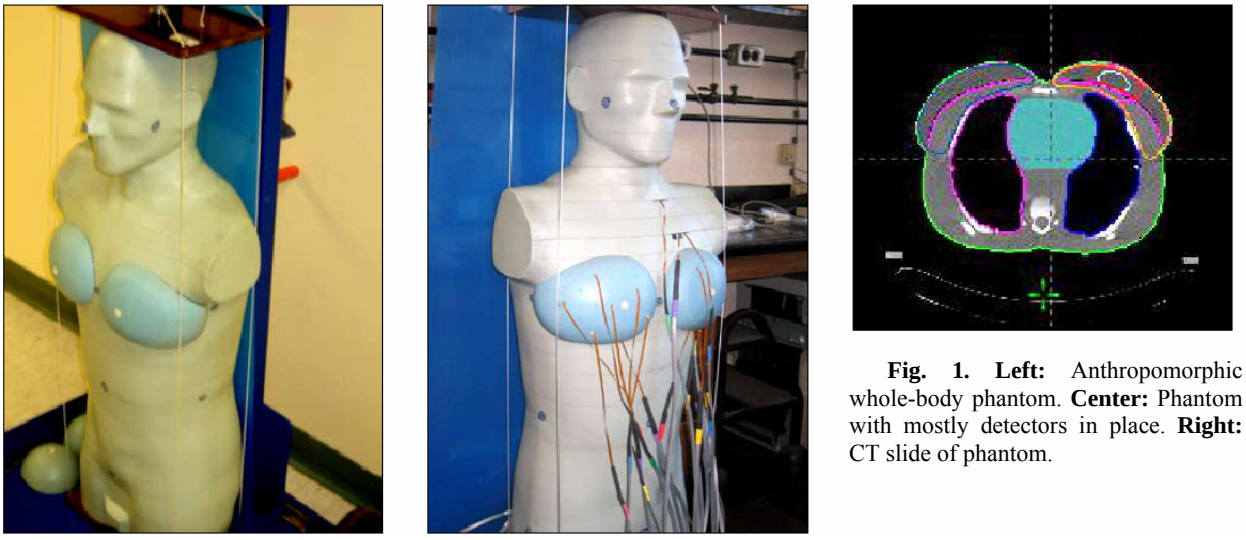

Fig. 1. Left: Anthropomorphic whole-body phantom. **Center:** Phantom with mostly detectors in place. **Right:** CT slide of phantom.

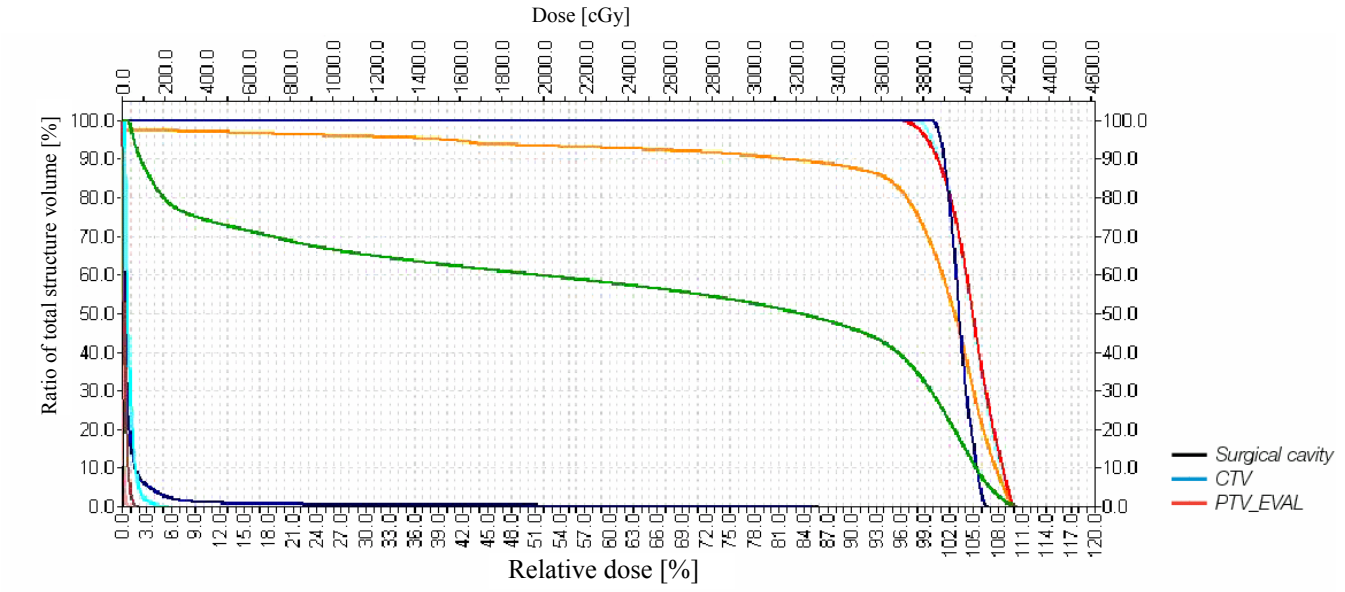

Fig. 2. Typical dose-volume histogram from a breast radiation therapy plan showing dose in three different patient volumes.

Breast and lung cancer risks were calculated from calculated dose-volume histograms (Fig. 2) using a recent validated mechanistic model[1] which incorporates pre-malignant stem cell initiation, inactivation and, crucially, proliferative repopulation. Proliferation of pre-malignant cells during postirradiation repopulation explains why cancer risks do not decrease sharply at high radiation doses, as is now clear from recent epidemiological data.

Preliminary estimates have been made of the absolute lifetime second cancer risk associated with the radiation exposure (ipsilateral breast, contralateral breast, ipsilateral lung, contralateral lung) for women treated at ages 40-70 with the six different APBI techniques. Each APBI technique delivered 10 fractions of 3.85Gy/fraction for a total APBI dose of 38.5Gy. The estimated risks decreased with increasing age, quite rapidly for the breast (more than a factor of 10 between ages at exposure 40 to 70), and quite slowly for the lung (less than a factor of 2 between ages at exposure 40 to 70). Despite the fact that the doses to the lung were far less than those to the breast, the absolute cancer risks were quite similar for breast vs. lung, for a woman treated at, say, age 60.

The six treatment protocols resulted in quite different predicted second cancer risks for all the sites studies. This effect was particularly marked for the ipsilateral lung, which represents the largest predicted risk for women exposed over age 60; here, the different plans resulted in predicted ipsilateral lung cancer risks which varied by more than a factor of 10.

Among the six APBI techniques studied, IDMLC followed by 3D-CRT gave the lowest estimate lifetime cancer risks, reflecting lower mean doses to both breasts and both lungs. Different APBI techniques in breast conserving therapy result in quite different dose distributions and mean doses to the ipsilateral and contralateral breast and lung, and thus quite different predicted risks of radiation- induced second breast cancer and lung cancer. 3D-CRT and, particularly, IDMLC result in much lower doses and risks than other techniques. This is particularly important for radiation-induced ipsilateral lung cancer, where, for example, the estimated lifetime risk for a 60 year old woman can be reduced from 2.3% to 0.24% by using an appropriate technique.

While the benefits of breast irradiation in breast conserving therapy certainly outweigh the risks of developing subsequent radiation induced cancers, the excellent long-term survival rate for women undergoing breast conserving therapy suggests that it is imperative that second-cancer risks be reduced as much as possible. Consideration should be given to breast treatment planning techniques that decrease the radiation exposure to the contralateral breast and lung and, particularly, the uninvolved ipsilateral breast and the ipsilateral lung. These considerations hold for *all* women treated with radiation therapy for breast cancer, not only those treated at a young age, with a positive family history, and/or BRCA1/2 mutation carriers.

References

1. Sachs RK and Brenner DJ. Solid tumor risks after high doses of ionizing radiation. *Proc Natl Acad Sci USA* **102**:13040-5, 2005. ■

Mechanisms of Radiation-Induced Leukemia at Radiotherapeutic Doses

Igor Shuryak, Rainer K. Sachs,[a] Lynn Hlatky,[b] Mark Little,[c] Philip Hahnfeldt[b] and David J. Brenner

Radiation therapy inevitably results in ionizing radiation exposure to normal healthy organs, causing an increased risk of a radiation-induced second cancer. Patients who undergo radiotherapy for common cancers such as prostate and breast are undergoing treatment at younger ages and with increasing survival times, and thus the issue of radiation-induced second cancer has become increasingly pertinent. There is particular interest in radiotherapy-induced leukemias, because the latency time between radiation exposure and leukemia is typically only a few years, far shorter than for solid tumors.

There is a considerable literature on epidemiological studies of second cancers after radiotherapy, but, as treatment techniques are changing rapidly, the results of these studies, typically referring to treatment techniques some decades ago, cannot be directly applied to modern-day protocols. Thus, there is increasing interest in being able to predict radiation-induced second-cancer risks based on the organ doses or dose distributions produced by current radiotherapeutic treatments. Quantitative, biologically based modeling of cancer can lead to such predictions, as well as giving insight into the basic mechanisms of carcinogenesis.

A recent mechanistically-motivated model of high-dose radiation-induced cancer successfully estimated risks of second solid tumors, by incorporating proliferation of radiation-damaged stem cells as a counterbalance to radiation-induced cell killing. However, this model overestimates the high-dose leukemia risk. We have extended the model to radiation-induced leukemia, by incorporating repopulation of hematopoietic stem cells through cells that have migrated via the blood stream. In contrast to second solid cancers, these repopulating cells often originate at locations distant from the treatment volume, and are thus largely undamaged and contribute minimally to the leukemia risk.

As shown in Figure 1, using parameter values derived from biologic data, the model generates risk estimates for radiation-induced leukemia that are consistent with epidemiological data both for radiotherapy-induced second cancer data, and for A-bomb survivors.

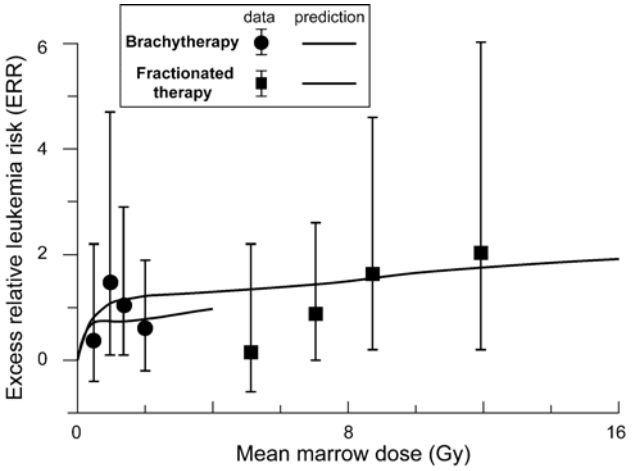

Fig. 1. Model-based predictions for excess relative risk (ERR) of radiation therapy-induced leukemia, and corresponding epidemiologic data. Points refer to epidemiological data for brachytherapy and fractionated external-beam radiation therapy. The model predicts a steep initial increase in ERR with increasing dose of radiation, a subsequent leveling off that is much more pronounced than that predicted for solid tumors by the initiation–inactivation–proliferation model without migration, and, in contrast to the standard linear–quadratic–exponential, predicts a substantial risk even at large doses.

Radiation-induced leukemia risks at radiotherapeutic doses are predictable using a model based on induction of pre-leukemic stem cells, stem cell killing, stem cell proliferation, and, uniquely for leukemia, stem cell migration. As well as providing practical algorithms for risk estimation, this approach provides quantitative insights into the mechanisms of radiation-induced leukemia. Realistic high-dose second-cancer risk estimates should significantly enhance modern radiotherapy treatment planning.

[a] *Departments of Mathematics and Physics, University of California, Berkeley, CA.*
[b] *Tufts School of Medicine, Boston, MA.*
[c] *Imperial College, London, UK.*

References

1. Sachs RK, Brenner DJ. Solid tumor risks after high doses of ionizing radiation. *Proc Natl Acad Sci USA* **102**:13040-5, 2005.
2. Shuryak I, Sachs RK, Hlatky L, Little MP, Hahnfeldt P, Brenner DJ. Radiation-induced leukemia at doses relevant to radiation therapy: modeling mechanisms and estimating risks. *J Natl Cancer Inst* **98**:1794-806, 2006. ■

A Comparison of Mantle vs. Involved-field Radiotherapy for Hodgkin's Lymphoma: Reduction in Normal Tissue Dose and Second Cancer Risk

Eng-Siew Koh,[a] Tu Huan Tran,[a] Mostafa Heydarian,[a] Rainer Sachs,[b] Richard Tsang,[a] David J. Brenner, Melania Pintilie,[a] Tony Xu,[b] June Chung,[b] Narinder Paul[a] and David Hodgson[a]

It has long been established that Hodgkin's lymphoma (HL) survivors experience increased risks of secondary cancer (SC) and cardiac disease attributable in part to radiotherapy (RT). This is of considerable significance for HL survivors, in that the 10-year survival rate for favorable early-stage Hodgkin's lymphoma is more than 90%. Indeed, for such patients, treatment-related mortality may exceed HL-related mortality. Most published estimates of SC risks after RT in HL survivors are based on results from patients treated with extended field RT (i.e., mantle, extended mantle or subtotal nodal RT fields that included both grossly enlarged lymph nodes as well as surrounding lymph nodes), widely used before the mid 1990s. Since that time, in large part to reduce the risks of SC and cardiac sequelae, extended field radiotherapy for HL has been widely replaced by involved field radiation therapy (IFRT) delivered following chemotherapy, resulting in a significant reduction in the radiotherapy treatment volume. Most IFRT protocols use the same prescribed dose as the corresponding extended-field treatment, but several trials have recently investigated reduced-dose IFRT, and interim analyses suggest that IFRT dose reduction to 20Gy may produce comparable early response for selected favorable and intermediate risk patients.

Because the advent of IFRT is relatively recent, while it has generally been assumed that IFRT will result in less late toxicity, there are no large-scale studies with sufficient statistical power to confirm and quantify this expectation. Only one study has been published comparing SC risks for IFRT and extended field RT at the same dose, and no second-cancer results will be available for some years for the comparatively-recent low-dose IFRT. The one published study, by the British National Lymphoma Investigation (BNLI), although quite large (600 patients), involved a number of confounding variables, such as subsequent therapy, mediastinal disease (which results in part of the breast and lung being in the treatment field, even for IFRT), age, and smoking.

Until recently, it was not practical to calculate SC risks after HL radiotherapy, because there was considerable uncertainty about the appropriate dose-responses for radiation-induced cancer at high radiation doses. However, our recent mechanistically-based analyses of epidemiological studies of radiotherapy-induced SC risks have now clarified the shapes of dose-cancer-risk relationships at high radiation doses, particularly for the key sites of breast and lung.[1] The current study therefore estimates the changes in dose distributions within the breast and lung due to the transition from 35Gy mantle RT to 35Gy IFRT and 20Gy IFRT, and uses these data to estimate the associated reductions in risk of radiotherapy-induced breast and lung cancer. In addition, the reduction in cardiac and thyroid dose is evaluated.

Organ-specific dose-volume histograms (DVH) were generated for 41 patients receiving 35Gy mantle RT, 35Gy IFRT, or 20Gy IFRT, and integrated organ doses were compared for the three protocols. Organ-specific SC risk estimates were estimated using a "dosimetric + risk-modeling approach", analyzing DVH data with quantitative, mechanistic models of radiation-induced cancer.

Results are summarized in Table 1, which shows the estimated excess relative risk (ERR) of secondary breast and lung cancer 20 years after radiation exposure (95% confidence interval). Dose reductions resulted in corresponding

[a] *Princess Margaret Hospital, Toronto, Ontario, Canada.*

[b] *Department of Mathematics, University of California, Berkeley.*

Table 1.

	Female Breast		*Female Lung*		*Male Lung*	
	Age at RT (yrs)		Age at RT (yrs)		Age at RT (yrs)	
	20	30	20	30	20	30
35Gy mantle RT	4.6	2.1	18.4	7.6	12.6	5.2
(95% CI)	(2.5-13.3)	(1.07-6.1)	(7.0-56.3)	(3.0-21.8)	(5.3-26.4)	(2.3-10.1)
35 Gy IFRT	1.7	0.74	6.1	2.5	8.3	3.4
(95% CI)	(0.90-4.7)	(0.38-2.2)	(2.3-18.8)	(0.99-7.3)	(3.5-17.3)	(1.5-6.6)
20Gy IFRT	1.06	0.47	3.5	1.4	4.7	1.9
(95% CI)	(0.58-3.0)	(0.24-1.4)	(1.3-10.7)	(0.57-4.1)	(2.0-9.9)	(0.86-3.8)

reductions in predicted ERRs for SC induction. Moving from 35Gy mantle RT to 35Gy IFRT reduces predicted ERR for female breast and lung cancer by approximately 65%, and for male lung cancer by approximately 35%; moving from 35Gy IFRT to 20Gy IFRT reduces predicted ERRs approximately 40% more. The median reduction in integral dose to the whole heart with the transition to 35Gy IFRT was 35%, with a smaller (2%) reduction in dose to proximal coronary arteries.

The significant decreases estimated for radiation-induced SC risks associated with modern IFRT provide strong support for the use of IFRT to reduce the late effects of treatment. The approach employed here can provide new insight into the risks associated with contemporary IFRT for HL, and may facilitate the counseling of patients regarding the second-cancer risks associated with this treatment.

References

1. Sachs RK and Brenner DJ. Solid tumor risks after high doses of ionizing radiation. *Proc Natl Acad Sci USA* **102**:13040-5, 2005. ■

Automated Robotic System for High-Throughput Radiation Biodosimetry

Anubha Bhatla,[a] *Jian Zhang,*[a] *Alessio Salerno,*[a] *Nabil Simaan*[a] *and Lawrence Y. Yao*[a]

Introduction

The goal of this project is to develop a high-throughput radiation biodosimetry workstation, using robotic devices and advanced high-speed automated image acquisition. This report focuses on the design, analysis and implementation of robotic devices necessary to reach the desired throughput of 30,000 samples/day.

System layout

The robotic biodosimetry workstation consists of four main modules: centrifuge, cell harvesting system, liquid/plate handling robot and dedicated image acquisition/processing system.

The system depicted in Figure 1 is currently under development. The main tasks of this system are *i)* sample handling, *ii)* information logging and *iii)* imaging. Excluding the latter, an optimized system layout is reported in Figure 1a. The imaging system is described in the next section.

The layout shown in Figure 1 includes robotic centrifugation, service robot, cell harvesting and liquid/plate handling.

A SCARA robot is responsible to automate the blood sample transfer operations among the modules. To this end the SCARA workspace is augmented by designing an additional link capable of reaching safely into the workspace of the liquid/plate handling robot as shown in Figure 1b.

Robotic centrifugation module

An overview of the automated processing steps begins with loading blood samples, contained in PVC hematocrit capillaries, into a centrifuge which will isolate the lymphocytes. A challenge here is to meet the desired throughput and system reliability when handling capillaries.

To cope with this problem a novel multi-purpose robotic gripper is designed for *i)* centrifuge-buckets and microplates handling and *ii)* multiple handling of capillaries, see Figure 2.

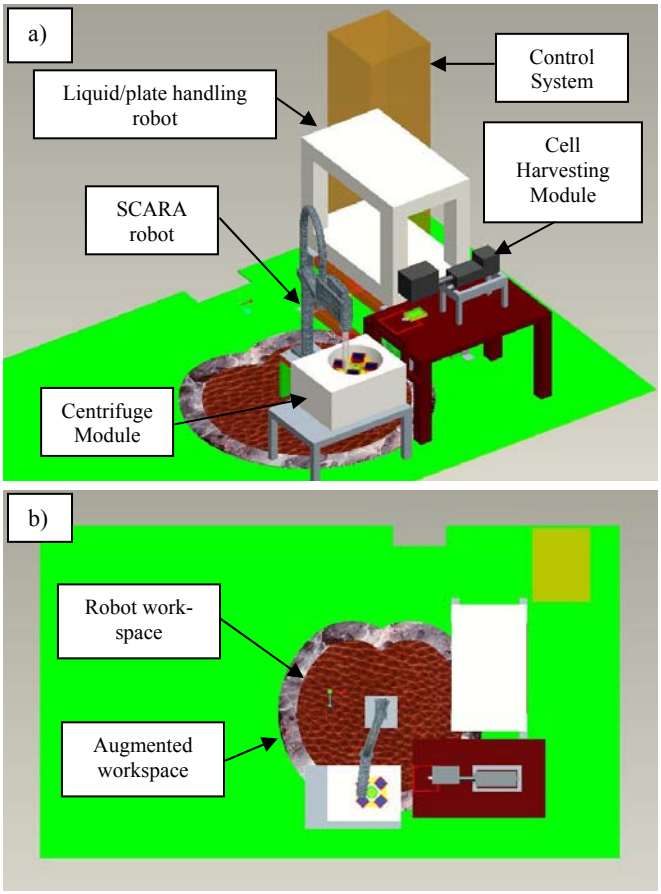

Fig. 1. Optimized System Layout isometric (a) and top view (b).

[a] *Department of Mechanical Engineering, Columbia University.*

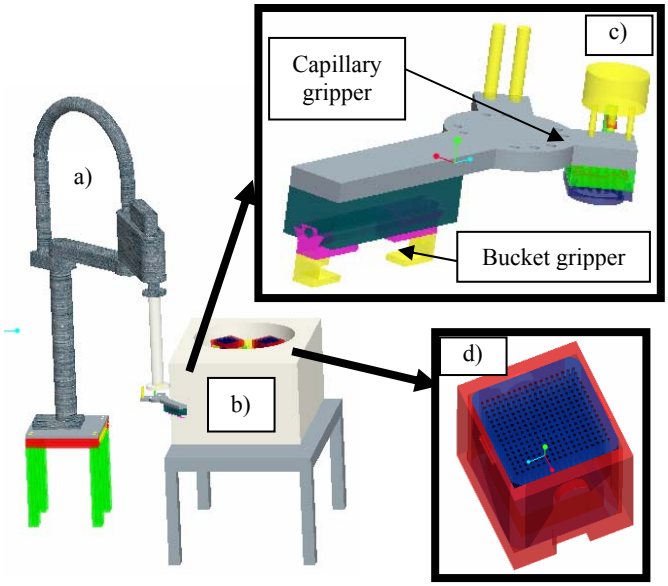

Fig. 2. Robotized Centrifuge Module made of SCARA robot (a), multi-bucket PC-controlled centrifuge (b), custom-made bucket/capillary/microplate gripper (c), and multi-position bucket adapter (d).

Cell harvesting module

After centrifugation the samples are transferred to a band recognition module, where cell harvesting is completed by cutting the hematocrit tube to select the lymphocytes. Plasma and lymphocytes are flushed into the appropriate well. A challenge faced here is the contactless automatic cutting of PVC hematocrit capillaries. To avoid cross-contamination associated with the use of non-disposable mechanical cutting tools, a laser-based cutting system is designed and tested on water-filled capillaries (Fig. 3a-b).

An automatic rotary stage is designed and implemented to allow for even distribution of the laser-delivered power along the circumference of the cut cross-section, see Figure 3c. A collet/solenoid-based gripper for automatic capillary back feed is designed, see Figure 3d.

Product development

Our product development strategy consists of three stages: breadboard, low-throughput prototype (6,000 samples per day) and high-throughput prototype (30,000 samples/day). In order to develop the breadboard a room was selected in such a way as to impose dimensional constraints that would increase system portability. The automated bio-

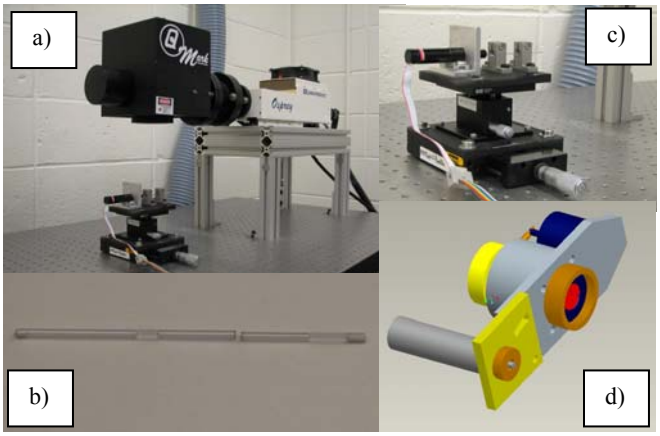

Fig. 3. Laser system (a) for capillary cutting (b), made of a custom-made rotary stage (b) and upgradeable with a back-feed gripper (d).

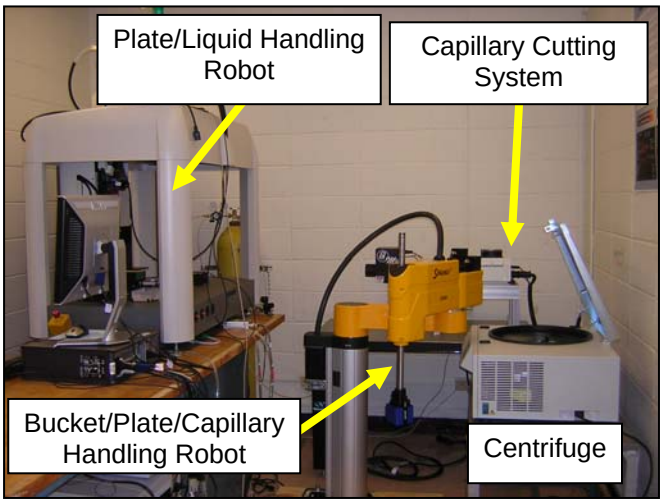

Fig. 4. Breadboard.

dosimetry room is located in the Mudd Engineering building at Columbia University Morningside Campus within the Department of Mechanical Engineering. The room has been equipped with an RS80 SCARA robot from Staubli, an O-Sprey UV laser system from Quantronix, a Sciclone ALH 3000 liquid handling robot from Caliper Life Sciences, a 5810RA Robotic Centrifuge from Eppendorf, and an industrial PC from iBASE technology running RTAI Linux for the low level control.

An implementation of the breadboard without the image acquisition/processing module is reported in Figure 4. ■

Dr. Michael Partridge, examining slides through a microscope.

Developing High-Throughput Imaging Systems For Biodosimetry

Guy Garty, Gerhard Randers-Pehrson, Oleksandra V. Lyulko and David J. Brenner

Introduction

Current automated imaging systems have limited throughput, mostly due to their non-specificity. For example the Metafer system (Metasystems, Germany) can perform rare cell detection, comet assays, metaphase spreads, location of dicentrics, micronucleus scoring and more on 100-200 slides per day as well as. This is about 1% of the required throughput for the biodosimetry workstation under design at the CMCR. We have therefore decided to build a dedicated high-throughput imaging system for performing the micronucleus assay exclusively, seeking creative solutions for rapid sample manipulation, automated focusing and image acquisition and analysis, using the experience gained from developing the automated microbeam workstation. The throughput of the imaging system currently under advanced stages of design and component testing is estimated at 5-6 minutes/96-well plate or 20,000-30,000 individual samples/day.

Sample manipulation

Commercial microscope stages such as the one used by the Metafer system are rather slow (70mm/sec); this is partially due to the fact that the main bottleneck in those systems is the generalized image acquisition and quasi-offline analysis and partially because of the desire to limit the accelerations experienced by living cells.

In our system both requirements are non-existent and so a much faster stage can be used. As in the microbeam, the

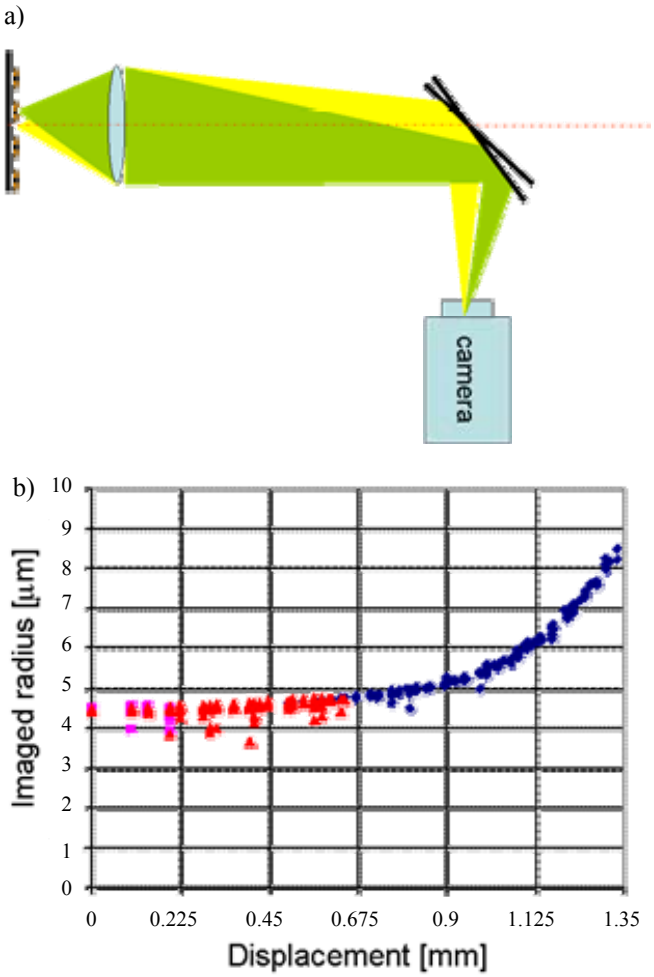

Fig. 1. a) Using mirrors to access off-axis fields of view. b) Imaged radius of a 10µm bead as a function of the distance from the objective lens axis. The larger image sizes above 1mm displacement are due to coma.

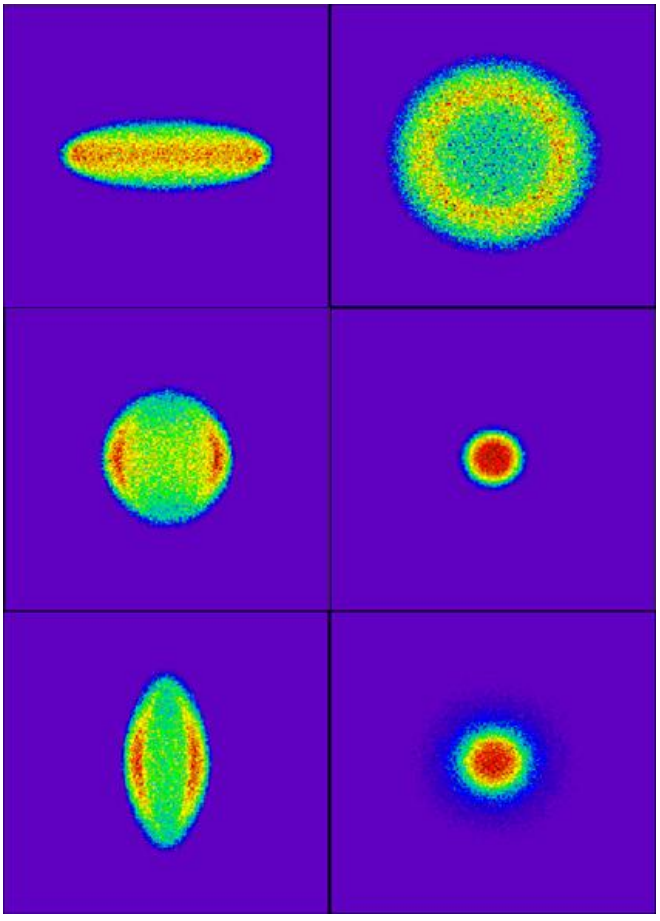

Fig. 2. Simulated images of a 10µm bead with (left) and without (right) a cylindrical lens in the beam path. The rows correspond to 10 µm above (top), at (center) and 5 µm below (bottom) focus.

motion of the sample is separated into two components. A slower coarse motion and a rapid fine motion. The coarse motion is performed by a high speed stage (Parker motion) capable of few-g accelerations. This motion is used to move between adjacent samples (9mm in 50msec). The fine motion between fields of view within a single sample is performed, not by moving the sample but rather by steering light, using fast galvanometric mirrors as shown in Figure 1. Typical transit times between adjacent fields of view of the microscope objective are 1-2msec.

Focusing

A major rate limiting step in automated imaging systems is focusing. In order to get good image quality, typically microscope objective lenses have a rather small depth of field and are sensitive to the roughness of the sample being imaged. The simple solution to this is to take several images at different object-lens distances, quantify "fuzziness" and search for the best setting. This process is very time consuming and therefore unacceptable. Our solution is to place a weak cylindrical lens in the optics path. Using an appropriately selected lens, a circular object will be imaged as circular when in focus and as elliptical when out of focus (Fig. 2), the aspect ratio being proportional to the distance from focus. The object-lens distance can then be corrected in one step.

Image acquisition and processing

For imaging we chose a CMOS camera, which has a much faster readout than the lower noise, CCD cameras typically used. The resulting loss in image quality may be significant for "all purpose" imaging systems, but is unimportant for detection of micronuclei. Analysis of the image is split between the camera and the frame grabber board to decrease the amount of data transferred to the controlling computer, the biggest bottleneck in current imaging systems. By using a dichroic mirror and two cameras attached to the same frame grabber board we can simultaneously "see" the nucleus and cytoplasm and rapidly analyze their overlap, obtaining the number and size of nuclei in each cell. ■

Ex vivo Gene Induction for Development of Radiation Biodosimetry Profiles

Sunirmal Paul and Sally A. Amundson

Introduction

One component of the recently established Center for High-Throughput Minimally Invasive Biodosimetry led by Columbia is the development of a self-contained biochip capable of rapidly measuring gene expression signatures to define radiation exposure, dose and injury. As a first step toward identifying these signatures, which will potentially consist of a hundred or more genes, we are measuring gene expression in *ex vivo* irradiated peripheral blood obtained from healthy donors.

The main goal of this biodosimetry project is to provide radiological triage to identify those individuals who will benefit from medical intervention, and those who will not, at an early stage following a large-scale radiological event. Individuals who receive whole-body doses above around 1.5Gy can benefit from antibiotics, platelet and cytokine treatment. There is also a critical need for biodosimetry at higher doses, because there is a relatively narrow dose window (approximately 7-10Gy) in which bone-marrow transplantation is a useful option. Below 7Gy, survival rates are good with antibiotic and cytokine treatment, while above 10Gy patients will generally have lethal gastrointestinal damage. Thus, our initial studies have been designed to span these critical dose ranges, and also to allow comparison with *in vivo* responses in patients undergoing total body irradiation (TBI) prior to transplantation.

Irradiation and culture

In our previous studies of gene expression in *ex vivo* irradiated peripheral blood,[1] we first isolated mononuclear cells by centrifuging the whole blood on a Lymphoprep™ gradient. The cells were then resuspended in RPMI 1640 medium and 10% fetal bovine serum (FBS), irradiated, and incubated for times from 4 to 72 hours to allow gene expression. In the current work, we were interested in exploring the possibility of irradiating whole blood, both to expedite the workflow, and to permit interactions between different blood components during the irradiation and recovery phases to more closely mirror possible effects *in vivo*. Donor blood was aliquotted and irradiated directly after drawing, then diluted 1:1 with RPMI 1640 supplemented with 10% FBS. The samples were incubated for 24 hours to allow gene expression.

Purification of RNA

Because the ultimate goal of this study is to perform microarray screening to develop multi-marker signatures of radiation response, the presence of red blood cells and hemoglobin in our samples was a concern. Extraction of RNA from whole blood yields mRNA containing a high percentage of globin message. In past studies, such preparations have been shown to limit the sensitivity of microarray experiments, or to skew the results.[2,3] In order to avoid such

potential effects, we investigated a number of methods for preparation of RNA with reduced hemoglobin message content. The Versagene™ Blood RNA Purification System (Gentra Systems) uses an initial step to differentially lyse red blood cells and wash away the nucleic acids released prior to lysis of the white blood cells and isolation of their RNA. This protocol yielded high quality RNA, and RT-PCR analysis demonstrated a reduced level of globin RNA compared to the same samples processed without differential red cell lysis (Fig. 1). However, relatively high levels of globin still remained when compared to RNA prepared from the TBI patients using treatment with GLOBINclear™ (Ambion). Applying the GLOBINclear™ protocol to the donor blood samples resulted in extremely low levels of globin mRNA, providing samples appropriate for comparison with the *in vivo* TBI samples (Fig. 1).

Optimal blood collection

In our initial studies, we collected the donor blood in tubes with sodium heparin to prevent clotting during the experiment. Some literature suggests, however, that using heparinized blood may inhibit down-stream enzymatic reactions, including amplification and labeling for microarrays. We therefore tested the relative efficiency of amplification and radiation induced expression ratios for the *CDKN1A* gene in blood from the same donor collected with sodium heparin or with sodium citrate as an anti-coagulant. Expression ratios did appear to be somewhat compressed in the heparin samples (Fig. 2), so we have elected to use sodium citrate as our anti-coagulant to avoid potential negative effects associated with heparin.

Dose Response of CDKN1A

We next examined the induction of the *CDKN1A* gene in *ex vivo* irradiated blood from a set of five independent donors using quantitative real-time PCR. We found a consistently increasing dose-response across the dose range studied, from 0.5 to 8Gy (Fig. 3). When these present data were compared to that from our earlier study,[1] which focused on the lower part of this dose range, we saw very good agreement within the overlapping dose range. This agreement was seen despite striking differences in the cell irradiation protocol (isolated lymphocytes versus diluted whole blood followed by globin reduction) and the method of gene expression measurement (quantitative dot blot versus quantititive real-time PCR).[4] This finding is encouraging, as it implies that the gene expression responses we are measuring are

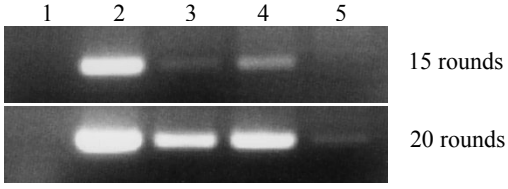

Fig. 1. *RT-PCR of β-globin RNA.* Lane 1: no RNA control. Lane 2: TBI patient whole blood. Lane 3: TBI patient with GLOBINclear™. Lane 4: *ex vivo* whole blood (Versagene™). Lane 5: *ex vivo* whole blood (Versagene™ plus GLOBINclear™).

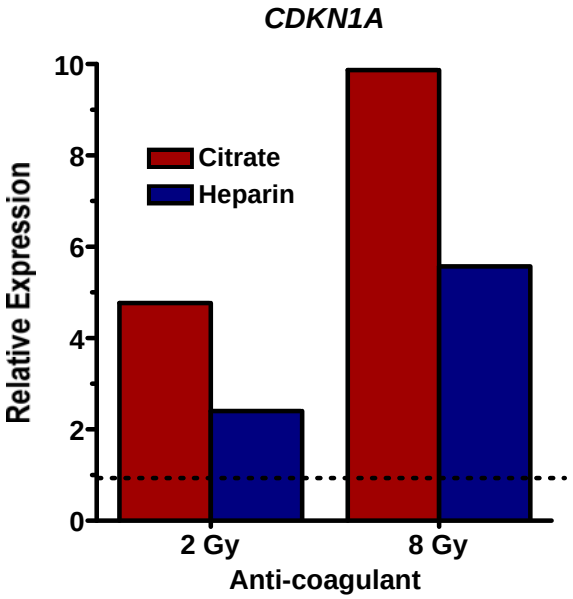

Fig. 2. Gene induction in ex vivo irradiated blood collected with different anti-coagulants. Dashed line: levels in untreated controls.

broadly conserved across individuals and different data sets, and are not easily affected by variations in the experimental details.

Interestingly, the dose-response relationship is not linear across the entire dose range, but rather appears bi-phasic. This response is virtually identical in shape to that previously seen in ML-1 human myeloid cells, where *CDKN1A* was induced with linear kinetics up to around 2.5Gy, then showed further linear increases with doses up to 20Gy, but with a much shallower slope.[5]

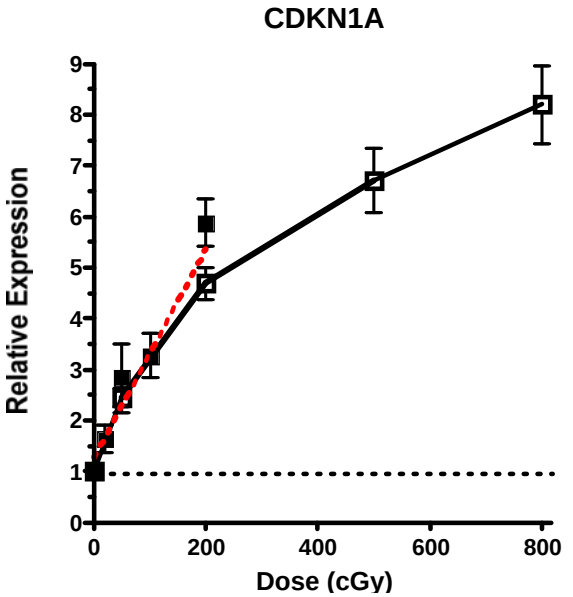

Fig. 3. *CDKN1A* expression 24 hours after *ex vivo* irradiation. Mean and SEM of real-time PCR (□; 5 donors) and prior dot blot studies (■; 4 donors).[1] Dashed line: untreated control levels. Red dotted line: linear fit to all data at 2Gy and below.

These same samples are now being hybridized to whole genome microarrays (Agilent). We anticipate that analysis of this first round of microarray data will provide valuable insights into the possibilities of biodosimetric gene expression signatures. Many additional experiments, including ongoing experiments with RNA from the TBI patients, will be needed to refine and validate signatures for practical biodosimetry, however. Our efforts are continuing in collaboration with investigators at the Center for Applied Nanobioscience (Arizona State University), where development of the self-contained biochip for gene profile analysis is progressing well.

References

1. Amundson SA, Do KT, Shahab S, Bittner M, Meltzer P, Trent J and Fornace AJ, Jr. Identification of potential mRNA biomarkers in peripheral blood lymphocytes for human exposure to ionizing radiation. *Radiat Res* **154**:342-6, 2000.
2. Feezor RJ, Baker HV, Mindrinos M, Hayden D, Tannahill CL, Brownstein BH, Fay A, MacMillan S, Laramie J, Xiao W*, et al.* Whole blood and leukocyte RNA isolation for gene expression analyses. *Physiol Genomics* **19**:247-54, 2004.
3. Liu J, Walter E, Stenger D and Thach D. Effects of globin mRNA reduction methods on gene expression profiles from whole blood. *J Mol Diagn* **8**:551-8, 2006.
4. Koch-Paiz CA, Momenan R, Amundson SA, Lamoreaux E and Fornace AJ Jr. Estimation of relative mRNA content by filter hybridization to a polyuridylic probe. *Biotechniques* **29**:706, 8, 12, 14, 2000.
5. Amundson SA, Do KT and Fornace AJ Jr. Induction of stress genes by low doses of gamma rays. *Radiat Res* **152**:225-31, 1999.

■

Lymphocyte-based Biodosimetric Assays For Robotic Handling

Giuseppe Schettino,[a] Aparajita Dutta, Guy Garty and David J. Brenner

Introduction

The two assays used for automated biodosimetry are the micronuclei assay and the γ-H2AX assay. Both these assays require the separation of lymphocytes from whole blood as a first step for our purpose. Whole blood is collected by minimally invasive procedures such as a finger stick and transferred into glass capillaries coated with lithium heparin as an anticoagulant (QBC diagnostic Accutube).

Lymphocyte extraction

For the lymphocyte separation, we have been successful in working with 50µl of whole blood. The blood is transferred into the accutube by capillary action, followed by 50µl of the lymphocyte separating medium, and centrifuged at a speed of 40g for 20mins. This yielded a good separation of the lymphocytes in the form of a clearly visible white band of lymphocytes with a count of 2100/µl of blood and about 80% purity. The lymphocyte separating medium, Ficoll Hypaque, with a density of 1.114g/ml was found to yield better counts of lymphocytes and sharper bands upon separation as compared to the separation medium with the lower density (1.077g/ml).

Although our current tests are with glass capillaries, we intend the final system to use plastic ones (such as Safe-T-Fill capillaries from RAM scientific), to increase safety and to facilitate capillary cutting. Initial tests indicate that the lymphocyte separation works as well with plastic capillaries.

[a] *Gray Cancer Institute, Mount Vernon Hospital, Northwood, Middlesex, UK.*

Lymphocyte culture in the 96 microwell plates and micronuclei assay

In order to reduce handling time and to facilitate medium exchange and the addition/removal of reagents without needing to pellet out the lymphocytes by centrifugation each time, we have designed a system for culturing lymphocytes in 96 microwell plates (Multiscreen plates from Millipore). We have used the plates with non-fluorescent filters with a pore size of 1.2µm for this purpose. The underdrains of the microwell plates are easily detachable so that it allows easy removal of the processed, stained lymphocytes, embedded in the filters from the wells for imaging.

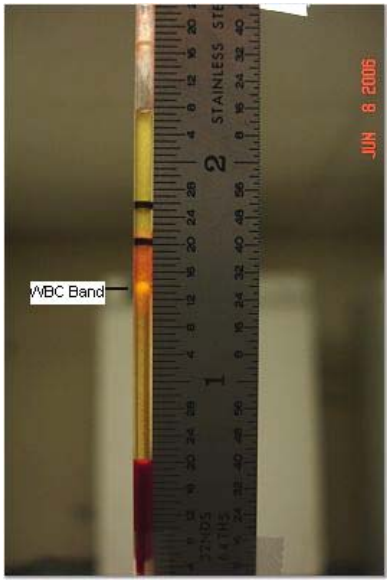

Fig. 1. Lymphocytes separated out from whole blood in a glass Accutube is seen as a white cloudy band on the upper half of the tube.

The lymphocytes within each capillary after centrifugation were separated from the RBC pellet and dropped within the microwell. Cultures were set up in each well with complete medium containing

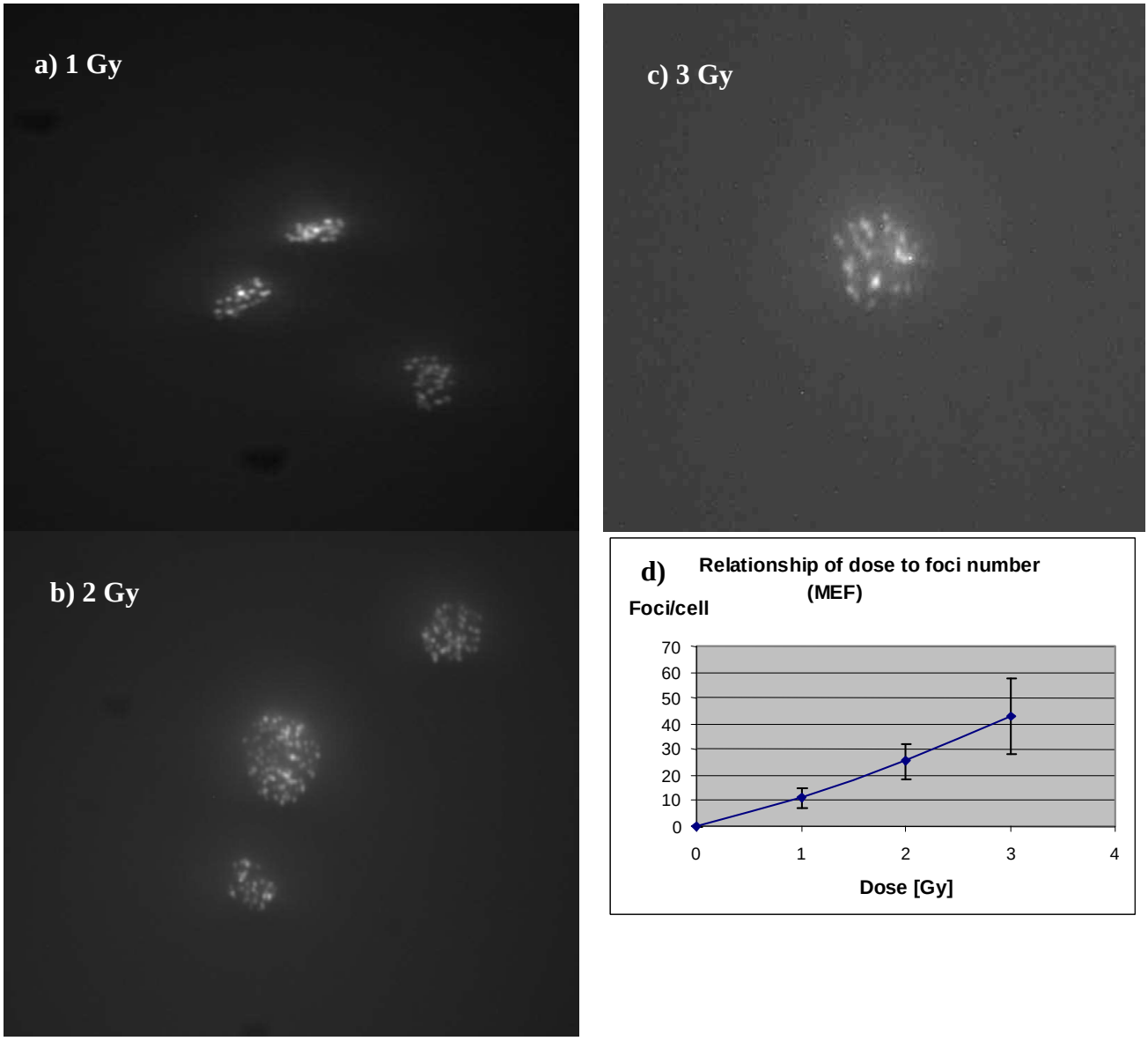

Fig. 2. (a)-(c) γ-H2AX foci formation on MEF cells in response to different doses of 250 kV X-rays. **(d)** Graph to show dose response of γ-H2AX foci formation in MEF cells.

15% heat inactivated FBS, PHA (M-form), L-glutamine and antibiotics. After incubation at 37°C for 44hrs cytochalasin B (in DMSO) was added in order to block cytokinesis. After 28hrs with the cytochalasin B at 37°C, cells were treated with hypo and fixed in Carnoy's fixative. Every time, the liquid already present within each well was drained out by the application of a positive pressure before the addition of any fresh reagents. Finally, the cells were allowed to dry and stained with Acridine Orange and DAPI, and viewed under a fluorescent microscope.

Optimization of the γ-H2AX foci staining protocol

The need to detect DNA damage by radiation requires specific markers that can be easily seen and quantified, and γ-H2AX foci formation is one such event that can be used in this scenario. It is known that H2AX phosphorylation is specific to sites of DNA damage and is also indicative of amount of DNA damage. However, in order to use γ-H2AX as a quick screening tool, it must be optimized for sensitivity and rapidity which is what we are aiming to achieve.

The first aspect that we addressed is the image quality of foci in cells as it is important for uses in testing or as a diagnostic marker. Certain parameters need to be used in order to test the efficacy of γ-H2AX and the best procedure for producing the images. Light intensity ratios of foci being one such parameter, can be optimized through antibody concentrations during chemiluminescence. The goal is to achieve the sharpest image possible and also to record the relationship between radiation level and foci counts. For the first experiments, to determine the γ-H2AX induction, we worked with MEF cells in culture. It was seen that there was an increase of foci with increasing doses (Fig. 2) of radiations in the fibroblasts. Experiments were also performed to measure which concentration of antibodies yielded the best

image quality based on the contrast between the cell background and fluorescence signal given by the γ-H2AX foci. Cells that exhibited the largest intensity ratio were deemed the best for viewing for clarity and with the most distinction between foci and cellular background. Cells were treated with antibodies using various concentrations of 1-100, 1-500, 1-1000, and 1-2000 dilution of both the primary and secondary antibodies. Cells were then imaged and compared. It was found that the 1:100 concentrations for the primary antibody and the 1:500 for the secondary antibody yielded the best intensities ratios so far (Fig. 3). A comparison was also done using different kinds of blocking agents, and it was found that even though Superblock (Pierce Biochemicals) yielded faster results, NFDM (non fat dried milk) provided clearer pictures of the foci.

So far all the experiments regarding the γ-H2AX foci have been done in MEF cells and we need to apply all these procedures to human lymphocytes and study the effects. We would also need to find out the dose response for γ-H2AX foci formation in response to very low doses of radiation. ■

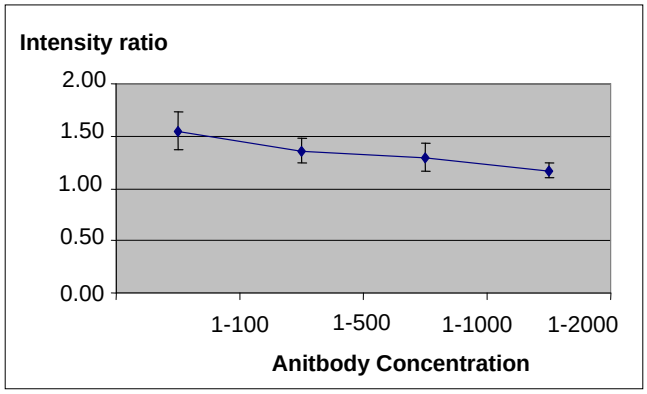

Fig. 3. Relationship of concentration of primary antibody to intensity ratio of γ-H2AX in MEF cells.

Podcasting Information in the Radiological Sciences To Health Care Professionals

Carl D. Elliston, David J. Brenner, Nitin Gumaste,[a] John Zimmerman[a] and Eric J. Hall

Particularly in the context of the potential for a large-scale radiological event, there is a growing necessity to train health care professionals at all levels in the radiological sciences. Correspondingly, there is increasing demand from health care professionals, most of whom have no background in the radiation sciences, for such information in an accessible format.

We have created an online educational resource to address this need. Our goal is to provide convenient access to the resource and to ensure that the user makes efficient use of their time during the learning activity. Another challenge is the potential long time span from the initial learning encounter until the user needs to apply the information; therefore, the educational strategy is to effect a long-lasting attitudinal change in the learning, while providing concise summary information for review and easy retrieval of detailed knowledge that may be required in an emergency.

Our solution to these challenges involves enhanced podcasting. A podcast is a media file that is distributed over the internet for playback on portable media players, such as an iPod, or on a personal computer. If the user subscribes to a podcast, all new files are automatically downloaded. Enhanced podcasting incorporates audio, images, links, and chapters in a podcast.

Our podcasts are based on a semiannual training course entitled *Radiological Science in the Context of Radiological Terrorism* which has been developed and implemented by faculty at Columbia, Harvard, and elsewhere. It covers a broad spectrum of topics to help participants understand 1) the nature of ionizing radiation; 2) how radiation is damaging to people; 3) how we know what we know about radiation risks; 4) potential radiological terrorist scenarios; and 5) emergency preparedness for a radiological event.

Fig. 1. Podcasts include audio of the lecture plus power point slides that can be played on video iPods or from a PC.

Each podcast consists of about 40 minutes of audio, playable on any iPod or similar player, optionally synched with accompanying Powerpoint slides viewable on a video iPod or a PC, as well a PDF handout giving an outline of the key topics covered.

A web page has been created to allow users to subscribe to the material in a simple, straightforward manner. The URL is:http://cmcr.columbia.edu/training/podcasts.html. ■

[a] *Columbia Center for New Media Teaching and Lecturing, New York, NY.*

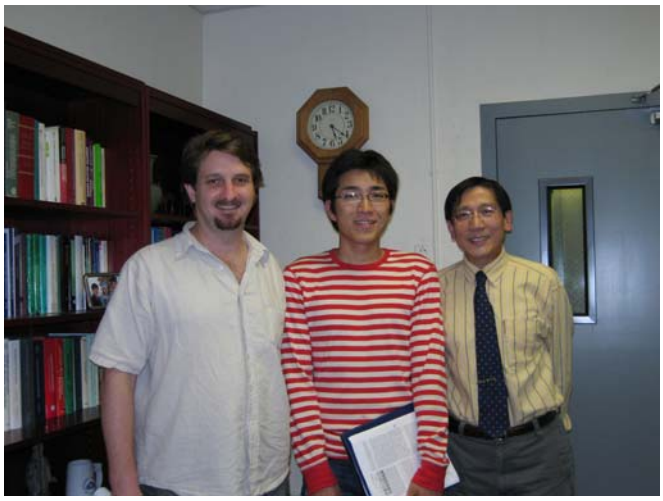

Mr. Takuro Fushimi, 3rd year student of Okayama University, Medical School, posted with Dr. Michael Partridge (left) and Dr. Tom K. Hei (right). Takuro had worked in Dr. Hei's lab for 3 months.

Ms. Ilana Yurkiewicz, a summer high school student in Professor Tom K. Hei's laboratory, was selected as one of the top twenty high school graduates in the United States in 2006 by the USA Today.

Clinical Radiation Oncology Residents, Drs. Jinesh Shag, Mori Suthen, Arther Ko, with their research mentor Professor Tom K. Hei.

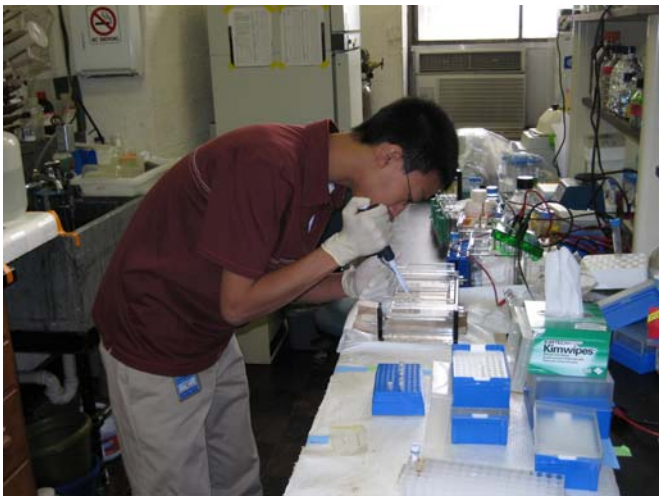

Albert Hei, is a summer high school student in Dr. Hei's lab. He came from Eleanor Roosevelt high School.

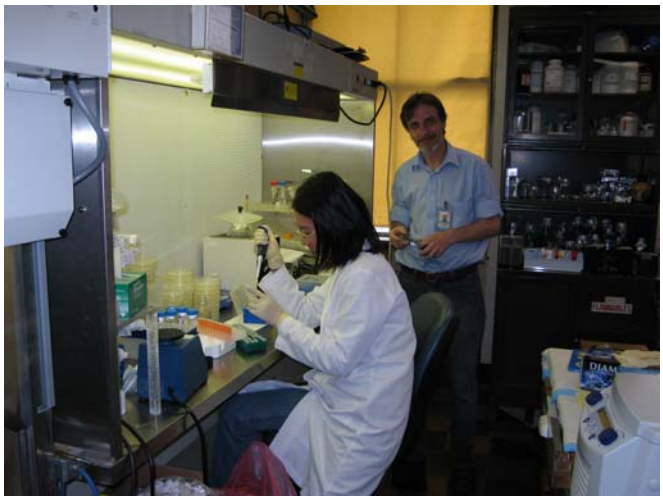

Dr. An Xu and Dr. Lubomir Smilenov.

Dr. Genze Shao, Post-Doctoral Research Scientist, left the Center for Radiological Research for new positions.

RARAF – Table of Contents

RARAF PROFESSIONAL STAFF

RARAF Staff *(l–r)*: Guy Garty, Yanping Xu, Andrew Harken, David Brenner, Sasha Lyulko, Gerhard Randers-Pehrson, Stephen Marino, Alan Bigelow, Brian Ponnaiya and Charles Geard. *Not shown*: Giuseppe Schettino, Gregory Ross and Gloria Jenkins-Baker.

David J. Brenner, Ph.D., D.Sc. **–** RARAF Director
Stephen A. Marino, M.S. **–** RARAF Manager
Gerhard Randers-Pehrson, Ph.D. **–** RARAF Associate Director, Chief Physicist
Charles R. Geard, Ph.D. – CRR Associate Director, Senior Biologist
Alan Bigelow, Ph.D. – Associate Research Scientist
Brian Ponnaiya, Ph.D. – Associate Research Scientist
Guy Y. Garty, Ph.D. – Staff Associate
Gregory Ross, M.S. – Programmer Analyst
Giuseppe Schettino, Ph.D. – Post-Doctoral Research Scientist
Yanping Xu, Ph.D. – Post-Doctoral Research Scientist
Andrew Harken, Ph.D. – Post-Doctoral Research Scientist
Gloria Jenkins-Baker, B.A. – Biology Technician

The Radiological Research Accelerator Facility

AN NIH-SUPPORTED RESOURCE CENTER – WWW.RARAF.ORG

Director: David J. Brenner, Ph.D., D.Sc.
Associate Director: Gerhard Randers-Pehrson, Ph.D.
Manager: Stephen A. Marino, M.S.

Introduction

This has been another momentous year for RARAF:

- RARAF is now 40 years old. It was started January 1, 1967 with the transfer of the 4.2 MV Van de Graaff that had been the injector for the Cosmotron at Brookhaven National Laboratory.
- Construction of over 2000 square feet of laboratory and office space was completed on the third floor, and was funded by a contribution from Columbia University.
- The new Singletron accelerator completed its first year of use.

Research using RARAF

The "bystander" effect, in which cells that are not irradiated show a response to radiation when in close contact with or even only in the presence of irradiated cells, continues to be the main focus of the biological experiments at RARAF, especially those using the microbeam. All but one of the biology experiments run this year examined this effect, observing a variety of endpoints to determine the size of the effect and the mechanism(s) by which it is transmitted. Evidence continues to be obtained for both direct gap junction communication through cell membrane contact and indirect, long-range communication through the cell media. Both the microbeam and the track segment facilities continue to be utilized in various investigations of this phenomenon. The single-particle Microbeam Facility provides precise control of the number and location of particles so that irradiated and bystander cells may be distinguished, but is somewhat limited in the number of cells that can be irradiated. The Track Segment Facility provides broad beam irradiation that has a random pattern of charged particles but allows large numbers of cells to be irradiated and multiple users in a single day.

Two special types of track segment dishes are being used to investigate the bystander effect using the Track Segment Facility: double-sided dishes and "strip" dishes. Double-sided dishes have Mylar foils glued on both sides of a stainless steel ring, 1cm apart, with cells plated on the inside surfaces of both foils. The interior is completely filled with medium. This type of dish is used for investigation of the non-contact, long-range bystander effect since the cells on the two surfaces are not in direct contact, can only communicate through the culture medium, and only the cells on one surface are irradiated. "Strip" dishes consist of a stainless steel ring with Mylar foil glued to one side in which a second dish is inserted. The Mylar foil glued to the inner dish has alternate strips of the Mylar removed. Cells are plated over the combined surface and are in contact. The Mylar on the inner dish is thick enough to stop the charged particles (usually ^{4}He ions) and the cells plated on it are not irradiated. These dishes are used for bystander experiments involving cell-to-cell communication.

Interest in irradiation of 3D systems has increased this past year, with several experimenters irradiating tissue samples using either helium ions or protons. Imaging systems for the Microbeam Facility are being developed to enable observation and targeting of cells that are not in monolayers; in the interim, cultured human tissue samples are being irradiated using the Track Segment Facility. The tissue samples are on membranes on the end of cylindrical plastic holders. Plastic discs have been constructed that fit in the spaces in the irradiation wheel and have small holes to provide precise alignment of the feet that are around the bottom edges of the tissue holders. A hole in the middle of each disc is fitted with two stainless steel half-discs that have a precise 0.001" (25μm) space between them. The tissue membrane is in contact with the stainless steel, which is thick enough to stop the charged particles. This provides a narrow line of irradiation across the center of the entire sample. The tissue samples are later sectioned, either parallel or crosswise to the line of irradiation, to observe bystander effects as a function of distance from the line of irradiation.

Table 1 lists the experiments performed at RARAF from January 1 through December 31, 2006 and the number of days each was run in this period. Use of the accelerator for experiments was over 59% of the normal available time, 6% higher than last year, which had been the highest we had attained at Nevis Labs. Fourteen different experiments were run during this period, about the average for 2000-2005. Eight experiments were undertaken by members of the CRR, supported by grants from the National Institutes of Health (NIH), the National Aeronautics and Space Administration (NASA), and the Department of Energy (DOE). Six experiments were performed by outside users, supported by grants and awards from NASA, the NIH, the DOE, the Japanese Nuclear Energy Crossover Research Program and the Japanese 21st Century Center of Excellence Program. Brief descriptions of these experiments follow.

Gerhard Randers-Pehrson and Alan Bigelow of the CRR continued development of a method to detect explosives in baggage (Exp. 82). The detection system is based on resonant elastic scattering of 0.43MeV neutrons by nitrogen and oxygen. Measurements of the neutron transmission through a liquid nitrogen sample were made using neutrons produced in a very thin target by the 7Li(p,n) reaction. A high voltage is applied to the target and scanned slowly up and down

Table 1. Experiments Run at RARAF, January 1 – December 31, 2006

Exp. No.	Experimenter	Institution	Exp. Type	Experiment Title	No. Days Run
82	G. Randers-Pehrson A. Bigelow	CRR	Physics	Detection of explosives	27.8
89	R.H. Maurer D. Roth J. Goldsten	Johns Hopkins University	Physics	Calibration of a portable real-time neutron spectrometry system	2.3
103	B. Hu C.R. Geard	CRR	Biology	Damage induction and characterization in known hit versus non-hit human cells	25.3
106	B. Ponnaiya C.R. Geard	CRR	Biology	Track segment α-particles, cell co-cultures and the bystander effect	6.2
110	H Zhou Y-C. Lien T.K. Hei	CRR	Biology	Identification of molecular signals of α-particle-induced by-stander mutagenesis	38.2
126	O. Sedelnikova W. Bonner (G. Jenkins)	NIH	Biology	γ-H2AX foci formation in directly irradiated and bystander cells	3.5
130	B. Ponnaiya C.R. Geard	CRR	Biology	Investigation of bystander responses in 3-dimensional systems	8.5
132	T. Funayama	JAEA	Biology	Quantitative analysis of the relationship between bystander response and DNA double strand breaks	9.8
133	J. Ahn, S. Ghandhi S. Amundson	CRR	Biology	Bystander effects in primary cells	9.4
134	P. Grabham C.R. Geard	CRR	Biology	Effects of track segment low-energy particles versus high-energy space-related radiations	1.3
135	K. Suzuki M. Yamauchi	Nagasaki University	Biology	Visualization of the effects of radiation on chromatin structure in bystander cells using 53BP1 foci as markers of chromatin disorganization	3.0
136	S. Amundson G. Schettino S. Paul	CRR	Biology	Bystander effects in 3D tissues	3.8
137	S. Bailey S.E. Williams (B. Ponnaiya)	Colorado State University	Biology	TRF2 recruitment in cells irradiated with α-particles	6.5
138	E. Azzam J. Santos O. Kovalenko	NJSMD	Biology	Investigation of the effect of mtDNA damage on apoptosis in hTERT cells	2.3

Note: Names in parentheses are members of the CRR who collaborated with outside experimenters.

across the proton energy required to produce neutrons with the required energy. The neutron transmission can then be measured over the range of a few keV under identical target and focusing conditions.

Richard Maurer, David Roth and John Goldsten of Johns Hopkins University continued the characterization of a neutron spectrometry system (Exp. 89) that may be used on the International Space Station and possibly the manned mission to Mars. They evaluated a tin-walled helium-3 gas detector with 0.84MeV neutrons for energy calibration and response. This detector is similar to a detector delivered to NASA Marshall Space Flight Center for a future balloon flight. The acquisition and pre-trigger times were the same as the balloon flight instrument and the detector was sampled at a data rate that accurately defined the acquired waveforms. A newly fabricated Eljen boron-loaded scintillator was evaluated for both energy calibration and waveform distributions at six neutron energies from 0.84 to 14MeV. This energy range is of primary concern when determining the neutron energy spectra produced in high energy collisions of protons and heavy ions with thick spacecraft material targets. Several acquisition parameters were altered to determine their effect on the recoil peak, capture peak and energy resolution. A recently refurbished 5mm thick silicon detector that is almost 5 times the diameter of the previously used silicon detectors was evaluated with 14MeV neutrons. Due to the increased area and consequent increased oblique path lengths, the response function used for the smaller 5mm detector needed to be modified.

Charles Geard and Burong Hu of the CRR continued

studies of the bystander effect, examining the relationship between the radiation-induced bystander response and genomic instability (Exp. 103). Normal human fibroblasts were cultured in double-sided Mylar dishes (see above) and one side was irradiated with 3Gy of ^{4}He ions using the Track Segment Facility. The range of the helium ions is very much shorter than the space between the two Mylar layers so that the cells on the other side of the dish were then bystanders, which could only be influenced by signal transfer through the medium. For microbeam studies, 20% of the nuclei of nearly confluent (in contact) fibroblasts were irradiated with 30 ^{4}He ions each, which ensures that only non-hit bystander cells can survive over many cell generations. In both scenarios cells were harvested at specific time points post-irradiation. Elevated levels of chromosomal damage in bystander cells were observed after G_2 PCC, reflecting signal transfer from irradiated cells and suggesting there is genomic instability in bystander cells after track segment and microbeam irradiation of cells. Preliminary mFISH results 5 cell divisions post-irradiation show chromosome 1 and 3 more frequently damaged in both of the experimental protocols. Experiments are continuing in order to confirm this interesting finding and investigate the signal transfer in bystander effect and genomic instability between the two kinds of irradiations.

Two other studies investigating the bystander effect were continued by Brian Ponnaiya and Charles Geard of the CRR. One study (Exp. 106) uses the Track Segment Facility for broad-beam charged particle irradiations of normal human fibroblasts plated on double-sided Mylar dishes to examine genomic instability in irradiated and bystander immortalized small airway epithelial cells (SAEC-htert). These cells were cultured on Mylar dishes and prior to irradiation, half the dish was covered with a metal shield. Cells on the non-covered portion of the dishes were irradiated with 0.1, 1 and 3Gy of ^{4}He ions, while cells on the covered portion of the dishes were bystander cells. Irradiated and bystander populations from each dish were separated and set up in culture. At various times post irradiation (7-28 days) G_2-PCCs were prepared from each culture using Calyculin A. The chromosomes were analyzed by both Giemsa staining (for gross chromosomal aberrations) and mFISH (for more subtle alterations, e.g., translocations). Giemsa staining revealed that both irradiated and bystander populations had elevated yields of chromosomal changes at 7 and 14 days post irradiation.

In a study of the bystander effect in artificial tissue systems (Exp. 130), EPI-200 epithelial tissue samples from MatTek Corp. were irradiated with ^{4}He ions or protons using the Track Segment Facility. Each sample was irradiated with multiple lines of particles down the center. This resulted in a 50μm line of irradiation in the center of a tissue sample 8mm in diameter. Samples were fixed at 15, 30, 45 and 60 minutes post-irradiation and sectioned perpendicular to the line of irradiation. Thus each section of tissue contained both irradiated cells (in the center) and bystander cells (at various distances away from the center). Immunohistochemical protocols were used to examine the expression of various phosphorylated proteins in these sections to determine the role of MAP kinases in the propagation of the bystander response. Enhanced phosphorylation of both Jnk and Erk were seen in both irradiated and bystander cells. Alterations in protein phosphorylation seemed to be dependent on the distance away from the line of irradiation; with closer bystander cells showing higher levels of the phosphorylated proteins.

Hongning Zhou, Yu-Chin Lien and Tom Hei of the CRR continued to use the single-particle Microbeam Facility to try to identify the cell-to-cell signaling transduction pathways involved in radiation-induced bystander mutagenesis (Exp. 110). Using the Microbeam Facility, they found that when 10% of the population of AA8 cells is lethally irradiated, the HGPRT$^-$ mutation frequency was about 4 times higher than the spontaneous yield. However, when 10% of V3 cells in the mixed population (90% AA8 and 10% V3) were irradiated, there was only a limited bystander mutagenesis response in AA8 cells when compared to bystanders of irradiated AA8 cells. A similar result was found when 10% of the AA8 cells in the mixed population (10% AA8 and 90% V3) were irradiated: there was only a limited bystander mutagenesis response in V3 cells when AA8 cells were lethally irradiated. These data indicate that DNA-PKcs deficient cells may have some problems in either delivering or receiving the radiation-induced bystander signals. A fraction of mitochondrial DNA deficient (ρ0) human hamster hybrid (A_L) cells were irradiated in the nucleus or the cytoplasm with ^{4}He ions and given doses that kill essentially all the irradiated cells. Mutagenesis at the CD59 locus for the surviving unirradiated cells was compared with that for wild-type cells. Preliminary data showed that the bystander effect induced by cytoplasmic irradiation was lower in ρ0 cells when compared with similarly irradiated wild-type cells, indicating that mitochondria may partially mediate the process. Interestingly, nuclear irradiation of ρ0 cells induced no bystander CD59 mutation, suggesting that mitochondrial function may play an important role in mediating the bystander signal initiated by nuclear-irradiation. The observed difference of bystander effects between cytoplasmic and nuclear-irradiated ρ0 cells suggests different mechanisms for the genotoxicity and biological consequences of cytoplasmic and nuclear damages. In addition, experiments were performed using the Track Segment Facility. Several cell lines, such as DNA-PKcs deficient cells, mitochondrial function deficient cells and normal human lung fibroblast cells were irradiated on "strip" dishes. They found that 0.5Gy of ^{4}He ions could induce 3.3 times the yield of mutants in AA8 bystander cells compared with the spontaneous background. However, the same radiation increased mutagenesis in bystander cells by a factor of 2.

The occurrence of non-targeted effects calls into question the use of simple linear extrapolations of cancer risk to low doses from data taken at higher doses. Olga Sedelnikova and William Bonner of the NIH, in collaboration with researchers from other institutions, are investigating a model for bystander effects that would be potentially applicable to radiation risk estimation (Exp. 126). They are evaluating the lesions that are introduced into DNA by alpha particles and the resulting non-targeted bystander effect. These lesions, and particularly the most dangerous–the double strand

breaks (DSBs)–can be revealed by the phosphorylation of histone H2AX. Human reconstructed EpiAirway tissues from MatTek Corporation were irradiated with ^{4}He ions in a line 25μm wide across their diameters using the Track Segment Facility and the slit system described above. After irradiation, each tissue was incubated for different time periods, up to 7 days post-irradiation. Control tissues went through the same procedure without being irradiated. A total of 215 tissues were used in the experiment. The tissues were then frozen and shipped to the University of Lethbridge, Canada for extraction of DNA, RNA, histones and proteins, and to the NIH for immunohistochemistry.

Tomoo Funayama, a visitor from the Japan Atomic Energy Agency, explored intracellular mechanisms of the bystander response (Exp. 132). The relationship between cell killing and induction of DNA double strand breaks (DSBs) in the Chinese hamster-human hybrid cell line A_L was analyzed and compared between direct-hit and bystander cells. The cells were irradiated with 0-2Gy of α-particles using the Track Segment Facility and clonogenic survival and induction of γH2AX foci were analyzed. Preliminary results suggest that the intracellular mechanisms of cell killing after induction of DNA double strand breaks are the same for medium-mediated bystander and direct-hit cells. A similar experiment analyzing gap-junction mediated bystander mechanisms using the Microbeam Facility was also carried out. A very limited number of cells in confluent cell colonies were irradiated using a circular irradiation protocol; however, no significant bystander DSB induction was observed.

A group led by Sally Amundson of the CRR continued two types of experiments concerning radiation-induced gene expression profiles in human cell lines using cDNA microarray hybridization and other methods (Exp. 133, 136). One experiment, performed by Shanaz Ghandi and Jaeyong Ahn, involved use of the track segment irradiation for comparison of gene expression responses to direct and bystander irradiation. Normal human fibroblast cells (NHLF and MRC-5) and epithelial cells: AEF-hTERT cells were plated on standard Mylar dishes for direct irradiation or "strip" dishes (see above) for direct-contact bystander irradiations. The cells were irradiated with 125keV/μm ^{4}He ions and assayed for micro-nucleus formation. The main goal of these experiments is to isolate total RNA and protein from the control, irradiated and bystander cells and measure the levels of PTGS-2/COX-2 mRNA and protein. They have found that irradiation with ^{4}He ions induces COX-2 mRNA in the epithelial cells, but the protein is barely detectable. In the case of MRC-5 cells, there are high basal levels of both mRNA and protein but no detectable response to irradiation. After confirmation of the bystander effect in fibroblast cells using the MN assay and/or COX-2 mRNA levels as initial indicators, they are currently using microarray analysis to search for pathways that will suggest novel gene targets involved in the bystander effect. The second experiment, performed in collaboration with Giuseppe Schettino and Surnimal Paul of the CRR, involved irradiation of artificial human tissue samples using the Track Segment Facility. EpiDerm tissues (EPI-200, consisting of fully differentiated cell layers) from MatTek were irradiated in a narrow line (~25μm) with protons having an initial LET of ~10 keV/μm using the same slit masks developed for Sedelnikova's experiment (Exp. 126). After 48h the tissues were removed from the culture insert and cut into narrow slices (200-400mm) parallel to the irradiation line. The strips were fixed on slides and scored for micronucleus formation. Micronucleus induction statistically significantly higher than background level was measured in samples irradiated with as little as 0.1Gy. Although a higher level of micronucleus induction was always detected in the irradiated cells, a bystander response was also measured up to 3mm away with no clear dose dependency.

Peter Grabham and Charles Geard began an assessment of the cytogenetic effects of particles with varying LETs (Exp. 134). Endothelial cells have been subjected to high energy particles at the NASA irradiation facility at Brookhaven National Laboratories and low energy particles at RARAF. Human umbilical vein endothelial cells (HUVECs) were irradiated at RARAF in standard Mylar dishes at varying doses using the Track Segment Facility. Chromosome damage at early stages after irradiation was assessed by giemsa staining. Much like the high energy particles, alpha particles (1Gy) caused widespread gaps and breaks in chromosomes. Studies to examine chromosome aberrations are currently being carried out using FISH analysis.

An investigation to visualize the effects of radiation on chromatin structure in bystander cells using 53BP1 foci as markers of chromatin disorganization in cells was initiated by Keiji Suzuki and Motohiro Yamauchi of Nagasaki University in Japan (Exp. 135). Cells stained with Hoechst 33342 were plated on microbeam dishes along with cells stained with Cell Tracker Red in a ratio of 1:1. Approximately 20% of the cells stained with the Hoechst dye were irradiated with ^{4}He ions using the Microbeam Facility and immunostained. Observation of 53BP1 foci in bystander cells confirmed the indirect effect of radiation on chromatin structure.

Susan Bailey and Eli Williams, a graduate student of Colorado State University, are conducting an experiment to observe recruitment of TRF2 in cells irradiated with α-particles (Exp. 137). Although damage induced by high intensity (e.g., multi-photon) laser irradiation resulted in the positive recruitment of TRF2, α-particles, well known for their ability to produce DSBs, failed to elicit this response. In seeking an explanation for this apparent discrepancy, the possibility was considered that damage from a single α-particle track might be insufficient to cause TRF2 recruitment. To address this issue, they utilized α-particles from the charged-particle Microbeam Facility. Cells were exposed to either 200 or 400 α-particles (roughly equivalent to 30 and 60Gy) in a defined nuclear area of less than 5μm^2 and fixed immediately, 30min, and 60min after irradiation, followed by immunostaining. This resulted in well-defined damage clusters marked by γ-H2AX and MDC1. However, even at these high fluences, producing thousands of DSBs in a limited nuclear volume, TRF2 recruitment was not observed.

Edouard Azzam, Janine Santos and Olga Kovalenko of the New Jersey School of Medicine and Dentistry are investigating whether mitochondrial DNA (mtDNA) damage by

itself can trigger apoptosis in hTERT cells (Exp. 138). Parental cells carrying wild type or a nuclear-only hTERT mutant are irradiated either in the nucleus or the cytoplasm using the Microbeam Facility, allowed to recover for approximately 24h, and stained with YOPRO-1 in order to score the percentage of apoptotic cells. Using the above cells and apoptosis as an endpoint, they are also investigating the expression of radiation-induced bystander effects under conditions wherein a small fraction of cells in the exposed population is targeted through the nucleus or cytoplasm by one or more ^{4}He ions.

Development of facilities

This year our development efforts concentrated on a number of extensions of the capabilities of our microbeam facilities including:

- Development of focused accelerator microbeams
- Non-scattering particle detector
- Advanced imaging systems
- Focused x-ray microbeam
- New laboratory space

Development of focused accelerator microbeams

The first quadrupole triplet for the double quadrupole lens, installed in 2003, continues to operate very reliably, with very few sparks. It has proven to be quite robust, surviving vacuum excursions caused by the occasional breakage of the ion beam exit window. An electrostatic phase space "confuser" has been installed just above the 90° bending magnet. By varying the voltages on 4 electrodes, the beam is continually steered in a non-repetitive way to eliminate any correspondence between particle position and direction. This has enabled us to focus a 6MeV ^{4}He beam down to a diameter of 2μm.

The parts for the second quadrupole triplet have been constructed in our shop and will be inserted into a separate alignment tube for testing, in place of the present lens once the permanent magnet microbeam (Fig. 1) is fully operational for biological irradiations. When the voltages on this second lens have been adjusted to produce the smallest beam spot attainable, the two lenses will be mounted in a single tube for testing of the compound lens system that will produce a sub-micron beam spot. After using this sub-micron beam for biological irradiations for a suitable period, the testing process will be repeated with two more triplet lenses so that we will eventually have two complete compound lenses, one of which will be used as a spare.

A second microbeam has been reassembled after construction of the 3rd floor. A beam of 5.3MeV ^{4}He ions or protons will be focused into a spot smaller than 10μm in diameter using a compound quadrupole triplet lens made from commercially available permanent magnets. Because the magnet strengths are essentially fixed, only a single energy proton or ^{4}He ion can be focused. The pair of quadrupole triplets is similar to the one designed for the sub-micron microbeam, the only difference being that it uses magnetic rather than electrostatic lenses. This system was originally designed to focus alpha particles from a ^{210}Po source during the dismantling of the Van de Graaff and the installation of

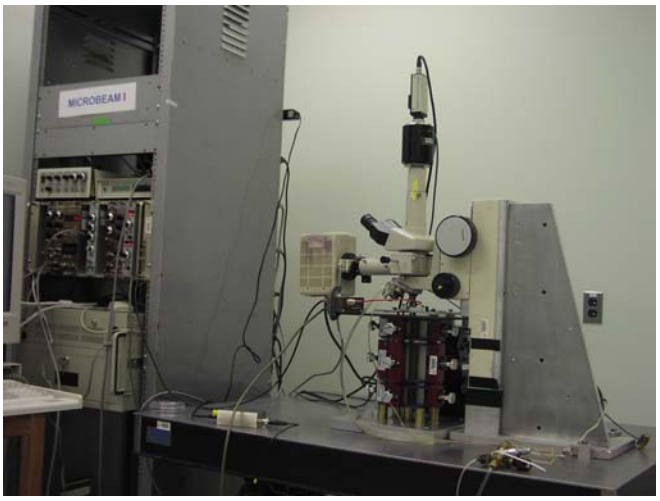

Fig. 1. A view of the Permanent Magnet Microbeam system in its new lab on the 3rd floor.

the Singletron. Using a charged particle beam from the accelerator will provide us with a much greater flux. The endstation for our original microbeam has been moved from the 2nd floor, where it was used for the collimated microbeam, to the new microbeam lab on the 3rd floor because additional room for the lens structure is required between the focal point and the final bending magnet

The helium beam from the Singletron accelerator is incident on a thin aluminum foil to produce a beam in which the particle location and direction are not coupled. This foil will soon be replaced by a magnetic steerer, which will reduce the energy spread in the beam, allowing the beam to be focused to a smaller diameter, and increasing the flux at the endstation. The lenses have been optically aligned and adjustment of the quadrupole magnet strengths has begun using micrometric screws to retract and extend the individual magnets of each quadrupole.

This system will be used for irradiations when the electrostatic system is unavailable because of development or repair.

Non-scattering particle detector

To irradiate thick samples, such as model tissue systems or oocytes, to use particles with very short ranges, such as the heavy ions from the laser ion source, and to allow irradiation of cell monolayers without removing the culture medium, a completely non-scattering particle detector is necessary upstream of the samples. A novel particle detector has been designed on the basis of a long series of inductive cells coupled together into a delay line. The Lumped Delay Line Detector (LD^2) will consist of 300 silver cylinders 3mm long with a 2.2mm inside diameter connected by inductors and capacitively coupled to ground. The cylinders are glued to a semi-cylindrical tube of dielectric material 1m long for mechanical support. The dielectric has a semi-cylindrical metal tube around it that can be rotated about its axis to adjust the capacitance. If the individual segment delays are set (by adjustment of the capacitance) such that the propagation velocity of the pulse equals the projectile velocity, the pulses capacitively induced in all segments by the passage of a single

charged particle will add coherently resulting in a fast electron pulse at each end of the delay line that is 150 times larger than the charge induced on a single cylinder. This easily detectable charge of at least 150 electrons will be amplified to provide the detection pulse for the particle counter. Two prototype LD^2 detectors (1/6 length) have been constructed for testing their signal propagation properties. Based on these results the parameters for a full-length LD^2 detector have been determined. The full-length detector is currently under construction. It is anticipated that this detector will become the standard detector for all microbeam irradiations.

Advanced imaging systems

Development continued on new imaging techniques to view cells without using stain and to obtain three-dimensional images of unstained cells. Two different techniques continue to be investigated: quantitative non-interference phase microscopy (QPm) and immersion-based Mirau interferometry (IMI). Both have been integrated into the Microbeam Facility and are being tested for applicability to rapid location and targeting of cells for microbeam irradiation without use of stain.

QPm is a non-interferometric approach to non-stain imaging. Reflected light images are obtained in focus and with the focus set slightly above and below the sample plane. These images are then used to approximately solve the light transport equation using the Fourier transform-based software from Iatia Vision Sciences. The results are used to create a new 2D map of the sample which is then fed back into the custom microbeam irradiation software. By streamlining the control program, including interleaving the image processing steps with the mechanical motions of the stage, the additional processing time required to convert the raw images into QPm images can be reduced such that it affects throughput by only about 10%. We are working with Iatia to improve this processing time by taking full advantage of the on-board dual processing, which will cut this factor in half.

In tests, some cells have been missed and there also have been false positives. In general, the quality of the images can be improved by carefully optimizing tuning of the parameters for the approximate solution to the transport equation. However, to optimize for our regular, automated use there is still work to be done in eliminating false cells and reducing missed cells. Several variables have been isolated and eliminated as causes: plating time, cell-type, cell phase, light color, cell growth surface, amount of medium (depth), percent of medium vs. buffer, and use of a cover glass. Continued efforts are aimed at finding a combination of these variables that may affect the images and at exploring other variables that have not yet been considered.

The immersion-based Mirau interferometric (IMI) objective is currently under construction (Fig. 2) and has been designed to function as an immersion lens with standard interferometric techniques using a short coherence length and to otherwise accommodate the endstation requirements for the microbeam at RARAF. The preliminary results in air on 10μm polystyroid beads were sufficiently encouraging to warrant the effort to design the new objective. As part of the testing for the design process we modified an off-the-shelf Mirau objective such that it became a water immersion lens, and we confirmed that the two equal-arm light pathways will indeed be restored and will then provide interference fringes in the environment with sufficient contrast to perform the biological experiments.

Preliminary results from the modified objective confirm that the contrast will be sufficient. The finished objective will support rapidly and automatically locating the cell nuclei under the no-stain scenario. “Banding” in some of the images indicates that further work must be done to eliminate both a slow drift in z-position and some very slight vibrational interference.

While it is possible that we ultimately will keep both forms of no-stain imaging in the endstation, QPm and IMI are being evaluated in competition with each other. Under consideration are: processing time, reliability, maintenance, and ease of use for the experimenter. IMI is slightly faster in the endstation under regular use than QPm but both are acceptable. QPm is likely to be improved, so they will score about the same. IMI, judging by the preliminary images, is much more reliable than QPm at this stage. QPm is a software solution and does not require introduction of fluids or cleaning, whereas IMI does. QPm does not require any additional equipment and can work in air, while the immersion-Mirau interferometer requires the end-user to use a custom objective and an immersion-based approach. It appears likely that the immersion-Mirau approach will ultimately be favored, but additional work will be done especially on the QPm reliability.

We are constructing a multi-photon microscope for our single-cell single-particle Microbeam Facility to detect and observe the short-term molecular kinetics of radiation response in living cells and to permit imaging in thick targets, such as tissue samples. The multi-photon capability is being built into the Nikon Eclipse E600-FN research fluorescence microscope of the microbeam irradiation system and will provide three-dimensional imaging. A Chameleon (Coherent Inc.) tunable titanium sapphire laser (140fs pulses at a 90MHz repetition rate) is the source for the multi-photon excitation. The scan head incorporates commercial scanners and a scan lens then focuses the laser beam to a point at an

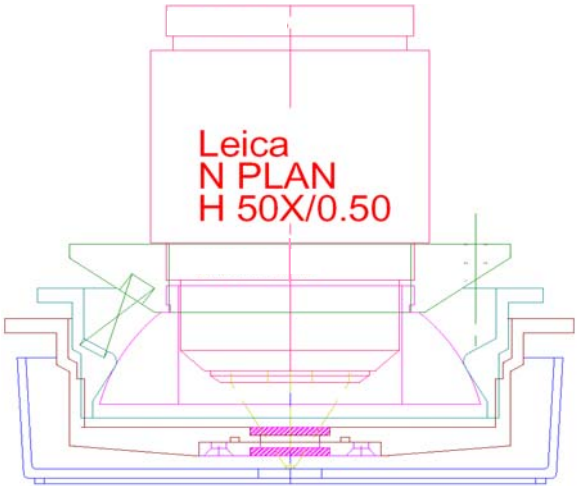

Fig. 2. Construction drawing of the immersion Mirau lens.

image plane of the microscope (a CCD camera is also placed at such an image plane for fluorescent microscopy). The incident laser beam will enter the microscope through the side of the trinocular tube of the microscope. A switch mirror will allow us to choose between multi-photon microscopy and standard fluorescence microscopy. The scanned laser beam establishes an optical section within the specimen, where multi-photon absorption preferentially occurs. Wavelengths available from the laser can penetrate to depths of about 100 microns in a biological sample by varying the z-position of the specimen stage. Returning along the collection pathway, light emitted from the specimen is selectively deflected by a series of dichroic mirrors to an array of photomultiplier tubes (PMTs). To control the multi-photon microscope, we are adopting the design and software of Karel Svoboda, Cold Spring Harbor.

Focused x-ray microbeam

There are considerable benefits in using soft x-ray microbeams for both mechanistic and risk estimation endpoints. The higher spatial resolution achievable with modern state-of-the-art x-ray optics elements combined with the localized damage produced by the absorption of low-energy photons (~1-5keV) represents a unique tool to investigate the radio-sensitivity of sub-cellular and eventually sub-nuclear targets. Moreover, as these x-rays do not suffer from scattering, by using higher energy x-rays (~5keV) it is possible to irradiate with sub-micron precision individual cells and/or part of them up to a few hundred microns deep inside a tissue sample in order to investigate the relevance of effects such as the bystander effect in 3D structured cell systems.

We have investigated expanding the microbeam to include soft x-rays, characteristic K_α x-rays from Al (1.49keV) and Ti (4.5keV). The use of higher energies is not feasible due to Compton scattering effects; we are limited to x-ray energies where the predominant mode of interaction is photoelectron absorption.

Zone Plate (ZP) lenses will de-magnify to a micron or sub-micron size spot a small X-ray source (i.e.~100μm D) produced by bombarding a thin solid target with high-energy protons using a microbeam triplet lens. We investigated the production of characteristic x-rays (K_α line) as a function of the proton energy for aluminum and titanium. The best x-ray production cross sections are at 2.9MeV for Al and 4.5MeV for Ti. By using the already focused proton microbeam to generate characteristic x-rays, it is possible to obtain a nearly monochromatic x-ray beam (very low bremsstrahlung yield) and a reasonably small x-ray source (~10μm diameter), reducing requirements on the subsequent x-ray focusing system.

The present design consists of 3 thin Al or Ti foils 15-20 μm thick separated by 5μm gaps through which cooled He is blown. Such a target is able to cope with a substantial amount of power from the proton beam, providing an x-ray dose rate suitable for many radiobiological experiments (~0.05Gy/sec), even with a sub-micron diameter photon beam. This target design has been tested with a laser beam by focusing 0.8W (800nm) into a 99μm spot. The measurements have exceeded the expectations based on simulations performed using a finite element analysis program (ANSYS), indicating that the designed target is able to cope with a considerable amount of power from the proton beam.

Based on these data, zone plate specifications have been worked out. The proposed zone plate will have a radius of only 80μm and an outmost zone width of 40nm, which implies a zone plate which is easy to manufacture (focusing efficiency closer to the maximum theoretical value) and easy to handle. The new zone plate will be placed close to the x-ray source (150mm) and have a focal length of 12.57mm (demagnification factor of ~12). The final expected dose rates to the sample, based on ANSYS simulations, are 0.03 to 0.6Gy/s for beam spots 0.4 to 2.1μm in diameter.

The main elements of the system have been manufactured in our machine shop and the zone plates are scheduled to be purchased this year.

New laboratory space

Because of a large homeland security research and development grant received by David Brenner and Gerhard Randers-Pehrson from the National Institute of Allergy and Infectious Diseases (NIAID), the Trustees of Columbia University contributed the funds required to build over 2000 square feet of new laboratory and office space on the third floor of the facility (Fig. 3). When RARAF was built in the early 1980s, this space had been intended for offices and a meeting room. Since there were never funds available to build these, the space had been used for storage. Construction began in April 2006 and was completed in December. Over half the area is a biology laboratory with provision for

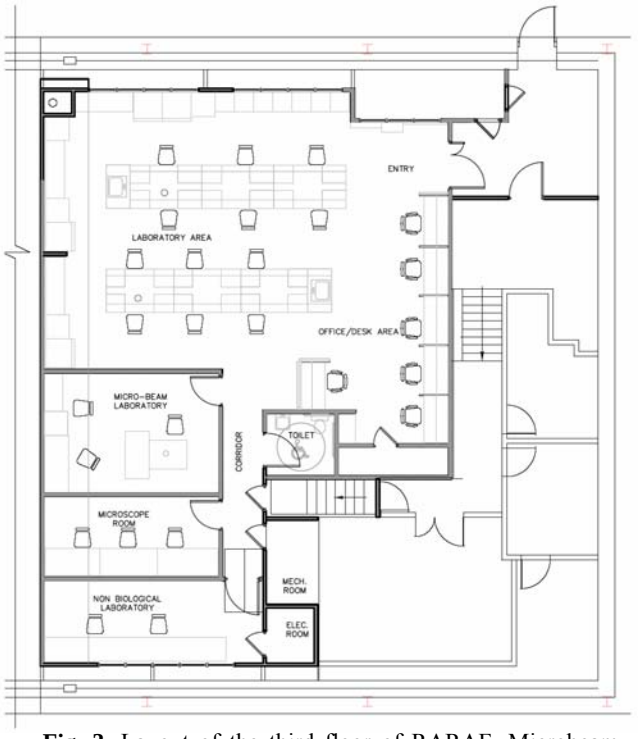

Fig. 3. Layout of the third floor of RARAF. Microbeam Lab III (permanent magnet lens system) is directly above the original microbeam laboratory. The wall on the left is ~58 feet long. Microbeam II, which houses the electrostatic lens system, is shown in the bottom right of center and is a half-floor below the new construction, shown with emphasized walls.

Fig. 4. The new Biology Lab as viewed from the entrance to the third floor lab space (upper right in Fig. 3). In view are the two islands that have work stations for up to 12 people. Sasha Lyulko is working in the new lab.

three laminar flow hoods, one of which is a class II hood, several incubators, refrigerators and freezers and two islands comprising a dozen work stations (Fig. 4). There are also six desks for technicians and postdocs. Two of the labs are a dedicated microscopy laboratory (Fig. 5) with three workstations and a physics laboratory that is being used for the NIAID project.

Included in the construction is a new lab for the permanent magnet Microbeam Facility. While this system was being developed as a stand-alone microbeam for use with a ^{210}Po alpha source, it was housed in a makeshift room on the 3rd floor. The magnetic quadrupole quadruplets and endstation for the system were removed before construction began. Now that construction is complete, the beam line has been reconstructed with the two quadruplet lenses, and the endstation with the microscope and electronics has been installed. The lab is fitted with a laminar flow hood and an incubator. The magnet system is being adjusted to provide the best focusing using proton and helium ion beams from the accelerator. When the focusing studies are complete, the system will be available again for biological irradiations.

Fig. 5. Dr. Brian Ponnaiya, Associate Research Scientist, is working in the new microscope laboratory on the third floor.

Singletron utilization and operation

Accelerator usage is summarized in Table 2. The Singletron was started at 7:30 AM on most days, often run into the evening, and occasionally run on weekends for experiments, development and repair. This has resulted in a total use that equals the nominal accelerator availability of one 8-hour shift per weekday.

Use of the accelerator for radiobiology and associated dosimetry increased by more than 10% over 2004-2005 to the highest level since RARAF has been at Nevis Labs and was about 30% higher than the average for 2000 to 2005. Over half the accelerator use for all experiments was for microbeam irradiations and 23% for track segment irradiations.

The Microbeam Facility is in great demand because it enables selective irradiation of individual cell nuclei or cytoplasm. In addition, because of the relatively low number of cells that can be irradiated in a day, microbeam experiments usually require considerably more beam time than broad beam (track segment) irradiations to obtain sufficient biological material, especially for low probability events such as mutation and bystander effects.

The Track Segment Facility is being used more efficiently, reducing the amount of accelerator time required to satisfy user demand. Because the irradiation times for samples are often 10 seconds or less, multiple users, sometimes as many as 5, are run on a single shift, sometimes using different LETs and different types of ions in the same day.

Radiological physics utilization of the accelerator increased slightly this past year, consisting mainly of the experiment to develop a system to detect explosives in luggage (Exp. 82).

Approximately 20% of the experiment time was used for experiments proposed by outside users, about 2/3 the average for the last five years. This is probably to be expected since operations had been interrupted for the last 6 months of 2005 due to the replacement of the Van de Graaff and it takes a while to get back up to speed.

Use of the accelerator for online development decreased by about 50% from last year. This is predominantly due to the fact that in 2005 there was a major push to get the stand alone microbeam system operational and this past year the emphasis was on radiobiology, to catch up for the 6 months required for the replacement of the accelerator .

Accelerator maintenance and repair time declined somewhat relative to last year, returning to the levels of 1986-2001 when the previous accelerator was running well. The new Singletron accelerator has operated reliably for over 15 months with a single exception: the RF power supply for the ion source. The accelerator has maintained a terminal potential as high as 5.5MV without sparking and probably can maintain an even higher voltage. No accelerator maintenance or repairs have been required for the charging and control systems. The RF tubes for the ionization source were replaced several times, each requiring an accelerator opening, before it was determined that the voltage from the terminal generator was too high. The system was assembled and tested in the Netherlands, where the electric system operates at 50 cycles per second. In the United States, the

Table 2. Accelerator Use, January–December 2006
Percent Usage of Available Days

Radiobiology and associated dosimetry	47%
Radiological physics and chemistry	12%
On-line facility development and testing	26%
Safety system	2%
Accelerator-related repairs/maintenance	8%
Other repairs and maintenance	3%
Off-line facility development	15%

system operates at 60cps. The higher frequency caused the motor that drives the generator to operate at a higher speed, which produced a higher supply voltage. A transformer tap for the RF supply was moved to a different position, lowering the voltage. The RF source has worked reliably for the last 9 months. There was one accelerator opening to replace the ion source bottle, which had become dirty after a year of service.

The terminal voltage, as expected, has very low ripple and produces beams with very little energy spread. Measurements of the Li(p,n) threshold show a very sharp rise in yield with terminal voltage because of the narrow beam energy. An unexpected feature of the accelerator has been some drift in the terminal voltage as the accelerator warms up after starting. The beam currents used for the microbeam irradiations are not large enough to permit slit regulation; therefore the GVM is the main control of the terminal voltage. Because the beam energy is so narrow, beam intensity decreases rapidly as the terminal potential changes by a few kilovolts during warm-up. The problem has been traced to changes in the spacing of the pick-up plates in the generating voltmeter (GVM) as the accelerator warms up. The GVM housing is presently being heated to a constant temperature at all times, greatly reducing the voltage change during warm-up. A more complex system is being constructed that will adjust the temperature of the GVM housing based on the load on the motor that rotates the GVM blades.

Training

The Small Group Apprenticeship Program continued for the third year. Five students from Stuyvesant High School in Manhattan spent at least two half-days each week for six weeks during the summer working on projects in biology or physics (Fig. 6). Stuyvesant is a high school specializing in science that is open to students throughout New York City by competitive admission. The students gave professional PowerPoint presentations to our group at the end of the program. Below is a list of the titles of the work presented followed by the name of the student and the name of his or her mentor:

1. The Bystander Effect: MAP Kinases and their roles in the phenomenon; JNK and Apoptosis – Kelvin Wong (Brian Ponnaiya).
2. Multiphoton Microscopy Prototype Design – Anthony Pang (Alan Bigelow).

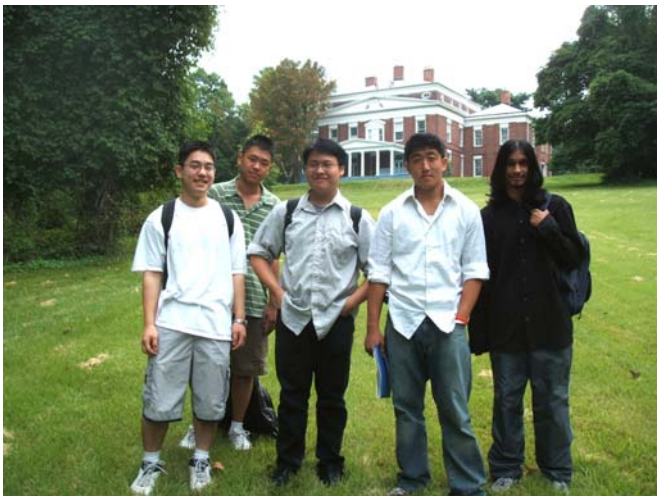

Fig. 6. Stuyvesant High School students who participated in the 2006 Small Group Apprenticeship Program (l-r): Edward Sung, Raymond Wu, Anthony Pang, Kelvin Wong and Ridwan Sami.

3. The Biological Effect of Dirty Bombs – Raymond Wu (Giuseppe Schettino).
4. Beam Stuff; Calculator Program – Ridwan Sami (Gerhard Randers-Pehrson).
5. Progress on the LD^2 Detector: Summer of '06 – Edward Sung (Guy Garty).

Several of the previous students have been co-authors of scientific journal articles, including one that was published in the prestigious Proceedings of the National Academy of Science (PNAS).

Dr. Tomoo Funayama of the Japan Atomic Energy Agency, who arrived in November, 2005 for a one-year visit at RARAF, returned to Japan in November, 2006. Dr. Funayama worked with Charles Geard and learned to perform experiments using the Microbeam and Track Segment Facilities.

Andrei Popescu, a student at Ossining High School in Westchester County, NY, is working with Brian Ponnaiya over the next year. He will be studying DNA breakage and micronucleus formation in mouse cells after x-ray irradiation.

Dissemination

A highlight this year was our hosting the 7th International Workshop of Microbeam Probes of Cellular Radiation Response, held at the Morningside campus of Columbia University, March 15-17, 2006. The two-day workshop featured over 100 scientists from eleven different countries.

RARAF also hosted an open house the day prior to the start of the Workshop. More than 35 researchers from around the world toured RARAF and received briefings on the new accelerator, the irradiation facilities and the research being conducted. Visitors also had opportunities to ask questions and have short discussions with the staff.

In October there was a tour of RARAF by 23 students and three professors from Concordia College in New Rochelle, NY.

Personnel

The Director of RARAF is Dr. David Brenner. The accelerator facility is operated by Mr. Stephen Marino and Dr. Gerhard Randers-Pehrson.

Dr. Alan Bigelow, an Associate Research Scientist, is continuing the development of the laser ion source and has begun the development of a two-photon microscopy system using a fast laser.

Dr. Guy Garty, a Staff Associate, is developing the secondary emission ion microscope (SEIM) and an inductive detector (LD^2) for single ions.

Mr. Greg Ross, a Programmer/Analyst, left RARAF in May. He had been assisting with various programming tasks and worked on new methods of imaging cells without stain.

Dr. Giuseppe Schettino, a Postdoctoral Fellow who left RARAF in December, worked primarily on the development of the x-ray microbeam and performed some biological experiments using tissues grown in culture.

Sasha Lyulko, a graduate student in the Physics Department at Columbia, began working at RARAF in September. She is learning to perform microbeam irradiations, will be involved in research in methods to image cells without stain, and spends half her time working for the NIAID project.

Two new postdocs arrived on the same day in January, 2007: Dr. Andrew Harken, who recently received his Ph.D. in Chemicals Material Engineering from the University of Nebraska at Lincoln, and Dr. Yanping Xu, who recently received his Ph.D. in Physics from North Carolina State University.

Several biologists from the Center for Radiological Research are stationed at the facility in order to perform experiments:

- Dr. Charles Geard, the Associate Director of the CRR and the Senior Biologist for the P41 grant that is the major support for RARAF, continues to spend most of each working day at RARAF. In addition to his own research, he collaborates with some of the outside users on experiments using the single-particle Microbeam Facility.
- Dr. Brian Ponnaiya is an Associate Research Scientist performing experiments using the Track Segment and Microbeam irradiation facilities.
- Ms. Gloria Jenkins, a biology technician, performs experiments on the Microbeam Facility for Dr. Geard. Unfortunately, Gloria will be retiring in May of 2007.
- Dr. Alexandre Mezentsev, an Associate Research Scientist, is working with cultured tissue systems and is starting to spend almost half his time at RARAF.

At the end of March, Yigal and Atara Horowitz from Ben Gurion University in Israel began a 1-year sabbatical at RARAF. Their project will be "Charged Particle Characterization of 'Slow-Cooled' LiF:Mg,Ti (TLD-100)" using the Track Segment broad beam irradiation facility.

Recent publications of work performed at RARAF (2005-2006)

1. Brenner DJ. Editor, The 7th International Workshop on Microbeam Probes of Cellular Radiation Response. *Radiat* Res **166**:652-89, 2006.
2. Calaf GM, Roy D and Hei TK. Growth factor biomarkers associated with estrogen- and radiation-induced breast cancer progression. *Int J Oncol* **28**:87-93, 2006.
3. Garty G, Ross GJ, Bigelow AW, Randers-Pehrson G and Brenner DJ. Testing the Stand-Alone Microbeam at Columbia University. *Radiat Prot Dosimetry*, 2006.
4. Hei TK. Cyclooxygenase-2 as a signaling molecule in radiation induced bystander effect. *Mol Carcinogenesis* **45**:455-60, 2006.
5. Ivanov VN, Zhou H and Hei TK. Gamma-irradiation and alpha-particle exposure sensitize human melanoma cells to TRAIL-mediated apoptosis through upregulation of TRAIL-R2/DR5 expression and translocation to the cell surface. *Exp Cell Res.* (submitted 2007)
6. Maurer RH, Zeitlin CJ, Haggerty DK, Roth DR and Goldsten JO. Compact Ion and Neutron Spectrometer (CINS) for Space Application. 2005 IEEE Nuclear Science Symposium Conference Record, N14-48, pp 428-432, Puerto Rico, 23-29 October 2005.
7. Ponnaiya B, Jenkins-Baker G, Randers-Pherson G and Geard CR. Quantifying a bystander response following microbeam irradiation using single cell rt-pcr analyses. *Exp Hematology* (accepted 2007).
8. Roy D, Calaf GM, Hande MP and Hei TK. Allelic imbalance at 11q23-q24 chromosome associated with estrogen and radiation-induced breast cancer progression. *Int. J. Oncol.* **28**:667-74, 2006.
9. Sedelnikova OA, Nakamura A, Kovalchuk O, Koturbash I, Mitchell SA, Marino SA, Brenner DJ and Bonner WM. DNA double-strand breaks form in bystander cells after microbeam irradiation of three-dimensional human tissue models. *Cancer Res* (accepted 2007).
10. Sykora GJ, Akselrod MS, Salasky M and Marino SA. Novel fluorescent nuclear track detectors for passive neutron dosimetry. *Radiat Prot Dosimetry* pp.1-6, 2007. doi:10.1093/rpd/ncm058.
11. Williams ES, Stap J, Essers J, Ponnaiya B, Luijsterburg MS, Krawczyk, PM, Ullrich, RL, Aten JA and Bailey SM. DNA double strand breaks are not sufficient to initiate the recruitment of TRF2. *Nature Genetics* (accepted 2007). ■

RSO – TABLE OF CONTENTS

RSO staff at various occasions

(L–r): Salmen Loksen, Ahmad Hatami and Jacob Kamen.

(L–r): Allison Powers, David Rubinstein, Charles Geraghty and Jaclyn Marcel.

(L–r): Jennifer Curiel, Roman Tarasyuk and Raquel Garcia.

(L–r): Charles Geraghty, David Park and Dae In Kim.

RADIATION SAFETY OFFICE

RSO Staff (s*tanding l-r):* Shinkyu Park, Charles Geraghty, Moshe Friedman, Jacob Kamen, Salmen Loksen, David Rubinstein, Thomas Juchnewicz and Roman Tarasyuk; (s*eated l-r):* Jaclyn Marcel, Allison Powers, Raquel Garcia, Jennifer Curiel and Ahmad Hatami; *not pictured:* Bruce Emmer and Dae In Kim.

PROFESSIONAL STAFF

Salmen Loksen, CHP, DABR; Director, Radiation Safety Officer
Ahmad Hatami, DABR, DABMP; Assistant Director
Thomas Juchnewicz, DABR; Assistant Radiation Safety Officer
Jacob Kamen, PhD, NRRPT, CHP; Assistant Radiation Safety Officer
Bruce Emmer, DABMP, DABR; Physicist
Dae In Kim, MS, Health Physicist
Shinkyu (David) Park, MS, Radiation Protection Supervisor
Charles Geraghty, BS, Jr. Physicist
Allison Powers, BS, Jr. Physicist

TECHNICAL STAFF

David Rubinstein, BS, Senior Technician
Jaclyn Marcel, MS, Technician B
Roman Tarasyuk, Technician B

ADMINISTRATIVE & OFFICE SUPPORT STAFF

Moshe Friedman, BRE, Office Administrator
Yvette Acevedo, AAS, Administrative Aide
Raquel Garcia, AAS, Senior Clerk
Milvia Perez, AAS, Clerk B
Jennifer Curiel, AAS, Administrative Staff/Clerk B

RADIATION SAFETY OFFICE

INTRODUCTION

On May 19, 1957 Grayson L. Kirk, President of Columbia University, distributed a memo entitled "Directive to All University Departments Having a Source of Ionizing Radiation," advising all parties of the expanded function of the Radiation Safety Committee.

Later, a notice entitled "Radiation Safety Guide for Columbia University," dated February 10, 1959, named Philip M. Lorio as Health Physics Officer for University Departments and Laboratories other than the College of Physicians & Surgeons, where Dr. Edgar Watts was named Health Physics Officer. The Chairman of the Radiation Safety Committee was Dr. Gioacchino Failla, who initiated the Radiological Research Laboratory in Columbia University's Department of Radiology.

By agreement between Columbia University and New York Presbyterian Hospital in 1962, the Radiation Safety Office was established as an autonomous unit for the purpose of maintaining radiation safety. The Joint Radiation Safety Committee (JRSC), appointed by the Medical Board of the New York Presbyterian Hospital and the Vice President for Columbia University's Health Sciences Division, was charged with the responsibility of defining and ensuring enforcement of proper safeguards in the use of sources of ionizing radiation.

Dr. Harald H. Rossi, Director of the Radiological Research Laboratory, was appointed Chairman of the Joint Radiation Safety Committee. Under his direction this committee developed a "Radiation Safety Code & Guide," the administration of which is assigned to the Radiation Safety Officer. Dr. Eric J. Hall, the next Director of the Radiological Research Laboratory, subsequently renamed the Center for Radiological Research, followed as JRSC Chairman until his retirement from that role in 2007. Dr. David Brenner, Director of the Radiological Research Accelerator Facility, is the current JRSC Chair.

The present Joint Radiation Safety Committee of Columbia University Medical Center, New York Presbyterian Hospital and New York State Psychiatric Institute came into existence through an agreement made on February 12, 1991 between the three institutions. The agreement combined several overlapping clinical and educational programs, including all programs for ensuring radiation safety. The current Director of the Radiation Safety Office and Radiation Safety Officer, Salmen Loksen, CHP, DABR, was appointed on December 16, 1996.

The Radiation Safety Office reports to and advises the Joint Radiation Safety Committee, which meets on a quarterly basis. At the present time the Radiation Safety Officer reports on professional and technical matters to Dr. David Brenner, Chair of the JRSC, and on budgetary matters to Dr. Robert Lewy, Sr. Assoc. Dean for Health Affairs, who represents Dr. Lee Goldman, Dean of Columbia University Medical Center. In addition, the Radiation Safety Office participates in the review of research protocols for the Radioactive Drug Research Committee (RDRC) under the jurisdiction of the U.S. Food and Drug Administration.

Radiation Safety Office staff are Columbia University employees. Columbia University, New York Presbyterian Hospital and New York State Psychiatric Institute fund the Radiation Safety Office budget via a cost sharing payback arrangement.

OVERVIEW OF RADIATION SAFETY OFFICE RESPONSIBILITIES

Collectively, Columbia University Medical Center, New York Presbyterian Hospital and New York State Psychiatric Institute form a large health sciences complex with extensive teaching, research, and clinical facilities. The basic goal of the Radiation Safety Office is to ensure the implementation of all protective measures necessary to guarantee that doses from ionizing radiation to patients, visitors, students, faculty and staff on campus, as well as to the community at large, remain "as low as reasonably achievable" (ALARA). Major entities supported by Radiation Safety Office services include:

- Columbia University Medical Center
- New York Presbyterian Hospital
- New York State Psychiatric Institute
- Columbia Presbyterian Eastside
- New York Presbyterian Hospital/Allen Pavilion
- CUMC Cyclotron Facility
- Dental Facilities throughout CUMC and elsewhere as described later in this report.

The projected completion of several additional buildings, as well as the Columbia University Medical Center Integrated Imaging Center will add to the responsibilities of the Radiation Safety Office in the near future. For the purposes of this report, this collection of entities will hereafter be referred to as CUMC/NYPH/NYSPI.

Reporting to the Joint Radiation Safety Committee of CUMC/NYPH/NYSPI, the Radiation Safety Officer and the staff of the Radiation Safety Office are responsible for obtaining and maintaining licenses authorizing the possession and use of radioactive materials and obtaining and maintaining registrations and permits for the operation of radiation producing equipment. In addition, the Radiation Safety Office is responsible for obtaining and maintaining permits necessary for the safe disposal or controlled release of research and medical wastes containing radioactivity.

The Radiation Safety Office ensures that authorized users of radioactive materials and radiation producing equipment comply with all governmental regulatory requirements and guidelines by means of training, education, consultation, and by a program of internal audits and inspections of facilities. Regulatory agencies charged with overseeing the pos-

session, use, or disposal of radioactive materials or radiation producing machines include:

- United States Environmental Protection Agency (EPA)
- United States Food and Drug Administration (FDA)
- United States Nuclear Regulatory Commission (NRC)
- New York State Department of Environmental Conservation (NYSDEC)
- New York State Department of Health (NYSDOH)
- New York City Department of Health & Mental Hygiene (NYCDOHMH), Office of Radiological Health

New York City Department of Health & Mental Hygiene, New York State Department of Environmental Conservation, and United States Food and Drug Administration conduct periodic inspections and audits of CUMC/NYPH/NYSPI facilities operating under their licenses or permits. The Radiation Safety Office works continuously to prevent regulatory violations and swiftly implements any regulatory recommendations.

The Radiation Safety Office also ensures compliance with institutional policies and procedures published in the "Radiation Code & Guide of Columbia University Medical Center, New York Presbyterian Hospital & New York State Psychiatric Institute."

SUMMARY OF RADIATION SAFETY OFFICE OPERATIONS FOR 2006

A summary of activities performed and services provided by the Radiation Safety Office is presented below. While inclusive of most major activities and services, the summary is by no means exhaustive, but is intended to provide a representative overview of departmental operations. An unabridged compilation of Radiation Safety Office activities and services may be found in the Minutes of the Quarterly Meetings of the Joint Radiation Safety Committee of CUMC/NYPH/NYSPI.

Statistical data presented are from the calendar year, January 1, 2006 through December 31, 2006. Activities are covered up to February 2007.

Maintenance of New York City Department of Health & Mental Hygiene, Office of Radiological Health Licenses, Registrations, Permits, Audits and Inspections

A primary activity of the Radiation Safety Office is the continued maintenance of City of New York Radioactive Materials Licenses, Certified Linac Registrations and X-Ray Permits. Currently this includes:

- Radioactive Materials License No. 75-2878-01 (Broad Scope Human Use)
- Radioactive Materials License No. 74-2878-03 (Non-Human Use)
- Radioactive License No. 52-2878-04 (Cyclotron Facility)
- Radioactive Materials License No. 93-2878-05 (Gamma Knife)
- City of New York Therapeutic Radiation LINAC Unit Certified Registration No. 77-0000019.
- Columbia-Presbyterian Hospital Radiation Installation Permit H96 0076353 86
- Columbia-Presbyterian-Allen Pavilion Radiation Installation Permit H96 0076383 86
- Columbia University Gymnasium, Morningside Campus or Baker Field Radiation Installation Permit H98 1005495
- Columbia University Physicians Metabolic Diseases Unit, Bone Density Permit H90 1162695

Activities performed in 2006 to maintain the City of New York Licenses, Registrations and Permits included:

Throughout the year the Radiation Safety Office reported to the Joint Radiation Safety Committee regarding several procedural and administrative requirements. The specifics of these requirements may be found in the quarterly reports of the Radiation Safety Office. Briefly, some of the topics covered were:

- Authorized Users need to report to the Radiation Safety Office any changes in the following: (1) handling or experimental procedures related to the use of radionuclides; (2) quantities and chemical/physical forms of radionuclides used; or (3) therapy physicists, authorized technicians, and radiation safety managers who use or oversee the use of radioactive materials.
- Human-use research protocols require IRB review at least once a year.
- The U.S. Food and Drug Administration recommends, as good practice, that all DMFs be updated annually.
- Certain conditions of the Radioactive Materials Licenses and Certified LINAC Registrations require that certain function procedures be performed only by and/or in the physical presence of specific individuals.
- Medical Physicists practicing in New York State are required to obtain professional licensure from the New York State Department of Education. At present, all senior officers of the Radiation Safety Office are certified either by the American Board of Health Physics, the American Board of Medical Physics, and/or the American Board of Radiology and are licensed to practice as Medical Physicists by the State of New York.
- RCNY 175.103(2) requires that: "(ii) The radiation safety officer shall: (A) investigate overexposures, misadministrations, accidents, spills, losses, thefts, unauthorized receipts, uses, transfers, and disposals, and other deviations from approved radiation safety practice and implement corrective actions as necessary."

NYCDOHMH conducts periodic audits of records and inspections of facilities at CUMC/NYPH/NYSPI operating under the Radioactive Material Licenses, the Certified Linac Registration, and the X-ray Permits. In 2006, these audits and inspections included:

- February 9–23, 2006, No. 74-2878-03 (Non-Human Use)
- February 2006, No. 77-0000077-19 (Certified LINAC Registration)
- January, February, and March 2006, Nos. H96 0076383 86, H96 0076353 86, H98 1005495 and H90 1162695 (X-ray Permits)
- August 7–September 6, 2006, No. 75-2878-01 (Human Use)
- August 29, 2006, No. 93-2878-05 (Gamma Knife)

- September 18, 2006, No. H960076353 86 (X-ray permit).
- December 3–6, 2006, No. 77-0000077-19 (Certified LINAC Registration)
- December 14–15, 2006, No. 52-2878-04 (Cyclotron

No deficiencies were cited during any of these inspections.

The RSO received an amended version of License No. 52-2878-04 (Cyclotron), dated February 2006. The most recent amendments to this license added David Wilson, R.Ph., as a pharmacist for the site, and Dae-In Kim, Health Physicist, as Authorized Users.

City of New York Radioactive Materials License No. 75-2878-01 is the Broad Scope License under which all human diagnostic, therapeutic and research use of radioactive material is authorized at CUMC/NYPH/NYSPI. The License is renewable for successive five year terms. The renewal process is complex, requiring hundreds of pages of documentation. On August 2, 2006, upon completion of the review process, the License renewal application was signed by the NYCDOHMH Office of Radiological Health. The renewed License is valid for the five year period ending March 13, 2011. Amendment No. 24, signed February 6, 2007, approved Dr. David J. Brenner as the new JRSC Chairman.

In 2006 the renewal application for City of New York Radioactive Materials License No. 74-2878-03 (non-human use) was submitted. In January 2007 the RSO received notice of the renewed License, valid through January 31, 2012.

As previously reported, on December 6, 2005, the Radiation Safety Office received an Order of the Commissioner from Thomas R. Frieden, M.D., M.P.H., Commissioner, NYCDOHMH. The Order requires the implementation of increased security controls over radioactive sources which exceed certain "quantities of concern." There are several sources throughout CUMC and NYPH which require these additional controls. In 2006 a number of actions were taken in response to the Order:

- Starting in January 2006, the Radiation Safety Office held meetings with all departments affected by the Order and implementation of the increased controls was discussed. The requirements, which limit unescorted access to the controlled sources to "trustworthy and reliable" individuals, were addressed.
- In February 2006, meetings were held with representatives from CUMC and NYPH Public Safety Departments where the requirements for monitoring, detecting, assessing and responding to unauthorized access were reviewed, and a walk-through of the areas affected by the Order was performed.
- In May 2006 security gates were installed in sensitive locations to restrict access to several high-activity sources. The keys to the gates were taken off master key access and a limited quantity of numbered keys was made for distribution only to individuals receiving dual approval from CUMC Public Safety and the RSO.
- On August 29, 2006, the NYCDOHMH, accompanied by a representative of the NYCPD Counter Terrorism Division, conducted the initial audit and inspection for compliance with the Order. The inspectors held an exit interview with Dr. Eric Hall, JRSC Chairman, and Salmen Loksen, Radiation Safety Officer. At the exit interview the inspectors verbally indicated their satisfaction with the implementation of the "increased controls" program, including new surveillance features, security gates, keys, and reliable and trustworthy assessments, although further security devices were recommended. Since that time a contractor was hired to perform installation of additional surveillance cameras and alarmed radiation monitors.

The Radiation Safety Office provided health physics assistance to JL Shepherd & Associates with the installation of a Mark I animal irradiator near the end of August 2006 in ICRC. Radiation Safety Office staff monitored ambient radiation levels during the delivery of the irradiator using survey instruments. The Mark I Cs-137 source falls into the cagtegory of radioactive materials included in the Order for increased controls. The RSO took responsibility for overseeing the regulatory and radiation safety requirements involved during the installation including provisions for increased security controls. At the same time, the RSO assisted JL Shepherd & Associates with the removal of another high activity radioactive source from storage in the Medical Center and its transfer to Los Alamos National Laboratory, as will be discussed in more detail below.

Radiation Safety Office professional staff provided ongoing Medical Health Physics and NYCDOHMH Licensing support for two projects in the Department of Radiation Oncology. One project involves the replacement of the Varian 2100CD Linear Accelerator with a Varian Trilogy Linear Accelerator. The other involved installation of a GE LightSpeed CT Simulator, and was completed in December 2006.

In another interaction with the NYCDOHMH, the Radiation Safety Office, together with the Emergency Department of New York Presbyterian Hospital, Allen Pavilion and Children's Hospital of New York applied for three grants from the City's 2006 Hospital Radiation Equipment Project. The three grants, each with a value of more than $23,600, were awarded for the purchase and maintenance of radiation safety emergency equipment. Under the terms of these awards, hospitals are able to choose equipment which they are responsible for maintaining. In the event of an emergency NYCDOHMH may requisition this equipment for its own use. In October, the NYCDOHMH Bioterrorism Hospital Preparedness Program conducted training for CUMC and NYPH staff, including RSO professional and technical staff, in the proper use of the emergency response equipment. In December 2006 the RSO received the shipments of the electronic equipment. The RSO is proceeding to meet with Emergency Room representatives to discuss relevant issues including storage, testing, staff training, installation and effective use of the equipment.

Maintenance of New York State Department of Environmental Conservation Permits, and Audits and Inspections

Another primary activity of the Radiation Safety Office is the continued maintenance of New York State Department of Environmental Conservation Radiation Control Permit No. 2-6201-00005/00006.

CUMC/NYPH/NYSPI conducts medical research and clinical activities that discharge limited and controlled quantities of radioisotopes to the atmosphere and to sewage systems as per the Conditions of the Radiation Control Permit and in compliance with New York State 6 NYCRR Part 380, Rules and Regulations for Prevention and Control of Environmental Pollution by Radioactive Materials.

The entities served by the Radiation Safety Office are situated within a densely populated urban area. The quantities of radioisotopes discharged and the resulting public radiation dose are closely regulated by the New York State Department of Environmental Conservation. Radiation doses to the general public resulting from atmospheric discharges of radioisotopes are required to not exceed the USNRC Constraint Limit of 10 mrem per year. This amounts to only a fraction of the annual naturally occurring background radiation level.

CUMC/NYPH/NYSPI are currently permitted a total of 15 atmospheric emission points from which radionuclides are discharged to the atmosphere. Monitoring, analyzing, reporting, and minimizing discharges from these emission points, in order to ensure compliance with the Conditions of the Radiation Control Permit, is one of the major continuing activities of the Radiation Safety Office.

Activities performed in 2006 to maintain the NYSDEC Radiation Control Permit included:

As required by New York State 6 NYCRR Part 380 and the Conditions of the NYSDEC Radiation Control Permit, the Radiation Safety Office will be submitting an Annual Report summarizing Discharges of Radioactive Effluents to the Environment from the fifteen atmospheric emission points and by controlled sewer disposal by the end of March 15, 2007. For the calendar year 2006, all atmospheric discharges were within the quantities authorized by the Radiation Control Permit, and the resulting public dose was within the U.S.N.R.C. constraint limit of 10 mrem per year. All discharges to sewers were well below the Effluent Concentration Limits as required by 6 NYCRR Part 380-11.7, Table of Concentrations.

As required by the Conditions of NYSDEC Radiation Control Permit 2-6201-0005/0006, on December 29, 2006, annual calibrations were performed on the monitoring systems of the Radioligand and Cyclotron exhaust stacks.

Members of the Radiation Safety Office continued to attend scheduled Design Meetings for the CUMC Integrated Imaging Center (NYSTAR Project). Actions taken to further the project in 2006 included:

- On October 10, 2006, at the Quarterly Construction Meeting of Columbia University Medical Center, the RSO was informed that the initial purchase order for the CUMC Integrated Imaging Center had been approved.
- The Radiation Safety Office performed shielding design evaluations for the project.
- At the PET Sub-Committee Meeting, held December 5, 2006, the RSO reminded the Committee of NYC DOHMH and NYSDEC regulatory requirements for the proposed new facilities. These include, but are not limited to: preparation and submission of a Radioactive Materials License Application or an Amendment to the current Radioactive Materials License for authorization to operate two RDS-111 Eclipse Cyclotrons, a Radiopharmacy, and a Radioligand Laboratory at 722 West 168th Street, Amendments for relocation of the PET imaging Center from Milstein Hospital Building under the Broad Scope Human Use License, and modification of the NYSDEC Radiation Control Permit to authorize new atmospheric discharge points.
- On December 12, 2006, the RSO received a letter from NYSDEC directing the CUMC to prepare to submit an application for a new Radiation Control Permit for the Integrated Imaging Center in the Mailman School of Public Health Building, as opposed to modifying the current Radiation Control Permit to include the new CUMC Integrated Imaging Center.

As required by the Conditions of the NYSDEC Radiation Control Permit 2-6201-0005/00006, all filters in the Cyclotron, Radioligand, PET Suite and Nuclear Medicine stacks were replaced both on May 21, 2006 and again on November 11, 2006.

On January 17 and 18, 2007 NYSDEC performed an audit of records, an inspection of facilities, and met with staff at CUMC/NYPH/NYSPI departments that are authorized to discharge radionuclides to the atmosphere under Permit No. 2-6201-00005/00006. Inspection results given at the exit interview confirmed that all facilities were in compliance.

On March 13, 2006, the Radiation Safety Office submitted a timely letter requesting renewal of the New York State Department of Environmental Conservation Permit No. 2-6201-00005/00006 in its existing form. On February 9, 2007, the Radiation Safety Office received a renewed Radiation Control Permit No. 2-6201-00005/00006 set to expire February 2, 2012.

Administration of Radioactive Material: Receipt, Distribution and Radioactive Waste Disposal

A major program of the Radiation Safety Office is the centralized administration of all authorized radioactive materials used at CUMC/NYPH/NYSPI. The use of radioisotopes by individual investigators is authorized by the Joint Radiation Safety Committee and controlled by the Radiation Safety Office. Human Use of radioactive materials is carried out by Authorized User Physicians. Authorized User status is granted following a review of credentials and a majority vote by a quorum of the Joint Radiation Safety Committee. Non-Human Use of radioactive materials by Responsible Investigators is granted after a review of applications and written permission of the Chairman of the Joint Radiation Safety Commission and the Radiation Safety Officer. In 2006 a number of new Responsible Investigators were reviewed and approved for non-human use of radioactive materials, and scores of current Responsible Investigators received renewal of their authorizations.

Activities in 2006 to administer, receive, distribute, and dispose of radioactive materials included:

1037 purchase orders for materials that contain radioisotopes were approved. 1830 packages containing radioactive material, excluding shipments to the Nuclear Medicine and Radiation Oncology, departments were received. Prior ap-

proval was given for all received shipments. Package surveys and wipe tests were also conducted to ensure that none of the packages were contaminated.

The Radiation Safety Office maintains inventory control of all radioactive materials received and distributed through the use of a computerized database. The orders referred to in Item 1 of this section resulted in the purchase of a total of approximately 1.9 Curies of activity. ^{35}S, ^{3}H, and ^{32}P were the isotopes purchased with the highest activities.

Low-level aqueous radioactive waste was disposed of through the sewer during 2006. The total activity of sewer-disposal aqueous radioactive waste was 264 mCi, of which 110 mCi was tritium (^{3}H), 144 mCi was ^{35}S, and 9.6 mCi ^{32}P, and 0.4 mCi was ^{125}I other. As required by 6 NYCRR Part 380 and the conditions of our NYSDEC Radiation Control Permit, the controlled sewer disposal of aqueous radionuclides was reviewed. The discharge for all isotopes was well below the concentration limits of 6NYCRR Part 380-11.7 Table II.

The Radiation Safety Office processed a total of 1148 waste requisitions from CUMC, NYPH, and NYSPI, and collected 190 black bags from NYPH for Decay-in-Storage. Black bags are collected from incontinent patients who have undergone nuclear medicine procedures.

On October 3, 2005, the Radiation Safety Office notified the New York State Department of Energy Conservation, Bureau of Hazardous Waste Regulation, that CUMC/NYPH/NYSPI was claiming the conditional storage and treatment exemption for Low Level Mixed Waste outlined in 40 CFR 266 Subpart N and adopted by New York State on September 2, 2005. Claiming the exemption allows for greater flexibility in the way mixed waste is managed. This flexibility will increase the ease with which the current mixed waste policy is implemented for both laboratory and radiation safety personnel.

Under current CUMC/NYPH/NYSPI mixed waste policy, short-lived liquid mixed wastes are held in storage for decay. Once the contained radioactivity is decayed to background levels, the wastes are transferred to the Environmental Health and Safety Office for disposal as non-radioactive hazardous waste. During 2006, 100L waste from the labs of Dr. Gautier, Dr. Dauer, and Dr. Dalla-Favera were transferred.

In the course of two shipments on February 15, 2006 and December 13, 2006, the Radiation Safety Office removed 38 drums of Liquid Scintillation Vials (LSV) and long half-life low level liquid mixed waste for disposal. The licensed shipper was Radiac Research Corporation. The total volume of the shipments was 152 cubic feet, the total weight was 5270 lbs., and the total activity shipped was 9.24 mCi of which 6.77 mCi was tritium (^{3}H), 0.19 mCi was ^{14}C, and 2.28 mCi was other isotopes.

On April 4, 2006, the RSO shipped a total of 87 drums of Dry Active Waste (eleven 55-gallon drums and sixty-nine 30-gallon drums) for disposal by Envirocare of Utah via GTS Duratek Super-Compaction. The same day, the Radiation Safety Office shipped a total of seven fiber drums of solid animal carcasses for incineration at Envirocare of Utah. The total volume of animal carcasses shipped was 28.07 cubic feet, weighing 525 pounds and containing 4.21 mCi of Tritium (^{3}H). The total volume of the dry shipment was 425.65 cubic feet, weighting 7,350 pounds. The total activity shipped was 34.061 mCi, of which 25.623 mCi was Tritium (^{3}H), 3.973 mCi was ^{14}C. CUMC Public Safety assisted in the pickup which occurred at 2 a.m. in several locations including the Hammer Health Sciences Building and the College of Physicians & Surgeons.

The Radiation Safety Office received, shipped and disposed of (or recycled) 246 mCi of Heyman ^{137}Cs sources. These sources were used by the Radiation Oncology Department for patient treatments. The Heyman sources were assessed and packaged by CoPhysics and were removed from the RSO storage facility on December 6, 2006 for temporary staging at Radiac in Brooklyn, NY. The sources will be shipped to the recycler/processor, RAM Services, Inc. in Wisconsin. This is a License-transfer of the sources; no disposal manifest is necessary. The RSO will be receiving a notice of License transfer from RAM Services.

The Radiation Safety Office received documentation regarding the shipment of 85 small activity orphan sources from Columbia University Medical Center to a Licensed recycler/processing facility. The sources, which were kept in radioactive waste storage room P&S B417, were assessed and packaged by CoPhysics and removed from CUMC on August 28, 2006 for temporary staging at Radiac in Brooklyn, NY. On November 2, 2006 the sources were shipped to the recycler/processor, RAM Services, Inc. in Wisconsin. This is a license-transfer of the sources; no disposal manifest is necessary. The RSO received notice of the license transfer from RAM Services and CoPhysics.

The RSO received confirmation notice of the completion of the shipment and the transfer of ownership of the 46 Ci Cs-137 irradiator source (SN 1307-198) to its new Licensee, Off-Site Source Recovery Project (OSRP), at Los Alamos National Laboratory. Over August 26 and 27, 2006, JL Shepherd & Associates service engineers, under RSO supervision, removed the source from its lead housing, packed it onto a 2R container, and transported it to Los Alamos National Lab by Federal Express Truck with special security provisions. The agreement between Columbia University Medical Center and Los Alamos National Laboratory stipulates that CUMC irrevocably relinquishes all rights, title and ownership in the sealed source to DOE/NNSA in furtherance of the OSRP. LANS accepts the sealed sources on behalf of DOE/NNSA upon the execution of the Acknowledgment of Receipt of the source by the designated LANS support subcontractor JL Shepherd & Associates. The RSO has received confirmation notice of the completion of the shipment and the transfer of ownership. The cost savings to CUMC due to participation in the Los Alamos Source Recovery Project is estimated to be approximately $85,000.

On February 25, 2007, the Radiation Safety Office filed a report with the NYS Energy Research and Development Authority for 2006 Low-Level Radioactive Waste.

Personnel Dosimetry, Bioassay and Area Monitoring

In accordance with regulatory requirements, the Radiation Safety Office operates an ALARA Program to ensure

that the radiation doses resulting from operations at CUMC/NYPH/NYSPI are both within the legal limits and kept "As Low As Reasonably Achievable."

The principal methods of monitoring radiation dose include the assignment of personnel radiation dosimeters to individuals, the posting of area and environmental dosimeters, and the monitoring of all discharges of radioactive materials.

Immediate action is taken, as appropriate, in response to unusual or high dosimeter readings. Quarterly ALARA reports are prepared and submitted to the Joint Radiation Safety Committee. These reports present the following: a) the doses of individual workers that exceeded ALARA I limits; b) summaries of investigations of doses to individual workers that exceeded ALARA II limits; and c) discussions of trends within departments that have historically experienced high individual doses. In addition, Quarterly Environmental ALARA reports are prepared and submitted to the Joint Radiation Safety Committee. The Quarterly Environmental ALARA report presents the quantities of radionuclides discharged to the atmosphere and the sewer system and the resulting dose to the general public.

In 2006, all doses to individual workers were less than the legal annual reportable limits as specified in RCNY Article 175, Radiation Control. All doses to the general public resulting from atmospheric discharges of radionuclides were less than the USNRC constraint limit of 10 mrem per year.

Activities performed in 2006 to maintain the ALARA Program included:

The Radiation Safety Office distributed approximately 10,000 personnel radiation dosimeters each quarter, including both monthly and quarterly badges. A total of approximately 40,000 dosimeters were distributed and collected in 2006. To maintain dosimetry records, the Radiation Safety Office uses dedicated computers with internet and direct modem access to the database of the dosimeter supplier, Landauer Inc.

The Radiation Safety Office received Annual Occupational Exposure Reports (NRC Form 5) from Landauer Inc. for the year 2005 and reviewed and forwarded these reports to radiation workers as required by the New York City Department of Health regulations.

The Radiation Safety Office notified 76 employees with ALARA Level I readings and investigated 21 cases of ALARA Level II readings as reported by Landauer Inc. Particular attention was paid to occupational groups that typically exceed the ALARA limits, i.e., workers and researchers at the Cyclotron Facility, Angiography, the Cardiac Cath Lab, and physicians in the PET Suite.

The Radiation Safety Office performed 72 bioassays on radiation workers who use radioactive iodine or handle greater than 10 mCi of ^{3}H or ^{32}P.

The Radiation Safety Office provided all workers who had declared pregnancy with health physics counseling concerning the risk factors of exposure to radioactivity. Also, additional monitoring of the fetus during the gestation period was provided, and personnel radiation exposure reports were closely followed. The work environments were evaluated and modified if necessary.

Routine Radiation Safety Compliance – Internal Inspections, Audits and Surveys

A major activity of the Radiation Safety Office is the performance of facility inspections and audits of records at approved clinical departments and research laboratories in order to ensure compliance with regulatory requirements as well as with the guidelines and policies of the Joint Radiation Safety Committee.

Routine internal compliance activities conducted in 2006 included:

Quarterly and annual inspections and audits were completed of all CUMC and NYPH clinical facilities using radioactive materials. The facilities audited include: NYPH Nuclear Cardiology, NYPH Nuclear Medicine, Allen Pavilion Nuclear Cardiology, Allen Pavilion Nuclear Medicine.

Quarterly inventory and biannual leak testing was performed for all radioactive sources located in the following facilities: Milstein Hospital Nuclear Medicine and Nuclear Cardiology, Kreitchman PET Suite, Radioligand and Cyclotron facilities, Allen Pavilion Nuclear Medicine, and CUMC laboratories. Leak Test Certificates were generated and issued.

476 routine radiation safety inspections and audits were performed in Columbia University Medical Center and New York State Psychiatric Institute research laboratories. The results were communicated to the Responsible Investigators. A total of 61 labs were cited with deficiencies, and these followed up to ensure compliance.

73 equipment clearance and laboratory exit/entry surveys were performed.

Airflow rates were measured in 194 fume hoods in areas where volatile radioactive materials are used. In all rooms where radioactive gases or aerosols are used, ventilation rates were measured, and spill gas clearance times were calculated and posted. Adjustments were made as required to air supply and exhaust systems to obtain negative pressure conditions. Researchers whose hoods did not meet safe flow rate standards were instructed to have their hoods repaired or replaced. Follow-up audits confirmed that corrective actions were taken.

371 live animal and carcass surveys were performed, in order to identify potential contamination in animal facilities and cages, protect animal care staff, and ensure proper disposal of animal carcasses containing radioactivity.

Calibration and maintenance services were provided for 262 radiation survey instruments used throughout CUMC/NYPH/NYSPI. The Radiation Safety Office maintains a supply of portable survey instruments available for loan to Responsible Investigators and in case of emergency.

The Radiation Safety Office conducted surveys of 55 inpatients and outpatients treated with ^{131}I by the Nuclear Medicine Department and 11 surveys of patients treated with ^{137}Cs or ^{192}Ir implants by the Radiation Oncology department in 2006.

In 2006 the Radiation Safety Office interviewed 40 outpatients who were being considered for treatment with Iodine-131 for cancer of the thyroid by the Department of Nuclear Medicine. Records of interviews are on file in the Radiation Safety Office.

Radiation Safety Training

Pursuant to Article 175 of the New York City Health Code, the Radiation Safety Office provides initial radiation safety training to all new employees of CUMC/NYPH/NYSPI prior to their beginning work with radiation equipment or radioactive materials. The Radiation Safety Office then provides annual refresher training as well. The Radiation Safety Office also provides training in the general area of Emergency Response Preparedness as prescribed by the Joint Radiation Safety Committee. The following radiation safety courses and training sessions were presented during 2006:

- 12 initial training sessions for individual researchers
- 12 annual refresher sessions for researchers
- 12 sessions for the Nursing Staff of NYPH
- Training sessions for Dental School residents
- Training sessions for Dental Assistant students
- Training sessions for Radiology residents
- Training sessions for Anesthesiology staff
- Training sessions for the Facilities Department.
- Training for Security Personnel at both the CUMC and Morningside campuses
- Training for Nursing students
- Training for Non-Radiology Users of X-ray Machines.

For employees who could not attend the regularly scheduled classes, the RSO administers a self-study program including the use of videotapes available at the CUMC Library. A passing grade on the quiz administered after viewing the video qualifies an employee working in Non-Human Use Applications to be issued a radiation monitor badge. If the individual's employment involves human use of radioactive material, a passing grade on the quiz results in obtaining a temporary badge until the next regularly scheduled new employee training session.

In addition to providing training to outside departments and institutions, personnel within the Radiation Safety Office itself are continually undergoing training to update their skills and qualifications. Training activities undertaken in 2006 included:

On March 29, 2006 and again on November 1, 2006, the Radiation Safety Office and the Office of Environmental Health and Safety conducted joint training sessions in order to review blood-borne pathogen safety, radiation safety, fume hood certification, increased controls for radioactive materials in quantities of concern, and record keeping requirements.

In April 2006 members of Radiation Safety Office staff attended a two-day seminar, "Radiological Sciences in the Context of Radiological Terrorism," presented by the Center for High-Throughput Minimally-Invasive Radiation Biodosimetry at the CUMC Center for Radiological Research. This Center is funded by a grant awarded by NIAID (National Institute of Allergy and Infectious Diseases) as a component of the federal funding for Centers for Medical Countermeasures against Radiation.

In July 2006 four Radiation Safety Office staff members attended RCRA refresher training presented by the Environmental Resource Center.

In August 2006 members of Radiation Safety Office staff attended a training program for operation of the JL Shepherd & Associates Mark I-30 Irradiator.

In October 2006 members of Radiation Safety Office staff attended an EAI Corporation Radiation Equipment Course under the auspices of the New York City Department of Health & Mental Hygiene. The training was provided pursuant to the NYC DOHMH Bioterrorism Hospital Preparedness Program radiation equipment grants of more than $23,600 each to New York Presbyterian Hospital, Children's Hospital of New York, and the Allen Pavilion., as discussed elsewhere in this report.

In addition, the Radiation Safety Office staff continues to attend regularly scheduled meetings with the departments of Environmental Health & Safety, Public Safety and Security, and Emergency Room staff to discuss and train for emergency response to any potential emergencies.

Professional Radiation Safety and Health Physics Support

The Radiation Safety Office provides professional radiation safety and health physics consultation to clinical departments, research laboratories, Authorized Users, and Responsible Investigators throughout CUMC/NYPH/NYSPI in order to ensure compliance with regulatory requirements and the ALARA program.

Specific examples of professional support provided by the Radiation Safety Office in 2006 include:

The Radiation Safety Office investigates spills, misadministrations, and other incidents involving radioactive materials and other sources of radiation. The Radiation Safety Office ensures that, when required, timely notice of reportable incidents is made to the New York City Department of Health, Office of Radiological Health. The Radiation Safety Office responded to the following 14 incidents in 2006 and early 2007. Further details are on file in the Radiation Safety Office and may also be found in the Radiation Safety Office's quarterly reports to the JRSC.

- On February 2, 2006, the Radiation Safety Office was notified that a routine wipe test of a recently received radiochemical vial had yielded counts above background. Radiation Safety Office staff surveyed the area and laboratory personnel who handled the vial. The contamination was restricted to the vial and determined to be well below regulatory limits.
- On Sunday, March 12, 2006 the Radiation Safety Office responded to the report of a flood in P&S room 7-501, a radiation area. After a GM survey was performed, a sample of the flood water, counted using the liquid scintillation technique, confirmed that no contamination was present.
- On March 28, 2006, a spill occurred in the PET Suite area. Approximately 1-2 mCi of ^{11}C Raclopride leaked onto the floor below an infusion pump due to a faulty connection. Decontamination procedures, including a wipe test, were performed. The area was cleared for use at 10 a.m. the following morning. Follow-up to the incident included a radiation safety in-service to PET Suite research staff.
- On May 11, 2006, the RSO responded to a contamination incident in the Radioligand Laboratory during the

synthesis of ^{18}F labeled aromatic sulfamide. All radioactivity, except for contamination to the researcher's left hand, was confined to Hot Cell 3.

- A minor spill occurred in the Department of Nuclear Medicine on May 17, 2006. A few drops of roughly 5 μCi of Tc-99m HMPAO solution leaked onto a patient's bed through a loose port connector. The Radiation Safety Office performed decontamination immediately and the room was isolated for decay. The next day the RSO cleared the room based upon the wipe test results in compliance with RCNY 175 specifications.
- On May 24, 2006, an ^{18}F spill occurred in the Radioligand Lab. Contamination was identified on two lab employees, the floor, a computer rack and a stepstool. Decontamination protocol procedures were carried out immediately and the area was covered with lead and plastic. Personnel radiation monitors were sent for analysis and were shown to be consistent with the contamination incident.
- A minor spill occurred in Nuclear Cardiology on July 25, 2006. About 3 μCi of Tc-99m MIBI leaked out of the connecting tubing. Contamination was identified on the treadmill. Decontamination procedures were immediate performed. The area was cleared by RSO staff on July 27, 2006.
- A minor leak occurred in the Epilepsy Monitoring Unit at Milstein Hospital on August 3, 2006. Approximately 2 μCi of Tc99m HMPAO leaked from a syringe port onto a medication preparation bench. Decontamination was performed immediately and the contaminated items were isolated for decay. The next day, RSO staff cleared the room based upon the wipe test results which met RCNY 175 specifications.
- A patient received administration of 76.4 mCi of ^{131}I on August 4, 2006 vomited into his bathroom sink on August 5, 2006 and RSO staff responded to the incident. The bathroom and sink were surveyed and found to read background level. The patient's thyroid and stomach were surveyed and levels were normal. It was concluded that little or no radiation was expelled through the vomit and treatment continued.
- On October 3, 2006, a minor spill occurred in Nuclear Cardiology. About 2 μCi of Tc-99m MIBI leaked out of connecting tubing. Contamination was identified on the treadmill. Decontamination procedures followed including a wipe test. The area was cleared by the RSO at 11:00 a.m. on October 5, 2006.
- On November 16, 2006 smoke was detected emanating from P&S 8-446, a laboratory cold room, and was reported to the Radiation Safety Office. The NYC Fire Department arrived quickly to control the location but did not enter the room due to RAM postings. Upon the RSO's arrival to the site it was evident that the incident was limited to a small bench-top apparatus that had overheated. The doorway was surveyed by the RSO and no radioactivity above background was identified. The smoldering device was subsequently attended to by FDNY and the responders were surveyed afterwards. The RSO obtained records of the radioactive material in possession by the principle investigator and advised the FDNY that the potential radiation hazards were minimal, as only a small quantity of ^{3}H was in possession of the P.I. at that time. After the incident the RSO performed an area survey and wipe test both of which revealed no radiation above background levels. After investigation, the piece of laboratory equipment was identified as an electrophoretic transfer apparatus used for a western blot procedure. In addition, it was confirmed that there was no radioactive material in the room at the time of the incident.
- On November 27, 2006 a minor leak was reported in the Epilepsy Monitoring Unit at Milstein Hospital. Roughly 2 μCi of Tc99m HMPAO leaked from the syringe port on the medication preparation bench. Decontamination was performed immediately and the contaminated items were isolated for decay. The next day the RSO cleared the room based upon the wipe test which complied with RCNY 175 specifications.
- A minor spill occurred in Nuclear Cardiology at 11:00 am on February 27, 2007. About two drops of blood containing Tc-99m MIBI leaked out of the site IV to the hallway floor. The RSO responded without delay. Decontamination procedures followed immediately. On the same day, at 1 pm, the area was cleared by the RSO as the wipe test results complied with RCNY 175 specifications.
- A water flooding event occurred in a PI Annex freezer room on March 8, 2007. A sprinkler had a mechanical failure and a water flood resulted. The Radiation Safety Office responded promptly. Clean-up and decontamination procedures were performed by NYSPI Housekeeping and Engineering staff. CUMC EH&S also responded. The Radiation Safety Office conducted a wipe test. All counts were below background level and the area was cleared.

Other examples of professional support provided by the Radiation Safety Office include:

The Radiation Safety Office, participates as a member of the IACUC Animal Care Protocol Review Committee by reviewing all procedures that utilize radionuclides in animal research and reviewing other animal protocols.

The Radiation Safety Office participates as a member of the JRSC executive committee in reviewing all Human Use protocols using radiation.

The Radiation Safety Office provides continuing radiation safety support for the Columbia University Cyclotron Facility and the Columbia University Radioligand Laboratory for production and synthesis of PET imaging radiopharmaceuticals. This support includes maintenance of licenses and permits, basic radiation safety services, personnel dosimetry, area radiation monitoring and quantitative measurement and ALARA analysis of radioisotope releases to the atmosphere, review of Authorized User credentials, and review of system modifications.

The Radiation Safety Office was requested by David Wilson, R.Ph., Director of the Radiopharmacy and Kreitchman PET Center, to develop a review of expenses and liabilities associated with the decommissioning of the CUMC-

owned RDS-112 Cyclotron. The decommissioning of this facility will likely require removal of neutron activated cyclotron components and disposal of activated concrete as low-level radioactive waste. Specifically, the RSO is responsible to ensure that: the radiation safety activities are performed in accordance with regulatory requirements, to report to management regarding radioactive materials issues, and to assist the JRSC in overseeing the use of licensed radioactive materials.

On May 25, 2006 a Bracco Diagnostics Rubidium-82 Infusion System for PET cardiac imaging was installed in the CUMC Kreitchman PET Center. The Rubidium-82 Infusion System is a standard diagnostic tool and is already authorized under the Human-Use License. PET Center staff, RSO staff, Cyclotron Radiopharmacy staff and Nuclear Cardiology staff received training from Bracco Diagnostics in the maintenance and use of the infusion system. The RSO is currently evaluating the radiation safety impact of the operation of the system, including staff exposure from operating and maintaining the system, verification of daily QC for dose assay, and disposal of the ^{82}Rb eluants contaminated with long half-life ^{82}Sr and ^{85}Sr.

In 2006 CUMC participated in the Los Alamos Source Recovery Project by transferring ownership of a 46 Ci ^{137}Cs source to the Los Alamos National Laboratory. The agreement stipulates that CUMC irrevocably relinquishes all rights, title and ownership of the sealed source to DOE/NNSA in furtherance of the OSRP. Also in 2006, 86 orphaned sources that had been transferred from CUMC research laboratories to the RSO were leak tested and packaged by CoPhysics and removed by Radiac Inc. Some of these sources were recycled and some buried.

The Radiation Safety Office also performed shielding design evaluations during the planning phases of the new Nuclear Cardiology SPECT/CT unit located in Milstein Hospital 2-020.

Professional Radiation Safety and Medical Physics Support for Non-Radiology X-ray Activities

The dental quality assurance program is designed to optimize the radiological safety and clinical quality of dental radiography. This program is based on recommendations for quality assurance that have been promulgated by a number of professional organizations, including the National Council on Radiation Protection & Measurements (NCRP), the Bureau of Radiological Health of the Food & Drug Administration, the American College of Radiology (ACR), and the American Academy of Dental Radiology Quality Assurance Committee. In this program, the Radiation Safety Office has primary responsibility for preliminary radiation safety shielding evaluation, acceptance testing, diagnostic quality assurance, and radiation safety surveys on all dental x-ray units installed at the following locations:

- Morningside Dental Associates (2 locations): 9 intraoral units, and 1 panoramic/cephalographic
- Ambulatory Care Networked Corporation (ACNC): 4 intraoral units and 1 panoramic/cephalographic unit
- Babies Hospital OR: 1 portable intraoral unit
- Vanderbilt Clinic Teaching & Research Areas: 1 panoramic unit, 1 panoramic/cephalographic unit, 23 intraoral units, and 1 intraoral–cephalographic unit
- Dentcare Clinic (Intermediate School 183): 1 intraoral unit
- Columbia Eastside: 6 intraoral units and 1 panoramic/cephalographic unit
- Columbia North: 5 intraoral units and 1 panoramic unit
- Mobile Dental Facility: 2 intraoral units
- Mannie L. Wilson Health Care Center: 5 intraoral units and 1 panoramic unit.
- Odyssey House Dental Clinic: 3 intraoral units
- Harlem Children's Health Initiative Dental Facility: 1 intraoral unit.

In agreement with the New York Presbyterian Hospital, the Joint Radiation Safety Committee has assigned the Radiation Safety Office responsibility for Radiation Safety and Medical Physics support for those clinical facilities outside the Department of Radiology that use x-ray equipment. The Radiation Safety Office and the Department of Radiology Medical Physics staff jointly run the audit program for these facilities. This program is conducted in accordance with the conditions of the CUMC/NYPH/NYSPI New York City X-ray Permits, as specified in Article 175 of the New York City Health Code. In this audit program, the Radiation Safety Office is primarily responsible for ensuring that each site follows the proper QA procedures, safety practices and keeps proper records, while Department of Radiology Medical Physics is responsible for performing all technical tests. The following locations are audited under this program:

- Urology Department, Atchley 11th Floor: 1 fluoroscopy unit
- Endoscopy Department, Atchley 13th Floor: 3 C-arm fluoroscopy units
- Spine Center, Neurological Inst., 5th Fl: 1 C-arm unit
- Sports Medicine, Dodge Fitness Center/Bakers Field: 1 mini C-arm unit
- Cystoscopy Suite, Milstein 4th Floor: 3 radiographic/fluoroscopic units
- Cardiac Care, Milstein 5th Floor: 1 C-arm unit
- Pain Management, Presbyterian Hospital 5th Floor: 1 C-arm unit
- Harkness Pavilion 9th Floor: 4 bone densitometery units, 1 Xtreme CT.

In 2006, the Radiation Safety Office provided the following support for the above programs:

Radiation safety surveys and machine performance evaluations, in addition to the standard annual Q/A tests described above, were performed at the following locations:

- Facility of the Columbia University College of Dental Medicine at VC 7-214C
- Harlem Children's Health Initiative Dental Facility
- Odyssey House Dental Clinic.

On June 9, 2006 the Radiation Safety Office shipped quality assurance equipment that is utilized in the dental program to Global Calibration Laboratory, in Cleveland, Ohio for calibration.

The Radiation Safety Office gave the annual lecture to the new Post-Docs on June 27, 2006, and the annual lecture for Radiology Fellows on July 5, 2006.

Radiation Safety Office Personnel

Personnel changes in the Radiation Safety Office technical staff include:

In April 2006 James Dolan resigned from his post as Junior Physicist, in order to accept a position in another institution. In April 2006 David Rubinstein was promoted from Tech B to Chief Technician. Also in April, Charles Geraghty was hired as a Technician B. In June 2006 Allison Powers was hired to fill a second Technician B position. In December 2006 both Charles Geraghty and Allison Powers were selected to fill open Junior Physicists positions. In January 2007 Jaclyn Marcel was hired to fill one of the vacant Technician B positions. The Radiation Safety Office is expecting to fill the other Technician B position shortly.

Changes in the Radiation Safety Office administrative and support staff include:

In May 2006 Moshe Friedman was hired as the Office Administrator, transferring from the Center for Radiological Research to the Radiation Safety Office. In January 2007, Yvette Acevedo resigned from her post as Administrative Aide and accepted a new position in the Center for Radiological Research. A replacement for this position is expected to be hired soon. In February 2007 Milvia Perez resigned from her post as Clerk B to accept a position in another CUMC department. Jennifer Curiel, who for years provided support for the Radiation Safety Office as a part-time casual employee, was hired to fill the Clerk B position.

In 2007 the Radiation Safety Office is looking forward to filling all remaining open positions in order to provide the best possible safety and support services to the Columbia University Medical Center, New York Presbyterian Hospital and New York State Psychiatric Institute.

Allison Powers, Jr. Physicist, working on some reports at her desk in the RSO.

Ahmad Hatmai, Assistant Director of the RSO, making a point about radiation safety in a CUMC laboratory.

Radiation Safety Office staff (Jacob Kamen, left; David Park, right; and Ahmad Hatami, near center) pose with FDNY members and other medical center emergency personnel during a routine safety drill that was conducted at CUMC and NYPH.

Professional Affiliations & Activities

AMUNDSON, SALLY A., Sc.D.

Member

Radiation Research Society, *Finance Committee*
International Congress of Radiation Research, *Program Committee*
National Academies of Science Radiation Shielding Study
National Council on Radiation Protection and Measurements (NCRP)

Reviewer

Advances in Space Research
Cancer Gene Therapy
Carcinogenesis
International Journal of Radiation Biology
International Journal of Radiation Oncology, Biology and Physics
Mutation Research
PLOS Medicine
Radiation and Environmental Biophysics
Radiation Research

Patent Award

"Method for detecting radiation exposure" (U.S. Patent #7,008,768)

BALAJEE, ADAYABALAM S., Ph.D.

Member

Radiation Research Society of North America
Indian Association for Radiation Biology

Reviewer

Advances in Space Radiation Research
Cancer Research
Cancer Research Campaign, UK
Current Medicinal Chemistry
Eurekah Bioscience
Molecular Cancer Therapeutics
Medical Science Monitor
Nucleic Acids Research
Radiation Research

BIGELOW, ALAN, Ph.D.

Member

American Physical Society
Radiation Research Society

Reviewer

Optics and Laser Technology

Student Mentoring

New York City Stuyvesant High School summer student apprenticeship

BRENNER, DAVID J., Ph.D., D.Sc.

Member

Columbia University Radiation Safety Committee, *Chairperson*
National Council on Radiation Protection and Measurements (NCRP)
International Congress on Radiation Research, *Program Committee*
TV and radio appearances on the topic of CT examinations
Joint Radiation Safety Committee, Chairperson; Radioactive Drug Research Committee, Chairperson

Editorial Work

Radiation and Environmental Biophysics, Assoc. Editor

CALAF, GLORIA M., Ph.D.

Adjunct Faculty

University of Tarapaca; Institute for Advanced Research, Arica, Chile, *Full Professor*

Member

Biology Society of Chile
Mastology Society of Chile
Chilean Society of Citology
Chilean Society of Cancer
New York Academy of Sciences
Tissue Culture Association
International Association of Breast Cancer Research
American Association of Cancer Research
Society of Experimental Biology and Medicine
Radiation Research Society

Student Mentoring

Politechnical University of Madrid, Spain, Ph.D. Advisor

Teaching

"Senescence and cell death," Ph.D. Program in Genetic and Cell Biology, Autonomous University of Madrid, Madrid, Spain. May 2-6, 2006.
Course "Apoptosis and Cancer," Univ. of Tarapaca.

Grant Reviewer

FONDECYT Grants, Chile

Manuscrit Reviewer

British Journal of Cancer
Mutation Research
International Journal of Radiation Oncology Biology Physics
International Journal of Radiation Biology
Environmental Health and Perspectives
Gynecologic Oncology
Cancer Detection and Prevention
Radiation Research
Endocrinology
Molecular Medicine
Endocrine Related Cancer

Grants

FONDECYT #1040300, scholar grant
CIHDE (#BIP20185093)

GEARD, CHARLES R., Ph.D.

Member

Radiation Research Society
American Society of Therapeutic Radiology and Oncology (ASTRO)

Environmental Mutagen Society
Advisory Committee on Radiobiology, Brookhaven National Laboratory
Scientific Review Panels, NASA

Editorial Work

International Journal of Radiation Biology, Editorial Board

Reviewer

Mutation Research
Radiation Research
Mutagenesis

HALL, ERIC J., D.Phil., D.Sc., FACR, FRCR, FASTRO, FSRP

Member

Royal College of Radiology
British Institute of Radiology
American Board of Radiology, *Radiotherapeutic Written-Test Committee*
American Society of Therapeutic Radiology and Oncology (ASTRO)
Radiation Research Society, *Past President*
American Radium Society, *Past President*
International Association of Radiation Research, *Past President*
Columbia-Presbyterian Medical Center, Joint Radiation Safety Committee; Radioactive Drug Research Committee
National Council on Radiation Protection and Measurements, Committee 1, *Emeritus Member*

Editorial Work

Intl Journal of Radiation Oncology Biology Physics, Editorial Board
International Journal of Brachytherapy
International Journal of Radiation Biology
Radiation Research
Radiology

HEI, TOM K., Ph.D.

Adjunct Faculty

Department of Radiological and Environmental Health Science, Colorado State University, Fort Collins, Co., *Adjunct Professor*
Department of Ion Beam Bioengineering, Chinese Academy of Sciences, Hefei, China, *Adjunct Professor and Doctorate Student Mentor*

Member

NIH Special Emphasis Group, *Chairman, Ad Hoc Review Panel*
Radiation Research Society, *Vice-Chairman, Commission F of Committee on Space Research*
American Association for Cancer Research
Environmental Mutagen Society
Oxygen Society

Students Mentoring

Doctoral Student of Environmental Heath Sciences, Columbia University, School of Public Health
New York City High School Science Students for Intel Science Project
Faculty Advisor for exchange medical students from Fudan University, China
Faculty Advisor for radiation oncology resident

Reviewer

Cancer Research
Carcinogenesis
Chemical Research in Toxicology
Clinical Cancer Research
Environmental Health Perspective
Environmental & Molecular Mutagenesis
Free Radical Biology and Medicine
International Journal of Radiation Biology
International Journal of Radiation Biology, Physics & Medicine
Mutation Research
Proceedings of the National Academy of Sciences
Radiation Research
Toxicology & Applied Pharmacology

Editorial Work

Advances in Space Sciences, Section Editor
Journal of Radiation Research

LIEBERMAN, HOWARD B., Ph.D.

Member

Summer Research Program for NYC Secondary School Science Teachers, Columbia University, *Advisory Board*
Israel Cancer Research Foundation, *Scientific Advisory Board*
Columbia University College of Physicians and Surgeons, *Faculty Council*
American Association for the Advancement of Science, Elected fellow
American Society for Microbiology
Environmental Mutagen Society
Genetics Society of America
Radiation Research Society
Sigma Xi
Theobald Smith Society

Grant Reviewer

Basic and Preclinical Subcommittee C of the NCI Initial Review Group, *Member*
Joint Center for Radiation Therapy Foundation, Harvard Medical School, *Ad Hoc*
Pennsylvania Department of Health

Manuscrit Reviewer

Radiation Research
Journal of Cellular Physiology, Associate Editor

MARINO, STEPHEN A., M.S.

Member

Columbia University Radiation Safety Committee
Radiation Research Society

PARTRIDGE, MICHAEL, Ph.D.

Member

Radiation Research Society

Grants

High Throughput Biodosimetry Pilot Project

PONNAIYA, BRIAN, Ph.D.
Member
Radiation Research Society
Reviewer
International Journal of Radiation Biology
Radiation Research
Oncogene

RANDERS-PEHRSON, GERHARD, Ph.D.
Member
Radiation Research Society
Reviewer
International Journal of Radiation Biology

SMILENOV, LUBOMIR, Ph.D.
Reviewer
Advances in Space Research
Cancer Letters

YIN, YUXIN, M.D., Ph.D.
Adjunct Faculty
Assistant Professor, Department of Environmental Health Sciences, Mailman School of Public Health, Columbia University
Member
American Association for Cancer Research
Students Mentoring
Advisor for a Ph.D. student in the Department of Environmental Health Sciences, Mailman School of Public Health, Columbia University
Course taught
Molecular Toxicology PHS8308
Reviewer
Cancer Research
European Journal of Gastroenterology & Hepatology
Molecular & Cellular Biochemistry
Molecular & Cellular Biology
Oncogene
Proc. Natl. Acad. Sci. USA

ZHAO, YONGLIANG, Ph.D.
Member
Radiation Research Society
American Association for Cancer Research
Grants
RSNA Research Seed Grant
NIEHS Center Pilot Grant
NASA Project Grant ■

Publications

1. Bao L, Chen S, **Wu L**, **Hei TK**, Wu Y, Yu Z and **Xu A**. Mutagenicity of diesel exhaust particles mediated by cell-particle interaction in mammalian cells. *Toxicology* **229**:91-100, 2007.
2. **Bigelow AW**, **Ross GJ**, **Randers-Pehrson G** and **Brenner DJ**. Multiphoton Microscope Design for the Columbia University Microbeam II Endstation. *Radiation Research (Extended Abstract)* **166**:664, 2006.
3. **Brenner DJ** and Sachs RK. Estimating radiation-induced cancer risks at very low doses: rationale for using a linear no-threshold approach. *Radiat Environ Biophys* **44**:253-6, 2006.
4. **Brenner DJ**. It is time to retire the computed tomography dose index (CTDI) for CT quality assurance and dose optimization. For the proposition. *Med Phys* **33**:1189-90, 2006.
5. **Calaf GM**, Roy D and **Hei TK**. Gene and protein expression altered by organophosphorous pesticides and estrogen in human breast epithelial. *Oncology* (in press).
6. **Calaf GM**, Roy D, and **Hei TK**, Growth factor biomarkers associated with estrogen- and radiation-induced breast cancer progression. *Int J Oncol.* **28**:87-93, 2006.
7. **Calaf GM**. Susceptibility of human breast epithelial cells in vitro to hormones and drugs. *Int J Oncol* **28**:285-95, 2006.
8. **Garty G**, **Ross GJ**, **Bigelow A**, **Randers-Pehrson G** and **Brenner DJ**. Testing the stand-alone microbeam at Columbia University. *Rad Prot Dosim* **122:**292-6, 2006.
9. **Garty G**, **Ross GJ**, **Bigelow AW**, **Schettino G**, **Randers-Pehrson G** and **Brenner DJ**. Status of the Stand-Alone Microbeam at Columbia University. *Radiation Research (Extended Abstract)* **166**:656, 2006.
10. **Garty G**, Schulte R, Shchemelinin S, Grosswendt B, **Leloup C**, Assaf G, Breskin A, Chechik R and Bashkirov V. First Attempts at Prediction of DNA Strand-Break Yields Using Nanodosimetric Data. *Radiat Prot Dosimetry* **122:**415-9, 2006.
11. **Hall EJ**, Worgul BV, **Smilenov L**, Elliston CD and **Brenner DJ**. The relative biological effectiveness of densely ionizing heavy-ion radiation for inducing ocular cataracts in wild type versus mice heterozygous for the ATM gene. *Radiat Environ Biophys* **45**:99-104, 2006.
12. **Hall EJ**. Antiprotons for radiotherapy? *Radiother Oncol* **81**:231-2, 2006.
13. **Hall EJ**. Intensity-modulated radiation therapy, protons, and the risk of second cancers. *Int J Radiat Oncol Biol Phys* **65**:1-7, 2006.
14. **Hall EJ**. The inaugural Frank Ellis lecture – latrogenic cancer: The impact of intensity-modulated radiotherapy. *Clin Oncol (R Coll Radiol)* **18**:277-82, 2006.
15. **Hei TK**, Cyclooxygenase-2 as a signaling molecule in radiation-induced bystander effect. *Mol Carcinog***.** **45**:455-60, 2006.
16. **Hei TK**, **Xu A**, **Huang S** and **Zhao Y**. Mechanism of fiber carcinogenesis: from reactive radical species to silencing of the beta igH3 gene. *Inhal Toxicol* **18**:985-90, 2006.

17. **Hei TK**, **Zhou H, Lien Y** and **Zhao Y**. Mechanism of radiation carcinogenesis: βigHe3, COX-2 and beyond. *Int. Congress Series* **1299**: 114-20, 2007.
18. **Hei TK**. Cyclooxygenase-2 as a signaling molecule in radiation-induced bystander effect. *Mol Carcinog* **45**:455-60, 2006.
19. **Hu B**, Wu L, Han W, Zhang L, Chen S, **Xu A**, **Hei TK** and Yu Z. The time and spatial effects of bystander response in mammalian cells induced by low dose radiation. *Carcinogenesis* **27**:245–51, 2006.
20. **Ivanov VN** and **Hei TK**. Dual treatment with COX-2 inhibitor and sodium arsenite leads to induction of surface Fas Ligand expression and Fas-Ligand-mediated apoptosis in human melanoma cells. *Exp Cell Res* **312**:1401-17, 2006.
21. **Ivanov VN** and **Hei TK**. Sodium arsenite accelerates TRAIL-mediated apoptosis in melanoma cells through upregulation of TRAIL-R1/R2 surface levels and downregulation of cFLIP expression. *Exp Cell Res* **312**:4120-38, 2006.
22. **Ivanov VN**, Ronai Z and **Hei TK**. Opposite roles of FAP-1 and dynamin in the regulation of Fas (CD95) translocation to the cell surface and susceptibility to Fas ligand-mediated apoptosis. *J Biol Chem* **281**:1840–52, 2006.
23. Jin YJ, Wang J, Qiao C, **Hei TK**, Brandt-Rauf PW and **Yin Y**. A novel mechanism for p53 to regulate its target gene ECK in signaling apoptosis. *Mol Cancer Res* **4**:769-78, 2006.
24. **Jin YJ**, **Wang J**, Qiao C, **Hei TK**, Brandt-Rauf PW, **Yin Y**. A novel mechanism for p53 to regulate its target gene ECK in signaling apoptosis. *Mol Cancer Res* **4**:769-78, 2006.
25. **Lieberman HB**. Rad9, an evolutionarily conserved gene with multiple functions for preserving genomic Integrity. *J Cell Biochem* **97**:690–7, 2006.
26. Pandita RK, Sharma GG, Laszlo A, **Hopkins KM**, Davey S, Chakhparonian M, Gupta A, Wellinger RJ, Zhang J, Powell SN, Roti Roti JL, **Lieberman HB** and Pandita TK. Mammalian Rad9 plays a role in telomere stability, S- and G2-phase-specific cell survival, and homologous recombinational repair. *Mol Cell Biol* **26**:1850-64, 2006.
27. **Partridge MA**, Davidson MM and **Hei TK**, The Complete Nucleotide Sequence of Chinese Hamster (Cricetulus griseus) Mitochondrial DNA. *DNA Sequence* (in press).
28. **Ross GJ**, **Ponnaiya B**, **Bigelow AW**, **Randers-Pehrson G** and **Brenner DJ**. Update on Incorporating No-Stain Imaging into Microbeam Endstation, *Radiation Research* **166**:667, 2006.
29. Roy D, **Calaf GM** and **Hei TK**. Allelic imbalance at 11q23-q24 chromosome associated with estrogen and radiation-induced breast cancer progression. *Int J of Oncol* **28**:667-74, 2006.
30. Shao G, Berenguer J, Borczuk AC, Powell CA, **Hei TK** and **Zhao Y**. Epigenetic inactivation of Betaig-h3 gene in human cancer cells. *Cancer Res* **66**:4566-73, 2006.
31. Sharma S, Stumpo DJ, **Balajee AS**, Bock CB, Lansdorp PM, Brosh RM Jr and Blackshear PJ. RecQL, a member of RecQ family of DNA helicases, suppresses chromosomal instability. *Mol Cell Biol* **27**:1784-94, 2007.
32. **Shen WH**, **Balajee AS**, Wang J, Wu H, Eng C, Pandolfi PP and **Yin Y**. Essential role for nuclear PTEN in maintaining chromosomal integrity. *Cell* **128**:157-70, 2007.
33. **Shen WH**, **Wang J**, Wu J, Zhurkin VB and **Yin Y**. Mitogen-activated protein kinase phosphatase 2: a novel transcription target of p53 in apoptosis. *Cancer Res* **66**:6033-9, 2006.
34. Shuryak I, Sachs RK, Hlatky L, Little MP, Hahnfeldt P and **Brenner DJ**. Radiation-induced leukemia at doses relevant to radiation therapy: modeling mechanisms and estimating risks. *J Natl Cancer Inst* **98**:1794-806,2006.
35. **Smilenov LB**, **Hall EJ**, Bonner WM and Sedelnikova OA. A Microbeam Study of DNA Double-Strand Breaks in Bystander Primary Human Fibroblasts. *Radiat Prot Dosimetry* **122**:256-9, 2006.
36. Travis LB, Rabkin CS, Brown LM, Allan JM, Alter BP, Ambrosone CB, Begg CB, Caporaso N, Chanock S, DeMichele A, Figg WD, Gospodarowicz MK, **Hall EJ**, *et al.* Cancer survivorship--genetic susceptibility and second primary cancers: research strategies and recommendations. *J Natl Cancer Inst* **98**:15-25, 2006.
37. **Xu A**, **Smilenov LB**, He P, Masumura K, Nohmi T, Yu Z and **Hei TK**. New insight into intrachromosomal deletions induced by chrysotile in the gpt delta transgenic mutation assay. *Environ. Health Perspective* **115**:87-92, 2007.
38. **Zhao Y**, El-Gabry M and **Hei TK**. Loss of Betaig-h3 protein is frequent in primary lung carcinoma and related to tumorigenic phenotype in lung cancer cells. *Mol Carcinog* **45**:84-92, 2006.
39. **Zhou H**, **Xu A**, Gillispie JA, Waldren CA and **Hei TK**. Quantification of CD59- mutants in human-hamster hybrid (A_L) cells by flow cytometry. *Mutat Res* **594**:113-9, 2006. ■

Center for Radiological Research 2006 Christmas Party (*l-r*): Dr. Sally Amundson, Dr. Charles Geard, Ms. Mary Coady and Dr. Eric Hall.

Center for Radiological Research 2006 Christmas Party (*l-r*): Dr. Peter Grabham, Ms. Monique Rey, Dr. Tom Hei, Mrs. Bernice Hall, Ms. Mary Coady, Dr. Charles Geard, Mrs. Margaret Geard and Ms. Heidy Hernandez.

The multi-talentd Drs. Lubomir Smilenov, Corinne Leloup and Alan Bigelow performing at the Annual Christmas Party, together with the singing quartet of CRR (*l-r*): Dr. An Xu, Dr. Yu-Chen Lien, Ms. Sarah Huang and Ms. Jingjing Wu.